Preparation of amorphous silica-aluminas with enhanced acidic properties and spectroscopic identification of their acid sites

Xiaojing Jin

Université Pierre et Marie Curie

Ecole doctorale Physique et Chimie des Matériaux (ED397)

Laboratoire de Réactivité de Surface

Preparation of amorphous silica-aluminas with enhanced acidic properties and spectroscopic identification of their acid sites

Par Xiaojing JIN

Thèse de doctorat de Chimie

Dirigée par Pascal Man & Juliette Blanchard

Date prévisionnelle de soutenance: 25 octobre 2017

Devant un jury composé de:

Mme Françoise Maugé, Directrice de Recherche	Rapporteur
M. Francis Taulelle, Directeur de Recherche	Rapporteur
Mme Sophie Cassaignon, Professeur	Examinateur
Mme Catherine Especel, Maître de conférences	Examinateur
Mme Céline Chizallet, Ingénieure Recherche	Examinateur
M. Yannick Millot, Maître de conférences	Examinateur
Mme Juliette Blanchard, Chargée de Recherche	Examinateur
M. Pascal Man, Directeur de Recherche	Examinateur

To my father

Acknowledgements

This manuscript represents not only my work during these last months at my keyboard, it is a milestone for a twenty-two years' journey from elementary school to University and, of course, more specifically, for the past three years in LRS, an unexpected, exciting and rewarding experience!

I need to thank Catherine Louis first, as she is the person who forwarded my application email to Juliette Blanchard that ended up with this opportunity to work at the LRS. Besides, I gratefully acknowledge the funding agency China Scholarship Council (CSC) that made my Ph.D. work possible.

I would like express my highest appreciation and thanks to my supervisor Juliette Blanchard. She is very nice, responsible and acknowledgeable. In the past three years, she has devoted much time and efforts not only to my research work but also to my life. She helped me registration and lend me money for the tuition when I was in poverty. I clearly remembered that I came to UPMC fresh and ambitious but knowing not much about what awaited me in the totally new environment. Juliette has been always there for me kindly and supportively. I appreciate her guiding and directing while giving me adequate freedom on this interesting project and significant support to try any new experiments. When I was in lost, she gave me much encouragement and consolation. I remembered when I felt confused to my subject, she told me that "We expect Ph.Ds to be brain as much (and maybe more) than arms. Your research subject is a very challenging one and you cannot succeed in it by doing thousands of experiments but rather by doing the right ones. Those who are successful are those who work hard and really tackle their research subject." These words would influence me all my life. Her advice on both research as well as on my career have been priceless. I appreciate all her contributions of time, energy and ideas to make my Ph.D. experience productive and stimulating. The joy and enthusiasm she has for her research was contagious for me, even during tough times in the Ph.D. pursuit. Her abundant knowledge was motivational for me to

enlarge my knowledge scopes. She revised my thesis quite carefully and meticulously. She is the first person I knew who is such responsible to me except my parents. I could not imagine having a better advisor and mentor for my Ph.D study.

I am also deeply grateful to Yannick Millot for his guidance on my research especially for NMR. He is very patient and good-tempered. Every time when I made troubles, he never blamed me and on the contrary, he gave me understanding and comfort. He never refused to measure any samples when I asked him. He answered my question patiently and repeatedly until I understood. His guidance helped me in all the time of research and writing of this thesis. He not only revised my thesis but also explained the reason to me. The beautiful figures he drawn give me a deep impression and encourage me to pay attention to every details to match them.

My sincere thanks also goes to Pascal Man. He gave me a warm welcome when I first entered the lab. He introduced the people working in the lab and made me be familiar with others quickly. He directed me how to typesetting and arrange time reasonably. He also helped a lot, by his advices and his wide ranging expertise in theoretical aspects of NMR, in the realization of the NMR experiments reported this manuscript.

I am also much indebted to Céline Sayag for all the catalytic setup and test. As that was the first time I made catalytic test, endless problems emerged with the setup, furnace, GC, reactant, etc. Correspondingly, various attempt and adjustments needed to make. She seemed to be always there whenever any help was needed. She encouraged me to install and modify the setup by myself and made my operating capacities improve greatly.

I acknowledge all the professors and secretaries in the LRS. In particular, I would like to thank Jean-Marc Krafft for helping me a lot with the technical problems and processing data on IR throughout my research. Many thanks to Laetitia Valentin for training me in FTIR experiments for adsorption of pyridine and helping me measuring samples for FTIR experiments on CO adsorption. Thanks to Cyril Thomas for helping me adjusting the BEL apparatus for high temperature pretreatment. Thanks to Guylène Costentin for lending me

quartz reactors and Laurent Delannoy for the Ag catalysts.

My time in Paris was quite enjoyable due to many friends. Thank you all for the good times that we shared together. Special thanks go to my office mates Sarah Petit, Sarah Diallo-Garcia, Marie-Nour Kaydouh, Karam Jabbour, Priyanka Gairola. It was great having you all around and the good atmosphere in the office. Thanks to Diaa Obaid and Yuriy Sakhno for sharing insight into their culture with me. I'm also obliged to my chinese friends, Xiaolu Su, Meng Lin, Sijin Li, Yang Peng, Zongbei Dai, Xuepeng Wang, Zhao Wang, Longfei Lin, Lu zhang, Miao Zhang, Shuaiyuan Han, Yufeng Ren, Yan Li, Jing Luo,…Thanks a lot for the great company and the many dinners we've had together.

A special thanks to my family. Words cannot express how grateful I am to my grandparents and parents for all of the sacrifices that they've made for me.

Additionally, I would also like to thank my thesis committee members for taking precious time to review my thesis and attend to my thesis defense. I also want to thank all of you for letting my defense be an enjoyable moment, and for your brilliant comments and suggestions, thanks for your insightful comments and encouragement, but also for the hard question which incented me to widen my research from various perspectives.

Lastly, my sincere thanks to every person who cared for me, helped and supported me during my life. I will bear it in mind forever. Bless all of you and wish you happiness forever!

Glossary

23DMB1	2,3-dimerthylbut-1-ene
23DMB2	2,3-dimerthylbut-2-ene
33DMB1	3,3-dimethylbut-1-ene
Acac	Acetylacetone
Al^{IV}	Four-coordinated Al
Al^{V}	Five-coordinated Al
Al^{VI}	Six-coordinated Al
ASA	Amorphous Silica-Aluminas
BAS	Brønsted acid sites
BET	Brunauer, Emmett and Teller
BJH	Barret, Joyner and Halenda
CA	Citric Acid
DBM	Dibenzoylmethane
D-HMQC	Dipolar-Heteronuclear Multiple Quantum Coherence
$D^{i}BAH$	Diisobutylaluminium hydride
DP	Direct Polarization
DQ	Double Quantum
FTIR	Fourier Transform Infrared Spectroscopy
GC	Gas Chromatography
HETCOR	HETeronuclear CORrelation
I	Spin quantum number

LAS	Lewis acid site
MAS	Magic angle spinning
MQ	Multiple Quantum
NMR	Nuclear Magnetic Resonance
REAPDOR	Rotational Echo Adiabatic Passage DOuble Resonance
SQ	Single Quantum
TGA	Thermal Gravity Analysis
$T^{i}BA$	Triisobutylaluminium
TPD	Temperature programmed desorption of ammonia
XRD	X-ray Diffraction
δ	Chemical shift

Contents

Introduction Générale

Grâce à leurs propriétés acides, les silice-alumines sont utilisées dans de nombreux processus catalytiques tels que le raffinage du pétrole, la pétrochimie ou la chimie fine : comme supports de métaux nobles ou de sulfures dans les réactions d'hydrocraquage, échangées au nickel comme catalyseur d'oligomérisation des alcènes et telles quelles pour des réactions d'alkylation, de déshydratation, d'isomérisation… Les matériaux traditionnellement utilisés sont d'une part, les zéolithes (des aluminosilicates cristallins qui présentent l'avantage d'une acidité forte mais l'inconvénient d'une accessibilité difficile aux sites actifs du fait de leur microporosité) et d'autre part, les silices alumines amorphes (généralement mésoporeuses elles offrent une bonne accessibilité aux sites acides mais présentent une acidité plus faible que celle des zéolithes). Le développement de nouveaux matériaux combinant l'acidité forte des zéolithes et une porosité plus ouverte fait actuellement l'objet d'une recherche intense. Cette recherche est cependant ralentie par le fait que la nature des sites acides de Brønsted des ASA n'a pas encore pu être clairement établie (l'acidité des zéolithes est, quant à elle clairement associée à la présence de ponts Si-OH-Al).

Cette thèse a deux objectifs:

Le premier est de préparer des silice-alumines avec des propriétés acides améliorées en utilisant diverses voies de synthèse (modification de silice-alumines commerciales ou greffage de précurseur d'aluminium sur des silices). Il s'agira de déterminer les conditions de synthèse permettant d'obtenir des silice-alumines avec des propriétés acides améliorées sur la base de leur activité catalytique (isomérisation du 3,3-dimethylbut-1-ene) et de l'évaluation de leur acidité par adsorption de molécules sondes (pyridine et ammoniac). Ces silices alumines devront non seulement présenter des propriétés acides supérieures à celles des silice-alumines commerciales mais aussi présenter un taux plus élevé de sites acides par atome d'aluminium.

Le deuxième objectif est d'obtenir des informations sur la structure chimique des sites acides à l'aide de la RMN du solide. Les noyaux utilisés seront l'aluminium-27 et le proton du fait de leur abondance naturelle élevée. Les silice-alumines améliorées obtenues dans les chapitres consacrés à la synthèse trouveront ici toute leur utilité en particulier grâce à

l'augmentation du taux de site acide par atome d'aluminium. Les techniques de transfert de polarisation entre deux noyaux (^{1}H-^{1}H, ^{27}Al-^{27}Al mais également ^{27}Al-^{1}H) seront également très utiles pour obtenir des informations sur la proximité entre protons et aluminium et ainsi d'identifier les protons et les atomes d'aluminium qui participent à l'acidité.

Chapter 1. Bibliographic report

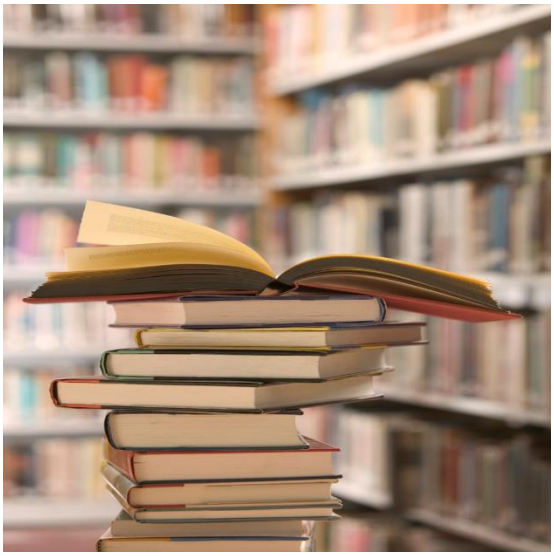

Abstract

In this first chapter, we will report and discuss different aspects of the literature related aluminosilicates and more specifically of amorphous silica alumina (ASA). As these ASA are complex materials because of their amorphous nature we will also, when necessary discuss the literature related to their crystalline counterpart, the zeolites. We will focus on several aspects of ASAs such as their catalytic applications, their preparation, the current hypotheses regarding the structure of their acid (Lewis or Brønsted) sites and the characterization of their acidic properties using mostly spectroscopic characterization tools with an emphasis on the use of solid state NMR. We will finish this chapter by a short sum-up of this analysis of the literature and the presentation of the objective of this thesis.

1.1 Applications of ASAs in catalysis

Aluminosilicates, such as zeolites and amorphous silica-alumina (ASA), have been extensively used in oil refining, petrochemistry and fine chemicals production and their catalytic activities are associated with their surface acidity properties.[1,2] Zeolites are crystalline materials that possess an exceptional combination of properties such as high thermal stability, high Brønsted acidity, and microporosity. The presence of regular micropores of molecular dimensions is responsible of their unequalled shape selectivity in catalytic conversions and separations.[3] However, in many applications, this microporosity induces diffusional limitations due to the restricted transport of molecules to the active sites.

ASA are mesoporous materials that lack long-range order and are therefore XRD amorphous. Their mesoporosity facilitates physical transport of reactants and products. In addition, ASA generally exhibit fewer and milder Brønsted acid sites than zeolites. Busca reviewed the application of these materials in industrial processes.[4] Although zeolites have supplanted ASA in many catalytic processes thanks to their stronger Brønsted acidity, ASA are still preferred to zeolite as hydrocracking supports when higher selectivity for middle distillates is desired or for the conversion of bulky molecules. They also are still used in dehydrochlorination of halided hydrocarbon and as support of sulfide for hydrotreatment and

of metal for ring opening reactions.[4] Beside conventional silica-alumina, other amorphous aluminosilicates are used: Al rich silica-aluminas are possibly used in the production of dimethylether (DME) or the coproduction of methanol and DME from syngas,[4] whereas silicate alumina (prepared by grafting TEOS on alumina) have been reported to be used in the dehydration of terbutyl alcohol to isobutylene.[4] At the other side of the composition, aluminated silica (prepared by addition of alumina precursors to preformed silica) are likely to be the catalysts used for the cracking of Methyl tert-butyl ether (MTBE) to isobutylene.[4] Another specificity of ASA is their high density of Lewis sites, which could also lead to their application in Lewis catalysed reaction (e.g. Meerwein–Ponndorf–Verley (MPV) reduction of carbonyl compounds). The strong Lewis acid sites of ASA have been reported to contribute to the Sanderson electronegativity of the support and hence to the increase in the electronegativity of supported metallic particles (e.g. Pt nanoparticles) and in turns to an increased activity of these particles in C-H bond cleavage and enhance their activity toward neopentane hydrogenolysis.[5]

ASA could also find application in reactions related to the biomass conversion such glycerol dehydration that requires mild acid sites[6] and for the conversion of lignocellulosic biomass in aqueous reaction media.[7]

1.2 Brønsted and Lewis acidity in ASA

As emphasize above, Brønsted and Lewis acidic properties of ASA have numerous and different applications in catalysis. Therefore, knowing and controlling the acidic properties of the catalysts are of great importance to understand the reaction mechanism and also to design more efficient acid catalysts. Hence, acid properties of ASA, such as acid type (Brønsted vs. Lewis), concentration, strength, location as well as cooperative effect between Lewis and Brønsted acids, attract considerable attention.

1.2.1 Brønsted acid sites

Zeolite, which play a dominant role industrial catalytic processes, generally have a higher catalytic activity than ASA and the structure of their Brønsted acid sites is well understood

based not only on experiments[8,9] but also on theory[10]). The strong Brønsted acidity resides in the bridging hydroxyl group originating from the replacement of a Si^{4+} in their crystalline framework by an Al^{3+} [≡Al–(OH)–Si≡].[11] Zeolite acidity depends on the local environment and the Al content. Indeed as the number of Al^{3+} atoms in the second coordination sphere (i.e. in the shell of 12 or less T atoms surrounding the $Al(OSi)_4$ site)increases, the strength decreases gradually.[12] Zeolites with high Al^{3+} content exhibit a high density of acid sites of low strength, while on the other side, dealuminated zeolites have a low density of acid sites, but of higher acid strength. In addition, high Al^{3+} content favour the tendency of zeolites to produce extraframework aluminium species (EFAL), thus generating Lewis acid sites.[12] The presence of Lewis acid sites can also influence the Brønsted acidity, thanks to a Lewis/Brønsted acid sites synergy that remarkably enhances the Brønsted acid strength.[13-15] The acidity of the zeolites is also influenced by the dimension of the cavities. It has been found that for similar chemical composition, the strength of acid sites in medium pore size zeolites is higher than that found in large pore size zeolites.[16]

In contrast to zeolite, due to the amorphous nature of these materials, acid sites in ASA are much less defined, and their structure is still far to be understood despite important contributions in the literature on this subject.[5,17-28] The original structural models of ASA proposed that Brønsted acidity arise from proton compensating the electronic charge of the surface.[29] Recently, many efforts have been made to study the Brønsted acid sites of ASA, based on probe molecule adsorption.[5,18,22,26,27] Trombetta et al.[28] suggested that, in mesoporous aluminosilicates, BAS originate from non-bridging SiOH groups in the vicinity of framework Lewis aluminium species. In presence of a basic molecule, a bridge is formed between the silanol and the Lewis aluminium (see Figure 1-1).

In 2005, Gora-Marek et al.[30] reported the detection, on the spectra of two ASAs, of a weak band located at ca. 3600-3610 cm^{-1}. They concluded to the presence of Si-OH-Al bridges in ASA and assigned the strong Brønsted acidity of ASA to these sites. In order to explain the weak intensity of this band, they proposed that it was due to a very low absorption coefficient for this band.

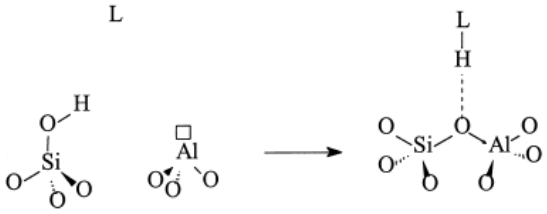

Figure 1-1 Structure of the terminal Brønsted acidic silanols in ASA (L: a base)[28]

One year later, Busca et al.[31] invalidated this hypothesis based on the fact that they could observe, on aluminated silica, sites of similar strength and in similar amount, independently of the presence of this band. Hence, they proposed that SiOH, Al^{3+} pair form a drawbridge that can be either closed (zeolite) or open (ASA). The closed drawbridge requires the rigidity of the zeolite framework to be stabilized and can therefore not exist in ASA.

In 2006, Crépeau et al.[20] also concluded that the Brønsted acidity of ASA arose from a Si-OH, Al^{3+} pair but ruled out the hypothesis of Trombetta et al.[28] concerning the formation of the $Si\text{-}O^{-}\text{-}Al$ bridge upon adsorption of a base (at least when the adsorbed base is CO) based on the fact that $\Delta\nu$(OH) vs. ν(CO) of CO adsorbed on the acid sites of ASA follows the same linear correlation as in the case of zeolites. They also proposed that the detection of Brønsted acid sites with different strength is related to the number of tetrahedral Al atoms in the vicinity of the acidic silanol.

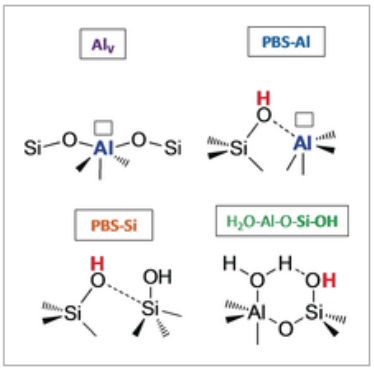

Figure 1-2 Brønsted and Lewis acid sites on the theoretical ASA surface model[32]

In 2009, Chizallet and Raybaud[19] have proposed the first theoretical model for ASA. This model is based on the coating of a γ-alumina surface by a monolayer of silica. This modified

surface has been optimized by periodic DFT. They identified pseudo-bridging silanols (PBS) (i.e. in electrostatic interaction with acceptor Al (PBS–Al) or Si (PBS–Si) (Figure 1-2), but not covalently bonded to it as they are in zeolite). When a strong enough base is adsorbed on these silanols, the pseudo-bridge (so-called drawbridge by Busca et al.) becomes a bridge that stabilizes the silanolate. Interestingly, the calculations of Chizallet et al. reconciliate the observation of Crépeau et al.[20] vs. Trombetta et al.[28]. Indeed, based on these calculations, the closing of the drawbridge requires a strong enough base (such as lutidine), whereas, upon adsorption of a weak base such as CO, the drawbridge remains open. On the other side, based on their calculation, Chizallet et al. discarded the hypothesis of Crépeau et al. who suggested that the Brønsted acidity arose from silanols directly connected to a Lewis aluminium, as they indeed observed the presence of such species on their calculated ASA but, based on their interaction with basic probe molecules, these sites should be classified as very weak Brønsted sites. Nevertheless, one must keep in mind that the model of ASA they used (atomic film of Si on an alumina surface) is very different from the ASA commonly studied (where Al and Si are more intimately mixed and which usually contain a high fraction of silica). Baiker group also concluded that tetrahedrally coordinated aluminium in the vicinity of silanol groups results in moderate Brønsted acidity.[33] According to them, sites with high Brønsted acidity (sites whose strength is similar or higher to that of Si-OH-Al bridges of zeolite) are due to silanols interacting simultaneously with a tetracoordinated and a pentacoordinated.[33]

1.2.2 Lewis acid sites

Lewis acid sites (LAS), are considered to play a key role in numerous reactions in heterogeneous catalysis either by themselves (e.g. MPV reaction[34]) or by playing a synergetic role on the Brønsted Lewis sites.[35-38] Reports on the structures of LAS of ASAs are very scarce. Hence we will present here briefly the literatures on LAS of zeolite.

LAS are associated with coordinatively unsaturated sites, and, for zeolites, very often assigned to Extra-Framework Aluminium species (EFAl). EFAl may occur in different forms such as Al^{3+}, AlO^{+}, $Al(OH)^{2+}$, $[Al(OH)_2]^{+}$, AlO(OH), $Al(OH)_3$, and Al_2O_3.[39] Among these compounds, the cationic extra-framework aluminium species Al^{3+}, AlO^{+}, and $Al(OH)^{2+}$ have

been reported to act as strong Lewis acid sites. The other species ($Al(OH)_3$, Al_2O_3 and AlO(OH)) are associated to a mild Lewis acidity, similar to the one of alumina.

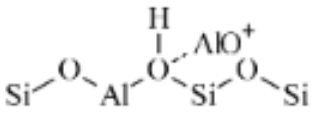

Figure 1-3 Possible superacid site formed by EFAl species with the Brønsted acid sites[40]

Regarding the synergetic effect of Lewis acid sites on Brønsted acid sites in zeolite, the origin of this phenomena is usually assigned to the interaction of the EFAl with the electron pairs of the framework oxygen atoms, which leads to a delocalization of the electron density near the Brønsted acid sites, and hence to an increase acidity of this site (Figure 1-3 and ref.[40]). Besides framework Al, the presence of framework Lewis sites has also been proposed in zeolites. Basically this framework Lewis site should be a tricoordinated Al (formed via the dehydroxylation of the bridging OH), but the presence of this species remains difficult to ascertain. Indeed, although XANES (at the Al Kedge) and XPS experiments (Bokhoven et al.[41,42]) have provided clear evidences for the formation of distorted Al species, the exact nature of these species remains difficult to ascertain and the formation of distorted tetrahedral Al species by interaction of a tricoordinated Al with an oxygen from the zeolite framework has been proposed.[43] Moreover, tricoordinated silicon species, whose formation has been postulated but never experimentally proven, could also contribute to the strong Lewis acidity.[44-46]

Although little is known regarding LAS of ASA, EFAl species described for zeolite are probably not the main LAS in ASA because they require the stabilisation of the zeolite cages, and LAS sites of ASA are probably mostly related to the second type of LAS, i.e. framework Lewis sites.

1.3 Formation of ASA

The amorphous nature (and hence complex surface structure) of ASAs makes very

difficult not only to the understanding of the origin of their Brønsted and Lewis acidities, but also to the accurate control of the acidic properties of these materials. Added to this, ASA can be prepared via a wide range of synthesis procedures and the choice of the synthesis method, together with the composition (SiO_2/Al_2O_3 ratio) strongly influence the distribution of silicon and aluminium atoms through the particles and can lead to different acidic properties. Moreover, the comparison of the acidic properties of ASA obtained by different procedures is made difficult by the fact that different techniques can be used to evaluate their acidity (e.g. NH_3-TPD, pyridine FTIR or catalytic activity in a model reaction). Recently, important developments in the synthesis of ASA via the sol-gel method,[18,20,22,47-49] coprecipitation method,[18,23,50] homogeneous deposition–precipitation,[22] grafting process,[17,50-56] flame-spray pyrolysis[33] have been reported.

Crépeau et al.[20] compared the acidic properties (based on FTIR of adsorbed pyridine and adsorbed CO) of samples prepared by impregnation (impregnation of alumina with silica, Siral series from Sasol) to those of samples prepared by cogelification of a small amount of aluminium with a high amount of silicon precursors. They concluded that cogelation leads to more homogeneous samples with higher Brønsted acidity (both in terms of number and of strength). Hensen et al.[22] studied the acidity (*n*-heptane, FTIR of adsorbed pyridine) of aluminosilicates prepared by homogeneous deposition precipitation (pH jump by urea thermal decomposition) of aluminium nitrate on silica. They concluded to the presence, in these ASA, of very small fraction of strong Brønsted acid sites, similar to those of zeolites. Moreover, they observed that a higher temperature of calcination results in a higher amount of strong Brønsted acid that they associated to the diffusion of Al atoms into the silica network. Baiker group[33] investigated an original preparation route for the synthesis of ASA based on flame-spray pyrolysis of a solution of aluminium acetylacetonate and tetraethoxysilane. These ASA exhibit a tunable Brønsted acidity ranging from moderate to zeolite-like depending on the aluminium content.

Controlled grafting of aluminium alkoxide or silicon alkoxide precursors respectively onto a silica or alumina support is also an efficient synthesis method to prepare ASA. Mokaya

et al.[55] synthesized ordered mesoporous aluminosilicate (Al-MCM-41) by grafting aluminium isopropoxide on silica in nonaqueous media or by grafting aluminium chlorohydrate in aqueous solution. These materials exhibited higher Brønsted acid content compared to Al-MCM-41 prepared via the conventional direct synthesis method. Caillot et al. prepared Al/SiO_2 and Si/Al_2O_3 by grafting aluminium (respectively silicon) alkoxides on silica respectively alumina under various conditions: liquid-phase (water free or water-added conditions) and gas-phase. They investigated the influence of several parameters on the deposition and came to the following conclusions: (1) for grafting in anhydrous liquid phase conditions, when the density of OH groups of the support is no longer the limiting factor, deposition is saturated when the surface of the support oxide has been completely covered with a monolayer of precursor molecules; (2) following a first grafting, new species can be grafted after a calcination step that allows recovering of hydroxyl groups; (3) temperature and water/precursor ratio can control the structure of the deposit.[50] In another study of the same team, the acidity of Al/SiO_2 prepared by grafting aluminium isopropoxide on silica was examined and results suggested that the nature of the Brønsted acid sites strongly depends on the method used for ASA synthesis.[52] For synthesis performed in presence of added water, grafting was less controlled leading to alumina agglomerates possessing weak and medium Lewis acid sites but no Brønsted acidity.[52] This team also found that ASAs prepared by cogelation has Brønsted acid sites with strength similar to those in zeolites, while grafted ASAs possess specific Brønsted acid sites that differ from those of zeolites.[18] More recently, this team performed DNP NMR experiments and DFT calculation on ASA obtained by grafting either Al on silica or Si on alumina. Based on these analyses, they proposed a detailed atomic level description of the preparation procedure and formation of Brønsted acid sites: on silica and alumina surfaces, molecular aluminium and silicon precursors are, respectively, preferentially grafted on sites that enable the formation of Al^{IV} and Si^{IV} interfacial sites and the genesis of Brønsted acidity is related to the formation of Si^{IV}-O-Al^{IV} linkages.[57]

This analysis of the literature related to the preparation of ASA highlights the complexity of these amorphous materials and clearly shows that the understanding the acidic properties of

ASA (nature, strength, concentration) and their relation with the synthesis procedure is of great importance to develop a synthetic route for the design novel solid catalysts with improved acidic properties. It also indicates that this goal can probably only be achieved by a carefully spectroscopic analysis of the environment of the Al and Si atoms.

1.4 Acidity Characterization

Various techniques can be used for acidity characterization. The traditional methods performed in solution (such as Boehm titration[7]) may give information about acid strength and concentration but their applications is limited due to (i) the fact that the measurement is performed in water (and hence, the acidity of the solid evaluated in these conditions may differ significantly from the acidity in gas phase) (ii) the slow diffusion, in aqueous solution of the probe into the micro- or mesopores of the solid. They remain very interesting when it comes to characterize the acidity of aluminosilicates for application in aqueous solution.[7] Characterisation of the acidity by adsorption of a basic probe molecule can also be performed in the gas phase. The probe molecules that are most usually used are, by increasing proton affinity (PA): CO (PA = 594 kJ/mol); ammonia (PA = 854 kJ/mol); pyridine (PA = 930 kJ/mol); lutidine (PA = 963 kJ/mol). Two approaches can be followed to detect the probe molecule: either a simple detection (TCD or mass spectrometry) of the molecule in the gas phase to follow its desorption during a temperature ramp, or a detection of the adsorbed probe molecules (mostly by FTIR). Probe molecules are especially useful for the quantification of the acid sites (either only the total amount, or a more detailed evaluation, e.g. BAS vs. LAS or strong vs. weak). Beside the characterization of the acidic properties of the solid by probe molecules, a direct spectroscopic characterization of the solid can also be performed. In this domain, beside FTIR (direct observation of the OH groups via the ν(OH) stretching band), high resolution solid state nuclear magnetic resonance (SSNMR) is a powerful tool for the determination of the geometry of the acid sites.

1.4.1 Characterization of the structure of the acid sites

1.4.1.1 SSNMR

Solid state NMR spectroscopy is undoubtedly one of the most powerful techniques for determining molecular-level structure of solids. Solid state NMR spectroscopy plays a key role thanks to the developments of methodologies appropriate to the investigation of quadrupolar nuclei (for more than 63% of the elements, the only NMR active isotopes are quadrupolar (absence of I = 1/2 isotope)). NMR is element selective, and the signal of the element will depend on its local environment. For aluminosilicates, the elements of interest are ^{1}H (S = 1/2, natural abundance 99.98%), ^{27}Al (S = 5/2, natural abundance 100%), ^{29}Si (S = 1/2, natural abundance 4.7%). Another isotope of interest is ^{17}O (S = 5/2) but, due to its very low natural (0.037%), its observation generally requires the preparation of enriched samples. To get an image of the acid sites, the observation of a single element is usually not enough and the recent developments in heteronuclear correlation bring new opportunities in the characterization of these sites.

^{27}Al nuclei

A- *^{27}Al MAS NMR*

^{27}Al MAS NMR have been extensively applied to determine local structure of aluminium sites, providing various information about aluminium coordination numbers. ^{27}Al with 100% natural abundance and a rather high gyromagnetic ratio, has a relatively high NMR sensitivity. But as a quadrupole nucleus with spin quantum number I = 5/2 and a relatively large quadrupolar moment ($eQ = 14.66\times10^{-30}$ m^2), the central transition of the Al NMR line is, under MAS conditions, broadened by the second-order quadrupole interactions. As a consequence, the Al signals can be rather large, and a part of the signal can become invisible (so-called NMR invisible aluminium). Moreover, chemical shift in 1D spectrum may vary with the magnetic field strength. The magnitude of the coupling (and hence, the broadening of the NMR signal) of a quadrupolar nuclei depends on the symmetry of the electric field gradient around the nuclei and hence on the symmetry of the distribution of charge of mostly (but not only) the

coordinating oxygen atoms. For perfect tetrahedral or octahedral symmetry the CQ value is 0 but it increases gradually with the decrease in the symmetry (Figure 1-4).

For high surface area aluminosilicates, the hydration level of the sample modifies dramatically the spectra. Figure 1-5 shows the ^{27}Al MAS NMR spectra of an amorphous aluminosilicates recorded without any specific pretreatment (and hence partially hydrated, H-MSA), fully dehydrated (dried H-MAS) and fully hydrated (H-MSA EQ60d). On the spectra recorded after drying, a broad signal is observed whose intensity corresponds to only 20% of expected one (large fraction of "invisible Al"), and, on the spectra recorded without specific pretreatment, still 50% of the NMR signal is invisible. Only a complete rehydration (or the adsorption of a basic molecule such as NH_3) allows a quantitative observation. This is the reason why, the aluminosilicates samples are usually rehydrated prior to the measurement of the ^{27}Al MAS NMR spectra of aluminosilicates.

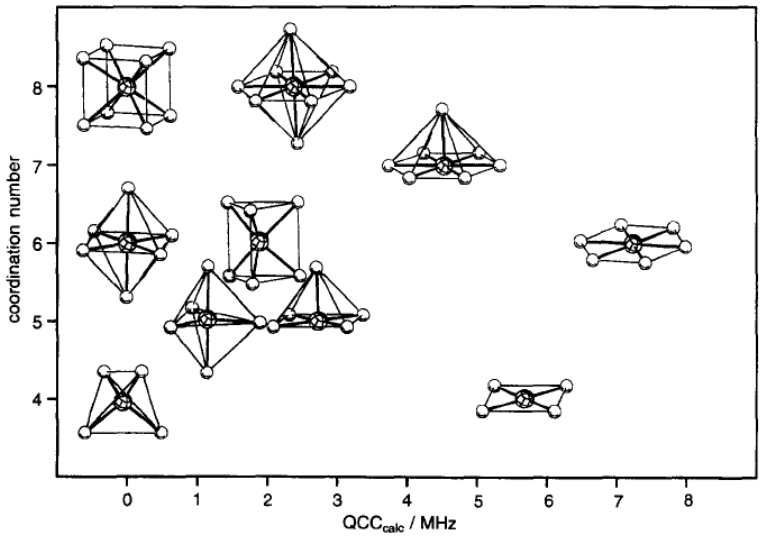

Figure 1-4 Relationship between QCC values and the Na coordination numbers[58]

This loss of signal for fully dehydrated aluminosilicates (and its recovery by rehydration or adsorption of basic molecules) has also been observed for zeolites.[59,60] The dramatic broadening of the peak associated to tetrahedral aluminium upon dehydration is assigned in zeolite to the formation of the Si-OH-Al bridge. Koller et al.[61] reported that the electric field gradient that surrounds an Al atom in a zeolite (calculated using DFT), is considerably larger for the protonated site (Al(OHSi)(OSi)$_3$ than for the unprotonated one ([Al(OSi)$_4^-$, H_3O^+]) due

to the weakening of the Al-O bond upon protonation.

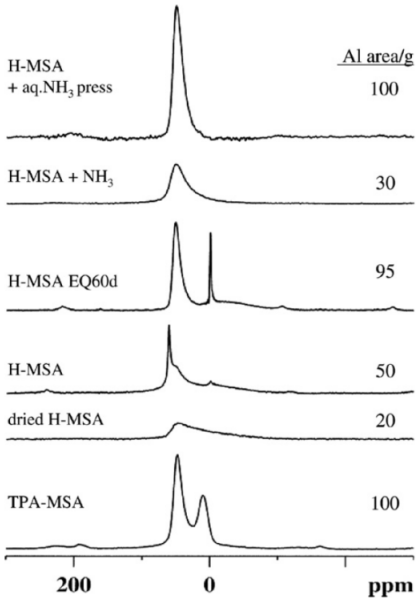

Figure 1-5 ^{27}Al MAS NMR under different hydration and NH_3 treatment[47]

On the spectrum of most ASAs, three signals are usually observed:

1) The peak observed at around 60 ppm is assigned to tetrahedral aluminium species, but, at variance with zeolites, only a small fraction of the aluminium atoms in tetrahedral coordination show Brønsted acidic properties (see Figure 1-6). Because of this, the term "framework aluminium" that is often used to qualify tetrahedral aluminium in ASA should be avoided as it is misleading.

2) The band at ca. 0 ppm is assigned to octahedral aluminium. The presence of Al in octahedral coordination is sometimes associated to the presence of transitional alumina domains or at least to some polymeric form of Al, as octahedral Al is the dominant coordination in many transitional aluminas[62]; octahedral Al is therefore often described as "extraframework Al". Although this assertion is mostly true for alumina-rich ASA, octahedral Al in silica-rich ASA has been shown partially[25,63,64] or even fully (see Figure 1-5) convert to tetrahedral Al upon adsorption of NH_3. The changes in the coordination of octahedral Al upon exposure to ammonia indicates that these Al are still connected to the framework via oxygen atom(s). Omegna et al.[25] concluded that the flexible coordination is limited to the aluminium atoms

which are part of an amorphous silica alumina character, as no change in Al coordination upon adsorption of NH_3 is observed for γ-alumina. This reversibility in Al coordination in presence of NH_3 was used for the evolution of the fraction of Al in silica alumina domains in ASA.[25,65]

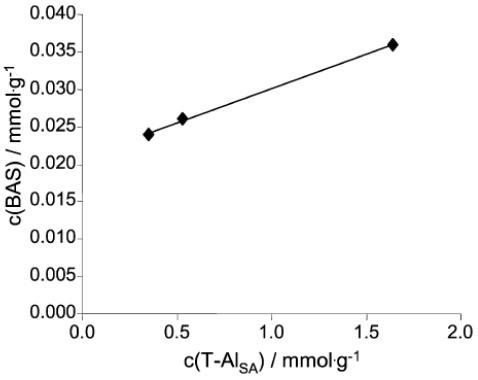

Figure 1-6 Concentration of BAS as a function of tetrahedrally coordinated Al in ASA (T-Al_{SA})[65]

3) The third signal is centered at 30 ppm. Two possible assignments have been initially proposed: either five coordinated Al or distorted tetrahedral species but MQ-MAS experiments (see below) have allowed assigning this signal to pentacoordinated Al. 5-coordinated Al are also present in gamma alumina and are associated in this oxide to surface Al atoms.[66] In Al rich ASA, these Al^V can be related to the presence of an alumina phase and be associated with surface sites of this alumina phase. However, these sites are also observed in Si-rich ASA. De Witte et al.[67] associated the presence of Al^V to the interface between the alumina and the silica-alumina phase. They observed, using ^{27}Al MAS NMR spectroscopy, that the proportion of this phase increases upon dehydration of the sample and also upon calcination (for ^{27}Al NMR spectra recorded on hydrated samples). However, Wang et al. came to a different conclusion as they observed, in ASA prepared by flame spray pyrolysis, a high population of homogenously dispersed Al^V in the absence of any bulk alumina phase and these sites were accessible to guest molecules.[68] Besides, these Al^V have been shown to contribute to the Brønsted acidity of the ASA (based on ^{27}Al DHMQC experiments that indicate a close proximity of NH_4^+ cations with these sites).[69]

B- ^{27}Al MQ MAS

As mentioned above, ^{27}Al MAS NMR spectroscopy provides information about the

coordination of the aluminium species. However, the spectral resolution is reduced by the second-order quadrupolar interaction that can only be partially averaged by MAS. This interaction also shifts the position of the central transition resonance away from its isotropic chemical shift. In 1995, Frydman and Harwood[70] introduced multiple quantum (MQ) ^{27}Al MAS NMR spectroscopy. This experiments produces a 2D spectrum that allows to obtain, not only a spectrum free of quadrupolar interaction (F1 dimension), but also information on the quadrupolar parameters of the nuclei (F2 dimension). In this sense, what was the main drawback of quadrupolar nuclei, becomes an advantage as it allows differentiating atoms as a function of their quadrupolar parameters. Moreover, the values of the isotropic chemical shifts and quadrupolar parameters determined from the analysis of the MQ MAS NMR spectra can be used to simulate the ^{27}Al MAS NMR spectra, leading to quantitative information on the aluminium species.Furthermore, as the quadrupolar parameters are related to the electric field gradient around the observed atom, it is possible to relate them to the local structure of this atom (usually based on theoretical calculation).

Figure 1-7 shows the ^{27}Al MQ MAS spectrum of a dehydrated HZSM-5.[71] This experiment allows differentiating 4 types of aluminium environments: two weak peaks associated to hexacoordinated and pentacoordinated Al and indicative of a slight extraction of framework aluminium and two types of tetracoordinated Al with close chemical shifts but very different C_Q value. The peak with the higher C_Q value (and hence the less symmetrical environment) can be assigned to a framework Al which is charge compensated by a H^+; the peak with the lower C_Q value (hence corresponding to the most symmetrical environment) can be assigned to a framework Al which is charge compensated by a cation other than H^+. This large difference in C_Q between these two tetrahedral environments is due to the fact that when the charge compensating cation is a proton, it corresponds to the formation of Si-OH-Al bridge and leads to one longer Al-O bond.

^{27}Al 3Q and 5Q MAS experiments have also been used to increase the resolution of the spectrum. This allowed, for example, to observe two tetrahedral Al environments in beta zeolite corresponding to different crystallographic sites[72] and to demonstrate that the coordination of

the Al atoms associated with the peak observed at ca. 30 ppm is five[65].

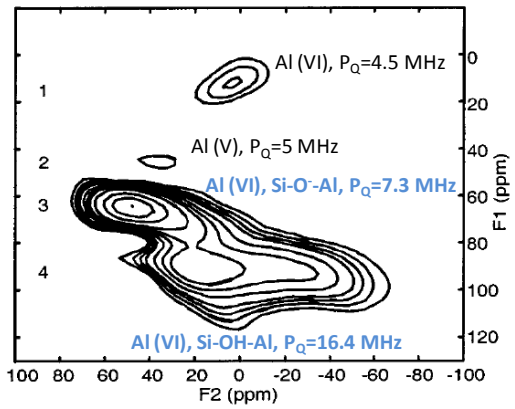

Figure 1-7 ^{27}Al MQ-MAS spectrum of a dehydrated HZSM-5 (field 14.1 T, spinning rate 27 kHz), with

$$P_Q = C_q * \sqrt{1+\frac{\eta^2}{3}} \approx C_q$$ (adapted from Kentgens[71])

On highly dehydroxylated aluminosilicate, one could expect a forth type of coordination for Al with the formation of tricoordinated aluminium. However, the observation of these species by ^{27}Al MAS NMR has not been reported until very recently. In a recent work Brus et al.[73] proposed, based on MQ MAS experiments and theoretical calculations, that framework trigonal Al in zeolites would be associated with a peak with the following parameters: δ_{iso} = 65 ppm, C_Q = 20 MHz and η = 0.1. However, this assignment is questionable as the C_Q value is close to the one of the Al engaged in Si-OH-Al bridges, and the values of C_Q reported by these authors for the Al of Si-OH-Al bridges (ca. 3.5 MHz) is not consistent with the numerous reports for this type of sites in the literatures.[60,71,74] The ^{27}Al spectra were probably misinterpreted in this work, likely due to an inappropriate sample preparation (adsorption of water molecules).

C-*^{1}H nuclei*

^{1}H NMR is one of the reliable and sensitive methods to investigate protons on solid owing to ^{1}H ≈100% natural abundance, high resonance frequency, S = 1/2 spin and large chemical shift rang. In zeolites, ^{1}H NMR spectroscopy not only allows to clearly distinguish the different types of hydroxyl groups (silanol nest, terminal silanol, hydrogen-bonded hydroxyl and bridging hydroxyl (Si−(OH)−Al)) via their chemical shift, but also for the quantitative analysis

of the different types of species. Quantification will be discussed in a separate part.

The properties of proton of surface OH groups of ASA are mainly influenced by local effects, such as oxygen coordination, bond geometry, and type of metal atoms in their local structure. ^{1}H NMR chemical shifts in aluminosilicates are illustrated in Table 1-1.

Table 1-1 Assignment of ^{1}H NMR chemical shift in Aluminosilicates

Abbreviation	δ_{1H} / ppm	Type	References
SiOH	1.9	nonacidic terminal silanol group	75
	2.2-2.3	silanol nests	75,79
H-bonded SiOH	6.1-6.5	silanol groups forming weaker hydrogen bonds	80,81
H_2O	4.7-4.9	water molecules adsorbed on silicalite	82,83
AlOH	0.4-0.6	non-framework AlOH (terminal)	84
	2.6-3.6	non-framework AlOH (bridging)	84-86
Si(OH)Al	3.6-4.3	bridging OH located in large cages and channels	86-88
	4.6-5.2	bridging OH located in small cages and channels	86,87
NH_4^+	6.5-7.0	ammonium ions	79,82,89

Signals at δ_{1H} = 1.2 − 2.3 ppm indicate the presence of SiOH, which may shift slightly due to interaction of their hydrogen with a neighboring oxygen (H-bond donor). Isolated terminal silanol groups appear at 1.9 ppm, and move to 2.1 ppm upon increasing temperature from 20 to 400°C.[75] In zeolites, silanol nests (produced by dealumination with alkaline solution) appear at 2.2 ppm. In amorphous silica, the presence of three types of silanols was evidenced by ^{1}H NMR, located at 1.8, 2.9 and 4.0 ppm. The first peak was assigned to isolated silanols, whereas the two others were assigned to H bonded (H-donors) silanols.[76] Yesinowski established a linear relationship between the distance between the two oxygens involved in the H-bond (picometer) and the chemical shift of the proton (ppm): $\Delta\delta_{1H}$ = 79.05 − 0.255 d(OH−O).[77] Hence, very high ^{1}H chemical shift can sometimes be observed in zeolite and silicates, indicative of very short H-bond. This is, for example, the case in phyllosilicates such as RUB-18 (Ilerite) for which a ^{1}H peak is observed at a chemical shift of 10.4 ppm which is associated with a ≡Si-OH…⁻O-Si≡H bond of ca. 250 pm.[78]

In zeolites, AlOH group of extra framework Al are responsible for peaks at 0.4 − 0.6 or

2.6 − 3.6 ppm.[84] Similar chemical shifts have been reported for surface OH in gamma alumina by Delgado et al: a chemical shift of about 0.4 ppm for terminal Al-OH (μ_1Al-OH) and of about 2.7 for bridging Al-OH-Al (μ_2AlOH). Similarly to silanols, the position of these peaks can be shifted toward higher chemical shift (low-field resonance shift) if they are involved in a H bond.[90]

Based on ^{1}H MAS NMR experiments, bridging Si-OH-Al hydroxyls have only been reported in zeolite and their presence has never been clearly ascertained in ASA. Zeolite pore channels influence the ^{1}H chemical shift of the acidic proton. For instance, the chemical shift of Brønsted bridging OH groups located in large cages and channels is in the range 3.6 − 4.3 ppm, while, when located in small cages and channels, it is shifted to lower field.[86,87]

Generally speaking, ^{1}H chemical shift can be regarded as an index of acid strength: the higher the ^{1}H chemical shift of hydroxyl groups over zeolite, the higher the acid strength, since the hydroxyl groups are isolated over zeolites (a higher acidity corresponds to a higher atomic charge on the hydrogen. This induces a reduction in the shielding of the external magnetic field on this hydrogen and hence a higher chemical shift[91]). The higher acid strength of silanol groups in the vicinity of framework aluminium atoms in mesoporous aluminosilicates in comparison with terminal SiOH groups is caused by the flexible local structure of these surface sites.[82]

Adsorption of ammonia as probe molecule is a very suitable method to highlight and quantify strong Brønsted acid sites. Upon formation of ammonium ions (NH_4^+) by protonation of the ammonia molecules by strong enough acidic OH groups, a narrow ^{1}H MAS NMR signal appears at δ_{1H} = 6.5~7.0 ppm[33,82,86] which cannot overlap with most of the OH signals and whose intensity is four times larger compared with that of the ^{1}H NMR signal of the acidic OH in the unloaded material. This can be used to quantify the number of accessible acid sites with high accuracy.[33,82]

In order to attribute signals in ^{1}H NMR spectra of solid, exploring the correlation between ^{1}H chemical shifts and the FTIR wavenumber of the O-H stretching vibration bands of

hydroxyl groups over various zeolites is of significant meaning. Several studies on this subject have been reported in the literature.[79,91,92] Based on these studies, a linear relationship between ^1H chemical shifts and the wavenumber of the O-H was established for non-interacting hydroxyl groups: δ_{1H} / ppm = 57.1 – 0.0147υOH/cm^{-1}.[92]

1.4.1.2 FTIR

FTIR spectroscopy have received considerable attention mainly as a tool to discriminate hydroxyl groups. The frequencies of the IR bands of the O-H stretching vibrations in the range of 3800-3200 cm^{-1} are used for primary characterization of the types of hydroxyl groups. Generally, four main bands appear in the region of OH stretching vibrations:

1) The band at 3745 cm^{-1} is characteristic of silanols located on the outer surface.[93-97]

2) the bands in the range ca. 3530 to 3620 cm^{-1} are attributed to bridging Si-OH-Al groups (strong Brønsted acid sites).[79,96]

3) the very broad IR adsorption band around 3500 cm^{-1}, is assigned to nest silanol groups[94,95] or Si-OH groups strongly disturbed by multiple hydrogen bonding[24,98] or H_2O interacting with the oxygen atoms of the framework.[99]

4) the bands at 3780, 3705 and 3670 cm^{-1} are attributed to OH groups bonded to extraframework aluminium.[79,97]

1.4.2 Quantitative evaluation of the acid sites

1.4.2.1 TPD (NH_3 and other bases)

The most direct way to evaluate the acidity of the sample is to adsorb a base on it and follow its desorption vs temperature (Temperature Programmed Desorption – TPD experiments). Ammonia is, by far, the most commonly used base, but the use of other basic molecules such as isopropylamine,[5] pyridine[65] and ethanol[18,52,100] has also been proposed.

Ammonia TPD is usually used for primary characterization of acidic properties. Ammonia is a strong base which is an appropriate probe for most OH groups, even in zeolites with small cavities, thanks to its small size (3.70 × 3.99 × 3.11 Å^3).[101] Experimentally, its simplicity and its low cost, make ammonia TPD a convenient method for quick determination

of the acidic properties. The desorbed amount of ammonia gives information about the amount of acid sites, whereas information on the strength are obtained by the analysis of the desorption temperature. Unfortunately, quantitative determination of the acid strength distribution may be complicated and measurements made using different experimental conditions are often not easily reconciled. The desorption peak has an unsymmetrical shape (related to the equilibrium between adsorbed NH_3 and NH_3 in the gas phase) and the peak shape and position depend on the experimental conditions (mass of sample, heating rate or gas flow), as well as on kinetic phenomena such as readsorption and/or slow diffusion. The fitting of the peaks is therefore very challenging.[102,103]

Nevertheless, under identical experimental conditions, the peak position gives comparative information about the relative acid strength and the width of the peak about the distribution of strength. Ammonia is usually adsorbed at 150ºC to eliminate the contribution of very weak acid sites and improve the spectrum resolution. Generally, two desorption peaks are observed, indicating the existence of at least two different types of adsorbed NH_3.[104,105] The first one, between 170 and 280ºC is referred to as the low temperature (LT) and is ascribed to the desorption of ammonia from acidic hydroxyls[106] or weak Lewis acid such as $Al(OH)_2^+$ and $Al(OH)^{2+}$[107], it is also sometimes assigned to over-adsorbed NH_3 (i.e. NH_3 molecules adsorbed on NH_4^+)[102]. It is usually considered as related to sites with no catalytic importance.[106,108] The second one, located between 350 and 440ºC, is called the high temperature peak (HT), and usually attributed to ammonia desorption from strong Brønsted and Lewis acid sites.[104]

However, the overlapping of the LT and HT peaks introduces some confusion in the interpretation of the TPD curves. The two peaks have to be separated to obtain the concentration of each type of acid site. Karge et al.[109] have reported a curve-fitting method to analyze TPD curve according to a simple Gaussian function based on the assumption of no readsorption of ammonia. However, the simulation is not robust and produces ambiguous results. Alternatively, the HT and LT peaks can be fitted with Haarhoff-Van der Linde (HVL) functions, but, although the use of this function allows a good fit for the experimental data, it can still lead to ambiguous results.[102]

It is clear that ammonia TPD is a useful technique for detection of the total acidity. But further distinguishing BAS and LAS far exceeds its power. Despite some limitations, it is still an ideal method to make a first evaluation of the acidity.

1.4.2.2 FTIR of adsorbed probe molecules

What differs between a probe molecule adsorbed on a Lewis and a Brønsted site is the mode of interaction of the probe with the site. For a strong base (e.g. pyridine or NH_3), the adsorption on a Brønsted site is associated with the protonation of the base (provided that the acid site is strong enough) or the formation of H-bond between the probe and the acid site (for probes with weak basic properties). On a Lewis site, the adsorption of a base leads to a coordination bond.

Figure 1-8 illustrates, with the example of pyridine, the different types of bonds that can be formed between the probe and the acid sites. The spectroscopic detection of the mode of adsorption of a base requires that different modes of adsorption have different signature. Although several other technics can be used (e.g. NMR or XPS), FTIR remains the choice spectroscopy for this application.

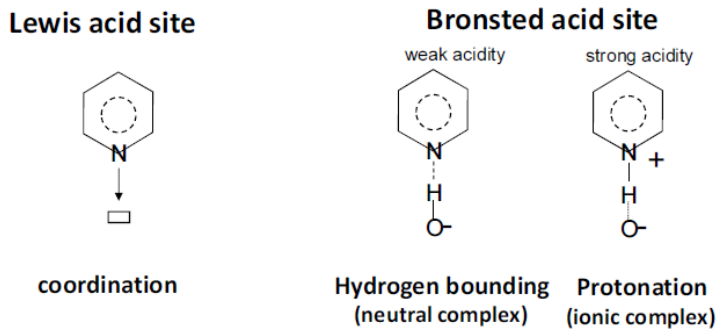

Figure 1-8 Bonds formed between probe (in this example, pyridine) and acid sites

A- FTIR of adsorbed pyridine

Pyridine is the most commonly used probe molecule for the investigation of the properties of acid sites. Pyridine presents the advantages of giving rise to very distinct vibrational bands to distinguish LAS from BAS and allows therefore to determine the concentration of Lewis and Brønsted sites using the absorption coefficients of these two bands.

Adsorption of pyridine is performed by saturation of the sample with pyridine and evacuation at increasing temperature, allowing therefore to also extract information on the strength of the acid sites (the stronger sites corresponding to the higher desorption temperature).

Table 1-2 Typical frequencies (cm^{-1}) for adsorption of pyridine on a solid acid[110]

	ν_{8a} ν(CC)	ν_{8b} ν(CC)	ν_{19a} ν(CN)	ν_{19b} ν(CN)
Gas	1584	1580	1483	1440
H-bond	1595	1580	1490 ww	1445
Lewis	1630–1600	1580 ww	1490 ww	1450
Brønsted	1640	1610	1490	1545

The bands due to the 19b and 8a vibration modes (Table 1-2) are very sensitive to coordination on the nitrogen and are commonly used to identify and quantify the sites of BAS and LAS: wavenumber of υ19a band at about 1450 cm^{-1} is characteristic of LAS while υ19b band at about 1550 cm^{-1} is for BAS. The shift of 8a mode is also sometimes used to measure the strength of LAS (the stronger the LAS, the higher the frequency).[20] Activation temperature changes the nature of the acid sites of ASA, due to dehydroxylation reactions: the higher the temperature of activation, the more LAS and the less BAS.[20]

Table 1-3 Compilation of molar absorption coefficients for pyridine adsorption

ε_{1550} (BAS) cm/μmol^{-1}	ε_{1540} (LAS) cm/μmol	Solid	Ref.
3.03	3.88	NH_4Y (BAS); SiO_2-Al_2O_3 (LAS)	111
0.73	1.11	HY (BAS); Al_2O_3 (LAS)	112
1.67	2.22	Zeolites, SiO_2-Al_2O_3	113
1.24	1.56	SiO_2-ZrO_2	114
0.57	1.50	SiO_2-Al_2O_3	115

Quantification of IR data is a key point that generally requires the measurement of molar absorption coefficients (ε). The values of ε determined by various workers can be very different (see Table 1-3). Possible reasons for this are the presence of physisorbed pyridine or the adsorption of a significant amount of the probe on the cell walls. Moreover, the zeolite structure may influence the dipolar moment of the probe molecule (and hence its absorption coefficient).

Hence, the molar absorption coefficients are considered to be strictly valid for only one given solid.[116] For this reason, the amount of Lewis and Brønsted acid sites determined by this method must be regarded as an approximation. Nevertheless, comparison remains relevant when the results are obtained on samples of similar nature and using the same experimental conditions.

Pyridine desorption temperature can also be used to evaluate the strength of the acid site. For this type of measurement, the amount of residual pyridine on BAS and LAS after desorption at different temperatures (e.g. 150, 250 and 350°C) is measured. The amount of strongest sites is estimated from the amount of adsorbed pyridine after desorption at high temperature. However, as the amount of residual pyridine is evaluated for discrete values of desorption temperature, the accurate evaluation of the amount of strong Brønsted acid sites by this method remains difficult.[117]

B- FTIR of adsorbed CO

Pyridine is, by far, the most common probe for determining the amount of Brønsted and Lewis acid sites by FTIR. However, its basicity is not strong enough to protonate on weakly acidic OH groups, and the estimation of the strength of acid sites using this probe remains difficult. Carbon monoxide is, for these two aspects, a particularly suitable probe. CO is a very weak base, which is not protonated but can perturb the proton by interaction with its carbon atom. Since its interaction with acid sites is very weak, the adsorption must be performed at low temperature (normally obtained by placing the IR cell in a liquid nitrogen bath). Using CO as a probe molecule brings an additional advantage: its small size allows easily access to most of the sites.

The strength of the interaction (and hence the strength of the acid site) will be related to the shift of the ν(CO) and ν(OH) bands. On BAS, the υ(CO) vibration band can shift from ca. 2152 cm^{-1} (very weak BAS such as silanols) up to ≈2180 cm^{-1} (very strong BAS such as those found in low Al zeolites) (see Figure 1-9). On LAS, it can shift from 2230 cm^{-1} for very strong LAS (such as those found in ASA and in zeolites) down to 2200 - 2180 cm^{-1} for weak LAS

(such as those of alumina[118]). 2170 - 2160 cm^{-1} corresponds to even weaker LAS (e.g. Na^+ cations in ion exchange position in zeolite[119]).

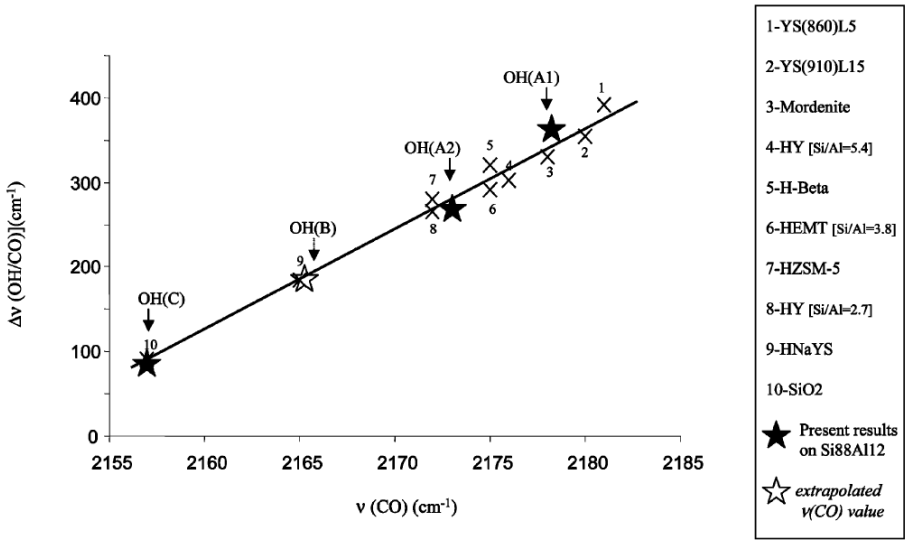

Figure 1-9 Relationship between Δν(OH/CO) and ν(CO) for CO adsorbed on various zeolite and ASA; For ASA(Si88Al12), the υ(OH) before adsorption is taken as the ν(OH) of silanol (3745 cm^{-1})[20].

Although the ν(CO) of LAS and BAS are expected in different frequency range, there is a small overlap of their respective ranges. Thus, discriminating between CO in interaction with LAS from CO in interaction with acidic OH groups is not always straightforward from analysing solely the CO stretching frequency zone. A parallel study of υ(CO) and υ(OH) zone is often necessary to distinguish between CO interaction via coordination or via H bonding. CO in interaction with OH groups of metal oxides or zeolites leads to the formation of a H-bond between CO and the hydroxyl that perturb the υ(OH) band. Hence the original ν(OH) bands disappear upon CO adsorption and are replaced by perturbed bands, ν(OH•••CO). Moreover, the extent of the shift of the υ(OH) band upon perturbation, Δν(OH•••CO), is proportional to the ν(CO) shift but extend over a wider frequency range. This relationship has been established by Cairon et al. using a series of zeolites with different acid strengths.[120] This correlation was later used by Crépeau et al.[20] to conclude that ASA contain very strong BAS (OH(A1) on Figure 1-9, ν(CO) = 2177 cm^{-1}), together with strong BAS (OH(A2) on Figure 1-9 ν(CO) = 2174 cm^{-1}) and that these sites where terminal silanols (ν(OH) ≈ 3747 cm^{-1}, ν(OH•••CO) = 3393 cm^{-1} & ν(OH•••CO) = 3456 cm^{-1}) and correspond to silanols located in

close vicinity to a tetrahedrally coordinated Al, possibly buried beneath the surface Al^{IV} Lewis sites.

Beside the bands of CO adsorbed on acid sites, a band at 2138 cm^{-1} is also often observed at high CO coverage that corresponds to physisorbed CO (as there is no chemical interaction with the surface, the position of this band is similar to that of liquid CO).

Similar to pyridine, CO can, in theory, be used for a quantitative determination of the number of sites based on the molar absorption coefficients of the ν(CO) band on the various sites. However, at variance with pyridine, there are relatively few reports regarding the values of these absorption coefficients. Moreover, many authors assume a common value for these coefficients, independently of the kind of acid site (and of its strength).[5,116]

1.4.2.3 Quantification of Protons

An important advantage of solid-state NMR spectroscopy is the linear relation between the signal intensity and spin concentration for spin $I = 1/2$ nuclei (and also for spin $I > 1/2$ nuclei for non-selective excitation with very short radio frequency pulses). Therefore, ^{1}H SSNMR is a convenient, direct, and non-invasive method to study different hydrogen species and provides information on site concertation, structural defects, dealumination and realumination mechanisms and surface functionalization. Classical quantification methods have their limitation: NH_3-TPD methods may suffer from multiple adsorbates per acid site, extreme sensitivity to subtle changes in the experimental parameters (flow rates, catalyst bed depths, temperature gradients, etc.) and its inability to distinguish between Brønsted and Lewis acid sites; Quantification by infrared methods is limited by the necessity to use molar extinction coefficients for either direct observation of acidic hydroxyl groups or for observation of adsorbates such as pyridine. This is a strong limitation especially when considering that that molar absorption coefficients, should, strictly speaking be considered as valid for only one given solid.

Generally, quantification of the concentration of protons in solid catalysts by ^{1}H NMR spectroscopy is obtained by the comparison of the signal intensities of the sample under study

with the signal intensity of an external standard with similar spectroscopic parameters (especially with a similar amount of proton) or with the signal intensity of an internal standard. A suitable external intensity standard allows application of identical experimental parameters for the samples and for the standard.

Wang et al.[121] reported the first quantification of hydroxyls in zeolite based on ^{1}H MAS NMR spin-counting method. They used poly(dimethylsiloxane) (PDMS) as an internal reference. This approach involves handling and accurately weighing microgram quantities of the sample and the internal standard in a glovebox and reproducibly centring them in the middle region of the rotor to avoid effects of the radio frequency field inhomogeneity. Although it seems an experimentally sound approach, the complicated sample preparation heavily restricts its routine application. In addition, this technique cannot be used when heating of the sample is required because of possible reactions of the internal standard with the material of interest. Later, Kennedy et al.[122] proposed a simplified method for the quantitative determination proton by ^{1}H MAS NMR using octakis(trimethylsiloxy)-silesquioxane, more commonly known as Q8M8, as an external standard to prevent any reaction with the sample under study. However, the necessary confinement of the sample volume to the middle region of the rotor was not mentioned. Marichal group[123] established a protocol for measuring absolute amount of proton in silica through calibration with three external standard (PDMS, HMB, and camphor) and confinement of the sample in the middle region of a 2.5 mm rotor using two specifically designed spacers. They compared the results obtained with this setup and without and observed that the measurement performed without led to underestimation of the proton concentration of 8 to 15%. The proton spin counting results they obtained gave proton concentrations that were consistent with the data obtained from classical thermogravimetric analysis and ^{29}Si MAS NMR.

Though ^{1}H NMR is a direct and quantitative methodology to identify, measure, and monitor these hydrogen species, it is noteworthy that ^{1}H chemical shift range ($\Delta\delta$ ~ 20 ppm) is narrower than other nuclei, such as ^{13}C ($\Delta\delta$ ~ 250 ppm) and ^{31}P ($\Delta\delta$ ~ 650 ppm), causing a relative lower resolution. Another disadvantage of ^{1}H MAS NMR study of acidity is that

detailed structure of acid sites cannot be observed. Therefore, in order to characterize in details the acid sites of solid catalysts, it is necessary to combine ^{1}H NMR with other techniques.

1.5 Model reaction for Brønsted acidity: Isomerization of 33DMB1

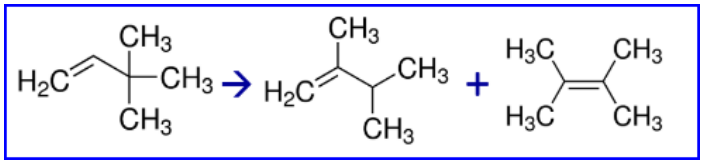

Model reactions constitute an efficient tool not only for checking the suitability of solid acids as catalysts but also for characterizing the surface acidity (type, strength and density). A variety of reactions are available to assess the acidity of the synthesized catalysts, including dehydration, isomerization, and cracking. Ultimately, considering its moderate reaction temperature (ca. 150°C), its sensitivity to mild Brønsted acidity and the fact that no water molecule is produced by this reaction (hence appropriate for a study of the effect of water), 3,3-dimethylbut-1-ene (33DMB1) isomerization was chosen. Typically, the skeletal isomerization of 33DMB1 is a clean reaction, with low deactivation, and which produces only two major products: 2,3-dimerthylbut-2-ene (23DMB2) and 2,3-dimerthylbut-1-ene (23DMB1). Side products such as methylpentenes appear at higher temperatures (over 300^{o}C) with relatively strong acid sites.[124]

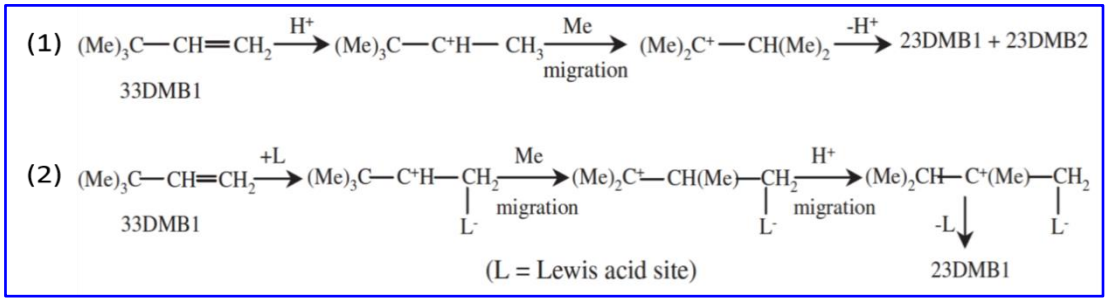

Figure 1-10 33DMB1 isomerization scheme, according to the reference[124]

33DMB1 isomerization proceeds through secondary carbonium ions mechanism. The two potential carbonium ion mechanisms are depicted on Figure 1-10. In mechanism (1) the alkene, after being protonated on the catalyst surface (the proton, coming from either BAS or adsorbed alkene fragments), undergoes methyl migration and then loses a proton to give one of the two products (23DMB1 or 23DMB2). Mechanism (2) involves adsorption of the alkene

onto a Lewis acid site followed by two rearrangements and release of 23DMB1 product. However, the probability that the 33DMB1 isomerization occurs through a pure protonic mechanism is the highest.[124-126] Kemball et al.[124,125,127] focused on the effects of hydrogen, water, and hydrogen sulfide on this reaction and demonstrated that this reaction did not occur on the Lewis acid sites (LAS) of alumina and was not poisoned by water and hydrogen sulfide. Consequently, the reaction rate of 33DMB1 isomerisation can be regarded as a measure of the concentration of BAS. Furthermore, more detailed studies confirmed that 33DMB1 isomerization occurs over the BAS of oxides with strong[128] and medium strength (desorbing pyridine at 220°C) acid sites,[128,129] and that weak acid sites such as surface OH groups were inactive for this reaction.[130]

1.6 Reactivity of aluminosilicates toward water

1.6.1 Role of water on aluminium coordination

Water plays a key role in zeolite dealumination by steaming. In this process, aluminium atoms are removed from the zeolite framework via hydrolysis of Si-O-Al bond by water vapour. Hence, the high reactivity of aluminosilicates and more specifically zeolites toward water is undeniable. In this chapter, we will not focus on this aspect of the interaction of water with aluminium atoms, but rather on the reversible modification of the coordination of the aluminium atoms in presence of water.

Van Bokhoven et al.[63] observed, using XANES (X-ray absorption near edge spectroscopy), that part of the aluminium atoms in two zeolites (H-beta and H-Y) have a flexible coordination depending on the presence of water: all Al atoms are in Al^{IV} coordination in vacuum up to 452°C. However, in presence of water, even at room temperature, part of Al^{IV} is converted to Al^{VI}. These Al^{VI} revert to Al^{IV} in absence of water (inert gas atmosphere) when temperature is 102°C or higher. Based on these observation, they concluded that part of the framework aluminium have a flexible Al coordination. As mentioned previously, there are other evidences for the flexible coordination of some of the Al atoms in zeolites and ASA using NH_3 instead of water as adsorbate, but the authors came to a different conclusion, which was

that Al with flexible coordination, both in ASA and zeolites, belong to an amorphous silica-alumina phase.[25]

Beside Al^{IV} and Al^{VI}, pentacoordinated Al^{V} are also present in ASA. As mentioned above, De Witte et al.[67] observed that the proportion of this phase increases upon dehydration of the sample and upon calcination (for ^{27}Al NMR spectra recorded on hydrated samples). Wang et al.[68] investigated the evolution of the coordination of the Al atoms upon hydration for an ASA prepared by flame spray pyrolysis. They observed that, at low Al loading, all the Al^{V} disappeared in presence of water and were transferred mostly to Al^{VI}. At higher Al loading, the disappearance of Al^{V} is only partial. They concluded that Al^{V} is fully accessible at low Al loading (and hence could play a role in the reactivity of ASA), whereas, at higher Al loading, part of Al^{V} is buried in the bulk of the material.

The modification of the local environment of Al upon dehydration is not limited to a decrease of its coordination: it is also accompanied by a decrease in the local symmetry around the Al and responsible for the considerable broadening of all peaks of the ^{27}Al NMR spectra and associated, at least in zeolites, to the formation of the Si-OH-Al bridges.

Beside simple water desorption, a reactive water desorption can also occur by elimination of a water molecule from two hydroxyls groups. This dehydroxylation reaction usually occurs during high temperature thermal treatment, especially if this treatment is performed under vacuum. In ASA, a modification of the nature of the acid sites upon high temperature dehydroxylation was evidenced by Kondo et al.[131] and Blanchard et al.[132], who observed using FTIR of adsorbed probe molecules (CO and/or pyridine) an increase of the fraction of the Lewis sites at the expense of the Brønsted sites.

1.6.2 Role of water to acidity and reactivity

The first experimental proof of the conversion of Lewis sites of ASA in Brønsted sites upon adsorption of water was reported in 1964 by Basila and co-workers.[133] They observed, using FTIR, that, when H_2O is added to an ASA sample where NH_3 or pyridine had been preadsorbed, the bands characteristic to NH_3 (or pyridine) adsorbed on the Lewis sites almost

disappear and the band corresponding to NH_3 (or pyridine) adsorbed on the Brønsted sites increases. They also observed that a simple treatment under vacuum was able to reverse the spectra to the initial form, indicating that the adsorption of water on the Lewis sites is weak in presence of NH_3 (or pyridine). The generation of BAS by adsorption of water molecules on undercoordinated aluminium, was again proposed by Lercher team[65] and Garrone group[134] based on FTIR of adsorbed CO and theoretical calculations, respectively. They concluded that H_2O adsorbed on Lewis sites is responsible for a new Brønsted acidity, with a strength similar to Si-OH-Al bridges in zeolites.

The possibility that the Brønsted sites formed by adsorption of water adsorbed on Lewis, contribute to the catalytic activities of ASA has always been envisaged. For example, Guisnet, in his article[129] about model reactions for the characterization of the acidity of solids, proposes to discard the reactions that produce water (such as alcohol dehydration reactions) for the characterisation of the Brønsted acidity of solids, due to the possible transformation of Lewis sites in Brønsted sites by adsorption of water. Even so, after activation under gas flow, one cannot exclude that the few ppm of water from the gas flow (for example, the specification for the amount of H_2O in N_2 U (Air Liquide) is: $H_2O \leq 5$ ppm), could contribute to the transformation of some of the Lewis sites into Brønsted sites. However, they are, only very few reports on the impact of water on the acidic activity of aluminosilicates and they seem controversial. In 1999, Panov et al.[135] observed that addition of water to the feed result in a loss of activity in the reaction of aldol condensation (condensation of two acetones molecules to form mesityl oxide, catalysed by Lewis sites, $T_{reaction} = 105°C$) on zeolites and concluded that water acts as a poison to the Lewis sites of zeolites. In 2004, Corma et al.[136] examined the impact of water on the kinetic of *n*-hexadecane hydrocracking at 400°C and observed no impact of the presence of water in the feed on the catalytic activity. More recently, Kim et al.[6] studied the influence of the addition of water on the selectivity of the reaction of dehydration of glycerol (selectivity toward acrolein catalysed by Brønsted acid sites, or toward 1-hydroxyacetone catalysed by Lewis acid sites) at 315°C on silica-aluminas. They observed that for molar ratio water/glycerol in the range 2–11, the conversion of glycerol was almost

unchanged but selectivity to acrolein increases (up to a factor of ca. 5) with the water content of the feed. In 2014, Xu et al.[137] studied the effect of water addition during alkylation of phenol either with propylene or with isopropanol (via its initial dehydration into propylene over acid sites) on HBEA zeolites. They observed a much higher conversion of phenol, not only when isopropanol was used as reactant but also when water was co-fed with propylene. Hence they concluded that water, either co-fed or generated *in situ* by the reaction of dehydration of propanol has a positive impact on the catalytic activity. Based on the characterisation of the acidic properties of the zeolite, they concluded that part of the Lewis sites was converted to Brønsted sites by adsorption of water molecules and that these new Brønsted sites participated to the activity. It is highly probable that the possibility of an impact of water adsorbed on Lewis site on the Brønsted catalytic activity strongly depends on the experimental conditions such as the temperature of reaction and the partial pressure of water: at a too high partial pressure, water may become a poison of the reaction either by competing with the reactant molecule for the Brønsted acid sites or by intervening in any other step of the reaction (e.g. by stabilising adsorbed intermediate[138]), and, at a too high temperature, water will desorb from the Lewis acid sites and hence have no or little influence on the activity. One must also mention that, although there are several reports of the positive impact of water on Brønsted acidity (and negative impact of water on the Lewis acidity), the role of water adsorbed on Lewis sites remains controversial as testified by the very recent publication of Busca and coworkers[139] and water is still often seen as a poison in zeolite catalysis, as discussed in a recent review.[140]

1.7 Objective and scope of this work

Zeolites and amorphous silica alumina are widely used as solid acid catalysts in the chemical industry. As we all known, in a perfect zeolite, a ratio of one BAS per Al is theoretical expected and values relatively close to the theoretical ones can be indeed observed.[141] In ASA, the majority of the Al is useless for acidity and inaccessible for catalysis. The proportion of acid sites on ASA per Al is generally significantly smaller than 1 and many of these sites are LAS. For this reason, ASA display rather low overall acidities and poor effective acidities (i.e. a low percentage of Al atoms contribute to the acidic properties), hereby lowering the potential

of catalytic applications of these materials.

The nature and detailed structure of BAS and LAS remain ambiguous and debatable issues mainly owing to lack of direct experimental evidence. Recent developments in solid state NMR could make possible the direct observation of these sites. Advanced SSNMR is the ideal tool for the investigation of the spatial proximity and connectivity between proton, aluminium and silicon and cold therefore provide direct experimental evidence for the structure of BAS and LAS. However, the large fraction of the Al atoms which are silent in terms of acidity in ASA heavily perturb the interpretation of NMR results.

Can the ratio of acid sites per Al be increased? Can the proportion of BAS to LAS been increased as well? Can we come to a strategy for development of materials combining the high acidity strength and high density of acid sites of zeolites with the open porosity of ASA?

This work is devoted to addresses these questions. More specifically, experiments will be dedicated to:

(1) synthesizing a series of ASA materials with improved acidity and higher percentage of acidic Al by a as controlled as possible method in order to facilitates their characterization by spectroscopic tools.

(2) learning more about the genesis of BAS and LAS in ASAs and their strength in order to establish structure−activity relationships and to design advanced materials with improved acidic properties.

The overall arrangement of this thesis is as follows:

This first chapter devoted to background information on the synthesis of amorphous silica-alumina and on their acidic properties and their characterization, Chapter 2 will describe the materials and experimental characterization methods that have been used in this thesis; Chapter 3 will introduce dealumination of amorphous silica alumina by acetylacetone and its influence on acidity and activity; Chapter 4 will investigate the preparation and characterization of ASA of enhanced acidity through citric acid treatment; Chapter 5 will be dedicated to the characterisation of ASA (selected among samples from Chapter 4) by advanced NMR

sequences; Chapter 6 will report on the preparation, characterization and comparison of ASAs by grafting various Al precursors on silica. This thesis will finally end up with conclusions and perspectives.

Reference

(1) Primo, A.; Garcia, H. *Chemical Society Reviews* **2014**, *43*, 7548.

(2) Weitkamp, J.; Puppe, L. *Catalysis and zeolites: fundamentals and applications*; Springer Science & Business Media, **2013**.

(3) Baerlocher, C.; Olson, D.; Meier, W. *Atlas of Zeolite Framework Types (formerly: Atlas of Zeolite Structure Types)*; Elsevier, **2001**.

(4) Busca, G. *Chemical reviews* **2007**, *107*, 5366.

(5) Hensen, E. J.; Poduval, D. G.; Degirmenci, V.; Ligthart, D. J. M.; Chen, W.; Maugé, F. o.; Rigutto, M. S.; Veen, J. R. v. *The Journal of Physical Chemistry C* **2012**, *116*, 21416.

(6) Kim, Y. T.; Jung, K.-D.; Park, E. D. *Applied Catalysis B: Environmental* **2011**, *107*, 177.

(7) Hahn, M. W.; Copeland, J. R.; Van Pelt, A. H.; Sievers, C. *ChemSusChem* **2013**, *6*, 2304.

(8) Acids, I. S. *Chemical Reviews (Washington, DC)* **1995**, *95*, 559.

(9) Bhan, A.; Iglesia, E. *Accounts of chemical research* **2008**, *41*, 559.

(10) Hafner, J.; Benco, L.; Bučko, T. *Topics in Catalysis* **2006**, *37*, 41.

(11) Van Santen, R.; Kramer, G. *Chemical Reviews* **1995**, *95*, 637.

(12) Sohn, J. R.; DeCanio, S. J.; Fritz, P. O.; Lunsford, J. H. *The Journal of Physical Chemistry* **1986**, *90*, 4847.

(13) Li, S.; Zheng, A.; Su, Y.; Zhang, H.; Chen, L.; Yang, J.; Ye, C.; Deng, F. *Journal of the American Chemical Society* **2007**, *129*, 11161.

(14) Yu, Z.; Li, S.; Wang, Q.; Zheng, A.; Jun, X.; Chen, L.; Deng, F. *The Journal of Physical Chemistry C* **2011**, *115*, 22320.

(15) Zhiwu, Y.; Qiang, W.; Lei, C.; Feng, D. *Chinese Journal of Catalysis* **2012**, *33*, 129.

(16) Huang, J.; Jiang, Y.; Marthala, V. R.; Bressel, A.; Frey, J.; Hunger, M. *Journal of Catalysis* **2009**, *263*, 277.

(17) Caillot, M.; Chaumonnot, A.; Digne, M.; Bokhoven, J. A. V. *ChemCatChem* **2013**, *5*, 3644.

(18) Caillot, M.; Chaumonnot, A.; Digne, M.; Van Bokhoven, J. A. *Journal of Catalysis* **2014**, *316*, 47.

(19) Chizallet, C.; Raybaud, P. *Angewandte Chemie International Edition* **2009**, *48*, 2891.

(20) Crépeau, G.; Montouillout, V.; Vimont, A.; Mariey, L.; Cseri, T.; Maugé, F. *The Journal of Physical Chemistry B* **2006**, *110*, 15172.

(21) Heeribout, L.; Vincent, R.; Batamack, P.; Dorémieux-Morin, C.; Fraissard, J. *Catalysis letters* **1998**, *53*, 23.

(22) Hensen, E.; Poduval, D.; Magusin, P.; Coumans, A.; Van Veen, J. *Journal of Catalysis* **2010**, *269*, 201.

(23) Hunger, M.; Freude, D.; Pfeifer, H.; Bremer, H.; Jank, M.; Wendlandt, K. *Chemical physics letters* **1983**, *100*, 29.

(24) Leydier, F.; Chizallet, C.; Chaumonnot, A.; Digne, M.; Soyer, E.; Quoineaud, A.-A.; Costa, D.; Raybaud, P. *Journal of Catalysis* **2011**, *284*, 215.

(25) Omegna, A.; van Bokhoven, J. A.; Prins, R. *The Journal of Physical Chemistry B* **2003**, *107*, 8854.

(26) Poduval, D. G.; Van Veen, J. R.; Rigutto, M. S.; Hensen, E. J. *Chemical Communications* **2010**, *46*, 3466.

(27) Xu, B.; Sievers, C.; Lercher, J. A.; van Veen, J. R.; Giltay, P.; Prins, R.; van Bokhoven, J. A. *The Journal of Physical Chemistry C* **2007**, *111*, 12075.

(28) Trombetta, M.; Busca, G.; Lenarda, M.; Storaro, L.; Pavan, M. *Applied Catalysis A: General* **1999**, *182*, 225.

(29) Thomas, C. L. *Industrial & Engineering Chemistry* **1949**, *41*, 2564.

(30) Góra-Marek, K.; Derewiński, M.; Sarv, P.; Datka, J. *Catalysis today* **2005**, *101*, 131.

(31) Bevilacqua, M.; Montanari, T.; Finocchio, E.; Busca, G. *Catalysis today* **2006**, *116*, 132.

(32) Larmier, K.; Chizallet, C.; Maury, S.; Cadran, N.; Abboud, J.; Lamic‐Humblot, A. F.; Marceau, E.; Lauron‐Pernot, H. *Angewandte Chemie* **2017**, *129*, 236.

(33) Huang, J.; van Vegten, N.; Jiang, Y.; Hunger, M.; Baiker, A. *Angewandte Chemie International Edition* **2010**, *49*, 7776.

(34) Kunkeler, P. J.; Zuurdeeg, B. J.; van der Waal, J. C.; van Bokhoven, J. A.; Koningsberger, D. C.; van Bekkum, H. *Journal of Catalysis* **1998**, *180*, 234.

(35) Corma, A.; García, H. *Chemical Reviews* **2002**, *102*, 3837.

(36) Almutairi, S. M.; Mezari, B.; Filonenko, G. A.; Magusin, P. C.; Rigutto, M. S.; Pidko, E. A.; Hensen, E. J. *ChemCatChem* **2013**, *5*, 452.

(37) Wang, Z.; Wang, L.; Jiang, Y.; Hunger, M.; Huang, J. *ACS Catalysis* **2014**, *4*, 1144.

(38) Perez-Beltran, S.; Balbuena, P. B.; Ramírez-Caballero, G. E. *The Journal of Physical Chemistry C* **2016**, *120*, 18105.

(39) Benco, L.; Demuth, T.; Hafner, J.; Hutschka, F.; Toulhoat, H. *Journal of Catalysis* **2002**, *209*, 480.

(40) Bhering, D. L.; Ramírez-Solís, A.; Mota, C. J. A. *The Journal of Physical Chemistry B* **2003**, *107*, 4342.

(41) van Bokhoven, J. A.; Van der Eerden, A. M.; Koningsberger, D. C. *Journal of the American Chemical Society* **2003**, *125*, 7435.

(42) Remy, M. J.; Genet, M. J.; Poncelet, G.; Lardinois, P. F.; Notte, P. P. *The Journal of Physical Chemistry* **1992**, *96*, 2614.

(43) Busco, C.; Bolis, V.; Ugliengo, P. *The Journal of Physical Chemistry C* **2007**, *111*, 5561.

(44) Gonzales, N. O.; Bell, A. T.; Chakraborty, A. K. *The Journal of Physical Chemistry B* **1997**, *101*, 10058.

(45) Elanany, M.; Koyama, M.; Kubo, M.; Broclawik, E.; Miyamoto, A. *Applied Surface Science* **2005**, *246*, 96.

(46) Chen, T.; Men, A.; Sun, P.; Zhou, J.; Yuan, Z.; Guo, Z.; Wang, J.; Ding, D.; Li, H. *Catalysis Today* **1996**, *30*, 189.

(47) Parker, W. O. N.; Wegner, S. *Microporous and Mesoporous Materials* **2012**, *158*, 235.

(48) Lemaire, A.; Su, B.-L. *Langmuir* **2010**, *26*, 17603.

(49) Sheng, Y.; Zeng, H. C. *ACS applied materials & interfaces* **2015**, *7*, 13578.

(50) Caillot, M.; Chaumonnot, A.; Digne, M.; Poleunis, C.; Debecker, D. P.; van Bokhoven, J. A. *Microporous and Mesoporous Materials* **2014**, *185*, 179.

(51) Anwander, R.; Gerstberger, G.; Palm, C.; Groeger, O.; Engelhardt, G. *Chem. Commun.* **1998**, 1811.

(52) Caillot, M.; Chaumonnot, A.; Digne, M.; Van Bokhoven, J. A. *ChemCatChem* **2014**, *6*, 832.

(53) Kerber, R. N.; Kerber, T.; Rozanska, X.; Delbecq, F.; Sautet, P. *Physical Chemistry Chemical Physics* **2015**, *17*, 26937.

(54) Kerber, R. N.; Kermagoret, A.; Callens, E.; Florian, P.; Massiot, D.; Lesage, A.; Copéret, C.; Delbecq, F.; Rozanska, X.; Sautet, P. *Journal of the American Chemical Society* **2012**, *134*, 6767.

(55) Mokaya, R. *Chemical Communications* **1997**, 2185.

(56) Mokaya, R. *Angewandte Chemie International Edition* **1999**, *38*, 2930.

(57) Valla, M.; Rossini, A. J.; Caillot, M.; Chizallet, C.; Raybaud, P.; Digne, M.; Chaumonnot, A.; Lesage, A.; Emsley, L.; Van Bokhoven, J. A.; Christophe, C. *Journal of the American Chemical Society* **2015**, *137*, 10710.

(58) Koller, H.; Engelhardt, G.; Kentgens, A. P.; Sauer, J. *The Journal of Physical Chemistry* **1994**, *98*, 1544.

(59) Jiao, J.; Kanellopoulos, J.; Behera, B.; Jiang, Y.; Huang, J.; Reddy Marthala, V.; Ray, S. S.; Wang, W.; Hunger, M. *The Journal of Physical Chemistry B* **2006**, *110*, 13812.

(60) Zhao, Z.; Xu, S.; Hu, M. Y.; Bao, X.; Peden, C. H.; Hu, J. *The Journal of Physical Chemistry C* **2014**, *119*, 1410.

(61) Koller, H.; Meijer, E. L.; van Santen, R. A. *Solid state nuclear magnetic resonance* **1997**, *9*, 165.

(62) MacKenzie, K.; Temuujin, J.; Smith, M.; Angerer, P.; Kameshima, Y. *Thermochimica acta* **2000**, *359*, 87.

(63) Van Bokhoven, J.; van der Eerden, A.; Koningsberger, D. *Studies in Surface Science and Catalysis*

2002, *142*, 1885.

(64) Wouters, B.; Chen, T.-H.; Grobet, P. *Journal of the American Chemical Society* **1998**, *120*, 11419.

(65) Williams, M.; Fonfé, B.; Sievers, C.; Abraham, A.; Van Bokhoven, J.; Jentys, A.; Van Veen, J.; Lercher, J. *Journal of Catalysis* **2007**, *251*, 485.

(66) Barrow, B. N. S.; Scullard, A.; Collis, N. *Johnson Matthey Technology Review* **2016**, *60*, 90.

(67) De Witte, B.; Grobet, P.; Uytterhoeven, J. *The Journal of Physical Chemistry* **1995**, *99*, 6961.

(68) Wang, Z.; Jiang, Y.; Yi, X.; Zhou, C.; Rawal, A.; Hook, J.; Liu, Z.; Deng, F.; Zheng, A.; Baiker, A. *arXiv preprint arXiv:1604.04839* **2016**.

(69) Wang, Z.; Jiang, Y.; Lafon, O.; Trébosc, J.; Kim, K. D.; Stampfl, C.; Baiker, A.; Amoureux, J.-P.; Huang, J. *Nature Communications* **2016**, *7*.

(70) Medek, A.; Harwood, J. S.; Frydman, L. *Journal of the American Chemical Society* **1995**, *117*, 12779.

(71) Kentgens, A. P.; Iuga, D.; Kalwei, M.; Koller, H. *Journal of the American Chemical Society* **2001**, *123*, 2925.

(72) Hajjar, R.; Millot, Y.; Man, P. P. *Comptes Rendus Chimie* **2008**, *11*, 380.

(73) Brus, J.; Kobera, L.; Schoefberger, W.; Urbanová, M.; Klein, P.; Sazama, P.; Tabor, E.; Sklenak, S.; Fishchuk, A. V.; Dědeček, J. *Angewandte Chemie International Edition* **2015**, *54*, 541.

(74) Jiao, J.; Kanellopoulos, J.; Wang, W.; Ray, S. S.; Foerster, H.; Freude, D.; Hunger, M. *Physical Chemistry Chemical Physics* **2005**, *7*, 3221.

(75) Munakata, H.; Koyama, T.-r.; Yashima, T.; Asakawa, N.; O-Nuki, T.; Motokura, K.; Miyaji, A.; Baba, T. *The Journal of Physical Chemistry C* **2012**, *116*, 14551.

(76) Brunet, F.; Charpentier, T.; Le Caer, S.; Renault, J.-P. *Solid state nuclear magnetic resonance* **2008**, *33*, 1.

(77) Yesinowski, J. P.; Eckert, H.; Rossman, G. R. *Journal of the American Chemical Society* **1988**, *110*, 1367.

(78) Hunger, M. In *Zeolites and Catalysis*; Wiley-VCH Verlag GmbH & Co. KGaA: **2010**, 493.

(79) Gil, B.; Zones, S. I.; Hwang, S.-J.; Bejblová, M.; Cejka, J. *The Journal of Physical Chemistry C* **2008**, *112*, 2997.

(80) Koller, H.; Lobo, R. F.; Burkett, S. L.; Davis, M. E. *The Journal of Physical Chemistry* **1995**, *99*, 12588.

(81) Huo, H.; Peng, L.; Grey, C. P. *The Journal of Physical Chemistry C* **2009**, *113*, 8211.

(82) Hunger, M.; Schenk, U.; Breuninger, M.; Gläser, R.; Weitkamp, J. *Microporous and mesoporous materials* **1999**, *27*, 261.

(83) Kasai, P. H.; Jones, P. M. *Journal of molecular catalysis* **1984**, *27*, 81.

(84) Huang, J.; Jiang, Y.; Marthala, V. R.; Thomas, B.; Romanova, E.; Hunger, M. *The Journal of*

Physical Chemistry C **2008**, *112*, 3811.

(85) Hunger, M.; Freude, D.; Pfeifer, H. *Catalysis Today* **1988**, *3*, 507.

(86) Hunger, M. *Solid state nuclear magnetic resonance* **1996**, *6*, 1.

(87) Müller, M.; Harvey, G.; Prins, R. *Microporous and mesoporous materials* **2000**, *34*, 281.

(88) Collart, O.; Cool, P.; Van Der Voort, P.; Meynen, V.; Vansant, E. F.; Houthoofd, K.; Grobet, P. J.; Lebedev, O. I.; Van Tendeloo, G. *The Journal of Physical Chemistry B* **2004**, *108*, 13905.

(89) Pfeifer, H.; Freude, D.; Hunger, M. *Zeolites* **1985**, *5*, 274.

(90) Delgado, M.; Delbecq, F. o.; Santini, C. C.; Lefebvre, F.; Norsic, S.; Putaj, P.; Sautet, P.; Basset, J.-M. *The Journal of Physical Chemistry C* **2011**, *116*, 834.

(91) Pfeifer, H. *Journal of the Chemical Society, Faraday Transactions 1: Physical Chemistry in Condensed Phases* **1988**, *84*, 3777.

(92) Brunner, E.; Karge, H.; Pfeifer, H. *Zeitschrift für Physikalische Chemie* **1992**, *176*, 173.

(93) Janin, A.; Maache, M.; Lavalley, J.; Joly, J.; Raatz, F.; Szydlowski, N. *Zeolites* **1991**, *11*, 391.

(94) Ichihashi, H.; Kitamura, M. *Catalysis today* **2002**, *73*, 23.

(95) Heitmann, G.; Dahlhoff, G.; Hölderich, W. *Journal of Catalysis* **1999**, *186*, 12.

(96) Chu, C. T.; Chang, C. D. *The Journal of Physical Chemistry* **1985**, *89*, 1569.

(97) Kiricsi, I.; Flego, C.; Pazzuconi, G.; Parker, W. J.; Millini, R.; Perego, C.; Bellussi, G. *The Journal of Physical Chemistry* **1994**, *98*, 4627.

(98) Zecchina, A.; Bordiga, S.; Spoto, G.; Marchese, L.; Petrini, G.; Leofanti, G.; Padovan, M. *The Journal of Physical Chemistry* **1992**, *96*, 4991.

(99) Halasz, I.; Senderov, E.; Olson, D. H.; Liang, J.-J. *The Journal of Physical Chemistry C* **2015**, *119*, 8619.

(100) Caillot, M.; Chaumonnot, A.; Digne, M.; Van Bokhoven, J. A. *ChemCatChem* **2014**, *6*, 2976.

(101) Webster, C. E.; Drago, R. S.; Zerner, M. C. *Journal of the American Chemical Society* **1998**, *120*, 5509.

(102) Rodríguez-González, L.; Hermes, F.; Bertmer, M.; Rodríguez-Castellón, E.; Jiménez-López, A.; Simon, U. *Applied Catalysis A: General* **2007**, *328*, 174.

(103) Barrie, P. J. *Physical Chemistry Chemical Physics* **2008**, *10*, 1688.

(104) Katada, N.; Igi, H.; Kim, J.-H.; Niwa, M. *The Journal of Physical Chemistry B* **1997**, *101*, 5969.

(105) Lónyi, F.; Valyon, J. *Microporous and Mesoporous Materials* **2001**, *47*, 293.

(106) Hidalgo, C. V.; Itoh, H.; Hattori, T.; Niwa, M.; Murakami, Y. *Journal of Catalysis* **1984**, *85*, 362.

(107) Woolery, G.; Kuehl, G.; Timken, H.; Chester, A.; Vartuli, J. *Zeolites* **1997**, *19*, 288.

(108) Niwa, M.; Sota, S.; Katada, N. *Catalysis today* **2012**, *185*, 17.

(109) Karge, H. G.; Dondur, V. *Journal of Physical Chemistry* **1990**, *94*, 765.

(110) Che, M.; Védrine, J. C. *Characterization of solid materials and heterogeneous catalysts: From structure to surface reactivity*; John Wiley & Sons, 2012.

(111) Hughes, T. R.; White, H. M. *The Journal of Physical Chemistry* **1967**, *71*, 2192.

(112) Datka, J.; Turek, A.; Jehng, J.; Wachs, I. *Journal of Catalysis* **1992**, *135*, 186.

(113) Emeis, C. *Journal of Catalysis* **1993**, *141*, 347.

(114) Rosenberg, D. J.; Anderson, J. A. *Catalysis letters* **2002**, *83*, 59.

(115) Pieta, I.; Ishaq, M.; Wells, R.; Anderson, J. *Applied Catalysis A: General* **2010**, *390*, 127.

(116) Thibault-Starzyk, F.; Maugé, F. In *Characterization of Solid Materials and Heterogeneous Catalysts*; Wiley-VCH Verlag GmbH & Co. KGaA: 2012, p 1.

(117) Hensen, E. J.; Poduval, D. G.; Ligthart, D. M.; van Veen, J. R.; Rigutto, M. S. *The Journal of Physical Chemistry C* **2010**, *114*, 8363.

(118) Daniell, W.; Schubert, U.; Glöckler, R.; Meyer, A.; Noweck, K.; Knözinger, H. *Applied Catalysis A: General* **2000**, *196*, 247.

(119) Cairon, O. *Physical Chemistry Chemical Physics* **2010**, *12*, 6333.

(120) Cairon, O.; Lavalley, J.-C. *Journal of the Chemical Society, Faraday Transactions* **1998**, *94*, 3039.

(121) Wang, X.; Coleman, J.; Jia, X.; White, J. L. *The Journal of Physical Chemistry B* **2002**, *106*, 4941.

(122) Kennedy, G. J.; Afeworki, M.; Calabro, D. C.; Chase, C. E.; Smiley, R. J. *Applied spectroscopy* **2004**, *58*, 698.

(123) Hartmeyer, G.; Marichal, C.; Lebeau, B.; Rigolet, S.; Caullet, P.; Hernandez, J. *The Journal of Physical Chemistry C* **2007**, *111*, 9066.

(124) Irvine, E.; John, C.; Kemball, C.; Pearman, A.; Day, M.; Sampson, R. *Journal of Catalysis* **1980**, *61*, 326.

(125) John, C. S.; Kemball, C.; Rajadhyaksha, R. A. *Journal of Catalysis* **1979**, *57*, 264.

(126) Bautista, F.; Campelo, J.; Garcia, A.; Luna, D.; Marinas, J.; Romero, A.; Urbano, M. *Reaction Kinetics and Catalysis Letters* **1998**, *64*, 41.

(127) Kemball, C.; Leach, H.; Skundric, B.; Taylor, K. *Journal of Catalysis* **1972**, *27*, 416.

(128) Martin, D.; Duprez, D. *Journal of Molecular Catalysis A: Chemical* **1997**, *118*, 113.

(129) Guisnet, M. R. *Accounts of chemical research* **1990**, *23*, 392.

(130) Gáti, G.; Halász, I. *Journal of Catalysis* **1983**, *82*, 223.

(131) Kondo, J. N.; Nishitani, R.; Yoda, E.; Yokoi, T.; Tatsumi, T.; Domen, K. *Physical Chemistry Chemical Physics* **2010**, *12*, 11576.

(132) Blanchard, J.; Krafft, J.-M.; Dupont, C.; Sayag, C.; Takahashi, T.; Yasuda, H. *Catalysis Today* **2014**, *226*, 89.

(133) Basila, M. R.; Kantner, T. R.; Rhee, K. H. *The Journal of Physical Chemistry* **1964**, *68*, 3197.

(134) Garrone, E.; Onida, B.; Bonelli, B.; Busco, C.; Ugliengo, P. *The Journal of Physical Chemistry B* **2006**, *110*, 19087.

(135) Panov, A.; Fripiat, J. *Catalysis letters* **1999**, *57*, 25.

(136) Corma, A.; Marie, O.; Ortega, F. *Journal of Catalysis* **2004**, *222*, 338.

(137) Xu, W.; Miller, S. J.; Agrawal, P. K.; Jones, C. W. *Catalysis letters* **2014**, *144*, 434.

(138) Zhi, Y.; Shi, H.; Mu, L.; Liu, Y.; Mei, D.; Camaioni, D. M.; Lercher, J. A. *Journal of the American Chemical Society* **2015**, *137*, 15781.

(139) Escribano, V. S.; Garbarino, G.; Finocchio, E. *Topics in Catalysis* **2017**, 1.

(140) Okuhara, T. *Chemical Reviews* **2002**, *102*, 3641.

(141) Thibault-Starzyk, F.; Stan, I.; Abelló, S.; Bonilla, A.; Thomas, K.; Fernandez, C.; Gilson, J.-P.; Pérez-Ramírez, J. *Journal of Catalysis* **2009**, *264*, 11.

Chapter 2. Experimental and Characterization

2.1 Materials

2.1.1 Commercial ASA

Two commercial ASA in their ammonium form produced by Grace-Davison were used as starting materials, containing 13 wt% (named GD13) and 25 wt% Al_2O_3 (named GD25). The ammonium forms were converted to the H-forms by an activation procedure made by calcining, in a muffle furnace, the ASA at 550°C for 5 h at a heating rate of 2°C/min. Calcined samples are referred to as GD13-H, GD25-H, respectively.

2.1.2 Commercial silica gel

Three high purity silica gel were used as support for the grafting of aluminium precursors:

- Davisil Grade 12, supplier: Sigma-Aldrich; pore size 22 Å, particle size 28-200 mesh particle size, denoted S2;
- High-purity grade 10180, supplier: Sigma-Aldrich; pore size 40 Å, 70-230 mesh particle size, named as S4.
- Davisil Grade 633, supplier: Sigma-Aldrich; pore size 60 Å, 200-425 mesh particle size, noted as S6.

Table 2-1 Textural properties and silanols density of the commercial silicas

Sample	S_{BET}	Pore Size	Pore Volume	n_{OH}	c_{OH}
	m^2/g	nm	cm^3/g	mmol/g	$\mu mol/m^2$
S2	574	3.3	0.06	6.17	10.74
S4	526	3.7	0.57	4.36	8.29
S6	477	4.8	0.90	4.30	9.13
S7	381	7.1	0.65	4.44	12.54

For sample S4, attempts were made at increasing the density of silanols by treatment of 5 g S4 in 50 ml of boiling water under reflux during 4 h. This sample is noted S7. The textural properties (N_2 sorption) and silanols density (based on mass -n_{OH} in mmol/g- or on m^2 –c_{OH} in $\mu mol/m^2$) of these silicas are reported in Table 2-1.

2.1.3 Preparation of high surface area silica

Silica gel with high surface was prepared according to a procedure adapted from the reference[1]: 5.8 ml distilled water was added dropwise, under stirring to 18 ml of TEOS diluted in 55 ml 2-propanol (i-PrOH). The reaction mixture was acidified with a given amount of HCl and its pH was measured (without correction for a nonaqueous medium). The acidic sol was placed in a sealed container, heated at 60°C under stirring (at 140 rpm) for 60 min. A given amount of ammoniac (37% in water) was subsequently added, and the resulting homogeneous sol was left to gel, with no further stirring. Following this general procedure, two sets of alcogels were prepared with molar compositions TEOS /H_2O /i-PrOH = 1 /4 /9.2 and HCl /TEOS = x (x = 0.005, 0.009) and NH_3 /HCl = 1. They are identified as HYD1000x (where x stands for the HCl /TEOS molar ratio). To strengthen the silica network, the alcogels were aged for 48 h at 60°C. This aging was first performed (during 24 hours) in the residual liquid. After that the gel was transferred in an aging solution containing TEOS, i-PrOH, and H_2O in the same proportions as used for gelation (5.8 ml distilled water + 18 ml of TEOS + 55 ml i-PrOH) for another 24 h period. After that, the gel was smashed to small particles and exchanged 3 times with 20 ml i-PrOH (in order to completely remove any residual water or TEOS). The washed gels were dried at 60°C under atmospheric pressure, partially covered, until the weight loss became negligible. The silica-gels were characterized and used without further calcination. Based on this procedure two silica gels with high surface area and either large or narrow mesopores are obtained (textural properties and silanols density of these two silica are summarised in Table 2-2).

Table 2-2 Textural properties and silanols density of high surface silicas

Sample	S_{BET} m^2/g	Pore Size Nm	Pore Volume cm^3/g	n_{OH} mmol/g	c_{OH} $\mu mol/m^2$
$S4_h$ (HYD7)	1022	3.7	0.77	13.4	13.1
S9 (HYD5)	1559	9.2	2.60	10.6	6.8

2.2 Characterization

The ASA samples prepared or modified in the present study were extensively

characterized using classical (N_2 sorption, XRF, TGA, NH_3-TPD…) as well as advanced techniques (FTIR of probe molecules, high resolution solid state nuclear magnetic resonance (SSNMR)), in order to investigate their acidic properties in relation with their textural properties and their synthesis protocols.

2.2.1 XRF

X-ray fluorescence (XRF) was employed to determine the elemental composition, which is expressed in weight% of Si and Al in the calcined samples. Calcined samples were directly filled in the tray for measurement at room temperature under He flow at rate of 80 L/h on a XEPOS spectrometer (SPECTRO, AMETEK).

2.2.2 XRD

X-ray diffractograms was obtained on a diffractometer (D8 advanced from Bruker Company) operating with Cu Kα radiation (1.5418 Å; 40 kV and 30 mA) with a Ni filter over the scattering angle of 2θ from 10° to 80° with a step size of 0.02°.

2.2.3 TGA

Thermogravimetric analysis (TGA) were used to quantify the silanol groups from the weight loss associated with the dehydroxylation process. TGA measurements were performed on a SDT Q600 (TA Instruments, Inc.). Samples were first heated from room temperature to 200°C at the rate of 7.5°C/min, and kept during 6 h (at this temperature in order to remove adsorbed water). After this plateau, temperature was increased up to 1000°C at a rate of 5°C/min. The whole thermal treatment was performed under air (100 ml/min).

Weight loss above 200°C (noted w_2) was ascribed to dehydroxylation. The concentration of hydroxyls can be estimated from Eq. 1 where M_{H2O} is the molar mass of water.

$$n_{OH}(mmol/g) = \frac{2 \times w_2(\%)}{M_{H_2O} \times 100} x1000 \qquad \text{(Eq. 1)}$$

2.2.4 N_2 physisorption

Nitrogen physisorption is a common method to study the porosity and surface area of

porous materials. The surface area can be determined by means of the BET equation, elaborated by Brunauer, Emmett and Teller.[2] The pore volume and pore radius was calculated by BJH method (Barret, Jonier, and Halenda).[3]

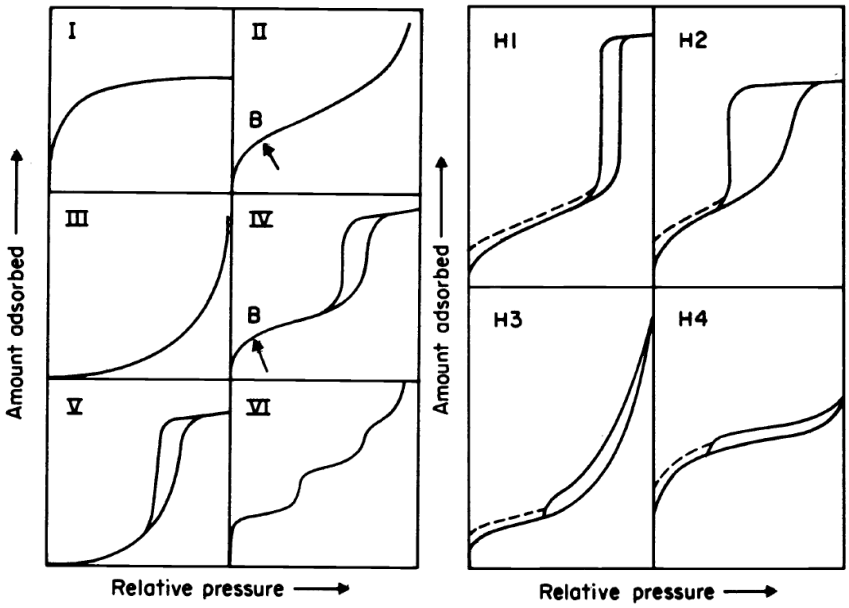

Figure 2-1 Different types of physisorption isotherms (left) and hysteresis loops (right)[4]

Adsorption isotherms are usually classified into six categories, displayed in Figure 2-1. Different properties in porosity give different types of isotherms. Type I is obtained when adsorption is restricted to a monolayer. Pores are typically microporous with the exposed surface residing almost exclusively inside the micropores, which, once filled with adsorbate, leave little or no external surface for further adsorption. Type II is frequently encountered and represent multilayer physical adsorption in nonporous (or pores larger than ca. 100 nm) materials. Type III, also corresponds to multilayer adsorption in nonporous materials but differs from type II by the absence of rapid initial uptake of gas. It corresponds to materials for which the interaction between the adsorbate and the adsorbent is low. Type IV occurs on porous adsorbents with pores in the range of 1.5 - 100 nm. The sharp adsorbate uptake at intermediate pressures corresponds to the filling of the pores (capillary condensation). A characteristic hysteresis loop between adsorption and desorption curves is observed. Type V is observed when interaction potential between adsorbate and absorbent is small (similar to type III) and is also associated with pores in the 1.5 - 100 nm range. Type VI is associated with layer by layer

adsorption on a highly uniform surface, which is rare.

Hysteresis appearing in the multilayer range of physisorption isotherms is usually associated with capillary condensation in mesoporous structures. Such hysteresis loops may exhibit a wide variety of shapes corresponding to different pore geometries. There are four types of hysteresis loops (H1, H2, H3, and H4) as shown in Figure 2-1. The H1 hysteresis is the result of adsorbents with a narrow pore size distribution of uniform and well defined cylindrical pore channels. The H2 hysteresis is usually observed when the porosity is generated by closely packed spherical particles with uniform size from a complex, interconnected pore network (ink-bottle shaped pores). The H3 hysteresis is observed from the aggregates of plate-like particles or adsorbents with slit-like pores. The H4 hysteresis results from adsorbents with slit-like pores in the microporous range.

The textural properties of the calcined samples were derived from N_2 adsorption/desorption measurement at -196^{o}C on a BelSorp Max equipment (BEL Japan, Inc.). Prior to the measurement, the samples were outgassed at 300^{o}C to a residual pressure below 10^{-2} KPa for 3.5 h. Total surface area was calculated using the Brunauer–Emmett–Teller (BET) method from the adsorption data obtained in the p/p_0 range of 0.05–0.3. The pore size distribution and mesoporous volume were measured using BJH method from the adsorption branch when the pore size is less than 5 nm in order to avoid the artifact peak[5] (usually appears at 4 nm). When the pore size is larger than 5 nm, the desorption branch was used.

2.2.5 NH_3-TPD

Total acid site concentration was determined by temperature programmed desorption of ammonia (NH_3-TPD) using a Micrometrics Autochem 2910 equipped with a thermal conductivity detector. Prior to NH_3 adsorption, the sample (about 0.2 g) was calcined in situ at 550^{o}C for 1 h under O_2 and, after that, the temperature was decreased to 150^{o}C. The NH_3 adsorption on the sample was carried out in a flow of 5 % NH_3/He during 60 min at 150°C. Afterward, loosely bonded NH_3 (physisorbed NH_3) was removed by flowing He on the sample at 150°C for 60 min. Typical NH_3 desorption was observed from 150^{o}C to 550^{o}C at a ramping

rate of 7.5°C/min in a He flow (20 mL/min). The NH_3 desorption curves of the ASA samples are typically made of two contributions. These two overlapping desorption peaks were decomposed into a peak at about 250°C (low temperature peak, LT) and a peak at about 350°C (high temperature peak, HT) using Gaussian and Haarhoff-Van der Linde (HVL) function separately, as reported in the literature.[6]

2.2.6 FTIR

Infrared spectroscopy on dehydrated samples has been used to characterize the surface hydroxyls of the samples and also to characterize their acidities (Brønsted and Lewis) by adsorption of two basic probe molecules, pyridine and CO.

2.2.6.1 FTIR of adsorbed pyridine

Experiments were conducted on self-supported wafers in an *in situ* IR cell. The sample about 20 mg was finely ground in an agate mortar and pressed into a self-supported wafer with a diameter 16 mm. This wafer was placed in a cell made of pyrex with, in its lower part, two CaF_2 windows for FTIR measurements, and, in its upper part, an oven for pretreatment and pyridine desorption, similar to the one depicted in elsewhere (**Annex III**, p217).[7] This cell is connected to a vacuum system. The spectra were recorded on a Bruker VECTOR 22 spectrometer equipped with a DTGS detector and using Bruker OPUS 5 software and acquiring 64 scans per spectrum with a resolution of 4.0 cm^{-1}.

Assembly for FTIR adsorption pyridine was displayed in **Annex IV**, p218. A typical experiment was carried out as follows: The wafer was activated by calcination from 50°C increase to 450°C at the rate of 2°C/min for 3 h under 200 Torr of O_2 (static pressure). Subsequently, the sample was treated at 450°C for 1 h under a secondary vacuum of 10^{-5} Torr. The background spectrum (empty cell) was recorded and then, after the wafer had cooled to ambient temperature, the IR spectrum of the sample was recorded. This spectrum will be subtracted to the spectra recorded after pyridine adsorption and desorption for the quantitative determination of BAS and LAS and its 3400-4000 cm^{-1} range will be used to study the nature of hydroxyl groups. The sample is exposed to 1.2 torr of purified and degassed pyridine vapor

at room temperature. Finally, the system was evacuated at RT and at different temperatures for 0.5 h under vacuum of 10^{-5} Torr and pyridine-adsorbed IR spectra were recorded at RT, 150°C, 250°C, 350°C, respectively. All spectra were normalized by the weight of the wafer.

Total Lewis acidity and total Brønsted acidity were calculated from the IR measurement results of pyridine adsorption at 150°C; weak Lewis and Brønsted acidities were obtained from the difference of adsorbed pyridine after treatment at 150 and 250°C; medium Lewis and Brønsted acidities were obtained from the difference of pyridine adsorbed at 250 and 350°C; strong Brønsted and Lewis acidities were estimated from the IR measurement results after pyridine adsorption at 350°C.

The concentration of BAS and LAS *c* (μmol/g) were be obtained using the relation

$$C = \frac{A\pi R^2}{w\varepsilon}$$

This equation is derived from the Beer Lambert law, where:

- *A* is the integrated surface of the peak on the difference spectra after baseline optimization;
- *R* (cm) is the radius of the wafer
- *w* (g) is the weight of the pre-treated sample
- ε (cm/μmol) is the molar absorption coefficient.

the values of molar absorption coefficients (ε) used for the quantification of BAS (band ν_{CN} at 1545 cm^{-1}) and of LAS (band ν_{CN} at 1450 cm^{-1}) are those reported by Emeis et al.[8]

2.2.6.2 FTIR of adsorbed CO

The set-up for FTIR of adsorbed CO is similar to the one described above for FTIR of adsorbed pyridine except that the cell is made of quartz and the bottom of the cell can be cooled down to about -173°C thanks to a bath of liquid N_2. Spectra were recorded using a Bruker Vertex 70 FTIR spectrometer, equipped with an MCT detector (resolution 2 cm^{-1}, 64 scans per spectrum). All the spectra related to CO adsorption experiment are reported in absorbance and after subtraction of the spectra of the sample before adsorption of any CO dose. Assembly for

FTIR adsorption CO was displayed in **Annex V**, p219.

The experimental protocol is as follows: wafers were first heated to 450°C at a rate of 2°C/min under O_2 flow (30 mL/min), they were kept at this temperature and under this atmosphere for 2 h, then evacuated under secondary vacuum before being cooled down to room temperature. The wafers were then transferred to the beam zone that was maintained under liquid nitrogen. Prior to the addition of CO, a He pulse (10 Torr, about 0.7 µmol He) was added in order to speed up thermal equilibration. The purpose of this step is to allow the wafer to reach its equilibrium temperature. Indeed, under vacuum, thermal equilibrium is very slow and very difficult to obtain before the addition of the first CO pulse. Hence, the progressive increase in pressure in the cell upon CO addition could result in a progressive decrease of the temperature of the wafer and therefore a shift of all the infrared peaks. As explained by Trukhan et al.,[9] this usually leads, on difference spectra, in distorted peaks and possibly to the appearance of artefact ones. Addition of a small amount of He increases the pressure in the cell sufficiently to reach thermal equilibrium in a few minutes. Spectra were recorded before and after the introduction of increasing doses of CO gas. After saturation with an equilibrium pressure of 133 Pa, an evacuation step was then carried out for 2 h until a residual pressure of about 10^{-5} Pa was reached.

2.2.7 Solid state NMR

2.2.7.1 1D MAS NMR

Solid state magic angle spinning nuclear magnetic resonance (MAS NMR) experiments were performed on a Bruker AVANCE500 spectrometer at 11.7 T in 4 mm zirconia rotors. The resonance frequency of ^{1}H and ^{27}Al were 500.16 MHz and 130.33 MHz, respectively. Chemical shifts, δ, were reported relative to TMS and aqueous $Al(NO_3)_3$ solution.

^{1}H MAS NMR spectra (Direct Polarization (DP)) are performed with a 90° pulse duration of 2.8 µs and a recycle delay of 5 s and 64 accumulations. The MAS equipment for rotation was carefully cleaned with ethanol to avoid spurious proton signals. Prior to ^{1}H NMR measurement, samples were loaded in the rotor and the sample (in the open rotor) was

dehydrated under vacuum at 200°C during 10 h in a N_2 sorption cell. After pretreatment the rotor was immediately closed to avoid rehydration.

^{27}Al MAS NMR spectra ((Direct Polarization (DP)) were recorded by small-flip-angle technique with a pulse of 1 μs (π/8), 0.5 s for the recycle delay and 2048 scans.

The simulation of the NMR spectra were performed using the Dmfit program.[10] For a quantitative comparison, spectra were normalized by sample weight (measure on hydrated or dehydrated sample). For aluminium, when MQMAS experiments were recorded, the quantification of the concentration for the different aluminium environments was done by fitting the corresponding 1D DP MAS spectra using, in first approximation, the quadrupolar product and the isotropic chemical shift determined in the MQMAS experiment. In other cases, the 1D DP MAS spectrum was decomposed using the CzSimple model.[11]

2.2.7.2 Quantification Proton

For proton quantification, camphor ($C_{10}H_{16}O$), poly(dimethylsiloxane) (PDMS, $(C_2H_6OSi)_n$), hexamethyl-benzene (HMB, $C_{12}H_{18}$) and adamatane ($C_{10}H_{16}$) were used as external references. These molecules were chosen for their low proton content (consistent with the proton content of ASA) and the simplicity of their NMR spectrum. For NMR measurement, the sample was restricted to the middle region of the 4 mm MAS rotor using an HR-MAS rotor (Figure 2-2). This type or rotor allows, thanks to two spacers, to restrict the available space to one-third of the initial volume, at the center of the rotor (where the magnetic field is homogeneous). A very small amount (as small as 0.1 mg) can be weighed precisely thanks to a microbalance and ^{1}H high sensitivity.

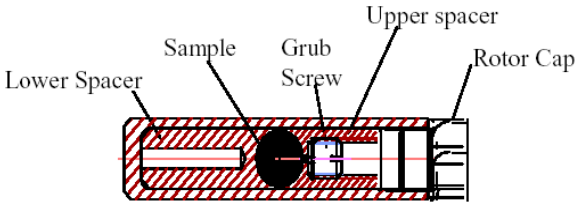

Figure 2-2 Structure chart of HR-MAS rotor

All spectra were recorded with exactly the same parameters and all the areas were

integrated from the spectrum subtracted from a background (empty rotor) using Topspin software. Figure 2-3 displays the experimental area of the proton resonances for each external sample as a function of the expected number of protons calculated from the chemical formula and the weight. A linear relationship going through zero was obtained and is characterized by a very good correlation coefficient value R^2 = 0.998. For a sample with an unknown proton concentration, using the integrated surface area of it ^{1}H NMR spectrum, its absolute proton concentration can be obtained by using the linear formula.

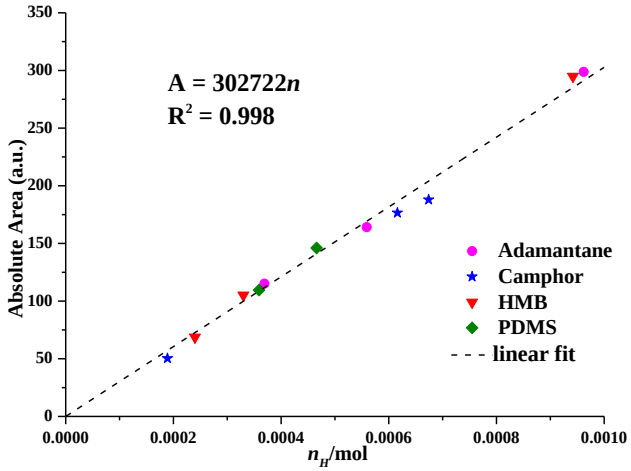

Figure 2-3 Area of the ^{1}H NMR spectra of different reference samples vs the number of proton in the rotor based on sample weight and chemical formulas a function of their theoretical number of protons. The dashed line is the linear regression best fit

This calibration curve was used to estimate the proton concentration of some silica and silica-alumina samples. For comparison, the proton concentration of these samples was also determined by TGA. Proton concentration based on TGA and ^{1}H MAS NMR are reported in Table 2-3. For all samples, the amounts of protons determined by these two methods were consistent, indicating that the two techniques could be used indifferently for the quantification of total proton in the sample. Based on this observation, total concentration of hydroxyls reported in the next chapters were determined based on the TGA results and the concentration of each type of proton in a sample was estimated based on the decomposition of its ^{1}H NMR spectrum (recorded in a conventional 4 mm rotor) and the total amount of proton derived from TGA. The reason we choose this protocol (instead of a direct quantification of proton by NMR using the HR-MAS rotor) is that measurements with HR-MAS rotor are difficult to perform

due to the instability of the HR MAS rotor at high spinning rate. Moreover, using a conventional rotor allows activating the sample in the rotor (for dehydration pretreatment) and the same rotor can be used for the recording ^{1}H, ^{27}Al and 2D spectra.

Table 2-3 Proton content of different samples measured by TGA and ^{1}H MAS NMR

Sample	H content (mmol/g)	
	TGA	^{1}H MAS NMR
S4	4.36	4.06
S2	6.17	6.24

2.2.7.3 Homonuclear NMR

2D double quantum quantum - single quantum (DQ/SQ) correlation experiment, using homonuclear DQ recoupling sequences (PC7 or $BR2_2^1$), has been used to probe the spatial proximity of two like-spins. The presence of a signal in the DQ/SQ MAS spectrum indicates that spins are in close proximity (< 5 Å), as the DQ coherences observed are strongly dependent on the internuclear distance. A schematic view of a DQ-SQ 2D spectra is shown on Figure 2-4. Peaks that occur along the diagonal (ω_A, $2\omega_A$) and (ω_B, $2\omega_B$) are autocorrelation peaks resulting from the dipolar interaction of spins with identical chemical shift, while pairs of off-diagonal peaks at (ω_A, $\omega_A+\omega_B$) and (ω_B, $\omega_A+\omega_B$) correspond to correlations between two spins with different chemical shifts. Usually, the strength of these cross peaks reflects the dipolar interaction between the spin pair. In other words, it reflects the distance between the two spins.

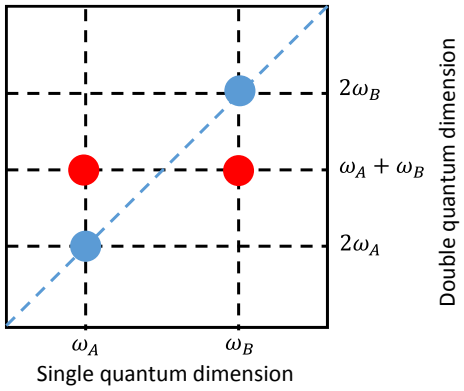

Figure 2-4 Schematic view of a 2D DQ/SQ MAS spectrum

The ^{1}H-^{1}H DQ/SQ experiments were performed using the POST C7 recoupling sequence

(Figure 2-5 (A)).[12] Typically 250 FIDs with 32 scans were recorded in t_1 dimension with rotor synchronized t_1 increment of 80 µs (ν_{rot} = 12.5 kHz). The rf nutation frequency (PC7 and π/2) was 87.5 kHz (= 7*ν_{rot}) with a relaxation delay of 5 s.

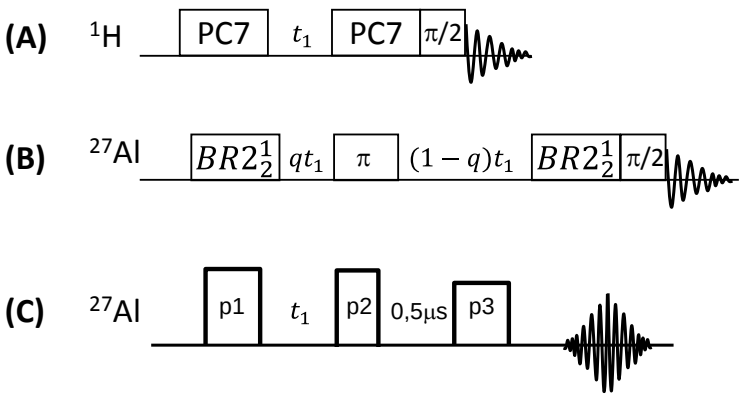

Figure 2-5 Pulse sequences of (A) ^{1}H DQ/SQ NMR (B) ^{27}Al DQ/SQ NMR (C) ^{27}Al MQ MAS NMR

The ^{27}Al-^{27}Al DQ/SQ spectrum used the supercycled symmetry-based $BR2_2^1$ sequence[13] for excitation and reconversion with τ_{exc} = τ_{rec} = 888 µs (Figure 2-5 (B)). The rotor-synchronized t_1 increment interval in the indirect dimension was set to 74.07 µs (ν_{rot} = 13.5 kHz). The relaxation delay was 0.4 s and the indirect dimension was acquired with 32 slices with between 8192 and 24960 transients each. The rf nutation frequency was 4.17 kHz for the central-transition π and π/2 pulses. The parameter q, for unequal incremented time period (qt_1 and $(1-q)t_1$), has been set to 0.2 and the 2D spectra have been re-scaled along F_1 to obtain the normal chemical shift values.

The MQ-MAS experiment allow to obtain 2D high-resolution NMR spectra of quadrupole nuclei with half-integer spin in solids, by refocusing the fourth-rank elements of the second-order quadrupole interaction in spin space. The 2D spectrum provides isotropic chemical shift in the F1 dimension but presents the second-order line shapes in the F2 dimension (MAS). ^{27}Al 3Q MAS spectra were acquired with the SPAM MQMAS sequence[10] (Figure 2-5 (C)). For the two first pulses P1 and P2, the applied RF field was about 80 kHz and for the third pulse P3 it was about 6 kHz. The pulse durations P1, P2 and P3 were set empirically to 5, 1.5 and 8 µs respectively. We used 50 t1 increments of 25 µs for F1 dimension acquisition. The number of accumulation varies from 1024 to 102400. Shearing transformation

and scaling of the F1 axis was realized with "xfshear".[14]

The quantification of the concentration for the diferent coordinated Al environments was done by fitting with dmfit[10] from the corresponding 1D DP MAS spectrum using the quadrupolar product and the isotropic chemical shift determined in the MQMAS experiment.

From the 3Q MAS spectra, isotropic chemical shift, δ_{iso}, and quadrupole product $C_{Q\eta}$ can be obtained by elsewhere,[15]

$$\delta_{iso} = \frac{17}{27}\delta_{F1} + \frac{10}{27}\delta_{F2}$$

$$C_{Q\eta} = I(2I-1)\frac{\omega_{cf}}{2\pi}\sqrt{\frac{40}{3\left[I(I+1)-\frac{3}{4}\right]}} \times \sqrt{\frac{17}{27}(\delta_{F1}-\delta_{F2})}$$

where δ_{F1} and δ_{F2} are the gravity centers of the signals in the F1 and F2 dimension, I = 5/2 is the spin quantum number of ^{27}Al and ω_{cf} is the carrier frequency of the spectrometer. The quadrupolar coupling constant C_Q can be estimated from $C_{Q\eta}$ by,

$$C_{Q\eta} = C_Q\sqrt{1+\frac{1}{3}\eta^2}$$

where η is the asymmetry parameters (limited to $0 < \eta < 1$).

2.2.7.4 Heteronuclear NMR

The dipolar heteronuclear multiple-quantum coherence technique (D-HMQC) is a recently developed NMR pulse sequence, which is particularly suitable for the investigation of spatial proximity between quadrupolar and spin 1/2 nuclei. Heteronuclear dipolar correlation techniques allow the edition of filtered 1D spectra or 2D correlation maps that qualitatively trace the spatial proximity between two species presenting different chemical nature. The heteronuclear dipolar coupling (averaged by MAS) is re-introduce by the use of dipolar recoupling sequences like $SR4_1^2$ (Figure 2-6).

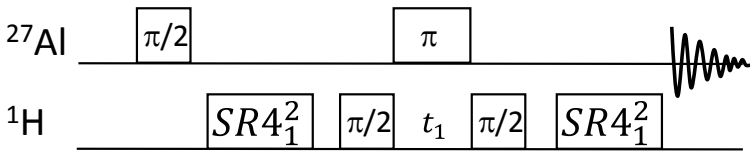

Figure 2-6 Pulse sequences of ^{1}H-^{27}Al D-HMQC NMR

The ^{27}Al-^{1}H D-HMQC experiments[16] were obtained with rf nutation frequencies of 8 and 90 kHz for ^{27}Al and ^{1}H, respectively. $SR4_1^2$ was used as the recoupling sequence to re-introduce ^{27}Al-^{1}H dipolar interaction with a rf field strength of 25 kHz (= 2*ν_{rot}) during 960 μs. Spectra result from averaging 15360 transients for each of 50 t1 increments with Δt_1 = 40 μs and a recycle delay of 0.4 s.

Rotational Echo Adiabatic Passage DOuble Resonance (REAPDOR) experiment[17] is based on the heteronuclear dipole interaction. This pulse sequence recouple the heteronuclear dipole interaction between an observed I = 1/2 spin and a quadrupole spin and allows the measurement of the interatomic heteronuclear distance. ^{27}Al-^{1}H REAPDOR experiments were carried out at three different spinning speeds (ν_{rot} = 8, 10 and 12 kHz) using rf field of 90 kHz for ^{1}H. For a partial adiabatic population inversion, the radio-frequency pulse in the ^{27}Al channel is of duration in the order of 1/3 of rotor period ($1/\nu_{rot}$). A recycle delay of 5 s and 16 accumulations were applied. The procedure used to obtain the value of the dipolar coupling and the internuclear distance is described in detail at this web address: *http://www.pascal-man.com/pulsesequence/double-resonance/REAPDOR.shtml*

2.2.8 Isomerization of 33DMB1 reaction

3,3-dimethylbut-1-ene (33DMB1) isomerization was chosen as model reaction to assess the acidity of the samples. The scheme of the test was displayed in **Annex VI, p**220 The reaction was carried out in a U-shaped, flow type quartz reactor (length = 195 mm, diameter = 6 mm, see p215 **Annex I**) at atmospheric pressure. The partial pressure of 33DMB1 in N_2 was adjusted by bubbling the gas through the liquid reactant in a saturator immersed in cryostat at 0°C. The catalyst (50 mg) was pretreated *in situ* with N_2 (50 cm^3/min) at temperatures 200°C at the rate of 2°C/min during 3 h. The sample was then cooled down in N_2 with the same flow to a reaction temperature of 120°. This temperature was chosen to avoid secondary reactions

and diffusional limitations. The products were analyzed online by gas chromatography (HP 6990) equipped with a flame ionization detector (FID) and a capillary column (CP-Sil PONA CB, 50 x 0.21 mm, Varian) and operated at 80°C. One of the result was displayed in **Annex II**, p216. The reagent partial pressure and flow rate were 20.4 kPa and 16.2 mmol/h (30 ml/min N_2), respectively.

Reference

(1) Fidalgo, A.; Rosa, M. E.; Ilharco, L. M. *Chemistry of materials* **2003**, *15*, 2186.

(2) Brunauer, S.; Emmett, P. H.; Teller, E. *J. Am. Chem. Soc* **1938**, *60*, 309.

(3) Barrett, E. P.; Joyner, L. G.; Halenda, P. P. *J. Am. chem. soc* **1951**, *73*, 373.

(4) Sing, K. S. *Pure and applied chemistry* **1985**, *57*, 603.

(5) Groen, J. C.; Peffer, L. A.; Pérez-Ramírez, J. *Microporous and Mesoporous Materials* **2003**, *60*, 1.

(6) Rodríguez-González, L.; Hermes, F.; Bertmer, M.; Rodríguez-Castellón, E.; Jiménez-López, A.; Simon, U. *Applied Catalysis A: General* **2007**, *328*, 174.

(7) Thibault-Starzyk, F.; Maugé, F.; Fan, F.; Feng, Z.; Li, C.; Jentoft, F. C.; Matsuoka, M.; Saito, M.; Anpo, M.; Jobic, H. **2012**, 1, 14.

(8) Emeis, C. *Journal of Catalysis* **1993**, *141*, 347.

(9) Trukhan, N. N.; Panchenko, A. A.; Roduner, E.; Mel'guno, M. S.; Kholdeeva, O. A.; Mrowiec-Białoń, J.; Jarzebski, A. B. *Langmuir* **2005**, *21*, 10545.

(10) Massiot, D.; Fayon, F.; Capron, M.; King, I.; Le Calvé, S.; Alonso, B.; Durand, J. O.; Bujoli, B.; Gan, Z.; Hoatson, G. *Magnetic Resonance in Chemistry* **2002**, *40*, 70.

(11) Neuville, D. R.; Cormier, L.; Massiot, D. *Geochimica et Cosmochimica Acta* **2004**, *68*, 5071.

(12) Hohwy, M.; Jakobsen, H. J.; Eden, M.; Levitt, M.; Nielsen, N. C. *The Journal of chemical physics* **1998**, *108*, 2686.

(13) Wang, Q.; Hu, B.; Lafon, O.; Trébosc, J.; Deng, F.; Amoureux, J. *Journal of Magnetic Resonance* **2009**, *200*, 251.

(14) Amoureux, J.-P.; Fernandez, C. *Solid State Nuclear Magnetic Resonance* **1998**, *10*, 211.

(15) Millot, Y.; Man, P. P. *Solid state nuclear magnetic resonance* **2002**, *21*, 21.

(16) Lu, X.; Lafon, O.; Trébosc, J.; Tricot, G.; Delevoye, L.; Méar, F.; Montagne, L.; Amoureux, J. *The Journal of chemical physics* **2012**, *137*, 144201.

(17) Gullion, T.; Academic Press: 1995; 117, 326.

Chapter 3. Dealumination of amorphous silica-aluminas with acetylacetone and its influence on acidity and activity

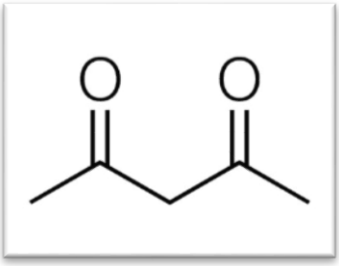

Abstract

The influence of dealumination of commercial ASA with acetylacetone on its textural properties, acidity and catalytic activity was studied by N_2-sorption, NH_3-TPD, FTIR of adsorbed pyridine as well as ^{1}H and ^{27}Al MAS NMR. Acetylacetone treatment increases the pore volume and surface area of GD13 without changing the pore size. More than half of the Al species are extracted from ASA but the total acidity is preserved or even slightly increased (for the ASA with higher Al content). The percentage of acidic Al is increased by a factor 2. Dealumination results in a better access to acid sites and an increase of medium BAS, leading to an increase catalytic activity of 33DMB1 isomerization.

3.1 Introduction

Amorphous silica−aluminas (ASA) are of considerable practical importance in industrial catalysis, where they are applied as a solid acid or serve as supports for finely dispersed metal sulfides or metals in a wide range of processes.[1,2] ASA are frequently present in modern bifunctional metal/acid catalysts to enhance selectivity toward middle distillates from hydrocracking of heavy oil fractions.[3] Compared to zeolites, ASA possess weaker and fewer Brønsted acid sites (BAS), and the structure of these sites are still subject to debate due to the amorphous nature of these materials. On ASA, the proportion of acid sites per Al is generally significantly smaller than 1 and many of these sites are Lewis acid sites (LAS). This indicates that only a fraction of the Al atoms in ASA develop acidic properties.

Dealumination is one of the available methods to remove these ineffective Al species from ASA. It has been successfully used on zeolites, the crystalline counterparts of ASA. For zeolites with low Si/Al ratio (e.g. faujasite Y), dealumination is commonly used to increase the Si/Al ratio in order to prepare active and stable catalysts. Dealumination not only improves the stability of the framework,[4,5] but also generates a secondary mesoporosity that increases significantly the accessibility of the acid sites and hence alleviate diffusion limitations and improves catalytic activity.[6] A significant number of papers have been dedicated to the effect of dealumination of zeolite on their acidity. In general, it was found that severe dealumination

decreases both Brønsted and Lewis acid sites, the former by removal of Al from the lattice by hydrolysis[7] and the latter by condensation of alumina moieties.[8]

Dealumination process is rather complicated, as many thermodynamic or kinetic factors will affect it significantly depending on the experimental conditions.[9] Dealumination can be achieved by steaming,[10] leaching with acids,[6,10-12] treatment with chelating agents such as hexafluorosolicate,[6] EDTA,[13,14] acetylacetone[15-17] and so on. Acetylacetone as a bidentate and nonacidic complexing ligand is a suitable chelating agent for mild dealumination leading to the extraction of "loosely bond" aluminium. Products of dealumination (e.g. $Al(acac)_3$) can be washed out from parent sample. Their extraction will depend on the type of structure, pore opening and extent of guest–host interaction.[18,19]

Dealumination of ASA has been far less investigated. Effect of dealumination of ASA by hydrochloric acid was studied by nuclear magnetic resonance.[20] A preferentially removal of octahedral aluminium was observed that occurred without modification of the catalytic properties.[20]

In the present study, we explored the dealumination of commercial ASA with acetylacetone, and proposed optimized dealumination conditions for this molecule. The influence of dealumination on the textural properties, acidity and catalytic activity was also studied. Furthermore, dealumination mechanism of ASA was explored.

3.2 Experimental

3.2.1 Synthesis

3.2.1.1 Starting ASA

Two commercial ASA GD13-NH_4^+ and GD25-NH_4^+ in their ammonium form and in their H form (calcined samples) GD13-H and GD25-H were used as starting materials (see details on §2.1.1 p47).

3.2.1.2 ASA dealuminated with acetylacetone

The starting ASA (2 g) was dried at 200°C overnight, then treated with 10 mL 38 wt%

of acetylacetone in toluene under magnetic stirring at room temperature or under reflux at 100°C for various time. Subsequently, the sample was immediately centrifuged with at a speed of 7000 rpm during 5 min, then washed thoroughly with acetone 3 times and dried at 110°C overnight. Prior to their use as catalysts, the modified ASA were calcined in a muffle furnace (550°C for 5 h at a heating rate of 2°C/min) to reveal the acidity and remove adsorbed acetylacetone. The obtained products were denoted as ASA-AHt or ASA-ARt, where A stands for acetylacetone, "t" is the reaction time (hour); H means reflux at 100°C, R means stirring at room temperature. A postfix ''a'' was used to distinguish the dried but uncalcined dealuminated samples. For simplification, GDxx-AHt means starting in ammonium form instead of GDxx-NH_4^+-AHt.

3.2.2 Characterization and catalytic test conditions

Characterization methods and Catalytic test conditions used in this chapter have been already been described in § 2.2.

3.3 Results

3.3.1 Textural properties

Table 3-1 Designation, Al content and textural properties of samples prepared by acetylacetone dealumination

Sample	Al	S_{BET}	Pore Size	Pore Volume
	mmol/g	m^2/g	nm	cm^3/g
GD13-H	2.3	445	4.8	0.70
GD13-AR1	2.0	456	4.2	0.69
GD13-AR24	2.0	549	3.7	0.68
GD13-AH4	1.1	539	4.2	0.77
GD13-AH24	1.0	550	3.7	0.77
GD13-H-AH4	1.4	477	4.2	0.68
GD25-H	4.0	421	4.8	0.70
GD25-AH4	1.4	559	4.8	0.81
GD25-H-AH4	1.7	477	4.8	0.71

Aluminium contents of the ASAs prepared by dealumination with acetylacetone under

various conditions are reported in Table 3-1. Treatment with acetylacetone results in various degrees of dealumination depending on experimental conditions. At room temperature, for the ASA prepared by subjecting GD13 to acetylacetone treatment during 1 h, only a small amount of aluminium was removed and extending time to 24 h, did not bring any change. This indicates that acetylacetone dealumination ability under ambient conditions is limited. The negligible amount of extracted Al in ASA under these conditions is consistent with previous reports on zeolites.[17,18] On the other side, upon treatment at higher temperature, dealumination is obvious: more than half of aluminium was removed from GD13 after reflux during 4 h. Upon prolonging time to 24 h, only a very small extra amount of Al was further extracted, indicating that the plateau in the dealumination was probably already reached after 4 h (all the reactive Al atoms are removed within 4 h). Therefore, optimal dealumination conditions are 4 h at 100°C.

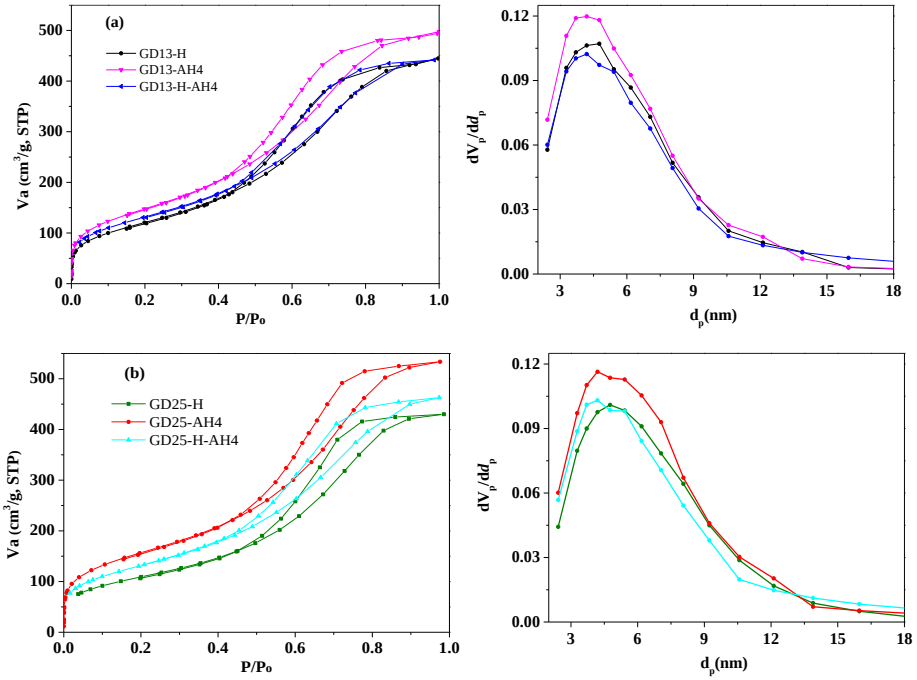

Figure 3-1 N_2 physisorption isotherms (left) and the pore size distributions (right) of (a) GD13-H and samples prepared by dealumination of GD13-NH_4^+or GD13-H; (b) GD25 and samples prepared by dealumination of GD25-NH_4^+ or GD25-H

Upon increasing the Al content in the starting ASA, the fraction of extracted Al significantly increases (from 52% for GD13 to 65% for GD25 under similar experimental conditions). Dealumination of calcined samples was also attempted. For the two ASA, the extent of dealumination is less than for the ammonium form.

To understand the effects of treatment with acetylacetone on the texture of the different samples, the porous properties of the dealuminated samples were compared (Table 3-1). It can be seen that, for treatments under ambient conditions (samples GD13-AR1 and GD13-AR24), no obvious effects of these treatments are observed. On the other side, for the samples obtained after reflux at 100°C of the ammonium forms of the ASAs, the surface area and the pore volume increase significantly compared to those of the starting ASA and the increase is more pronounced for the ASA undergoing the most important dealumination (surface area +20% for GD13-AH4, +39% for GD25-AH4). When dealumination is performed on the H-form ASA under the same conditions, the surface area also increases but to a lower extent and the pore volume chamges slightly.

Figure 3-1 shows the nitrogen adsorption desorption isotherms and pore size distribution curves of the samples synthesized under optimal dealumination conditions. All samples exhibit a type IV isotherm with a type H1 hysteresis loop, which is characteristic of mesoporous materials with a relatively narrow pore size distribution. Dealumination with acetylacetone did not change the pore size distribution, indicating that removal of the aluminium species occurs without destroying the pore structure. A possible explanation for the increase of the surface area is the removal of Al debris that were blocking the porosity, as previously reported by Fan et al. for the dealumination of steamed H-ZSM-5 by citric acid.[21]

3.3.2 Acidic Properties

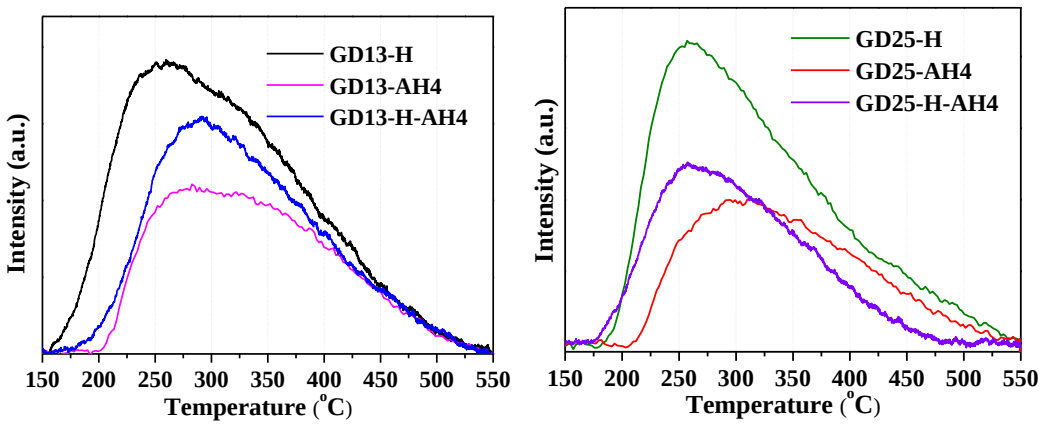

Figure 3-2 Acid properties of different samples determined by NH_3-TPD

The influence of treatment with acetylacetone on the acidity was explored by NH_3-TPD and FTIR of adsorbed pyridine. NH_3-TPD has been used to quantify total acidity (Brønsted and Lewis acidity) and the acid strength based on the peak position. Figure 3-2 displays the TPD curves; total acidity amount is summarized in Table 3-2. The TPD curved are clearly asymmetric and, in agreement with literature[22], two contributions were extracted, a low temperature peak (LT, between 170°C and 280°C), and a high temperature peak (HT, between 350°C and 550°C). The LT peak is ascribed to the desorption of NH_3 from weak acidic hydroxyls,[23] weak Lewis acid sites such as $Al(OH)_2^+$ and $Al(OH)^{2+}$.[24] It is also sometimes assigned to over-adsorbed NH_3 (i.e. NH_3 molecules adsorbed on NH_4^+).[22] Although the exact assignment of this peak is not clear, it is generally admitted that this peak does not correspond to an acidity relevant to catalysis.[25] The HT peak which is usually attributed to ammonia desorption from strong Brønsted and Lewis acid sites.[26]

Table 3-2 NH_3-TPD data of different dealuminated samples

sample	Total acid sites	Weak acid sites	Strong acid sites	Acidic Al
	mmol/g	mmol/g	mmol/g	%
GD13-H	0.42	0.16	0.26	18
GD13-AH4	0.24	0.05	0.19	22
GD13-H-AH4	0.26	0.07	0.19	19
GD25-H	0.46	0.12	0.34	12
GD25-AH4	0.25	0.05	0.20	17
GD25-H-AH4	0.20	0.06	0.14	12

Compared to GD13-H, GD25-H possesses only a slightly higher amount of total acid sites. Considering that the aluminium content is almost twice higher, this indicates that the fraction of non-acidic Al is much higher in GD25 than in GD13. The total acidity clearly decreases after treatment with acetylacetone. The acidity decrease seems to originate mostly from low temperature peak (assigned to weak acidic hydroxyls or weak Lewis acid), whereas the high temperature peak remains unchanged or decreases only slightly. This result suggests that dealumination occurs mostly on aluminium atoms involved in weak acid sites, which are not relevant for most catalytic applications. These results must nevertheless be taken with

caution as the decomposition of the TPD signal into two peaks is probably not very reliable due to the close proximity of the two contributions and to the unknown shape of the two individual TPD desorption signals.

FTIR of adsorbed pyridine was used in order to further differentiate the various acid sites present on the catalysts surface and more clearly assess the evolution of the acidity upon dealumination. Figure 3-3 presents the evolution of the pyridine vibration bands at different temperature for representative sample GD13-AH4 and the other samples displayed quite similar spectra on the right. The band at 1597 cm^{-1} is assigned to hydrogen bonded pyridine (weakly adsorbed pyridine). This band completely disappears upon thermal treatment. The bands at 1622, 1578 and 1457 cm^{-1} correspond to pyridine coordinated to LAS. The shoulder at 1640 cm^{-1} and the band at 1549 cm^{-1} are characteristic of pyridinium ions, indicating the chemisorption of pyridine on BAS.[27] The IR band at around 1622 cm^{-1}, associated to Lewis sites, shifts to higher frequency (1624 cm^{-1}) when the temperature of desorption increases. It is generally admitted that the band at higher frequency represents Lewis sites of a higher relative acid strength.[28] It is worth mentioning that a new peak appears at 1462 cm^{-1}. This band has been assigned by Flego et al. to a pyridine molecules interacting simultaneously with a Lewis site and a silanol.[29]

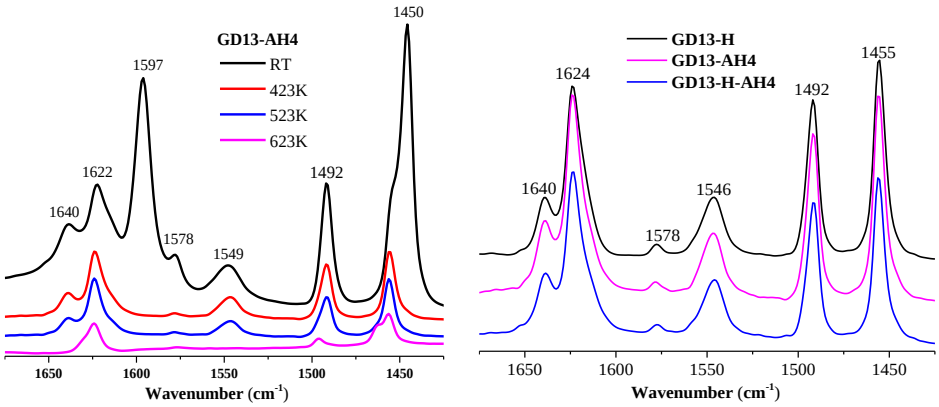

Figure 3-3 FTIR spectra of adsorbed pyridine on GD13-AH4 after evacuation at different temperatures (Left) and after evacuation at 150°C on a series of samples prepared by dealumination of GD13 with acetylacetone (right)

The bands at 1545 and 1450 cm^{-1} were used to quantify the amount of Brønsted and Lewis acid sites, respectively. The evolution of the intensities of these peaks with desorption

temperature (150, 250, 350°C) was used to evaluate the amount of total, medium and strong acid sites. The concentrations of mild (temperature of desorption between 150 and 250°C), medium (temperature of desorption between 250°C and 350°C) and strong (temperature of desorption higher than 250°C) Lewis and Brønsted acid sites are reported in Table 3-3. When the temperature reached 350°C, the band at around 1456 cm^{-1} remains while the band at 1549 cm^{-1} vanishes. This indicates the presence of strong LAS and absence of strong BAS.

Table 3-3 Acid type and strength distribution of the samples determined by pyridine-IR

Sample	Acidity (μmol/g)									Acidic Al
	total	BAS				LAS				
	B+L	weak	medium	strong	total	weak	medium	strong	total	%
GD13-H	101	23	11	0	34	21	11	36	67	4.4
GD13-AH4	102	11	25	0	35	10	13	43	67	9.2
GD13-H-AH4	84	24	6	0	31	10	9	33	53	6.1
GD25-H	110	31	10	0	40	21	9	40	70	2.8
GD25-AH4	121	28	13	0	41	27	8	44	79	8.8
GD25-H-AH4	94	25	10	0	36	14	6	38	58	5.4

Total acidity of GD25 is hardly higher than that of GD13, in agreement with the results of NH_3-TPD. However, the values of total acidity estimated by pyridine are considerably lower than those derived from NH_3-TPD. One obvious reason for this discrepancy is the presence of the LT peak on the NH_3-TPD curves that is not associated with relevant acid sites. It could therefore be more relevant to compare the total amount of acid sites evaluated by pyridine adsorption to those corresponding to the HT peak in the NH_3-TPD curves. Although the values get closer, the amount of acid sites evaluated via pyridine desorption is still more than two times smaller than that evaluated from NH_3-TPD. There could be two reasons for this: firstly, as mentioned above, the feasibility of the decomposition of the NH_3-TPD signal into two peaks is questionable because the exact shape of the TPD peaks is unknown. The amount of strong acid sites calculated based on NH_3-TPD measurement may therefore be inaccurate; secondly, the evaluation of the amount of acid sites by FTIR of adsorbed pyridine relies on the use of absorption coefficients. However, as discussed by Selli et al.,[30] the values that can be found for

these coefficients in the literature vary a lot, probably due to different experimental conditions. These authors reported absorption coefficients for the bands at 1455 and 1545 cm^{-1} that are about two times lower than those published by Emeis et al.[31] Nevertheless, although the quantities of Lewis and Brønsted acid sites may be underestimated by this method, the comparison of the values obtained for different samples is still correct, especially for all samples of the same type (here silica-alumina) and for spectra record in the exact same conditions.

Starting from GD13 (the ammonium form of GD13), dealumination with acetylacetone removes half of the aluminium species, but this removal occurs without modification in the total number of acid sites, indicating that acetylacetone removes selectively non acidic aluminium while preserving the acidic ones. It is consistent with previous results from the literature regarding dealumination of zeolite.[6] Quite interestingly, dealumination decreases both weak BAS and LAS while increasing medium BAS and strong LAS. This indicates that the removal of non-acidic aluminium is not without effect on the acidic properties of the ASA. One possible explanation would be that the removal of non-acidic aluminium in the close vicinity of acidic ones modifies their acidic properties. For the dealuminated samples prepared by using the H form ASAs, a decrease of the total acidity occurs, indicating that dealumination may be less selective when applied to the H form than on the ammonium one. For all ASA and whatever the dealumination conditions, strong BAS are never detected and the Lewis acidity is dominated by strong sites.

Dealumination with acetylacetone results in an increase of effective acidity (percentage of acid sites per Al) of a factor of two compared to GD13-H and three compared to starting GD25-H. The more important increase in effective acidity for the ASA obtained by dealumination of GD25 is consistent with the fact that GD25 contains a higher fraction of non-acidic Al, which makes dealumination more efficient on this sample than on GD13 (the dealuminated samples derived from these two ASAs have almost similar effective acidities). For the samples prepared by dealumination of the H form ASAs, the effective acidity increases only slightly as less Al was removed and total number of acid sites decreases.

3.3.3 Catalytic Performance

33DMB1 isomerization occurs through a pure protonic mechanism[32-34] (Lewis acid sites are not involved in this reaction) on strong and mild Brønsted sites. Moreover this reaction is, according to the literature, not poisoned by water.[35] Consequently, the percentage of conversion can be regarded as a measure of the concentration of Brønsted acid sites (BAS). Furthermore, 33DMB1 isomerization occurs over BAS with medium (or higher) acidic strength (corresponding to a pyridine desorption temperature of 220°C).[36,37] It is therefore well suited for the characterization of the acidity of ASAs. Figure 3-4 shows the conversion values as a function of time on stream for four ASAs.

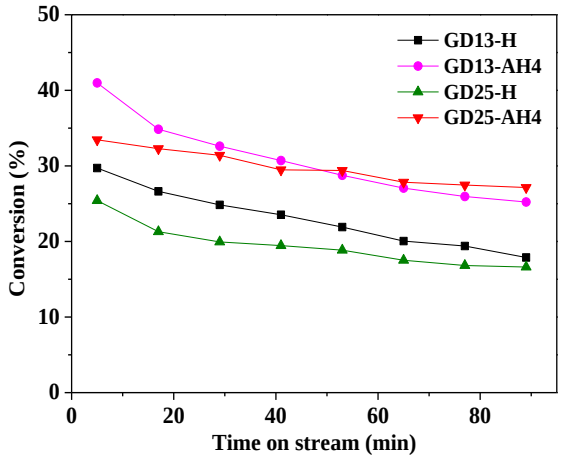

Figure 3-4 Conversion of 33DMB1 as a function of time on stream for the 2 starting ASA (GD13-H & GD25-H) and the dealuminated samples (dealumination of the NH_4^+ form)

For all samples, the conversion decreases with time on stream and finally stabilizes. This deactivation is probably due to the deposition of coke owing to other secondary reactions. The conversion observed for dealuminated samples is, at steady state, about 50% higher than that of their respective starting ASA. This increase may be related to the increase in the amount of medium Brønsted sites as 33DMB1 conversion is expected to be governed by BAS desorbing pyridine above 220°C (see Table 3-3, especially medium BAS). A more precise characterization of the acid strength of the Brønsted acid sites using FTIR of adsorbed CO would be helpful to investigate a possible modification of the strength of the acid sites upon dealumination.

3.3.4 Aluminium coordination

In order to gain insight into the dealumination mechanism, ^{27}Al MAS NMR was used to characterize the samples, not only in their calcined form but also in their intermediate form (treated with acetylacetone then dried without calcination, signaled by the postfix (a)). Spectra are shown in Figure 3-5. For a quantitative comparison, the amount of sample in the rotor has been weighted, and ^{27}Al NMR spectra were normalized on this weight.

For all samples, the ^{27}Al NMR spectrum has three contributions. The peak at 50-65 ppm corresponds tetrahedral aluminium species (Al^{IV}), whereas the one at ca. 0 ppm corresponds to octahedral aluminium (Al^{VI}). In zeolites, Al^{IV} and Al^{VI} are generally associated respectively to framework and extraframework aluminium species (with framework Al species corresponding to Brønsted acid sites and extraframework aluminium species usually associated with Lewis sites or alumina debris). In ASA the presence of Al in octahedral coordination sometimes points to the presence of transitional aluminas (especially for the aluminium-rich ASA) or at least to the presence of some polymeric form of Al, as octahedral Al is the dominant coordination in transitional aluminas.[38] The assignment of the signal centered at 30 ppm, has long been matter of debate (either distorted tetrahedral Al[39] or five coordinated Al[40]), but, based on MQ-MAS experiments it has been ascribed, at least on spectra recorded on hydrated samples, to five coordinated Al^{V}.[41,42]

Under the experimental conditions, we used complete hydration for the acquisition of the ^{27}Al NMR spectra, which is expected to allow full detection.[42] Hence by integrating a spectrum the contribution of each different coordination Al signals could be determined. To ascertain this, we verified that the evolution of the total Al area vs. the Al content (as determined by elemental analysis (Table 3-1) is indeed linear. Hence, we calculated, for each spectrum, the contribution, in mmol/g of each Al coordination, based on the amount of Al in the corresponding sample determined by elemental analysis. The peak assignments and the concentration of each Al coordination were summarized in Table 3-4.

The spectrum of GD13 (uncalcined ammonium form) shows two main peaks at 55.5 and

4.0 ppm, attributed to aluminium in tetrahedral (Al^{IV}) and octahedral (Al^{VI}) environment, respectively. The nonzero intensity between the two main lines indicates the probable presence of a weak amount of Al^{V}. For GD25, with nearly twice more Al than GD13, the spectrum exhibits a similar intensity for Al^{IV} whereas the intensity of the peak associated with Al^{VI} increases significantly. Therefore, most of the increase in the Al content between GD13 and GD25 contributes to Al^{VI}. Moreover, the signal at ca. 30 ppm corresponding to Al^{V} is clearly visible between these two main lines.

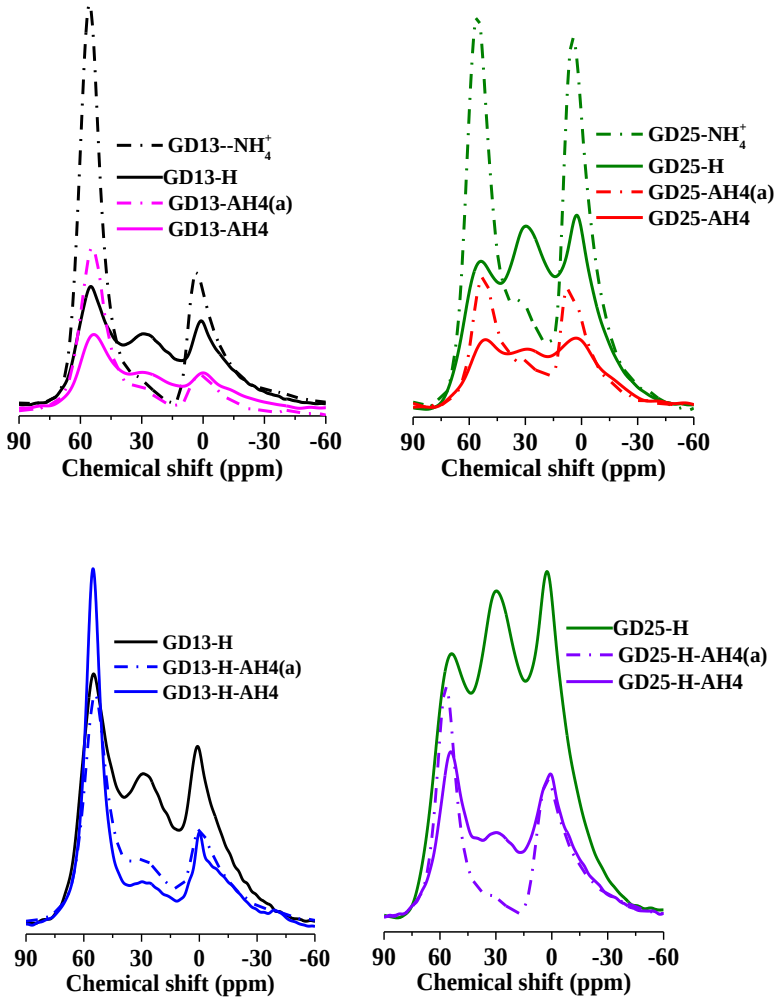

Figure 3-5 ^{27}Al MAS NMR of starting ASAs and dealuminated samples; left: GD13 series; right: GD25 series. All curves have been normalized by sample weight and calcined samples were rehydrated before measurement

After calcination (samples GD13-H and GD25-H), ammonium form of ASA changes into H form. Calcination leads, for the two starting ASA, to a significant increase in the proportion of Al^{V} at the expense of Al^{IV}. This modification in the speciation of Al between the H form and the NH_4^+ form ASAs is probably related to the flexible coordination of some of the Al

atoms in ASA, which has been evidenced by Omegna et al.[43] and Parker et al.[42] These authors observed that, upon exposure to NH_3, part of the Al^V changed their coordination to Al^{IV}. Flexible coordination of Al was associated to its belonging to a silica-alumina phase.

Table 3-4 Distribution of various aluminium species in samples based on the deconvolution of their normalized ^{27}Al MAS NMR spectra performed on hydrated samples

Sample	Al percentage (%)			Al content (mmol/g)		
	Al^{IV}	Al^V	Al^{VI}	Al^{IV}	Al^V	Al^{VI}
GD13-NH_4^+	64.5	3.6	32.0	1.48	0.08	0.74
GD13-AH4(a)	66.8	6.5	26.7	0.73	0.07	0.29
GD13-H	30.4	39.4	30.3	0.70	0.91	0.70
GD13-AH4	44.0	26.8	29.2	0.48	0.29	0.32
GD13-H-AH4	51.7	17.4	30.9	0.72	0.24	0.43
GD25-NH_4^+	45.2	3.6	51.2	1.81	0.14	2.05
GD25-AH4(a)	42.6	5.8	51.6	0.60	0.08	0.72
GD25-H	26.6	30.5	42.9	1.06	1.22	1.72
GD25-AH4	34.0	17.7	48.3	0.48	0.25	0.68
GD25-H-AH4	51.7	13.6	34.7	0.88	0.23	0.59

Comparison of the starting (uncalcined) ASA with the uncalcined samples obtained by dealumination of the ammonium form (GD13-NH_4^+ vs GD13-AH4(a); GD25-NH_4^+ vs GD25-NH4(a), shows a significant decrease of all aluminium peaks after treatment with acetylacetone. This is especially true for the sample derived from GD25-NH_4^+ (the ASA with the high Al content). This observation is consistent with the decrease of the aluminium concentration observed by elemental analysis. Although all peaks decrease in intensity, one can clearly see that the intensities of the peaks of Al^{IV} and Al^{VI} decrease in equal proportion while that of Al^V decreases less.

For the ASAs prepared by dealumination of the H form, the decrease (comparison of GD25-H and GD25-H-AH4) is more pronounced for the peak associated with Al^V than for the two others.

When comparing the spectra of the calcined starting ASAs with those of the dealuminated calcined samples (GD13-H, GD13-AH4, GD13-H-AH4; GD25-H, GD25-AH4, GD25-H-AH4)

one observe that, although all peak decrease in intensity, the fraction of tetrahedral Al increases and the fraction of pentacoordinated Al decreases for all samples.

3.3.5 Hydroxyl groups

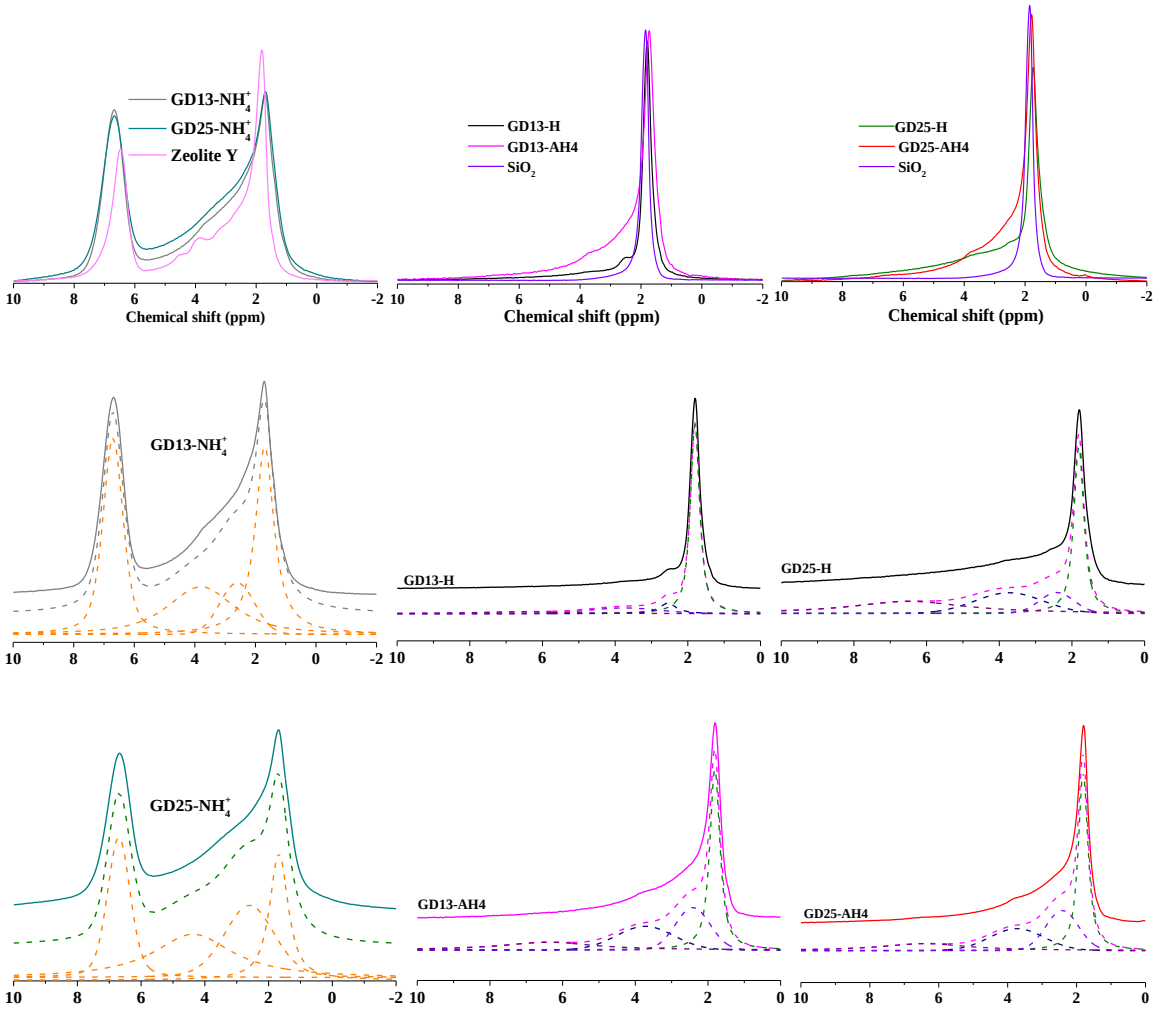

Figure 3-6 ^{1}H MAS NMR of various samples dehydrated at vacuum 200ºC (Top) and deconvolution with Lorentzian-Gaussian-shape peaks showing the contributions of various sorts of hydrogen groups (from top to bottom: Experimental, fitted and component spectrum)

^{1}H NMR spectroscopy allows not only to distinguish between the different types of hydroxyl groups (terminal vs bridging hydroxyl groups) and the ammonium ions via their chemical shift, but also to quantify each type of proton. The ^{1}H chemical shifts of surface OH groups on ASA are mainly influenced by local effects, such as oxygen coordination, bond geometry, and type of metal atoms in their local structure.[40] ^{1}H MAS NMR spectra are displayed on Figure 3-6.

Spectra of commercial zeolite Y (ammonium form, surface area 730 m^2/g, mole ratio SiO_2:Al_2O_3 = 12:1) and of a home-made silica (S9 (HYD5), see Table 2-2 on p48)) are also shown for comparison. The ammonium form zeolite Y showed four distinct signals at 1.8, 3.9, 4.5 and 6.7 ppm. The peak at 1.8 ppm is assigned to isolated or terminal Si-OH groups and the peak at 6.7 ppm is characteristic of the ammonium ions NH_4^+ formed by protonation of NH_3 on a Brønsted acid site. Two smaller at 3.9, 4.5 ppm represent bridging Si-OH-Al groups (Brønsted acid sites) in the sodalite cages and the supercages, respectively.[44] One would not expect the presence of Si-OH-Al bridges (at least from the supercages) in this sample which is in its ammonium form, but it should be noted that before ^{1}H MAS NMR measurement, a small amount of NH_3 may desorb during the pretreatment under vacuum at 200°C for 10 h.

Features of the ^{1}H MAS NMR spectra of the ammonium forms of the ASAs are similar to that of the NH_4Y sample. The signal at 1.7 ppm is assigned to isolated Si-OH groups[45] and/or terminal (H acceptor) silanols[46] and the one at 6.7 ppm to protons from NH_4^+. Beside these two sharp peaks, a broad shoulder is clearly visible at the right side of the peak at 1.7 ppm. Among the species one would expect in this range, Al-OH-Al group are expected at 2.6 ppm, similar to bridging surface μ_2-OH groups in gamma alumina[47] and Si-OH-Al bridging hydroxyl groups should be observed at 3.8 ppm based on the position of this species in zeolites.[48] However, considering that this sample is in its ammonium form, one can discard the presence of acidic species such as Si-OH-Al bridges, who should be mostly in the form Si-O^--Al, NH_4^+. Moreover, based on the spectrum of the pure silica sample, these last two peaks could also be due to the presence of weakly H-bonded silanols (donor of H bond, with a distance of about 2.95 Å (d = 3.8 ppm) and about 2.99 Å (d = 2.6 ppm))[46]. For the peak at 2.6 ppm it may contain contribution of both types (Al-OH-Al and H donor silanols). For the calcined samples, the peak assigned to NH_4^+ is no longer observed, in agreement with complete desorption of NH_3 during calcination. In the similar area where the NH_4^+ signal was located, a very broad new contribution centered at 6.5 ppm is observed. This signal is attributed to H-bonded Al-OH,[47,49] but one cannot discard the possibility that this species is related to water molecules in interaction with surface Al-OH species as these hydroxyls are more difficult to dehydrate than silanols.

As explained in **Chapter 2**, for the calcined samples, the total amount of hydroxyls was determined by TGA and based on the fraction of each type of proton deduced from the integration of the NMR spectra, the concentration (mmol/g) associated with each peak was calculated.

For the uncalcined samples the situation is a bit more complex as TGA weight loss will reflect desorption of water and ammonia. Considering that the NMR peak associated with the NH_4^+ proton stands for one NH_3 molecule and one hydroxyl, the fraction of NH_3 was taken as 1/4th of the surface of the peak at 6.7 ppm whereas the fraction of hydroxyls was taken as 1/4th of this peak. The totality of the others and the values in mmol/g were deduced from the percentage of weight loss (equal to(n_{NH3}×17+n_{OH}×18/2)×100).

Table 3-5 Assignment of the different bands in ^{1}H MAS NMR and the concentration of the various proton species in the starting and dealuminated samples

Sample	n_{OH} or n_{NH3} (mmol/g)					
	Total OH	1.8 ppm (Isolated and terminal SiOH)	2.6 ppm (AlOH and/or H donor SiOH)	3.8 ppm (Si-OH-Al bridges and/ or H donor Si-OH)	6.5 ppm (H donor Al-OH)	6.7 ppm n_{NH3} NH_4^+
GD13-NH_4^+	6.2	2.7	0.8	2.0	-	0.7
GD13-H	3.5	2.6	0.3	0.4	0.2	-
GD13-AH4	4.1	1.6	0.9	0.9	0.7	-
GD25-NH_4^+	7.8	2.0	1.6	3.6	-	0.6
GD25-H	3.6	1.3	0.4	0.8	1.1	-
GD25-AH4	4.5	1.9	1.0	0.9	0.7	-

The total density of OH groups is about twice higher in the ammonium forms of the starting ASA than in their H form. This is probably due to the fact that the ammonium forms correspond to uncalcined samples. The total density of OH groups increases slightly (+17%, between GD13-H and GD13-AH4, +25% between GD25-H and GD25-AH4) upon dealumination. This increase is consistent with the increase in the surface area upon dealumination (+20%, see Table 3-1).

The density of NH_3 is similar in the two starting ASA, in agreement with their close

acidic properties. These values are consistent but higher than those obtained by NH_3-TPD (see Table 3-2), which is not unexpected because they are obtained from uncalcined samples (whereas TPD values are obtained on freshly calcined samples). These values are also much higher than the amount of acid sites (Lewis + Brønsted) estimated based on FTIR of adsorbed pyridine (about 0.1 mmol/g, see Table 3-3)

The concentrations of the various OH groups have been deduced from the integration of their ^{1}H NMR signal. These integrated values confirm that the peak at 3.8 ppm cannot be assigned to Si-OH-Al bridges exclusively. Indeed, the density of hydroxyls associated with this peak varies between 0.4 and 3.6 mmol/g, which is well above the density of Brønsted acid sites estimated by pyridine adsorption FTIR (see Table 3-3). Hence, other species, most probably H bonded species also contribute to this signal. This confirms that the direct observation, in ASA, of BAS by ^{1}H MAS NMR spectroscopy is impossible.[50] For the peak at 2.6 ppm, the ratio of OH per Al for the dealuminated sample, would be rather high (0.4 OH per Al for example for GD25-AH4) but still possible. For all peaks, it is difficult to find a trend in their variation from one sample to another. This is probably due to the difficulty to determine accurately the contribution of each component as the 4 peaks used for the decomposition are broad and overlapped.

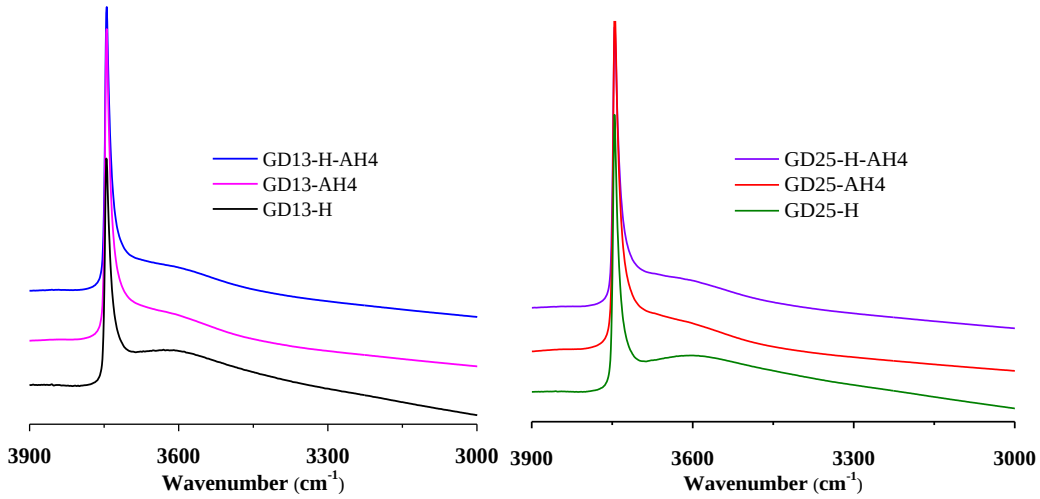

Figure 3-7 υ(OH) ranges of FTIR spectra of different samples activated at 450°C

Further information on the nature of hydroxyl groups in the samples was acquired by

FTIR spectra, as shown in Figure 3-7. All the samples displayed one sharp band at 3745 cm^{-1}, attributed to accessible, isolated silanol groups.[51-55] In addition, a broad envelop extending from 3700 to 3300 cm^{-1} is also detected, generally assigned to hydrogen-bonding Si-OH groups (H-donor)[56] and also to disturbed Si-OH-Al groups.[57,58] This broad envelop is more intense on starting ASAs than on dealuminated samples. The decrease of the intensity of this signal upon decreasing the Al content could indicate that this envelop also contains, in agreement with NMR data, a contribution of Al-OH-Al bridges (possibly H-bonded). It is worth mentioning that in all samples, no Si-OH-Al bridging hydroxyl groups were detected in agreement with previously published work on ASA.[27,40]

3.4 Discussion

The mechanism of dealumination of ASA by acetylacetone is related to the chelating property of this compound. The acetylacetone molecule, as a bidentate ligand, can chelate parts of "loosely bond" aluminium forming $Al(Acac)_x$ complexes on the surface. The formation of these complexes produces water and polarizes the Al-O bonds, a polarization that favours their breaking (by reaction with produced water).

$(MO)_nAl\text{-}OH + AcacH \rightarrow (MO)_nAl\text{-}Acac + H_2O$

$(MO)_{n-1}AcacAl\text{-}OM + H_2O \rightarrow (MO)_{n-1}AcacAl\text{-}OH + M\text{-}OH$

……

Where M is either Si or Al

The reactions may continue until $Al(Acac)_3$ is formed which can be washed out from parent sample resulting the Al elimination. The extraction of the Al atoms will likely depend on their next nearest neighbors. For the two ASA, Al elimination is only partial indicating that the ability of acetylacetone toward dealumination is limited (for the two starting ASAs, acetylacetone is present in excess in solution with regards to their Al content when considering the formation of $Al(Acac)_3$).

All dealuminated samples have a higher percentage of acidic Al (based on FTIR of

adsorbed pyridine) than the corresponding starting ASA (see Table 3-3). However, when dealumination is performed on the ammonium form ASA, the elimination of Al is more efficient than dealumination performed on the H-form ASA and the total amount of acid sites increases (whereas decreases slightly when dealumination is performed on the H-form of the ASA). Hence, dealumination is fully selective (AcacH only removes weakly bonded, non-acidic Al species) when performed in the ammonium form of the ASA and less efficient and only partially selective when performed on the H-form. The difference of efficiency of dealumination between ammonium form and H form ASAs is probably simply due to the fact that ammonium form is uncalcined and hence contains less condensed Al species (the density of hydroxyls in the ammonium form ASAs is about twice that of the calcined ones, see Table 3-5). The origin in the difference of selective is less straightforward. One could suggest that the NH_4^+ counter-ions somehow protect the acid sites from dealumination.

When comparing the series stemming from the two ASAs, one can see that the fraction of extracted Al is higher from the ASA with the high Al content (Table 3-1). This indicates a larger fraction of reactive Al in this ASA.

For all samples, Al removal is accompanied by an increase in the surface area and, the more Al atoms are removed, the more the surface area increases (see Table 3-1). This occurs without significant modification in the pore diameter (Figure 3-1) and, for the ASAs stemming from the ammonium form, with an increase in the pore volume. There could be two reasons for this modification in the textural properties of the ASAs upon dealumination: first, this could indicate that alumina-like debris that were blocking this access to a part of the porosity have been removed; second, as evidenced by the equations above, dealumination produce surface hydroxyls. These hydroxyls will undergo condensation reaction, either in solution or during calcination that can modify the textural properties of the ASA.

When comparing the Al distributions (^{27}Al MAS NMR spectroscopy of the calcined samples, see Figure 3-5 and Table 3-4), one can see that, for all Al coordinations, the amount of Al decreases upon dealumination with AcacH. However, the fraction of Al^{IV} slightly increases whereas the fraction of Al^{V} decreases. As Al^{IV} is associated, in zeolites, with Si-OH-

Al bridges, it is interesting to compare the density of Al^{IV} in the dealuminated samples with the density of acid sites. This comparison clearly shows that, even in the dealuminated samples, a large part of the Al^{IV} have no acidic properties.

3.5 Conclusion

Dealumination with acetylacetone in toluene under reflux, when performed on the uncalcined ammonium form of the ASAs, removes about half of the Al atoms and increases the surface area and pore volume. Dealumination is more efficient when performed on the ammonium form ASAs than on their H form. Moreover, it is fully selective in the sense that the acidic properties (FTIR of adsorbed pyridine) are not decreased (they are even slightly increased) upon dealumination on the ammonium form. The increase in the acidity and more precisely of the Brønsted acidity of the ASAs upon dealumination of their ammonium form is confirmed by the about 50% higher conversion of 33DMB1 of the dealuminated ASAs compared to their corresponding parent commercial ASA. The fraction of acidic Al is multiplied by 2-3 depending on the starting ASA, but remains low (below 10%), indicating that a large fraction of non-acidic Al is resistant to dealumination with AcacH (or where not accessible to this reactant). The characterization of the starting ASAs and the dealuminated samples by ^{27}Al MAS NMR reveals that all Al coordination undergo dealumination. However, when considering the calcined samples, the fraction of Al^{IV} increases whereas the fraction of Al^{V} decreases upon dealumination. The amount of Al^{IV}, even after dealumination exceed by far the amount of acid sites based on FTIR of adsorbed pyridine.

Although dealumination of ASA with AcacH allows to increase substantially the fraction of acidic Al by removing selectively non acidic ones, the percentage of acidic Al remains low after dealumination, indicating that AcacH may not be a strong enough dealuminating agent. Hence in the next chapter we will explore dealumination with another molecule: citric acid, which combines acidic and chelating properties and should therefore be a stronger dealumination agent.

Reference

(1) Acids, I. S. *Chemical Reviews (Washington, DC)* **1995**, *95*, 559.

(2) Busca, G. *Chemical reviews* **2007**, *107*, 5366.

(3) Scherzer, J.; Gruia, A. J. *Hydrocracking science and technology*; CRC Press, **1996**.

(4) Xu, B.; Bordiga, S.; Prins, R.; van Bokhoven, J. A. *Applied Catalysis A: General* **2007**, *333*, 245.

(5) Silaghi, M.-C.; Chizallet, C.; Raybaud, P. *Microporous and Mesoporous materials* **2014**, *191*, 82.

(6) Kumar, S.; Sinha, A.; Hegde, S.; Sivasanker, S. *Journal of Molecular Catalysis A: Chemical* **2000**, *154*, 115.

(7) Van Bokhoven, J.; Koningsberger, D.; Kunkeler, P.; Van Bekkum, H.; Kentgens, A. *Journal of the American Chemical Society* **2000**, *122*, 12842.

(8) Batonneau-Gener, I.; Yonli, A.; Hazael-pascal, S.; Marques, J. P.; Lopes, J. M.; Guisnet, M.; Ribeiro, F. R.; Mignard, S. *Microporous and Mesoporous Materials* **2008**, *110*, 480.

(9) Zhao, R.; Zhao, Z.; Li, S.; Zhang, W. *The Journal of Physical Chemistry Letters* **2017**, *8*, 2323.

(10) Li, S.; Huang, S.-J.; Shen, W.; Zhang, H.; Fang, H.; Zheng, A.; Liu, S.-B.; Deng, F. *The Journal of Physical Chemistry C* **2008**, *112*, 14486.

(11) Yan, Z.; Ma, D.; Zhuang, J.; Liu, X.; Liu, X.; Han, X.; Bao, X.; Chang, F.; Xu, L.; Liu, Z. *Journal of Molecular Catalysis A: Chemical* **2003**, *194*, 153.

(12) Chung, K.-H. *Microporous and Mesoporous Materials* **2008**, *111*, 544.

(13) Datka, J.; Kolidziejski, W.; Klinowski, J.; Sulikowski, B. *Catalysis letters* **1993**, *19*, 159.

(14) Agudelo, J.; Mezari, B.; Hensen, E.; Giraldo, S.; Hoyos, L. *Applied Catalysis A: General* **2014**, *488*, 219.

(15) Buckermann, W. A.; Huong, C. B.; Fajula, F.; Gueguen, C. *Zeolites* **1993**, *13*, 448.

(16) Zanjanchi, M.; Hemmati, M. *Materials chemistry and physics* **2004**, *85*, 334.

(17) Hosseini, M.; Zanjanchi, M.; Ghalami-Choobar, B.; Golmojdeh, H. *Journal of Chemical Sciences* **2015**, *127*, 25.

(18) Zanjanchi, M.; Razavi, A. *Spectrochimica Acta Part A: Molecular and Biomolecular Spectroscopy* **2001**, *57*, 119.

(19) Zanjanchi, M.; Mohabbati, E. *Journal of Molecular Structure* **2003**, *645*, 171.

(20) Man, P. P.; Peltre, M. J.; Barthomeuf, D. *Journal of the Chemical Society, Faraday Transactions* **1990**, *86*, 1599.

(21) Fan, Y.; Bao, X.; Lin, X.; Shi, G.; Liu, H. *The Journal of Physical Chemistry B* **2006**, *110*, 15411.

(22) Rodríguez-González, L.; Hermes, F.; Bertmer, M.; Rodríguez-Castellón, E.; Jiménez-López, A.; Simon, U. *Applied Catalysis A: General* **2007**, *328*, 174.

(23) Hidalgo, C. V.; Itoh, H.; Hattori, T.; Niwa, M.; Murakami, Y. *Journal of Catalysis* **1984**, *85*, 362.

(24) Woolery, G.; Kuehl, G.; Timken, H.; Chester, A.; Vartuli, J. *Zeolites* **1997**, *19*, 288.

(25) Niwa, M.; Sota, S.; Katada, N. *Catalysis today* **2012**, *185*, 17.

(26) Katada, N.; Igi, H.; Kim, J.-H.; Niwa, M. *The Journal of Physical Chemistry B* **1997**, *101*, 5969.

(27) Crépeau, G.; Montouillout, V.; Vimont, A.; Mariey, L.; Cseri, T.; Maugé, F. *The Journal of Physical Chemistry B* **2006**, *110*, 15172.

(28) Jia, C.; Massiani, P.; Barthomeuf, D. *Journal of the Chemical Society, Faraday Transactions* **1993**, *89*, 3659.

(29) Flego, C.; Kiricsi, I.; Perego, C.; Bellussi, G. *Catalysis letters* **1995**, *35*, 125.

(30) Selli, E.; Forni, L. *Microporous and mesoporous materials* **1999**, *31*, 129.

(31) Emeis, C. *Journal of Catalysis* **1993**, *141*, 347.

(32) Irvine, E.; John, C.; Kemball, C.; Pearman, A.; Day, M.; Sampson, R. *Journal of Catalysis* **1980**, *61*, 326.

(33) John, C. S.; Kemball, C.; Rajadhyaksha, R. A. *Journal of Catalysis* **1979**, *57*, 264.

(34) Bautista, F.; Campelo, J.; Garcia, A.; Luna, D.; Marinas, J.; Romero, A.; Urbano, M. *Reaction Kinetics and Catalysis Letters* **1998**, *64*, 41.

(35) Kemball, C.; Leach, H.; Skundric, B.; Taylor, K. *Journal of Catalysis* **1972**, *27*, 416.

(36) Guisnet, M. R. *Accounts of chemical research* **1990**, *23*, 392.

(37) Martin, D.; Duprez, D. *Journal of Molecular Catalysis A: Chemical* **1997**, *118*, 113.

(38) MacKenzie, K.; Temuujin, J.; Smith, M.; Angerer, P.; Kameshima, Y. *Thermochimica acta* **2000**, *359*, 87.

(39) Samoson, A.; Lippmaa, E.; Engelhardt, G.; Lohse, U.; Jerschkewitz, H.-G. *Chemical physics letters* **1987**, *134*, 589.

(40) Williams, M.; Fonfé, B.; Sievers, C.; Abraham, A.; Van Bokhoven, J.; Jentys, A.; Van Veen, J.; Lercher, J. *Journal of Catalysis* **2007**, *251*, 485.

(41) Fyfe, C. A.; Bretherton, J. L.; Lam, L. Y. *Journal of the American Chemical Society* **2001**, *123*, 5285.

(42) Parker, W. O. N.; Wegner, S. *Microporous and Mesoporous Materials* **2012**, *158*, 235.

(43) Omegna, A.; van Bokhoven, J. A.; Prins, R. *The Journal of Physical Chemistry B* **2003**, *107*, 8854.

(44) Li, S.; Zheng, A.; Su, Y.; Zhang, H.; Chen, L.; Yang, J.; Ye, C.; Deng, F. *Journal of the American Chemical Society* **2007**, *129*, 11161.

(45) Trébosc, J.; Wiench, J. W.; Huh, S.; Lin, V. S.-Y.; Pruski, M. *Journal of the American Chemical Society* **2005**, *127*, 3057.

(46) Brunet, F.; Charpentier, T.; Le Caer, S.; Renault, J.-P. *Solid state nuclear magnetic resonance* **2008**,

33, 1.

(47) Delgado, M.; Delbecq, F. o.; Santini, C. C.; Lefebvre, F.; Norsic, S.; Putaj, P.; Sautet, P.; Basset, J.-M. *The Journal of Physical Chemistry C* **2011**, *116*, 834.

(48) Asakawa, N.; Motokura, K.; Yashima, T.; Koyama, T.-r.; O-nuki, T.; Miyaji, A.; Baba, T. *The Journal of Physical Chemistry C* **2012**, *116*, 17734.

(49) Barrow, B. N. S.; Scullard, A.; Collis, N. *Johnson Matthey Technology Review* **2016**, *60*, 90.

(50) Luo, Q.; Deng, F.; Yuan, Z.; Yang, J.; Zhang, M.; Yue, Y.; Ye, C. *The Journal of Physical Chemistry B* **2003**, *107*, 2435.

(51) Janin, A.; Maache, M.; Lavalley, J.; Joly, J.; Raatz, F.; Szydlowski, N. *Zeolites* **1991**, *11*, 391.

(52) Ichihashi, H.; Kitamura, M. *Catalysis today* **2002**, *73*, 23.

(53) Heitmann, G.; Dahlhoff, G.; Hölderich, W. *Journal of Catalysis* **1999**, *186*, 12.

(54) Chu, C. T.; Chang, C. D. *The Journal of Physical Chemistry* **1985**, *89*, 1569.

(55) Kiricsi, I.; Flego, C.; Pazzuconi, G.; Parker, W. J.; Millini, R.; Perego, C.; Bellussi, G. *The Journal of Physical Chemistry* **1994**, *98*, 4627.

(56) Halasz, I.; Senderov, E.; Olson, D. H.; Liang, J.-J. *The Journal of Physical Chemistry C* **2015**, *119*, 8619.

(57) Pazé, C.; Bordiga, S.; Lamberti, C.; Salvalaggio, M.; Zecchina, A.; Bellussi, G. *The Journal of Physical Chemistry B* **1997**, *101*, 4740.

(58) Gil, B.; Zones, S. I.; Hwang, S.-J.; Bejblová, M.; Cejka, J. *The Journal of Physical Chemistry C* **2008**, *112*, 2997.

Chapter 4. Dealumination of amorphous silica-aluminas with citric acid and its influence on acidity and activity

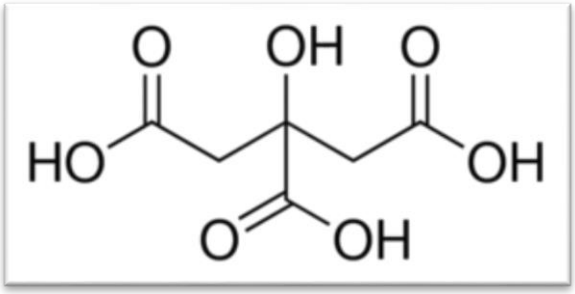

Abstract

A comprehensive study had been made on the modification of commercial amorphous silica alumina (ASA) by dealumination with citric acid (CA). The textural and chemical parameters that have been investigated are: pore structure and surface area (N_2 adsorption–desorption), acidity (NH_3-TPD, FT-IR of adsorbed pyridine and CO) and catalytic performances (3,3-dimethylbut-1-ene (33DMB1) isomerization). The effects of dealumination on the Al coordination and nature of hydroxyl group were investigated by ^{27}Al, ^{1}H MAS NMR and FTIR. It was found that CA dealumination decreases the Al content by a factor of 6 while increasing the surface area by about 50% and total acidity up to 41%. Moreover, the ratio of strong acid (Lewis or Brønsted) per Al can be increased up to 5 fold compared to the starting ASA. Dealumination under optimal conditions reveals Brønsted acid sites (BAS) similar in strength to those of zeolites based on CO adsorption FTIR and, by improving the access to acid sites, leads to an increased catalytic activity of 33DMB1 isomerization.

4.1 Introduction

As already introduced in **Chapter 3**, ASA contain a large fraction of Al atoms that are ineffective in terms of acidity. Dealumination is one of the available methods to reduce the fraction of these ineffective Al species and acetylacetone was used in **Chapter 3** for this purpose. Although interesting results were obtained using this molecule, the dealumination effectiveness, was limited. One possible reason for this limitation is the fact that acetylacetone acts only as a complexing agent. Compared to acetylacetone, Citric acid (CA) molecule has, not only three complexing groups (-COOH), allowing chelating interaction with aluminium, but also it is a polyacid (pKa_1 = 3.13, pKa_2 = 4.76 and pKa_3 = 6.39). Hence it acts both as acid leaching and chelating agent.[1] There are several reports regarding the use of this molecule for the dealumination of zeolites, either to remove framework aluminium (and more specifically Si(2Al) sites),[2] or to remove extra framework Al species.[3] In addition, Zaiku et al.[2] have shown that citric acid treatment can result in the insertion of extra framework Al into framework position (as evidenced by the decrease of the ^{29}Si NMR signal of Si(0Al) sites and increase of the Si(1Al) signal). Insertion of extraframework Al in framework position was later confirmed

by Fan et al.[4] for steamed HZSM-5 samples. These author also observed a recovery of the pore structure of steamed zeolite after citric acid treatment that they assigned to the removal of pore blocking extraframework debris. Therefore, it can be expected that dealumination effectiveness of CA would be superior to that of acetylacetone.

In the present study, treatment of commercial ASA with citric acid has been explored and dealumination conditions have been optimized. The influence of dealumination on the textural properties, acidity and catalytic activity was thoroughly studied. Furthermore, a mechanism for the dealumination of ASA with CA was proposed, which may result in a better comprehension for dealumination of ASA and provide guidance in the design of ASA with improved acidity and enhanced activity.

4.2 Experimental

4.2.1 Synthesis

4.2.1.1 Starting ASA

Two commercial ASAs in their ammonium form, GD13-NH_4^+ and GD25-NH_4^+ and in their H form (calcined samples), GD13-H and GD25-H were used as starting materials (see details in **Chapter 2** (§2.1.1 p47).

4.2.1.2 ASA dealuminated with citric acid

The starting ammonium form of ASA (2 g) was stirred during 4 h at room temperature in 10 ml of an aqueous solution of citric acid at a concentration ranging from 0.1 mol/L to 1.0 mol/L. Subsequently, the sample was immediately centrifuged, the supernatant was filtered with a CHROMAFIL ® syringe filters (0.20 μm) to get a solution free of solid phase for pH measurement and evaluation of Al and Si concentration in the solution. Then the solid was washed thoroughly with distilled water and dried at 110°C overnight. It was, thereafter calcined at 550°C for 5 h at a heating rate of 2°C/min. The obtained products were denoted as ASA-cCA, where "c" is the concentration of citric acid, CA represents citric acid. In absence of specific indication, the products are in calcined H form. For simplification, GDxx-cCA means starting in ammonium form instead of GDxx-NH_4^+-cCA.

In order to investigate the mechanism of dealumination with citric acid, reference samples were also prepared: (i) sample GD13-0.3CA(OH) was synthesized following the above procedure except for an extra step consisting in adding dropwise NaOH aqueous solution to adjust pH to 4.9 in the mixture (CA + ASA) at the beginning of the 4 h delay; (ii) sample GD13-HCl was obtained through treatment of GD13 with an HCl aqueous solution at pH = 1.6, i.e. a pH similar to the one of 0.3 mol/L CA (pH = 1.7).

4.2.2 Characterization and catalytic test conditions

Characterization methods and Catalytic test conditions used in this chapter have been already been described in § 2.2.

4.3 Results

4.3.1 Effect of dealumination on composition (Si/Al ratio) and texture

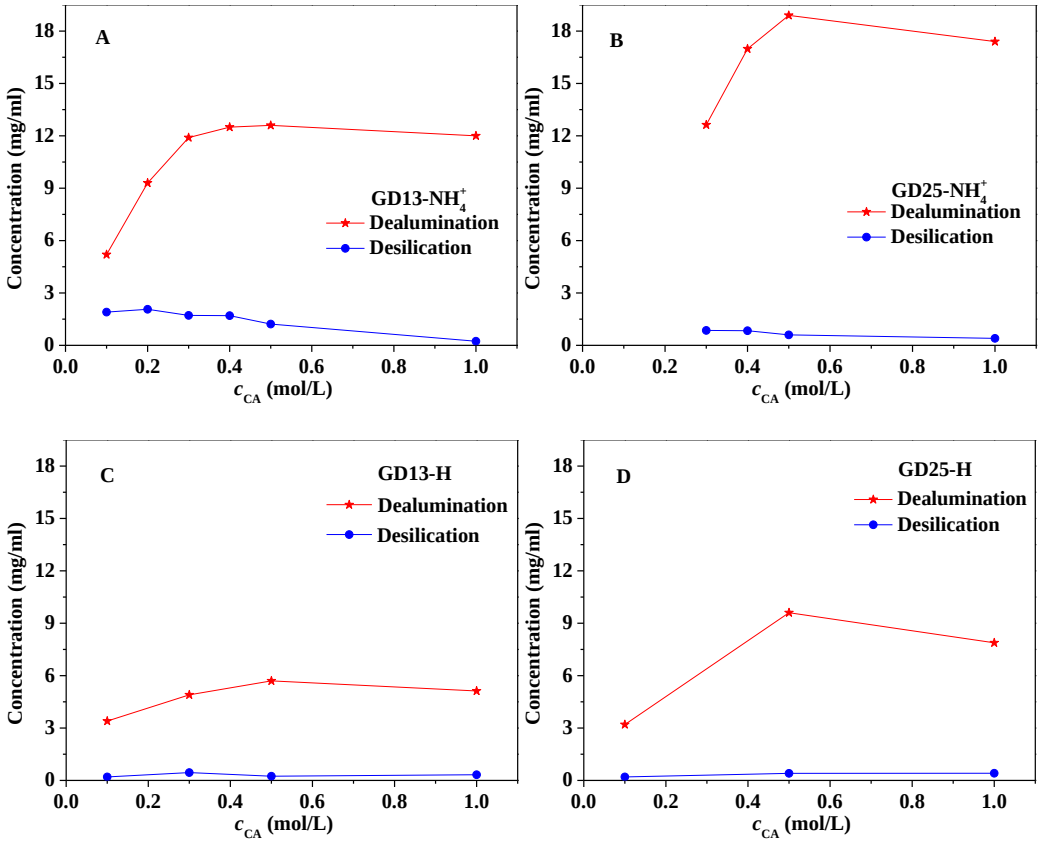

Figure 4-1 Influence of the concentration of CA on the concentration of Al (red curve) and of Si (blue curve) in the solution after dealumination, for: (A) GD13-NH_4^+; (B) GD25-NH_4^+; (C) GD13-H; (D) GD25-H

The influence of the concentration of CA in the dealumination solution on the extent of dealumination and desilication was monitored for several ASA by measuring the concentration

of Al and Si in the filtrate with XRF. The curves are shown in Figure 4-1. For all samples, a high concentration of Al and low concentration of Si in solution are detected for all concentration of CA. These values are consistent with the very low solubility of silicon[5] and the high solubility of aluminium, especially, in presence of citrate,[6] in the pH range 2-4 (considering the almost negligible solubility of silicon in this pH range, the small amount of silicon detected in the solution after dealumination could also be due to the presence of a small amount of remaining solid phase). Thus, dealumination rather than desilication is the dominant process in CA solution. The evolution of the extent of aluminium extraction with CA concentration is similar for all ASA: at low CA concertation, the amount of released Al increases with the concentration of CA and reaches a plateau at concentration of CA of 0.3-0.5 mol/L. As one could expect, the concentration of released Al, increases significantly between GD13-NH_4^+ (respectively GD13-H) and GD25-NH_4^+ (respectively GD25-H). Moreover, the amount of extracted Al is much lower for the H form ASAs than for their ammonium forms, indicating that dealumination is easier in the ammonium form. The pH of the CA solutions before and after treatment with ASA and the aluminium concentration in the calcined solid are reported in Table 4-1. At the end of the dealumination process, the pH of the solution is higher than initially. This can have two origins: firstly, the formation of soluble Al species and more specifically of $Al(H_2O)^{3+}$ implies the consumption of H^+ and should therefore increase the pH; secondly, considering the points of zero charge (PZC) of silica (PZC = 2-4) and of alumina (PZC = 8-9), surface hydroxyls will tend to become protonated at the low initial pH of the dealumination solution and hence a part of the protons from the solution could be consumed by this surface protonation. We will come back to this aspect more into details in the part dealing with the mechanism of dealumination.

The Al content of the dealuminated ASA was evaluated on the calcined solids using XRF (Table 4-1). These values are consistent with the Al concentration in the dealumination solution that have been commented above (the concentration of Al in solution is probably slightly overestimated by the calibration we used: indeed, for the GD13-0.5CA sample, based on the initial Al concentration and the final one, the samples undergoing the maximum dealumination,

the maximum Al concentration in solution should be 10.8 mg/mL, compared to 12.6 mg/mL measured experimentally). Treatment with CA results in remarkably high extents of dealumination when performed on the ammonium forms of the two ASAs (removal of 87% of initial Al for GD13-0.4CA and 75% for GD25-0.5CA). The extent of dealumination is significantly lower when the H forms of these ASA are used (-35% of Al for GD13-H-0.3CA and -43% of Al for GD25-H-0.5CA). It is worth mentioning that CA is much more efficient for the removal of Al form ASA than from zeolite.[4] A possible reason could be that ASA contains a larger fraction of Al species in the form of weakly bonded (polymeric) Al species than most zeolites.

Table 4-1 Al content and textural properties of different samples prepared by CA dealumination (pore size distribution was calculated by applying the BJH model to the adsorption curve and pore size value was taken at the maximum of the pore size distribution)

Sample	c_{CA}	Filtrate	Al	S_{BET}	Pore size	Pore volume
	pH	pH	mmol/g	m^2/g	nm	cm^3/g
GD13-H			2.3	445	4.8	0.70
GD13-0.1CA	2.1	4.1	1.7	453	4.2	0.72
GD13-0.2CA	1.8	3.4	1.0	517	3.7	0.78
GD13-0.3CA	1.7	2.8	0.4	598	3.3	0.69
GD13-0.4CA	1.7	2.6	0.3	699	3.3	0.63
GD13-0.5CA	1.6	2.5	0.3	662	3.0	0.55
GD13-H-0.3CA	1.7	2.2	1.5	445	4.2	0.66
GD25-H			4.0	421	4.8	0.70
GD25-0.3CA	1.7	3.3	1.9	537	3.7	0.55
GD25-0.5CA	1.6	2.6	1.0	619	3.3	0.54
GD25-1.0CA	1.4	2.3	1.0	636	3.3	0.53
GD25-H-0.5CA	1.6	2.1	2.3	509	4.2	0.72

Dealumination with CA has the unexpected consequence to change the textural properties of ASAs. These modifications are clearly seen by comparing the surface area, pore volume and pore size of the samples corresponding to different extent of dealumination (Table 4-1). It can be seen that, compared to the starting GD13-NH_4^+, the surface area of the dealuminated samples increases significantly upon increasing the extent of dealumination and

this increase reaches 56% (sample GD13-0.4 CA); the pore size (maximum of the pore size distribution, BJH calculation applied to the adsorption isotherm) decreases slightly with the CA concentration; the pore volume increases with CA concentration and reaches its maximum value for GD13-0.2CA and decreases afterwards. The series of samples prepared by dealumination of GD25-NH_4^+, displays the same tendency for the surface area (the maximum value is obtained for GD25-1.0CA and corresponds to an increase of surface area of 60%) and the pore size, whereas the pore volume decreases regularly with the concentration of CA in the dealumination solution. For the two starting ASA, when dealumination is performed on the H-form ASA, the surface area remains unchanged (GD13-H-0.3CA) or increases slightly (GD25-H-0.5CA), whereas the pore size decreases slightly.

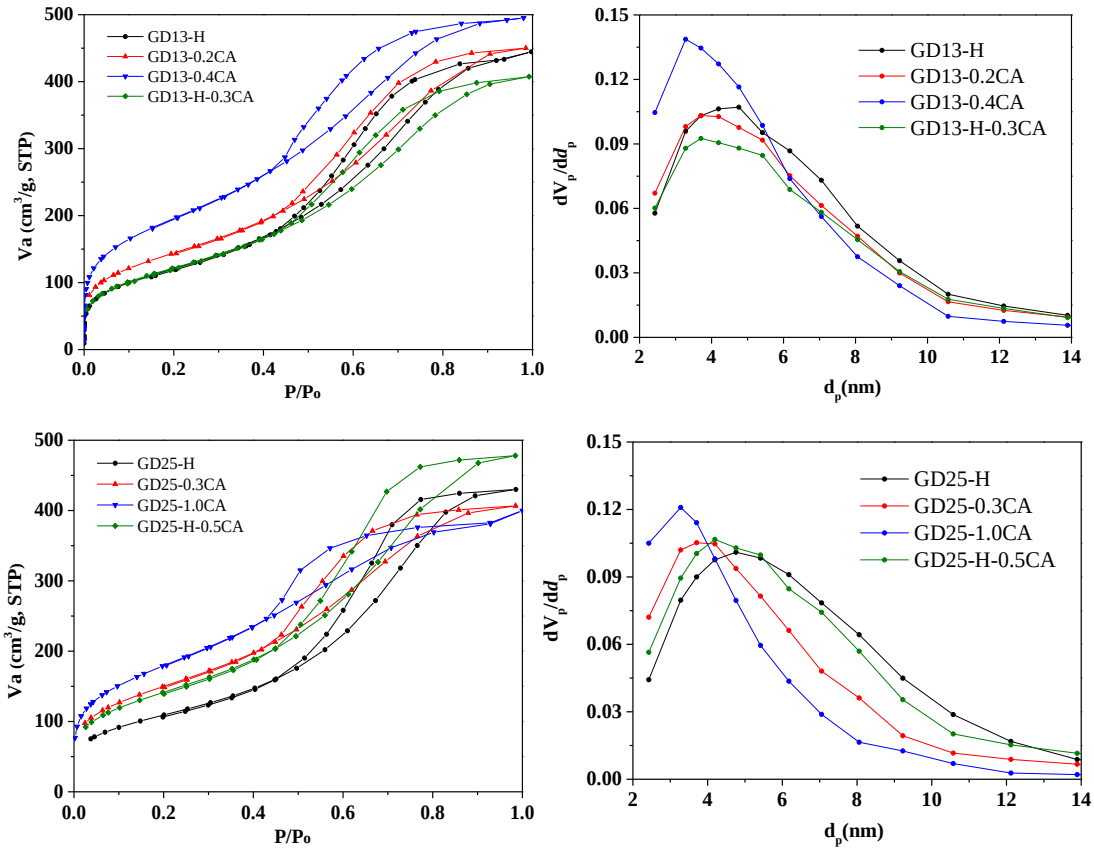

Figure 4-2 N_2 physisorption isotherms (left) and derived pore size distribution (right) of samples prepared by dealumination of GD13 (NH_4^+ and H form) (upper) and GD25 (NH_4^+ and H forms) (bottom)

Figure 4-2 shows the nitrogen adsorption-desorption isotherms and pore size distribution curves (BJH method applied to the adsorption isotherm) of representative samples. All samples exhibit a type IV isotherm with a type-H1 hysteresis loop, which is characteristic of

mesoporous materials with a relatively narrow pore size distribution and regular pores (by opposition with ink-bottle shaped pores). Dealumination of the ammonium forms of ASAs shifts gradually the pore size distribution to smaller value. When dealumination is performed on H form, no obvious change is detected.

Dealumination with CA (or other chelating acids such as oxalic acid[7]) has been investigated on zeolites, but, up to now, never been applied to ASA. An increase in the surface area and pore volume upon dealumination has also been reported for zeolites, and has been assigned to the removal of Al debris (extra-framework Al species) deposited on the external surface or located in the pore channel blocking the porosity.[4] The origin of the modification of the textural properties upon dealumination will be discussed latter on.

4.3.2 Acidic Properties

The influence of treatment with CA on the acidity was explored by ammonia temperature programmed desorption (NH_3-TPD) and FTIR of adsorbed probe molecules (pyridine and CO).

4.3.2.1 NH_3-TPD

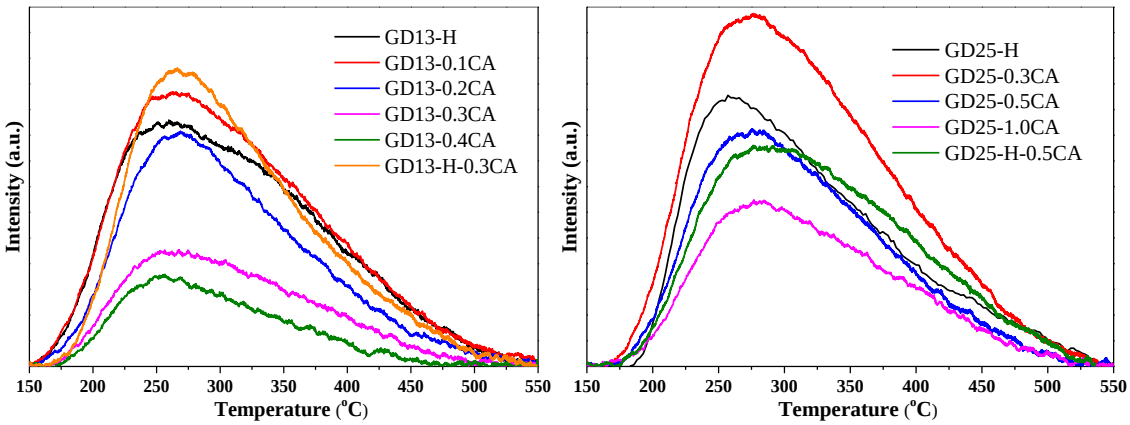

Figure 4-3 Acid properties of different samples determined by NH_3-TPD

NH_3-TPD has been used for a quantitative determination of the total acid site concentration (Brønsted and Lewis acidity). Figure 4-3 displays the TPD curves. Total amount of acid sites, based on the surface area of the desorption peak, are reported in Table 4-2, together with the ratio of acid sites per Al. Both starting ASA contain a relatively large amount of acid sites. As already reported in **Chapter 3**, GD25-H possesses only a slightly higher

amount of total acid sites as GD13-H. Considering that the aluminium content is almost twice higher, this indicates that the fraction of non-acidic Al is much higher in GD25 than in GD13. Removing a large amount of Al usually reduces the total amount of acid sites but increases the ratio of acid sites per Al.

Table 4-2 NH_3-TPD data of the CA dealuminated samples

Sample	Total acid sites	Weak acid sites	Strong acid sites	Acidity/Al
	mmol/g	mmol/g	mmol/g	%
GD13-H	0.42	0.16	0.26	18
GD13-0.1CA	0.47	0.20	0.27	28
GD13-0.2CA	0.33	0.13	0.20	32
GD13-0.3CA	0.19	0.07	0.12	44
GD13-0.4CA	0.13	0.06	0.07	39
GD13-H-0.3CA	0.37	0.16	0.21	26
GD25	0.46	0.12	0.34	12
GD25-0.3CA	0.50	0.14	0.36	26
GD25-0.5CA	0.31	0.11	0.29	30
GD25-1.0CA	0.23	0.12	0.11	24
GD25-H-0.5CA	0.44	0.13	0.33	23

As already discussed in **Chapter 3** (p68), the TPD curve is asymmetric and can be decomposed into two contributions corresponding to weak acid sites (Low Temperature –LT- peak) and strong acid sites (High Temperature –HT- peak). Peaks assigned to both weak and strong acid sites seem to loose intensity upon dealumination, but this result must be taken with caution because, as already commented on **Chapter 3**, although the presence of two contributions is not questionable, the decomposition of the TPD signal in these two contributions remains controversial, due to the strong overlap of the two contributions together with the unknown shape of the desorption peaks.[8]

4.3.2.2 FTIR of adsorbed pyridine

As NH_3-TPD does not allow to differentiate Lewis from Brønsted sites and because the evaluation of the fraction of strong acid sites by this method is questionable, quantification of acid sites by FTIR of adsorbed pyridine was also performed. The spectra after desorption of

pyridine at 150°C are shown on Figure 4-4.

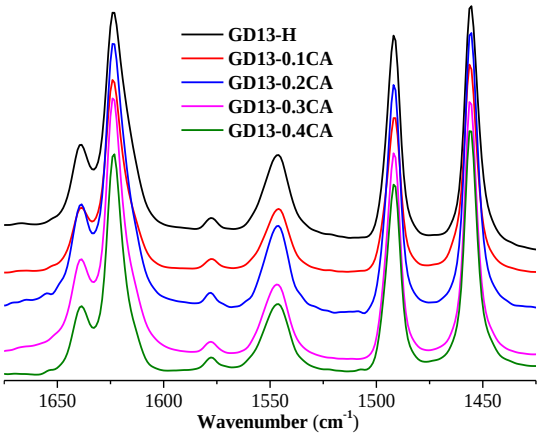

Figure 4-4 FTIR spectra of adsorbed pyridine after evacuation at 150°C on a series of samples prepared by dealumination of GD13 with citric acid

The evolution of the intensities of the bands at 1545 and 1450 cm^{-1} with desorption temperature (150, 250, 350°C) was used to evaluate the amount of total, medium and strong acid sites. The concentrations of mild (temperature of desorption between 150 and 250°C), medium (temperature of desorption between 250°C and 350°C) and strong (temperature of desorption higher than 250°C) Lewis and Brønsted acid sites (noted respectively LAS and BAS) are reported in Table 4-3.When the temperature reached 350°C, the band at around 1456 cm^{-1} remains while the band at 1549 cm^{-1} vanishes. This indicates the presence of strong LAS and absence of strong BAS.

The values reported in Table 4-3 clearly indicate that, under suitable concentration of CA, the total acidity increases. Starting from GD13-NH_4^+, under moderate dealumination conditions (0.2 mol/L of CA), little more than half of the aluminium species are extracted. However, this removal increases the total number of acid sites (+25%), and both Brønsted and Lewis acidity increased, respectively (from 34 to 43 μmol/g for the Brønsted sites and from 67 to 87 μmol/g for the Lewis sites). Starting from GD25-NH_4^+ (i.e. an ASA with a higher Al content), this increase is more pronounced: total acidity increases up to 41% and the increase in the amount of Lewis acid sites is stronger (from 70 to 104 μmol/g) than that of Brønsted acid sites. That increase could indicate that CA with suitable concentration can, not only remove selectively non-acidic aluminium while preserving the acidic ones, but also increase the total

acidity by opening an access to Al sites which were buried inside the pore wall. Alternatively, CA could also help to the transformation of non-acidic Al sites into acidic ones. Indeed, insertion of extra framework Al into framework position during CA treatment has been demonstrated for beta zeolites by Zaiku et al.[2] and later confirmed by Fan et al. for steamed HZSM-5[4]. Under more severe dealumination conditions (higher concentration of CA), the total acidity starts decreasing, however, even for the sample prepared with a CA concentration of 0.4 M, the amount of acid sites remains close to that of the starting ASA and the distribution of acid sites, in terms of strength and nature (Lewis vs. Brønsted) does not change significantly with the extent of dealumination. One can also observe that samples prepared by dealumination of GD25-NH_4^+ all exhibit a higher acidity than their GD13 derived counterpart, showing that the acidity of the dealuminated samples, is, at least partly inherited from the parent ASA. The distribution of acid sites, in terms of strength and nature (Lewis vs. Brønsted) does not vary significantly with the extent of dealumination.

Table 4-3 Acid type and strength distribution of the samples determined by pyridine-IR

Sample	Acidity(μmol/g)									Acidic Al (%)
	Total	BAS				LAS				
	B+L	Weak	medium	strong	total	weak	Medium	strong	total	
GD13-H	101	23	11	0	34	21	11	36	67	4.4
GD13-0.1CA	91	18	14	0	31	11	4	45	60	5.3
GD13-0.2CA	130	29	15	0	43	24	13	50	87	12.5
GD13-0.3CA	105	21	13	0	34	12	10	49	71	23.6
GD13-0.4CA	96	22	9	0	31	7	8	49	65	28.5
GD13-H-0.3CA	91	22	11	0	33	15	9	34	58	6.3
GD25-H	110	31	10	0	40	21	9	40	70	2.8
GD25-0.3CA	156	40	11	0	52	32	17	54	104	8.1
GD25-0.5CA	137	27	13	0	40	28	16	53	97	13.3
GD25-1.0CA	137	30	11	0	40	25	17	56	97	14.2
GD25-H-0.5CA	104	26	8	0	34	21	21	34	70	4.5

For the dealuminated samples prepared using the H form ASAs, a slight decrease of the total acidity occurs, indicating that dealumination may be less selective when applied on the H

form than on the ammonium one. For all ASA and whatever the CA concentration, strong BAS are never detected and the Lewis acidity is dominated by strong sites.

CA can very effectively remove Al without significant loss of the total acidity even under the most severe conditions. It has the additional benefit of increasing significantly the effective acidity (% of acidic Al): up to fivefold for GD13-NH_4^+ derived samples (from 4.4% for GD13-NH_4^+ to 28.5% for GD13-0.4CA see Table 4-3) and fourfold the GD25-NH_4^+ derived ASAs. The more important increase in effective acidity of GD13 is consistent with the facts that GD25 contains a higher fraction of non-acidic Al than GD13 and that CA dealumination upon this sample is less efficient than on GD13 (for GD13 up to 87% of the Al is extracted compared to 75% for GD25, see(Table 4-1). For the samples prepared by dealumination from the H form, the effective acidity improves only slightly as less Al was removed and total number of acid sites decreases.

4.3.2.3 FTIR of adsorbed CO

FTIR of CO adsorbed at low temperature is particularly suitable for probing the strength of acidic OH groups via the formation H-bond. Thanks to its weak basicity, CO interacts with all acid sites either strong or weak, Lewis or Brønsted. Moreover, as the interaction of CO with Brønsted acid sites occurs by the formation of an H-bond, CO can also inform on the strength of the Brønsted acid sites. Hence, depending on CO interaction mode, wavenumbers of υ(CO) bands can be directly related to the acidic strength of Lewis acid sites or hydroxyl groups (Brønsted acid sites, BAS).

FTIR of adsorbed CO was used on selected samples to further investigate the influence of CA dealumination on the acidity. Figure 4-5 presents the difference spectra during adsorption of increasing amount of CO on GD13-H and GD13-0.2CA and GD13-0.4CA; Figure 4-6 presents a comparison of the three samples after addition of ca. 250 µmol/g of CO. For GD13-H, with the first dose of CO (ca. 10 µmol/g), a negligible broad envelope appears at around 3450 cm^{-1} in the ν(OH) zone, indicating the adsorption of CO on acidic hydroxyl groups with different acidic strengths. Meanwhile, in the range of ν(CO), two bands appear at 2229

and 2173 cm^{-1}. After the second CO dose (ca. 30 µmol/g), the band at 3450 cm^{-1} becomes clearly visible and a new OH perturbed band is observed at 3562 cm^{-1}. The band at 2173 shifts a little to 2172 cm^{-1}. The bands at 2229 and 2172 cm^{-1} increase in intensity and additional bands at 2158 cm^{-1} and 2190 cm^{-1} become apparent. The introduction of additional doses (ca. 60, 150 and 250 µmol/g) leads to the appearance of a third OH perturbed component at 3654 cm^{-1}. All OH bands gradually increase but this band, together with the band at 3562 cm^{-1} become predominant. In parallel, in the CO zone, the bands at 2229 and 2192 cm^{-1} reach their maximum, indicating that CO saturates the strong and medium Lewis acid sites. The bands at 2172 cm^{-1} shifts to 2170 cm^{-1}; this band, and the one at 2157 cm^{-1}, keep increasing and become the two main peaks. A shoulder becomes visible at ca. 2138 cm^{-1} indicating the presence of physisorbed CO.

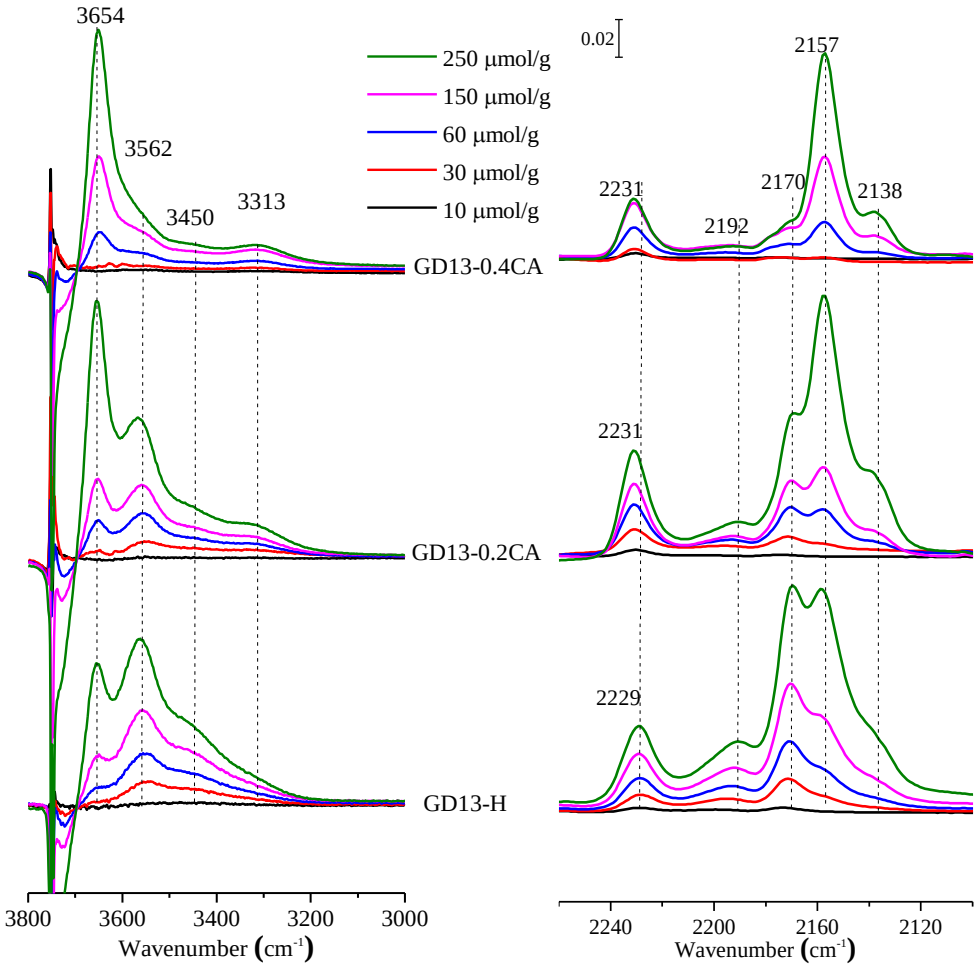

Figure 4-5 FTIR difference spectra of the ν(OH) zone (left) and ν(CO) zone (right) during adsorption of increasing doses of CO on GD13-H (top) and dealuminated samples GD13-0.2CA (middle) and GD13-0.4CA (bottom). All the spectra have been normalized by the weight of the wafer

The three perturbed-OH components at 3450, 3562, and 3654 cm^{-1} have been previously observed by Crépeau et al. [9] and Blanchard et al.[10] on ASA. The band at 3654 cm^{-1} is assigned to silanol groups (similar to those found in pure silica) perturbed by CO. Its appearance is associated with a negative band at 3751 cm^{-1} and the ν(CO) band at 2157 cm^{-1}. The band at 3562 cm^{-1} is indicative of the presence of mildly acidic OH groups (hydroxyls with a little higher acidity than silanols), while the band at 3450 cm^{-1} indicates the presence of strong acidic OH groups. Both bands are likely to be associated to the ν(CO) band at ca. 2170 cm^{-1}. The gradual shifts of this band from 2173 to 2170 cm^{-1} would be associated to the modification of the relative contributions of the associated bands in the ν(OH) range.

For sample GD13-0.2CA, beside the bands described above, a band, that was not detected upon adsorption of CO on GD13-H, can be clearly observed in the ν(OH) range at about 3310 cm^{-1}. Such high ν(OH•••CO) value is usually observed in zeolites and hence associated with the adsorption of CO on Si-OH-Al bridges.[11,12] This assignment cannot be fully ascertained based on the observation of the spectra of GD13-0.2CA due to the absence of the characteristic negative band in the 3570-3630 cm^{-1} range.[13] However, this negative band would be difficult to observe on the spectra due to the intense positive bands at 3560 and 3650 cm^{-1}. The presence of the band at 3310 cm^{-1} clearly indicates that GD13-0.2CA possesses BAS of zeolitic strength. Such band has been rarely observed in ASA and was, to the best of our knowledge, only reported by Hensen et al.[14] They observed, only for an ASA with a weak Al loading (5 wt% of Al_2O_3) prepared by deposition of Al on silica followed by calcination at high temperature (1073 K), a weak band at 3320 cm^{-1}, that was clearly visible at very low CO loading (between 2 and 14 μmol/g) upon adsorption of CO. They associated this band, to a band of ν(CO) appearing at 2178 cm^{-1} at very low CO loading. Moreover, cased on H_2/D_2 exchange experiments, that evidenced an OH band at 3630 cm^{-1}, associated with strong Brønsted acid sites, Hensen et al. concluded that the band at 3320 cm^{-1} was associated to hydroxyl band at 3630 cm^{-1}.

The comparison, at high CO loading (ca. 250 μmol/g), of the spectra of GD13-H and GD13-0.2CA (Figure 4-6) also reveals that mild dealumination increases the amount of strong Lewis sites, while apparently keeping mild Lewis (ν(CO) band at 2200 cm^{-1}), and mild

Brønsted sites (ν(OH) band at ca. 3450 cm^{-1}). This comparison also clearly shows that the strong Brønsted sites observed on the dealuminated sample were not present in the starting ASA (or in a significantly smaller amount).

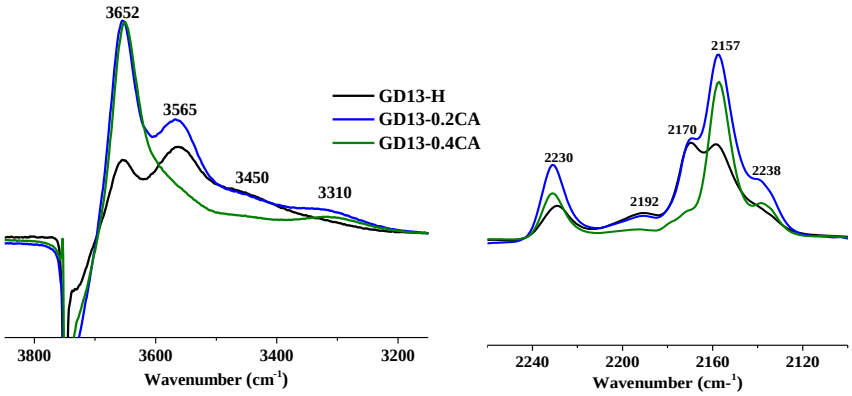

Figure 4-6 Comparison of the difference spectra of GD13-H, GD13-0.2CA and GD13-0.4CA at a CO loading of ca. 250 µmol/g, all the spectra have been normalized by the weight of the wafer

On the spectra of sample GD13-0.4CA, i.e. a sample prepared using more severe dealumination conditions, the peak at about 3310 cm^{-1} can still be clearly observed, while the bands corresponding to CO adsorbed on the mild (3450 cm^{-1}) and weak (3562 cm^{-1}) Brønsted acid hydroxyls strongly decrease in intensity and almost vanish. These observation indicates that the enhanced BAS of zeolitic strength were retained under these more severe dealumination conditions, whereas the Al atoms associated with the mild and weak acid sites were removed. In parallel, in the CO stretching zone, the intensities of the peaks associated with strong and mild Lewis sites are divided by a factor of ca. 2 and the peak associated with CO adsorbed on the Brønsted acid sites decreases strongly (with regards to GD13/0.2CA, see Figure 4-6). For this peak, one can clearly see two components, one located at ca. 2177 cm^{-1} (shoulder) and another one at ca. 2170 cm^{-1}. The first component is likely associated with the ν(OH•••CO) at 3310 cm^{-1} while the second one is probably due to the other two contributions at 3450 and 3562 cm^{-1}. Hence, severe dealumination modify significantly the acidic properties of the ASA. In these conditions, dealumination is not limited to the Al atoms without acidic properties. Nevertheless, the Al atoms associated with the strongest Brønsted acid sites are not removed from the ASA under these conditions.

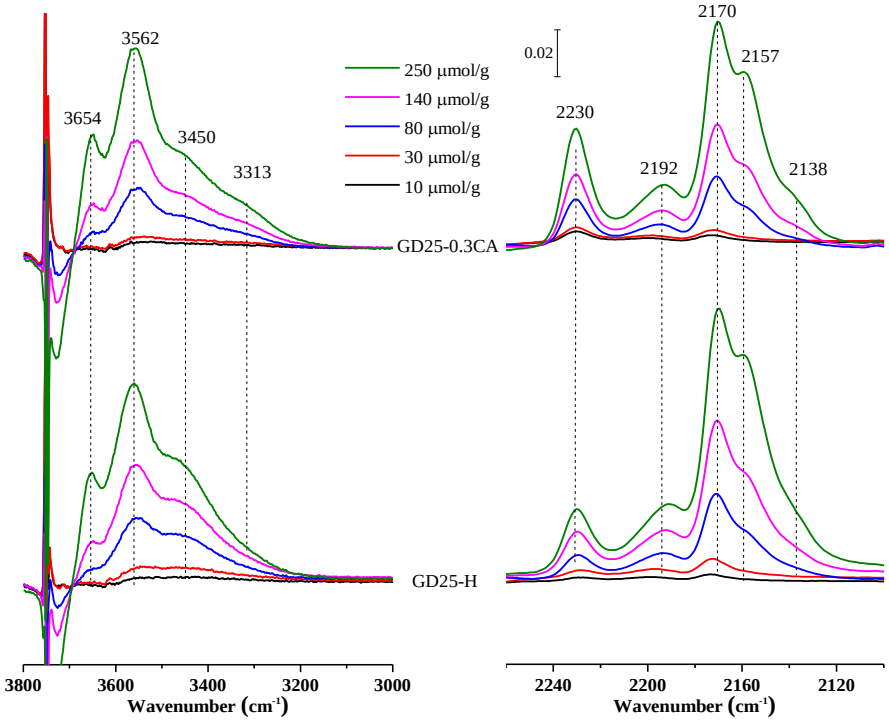

Figure 4-7 Difference FTIR spectra in ν(OH) (left) zone and ν(CO) (right) zone during CO adsorption on GD25-H and dealuminated sample GD25-0.3CA as a function of CO coverage. All the spectra have been normalized by the weight of the wafer

The influence of CA dealumination on GD25, i.e. an ASA containing a higher Al content has also been explored by FTIR of adsorbed CO. Figure 4-7 displays spectra of the adsorption of increasing amount of CO on GD25-H and GD25-0.3CA, while Figure 4-8 shows a comparison of the difference spectra of these two samples after adsorption of ca 250 µmol/g of CO. The difference spectrum obtained upon adsorption of CO on GD13-H at a similar CO coverage is also shown for comparison. The evolution of the difference spectra of these two samples with CO loading is the same as for the previous sample. We will therefore focus on the comparison at high CO loading (ca. 250 µmol/g, Figure 4-8).

The difference spectrum of GD25-H is quite similar to the one of GD13-H in both ranges. In the ν(CO) range, the bands characteristic of CO adsorbed on strong and mild Lewis acid sites and the bands of CO adsorbed on Brønsted acid sites and on silanols are observed. The intensity of the band of CO on strong LAS is similar for GD13-H and GD25-H whereas the intensities of the bands of CO on mild Lewis and on Brønsted sites are slightly higher on GD25-H than on GD13-H. Mild Lewis acid sites are similar to those found on γ-alumina. Hence, the

higher amount of mild Lewis sites is consistent with the higher fraction of non-acidic Al (likely alumina-like domains) in GD25-H.

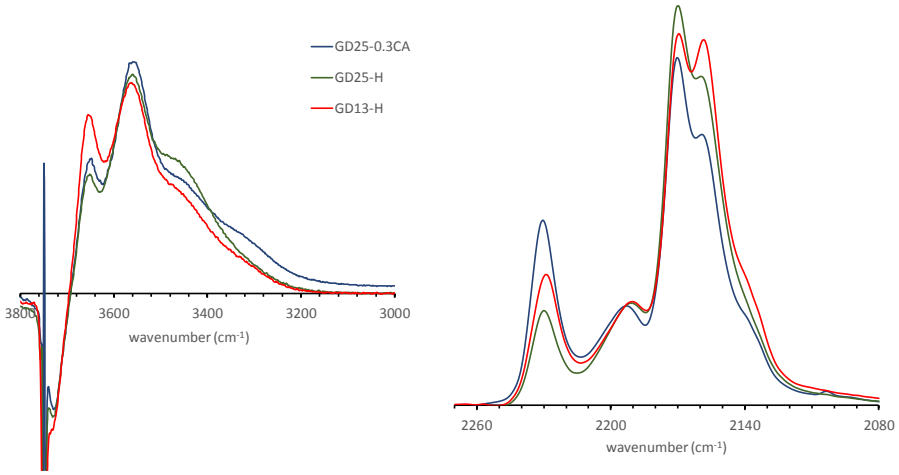

Figure 4-8 Comparison of the difference spectra in ν(OH) (left) zone and ν(CO)(right) zones after adsorption of ca. 250 µmol/g of CO adsorption IR spectra on GD13-H, GD25-H and GD25-0.3CA, all the spectra have been normalized by the weight of the wafer

The effect of CA dealumination on GD25-NH_4^+ is similar to what was observed for GD13-NH_4^+ after mild dealumination (GD13-0.2CA). In the ν(CO) range, the band associated with CO adsorbed on the strong Lewis sites increases significantly, while those associated with the mild Lewis acid sites and the Brønsted sites are almost unchanged. In the ν(OH) range, the band associated with CO adsorbed on the mild Brønsted sites (3450 cm^{-1}) decreases slightly, while a band corresponding to CO adsorbed on strong Brønsted sites (at ca. 3310 cm^{-1}), similar to those of zeolites is clearly visible.

4.3.2.4 Characterization of the acidic properties: conclusion

The acidic properties of the ASA and their modifications upon dealumination with CA have been investigated by means of NH_3-TPD, FTIR of adsorbed pyridine and FTIR of adsorbed CO. The characterization of the acidities of the samples using NH_3-TPD, did not give useful information because of the presence of over-adsorbed NH_3 (low temperature peak) and the resulting difficulty in the evaluation of the amount of strongly adsorbed NH_3 (high temperature peak). For the other two techniques, they give both valuable and consistent information. Based on pyridine adsorption, one can conclude that a mild dealumination increases the amount of Lewis and Brønsted acid sites, whereas, under more severe conditions,

the amount of Brønsted and Lewis sites starts decreasing slightly. FTIR of adsorbed CO confirms these results but also gives complementary information: under mild dealumination conditions, a new type of Brønsted acid sites is observed corresponding to strong Brønsted acid sites, similar to those found in zeolite. The amounts of the other types of acid sites are not significantly modified under these conditions. When more severe dealumination conditions are used, the amounts of all acid sites start decreasing except for the strong Brønsted acid sites, whose amounts are not modified. In briefly, mild dealumination removes only non acidic Al while revealing (or creating) strong Brønsted acid sites; severe dealumination removes non acidic Al but also a fraction of the Al atoms responsible for the acidic properties. The Al atoms associated with the strong Brønsted sites are not sensible to dealumination, even under these severe conditions.

4.3.3 Catalytic Performance for the isomerization of 3,3-dimethylbut-1-ene

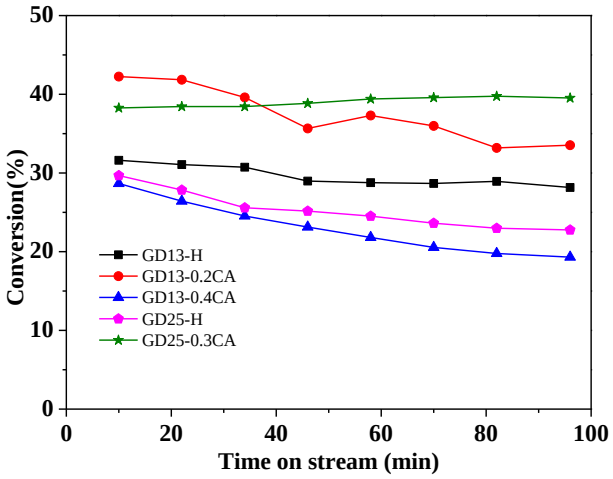

Figure 4-9 Conversion of 33DMB1 as a function of time on stream for the 2 starting ASA and the derived CA dealuminated samples

Figure 4-9 shows the conversion of the ASAs (starting ASAs and ASAs obtained by dealumination with CA) as a function of time on stream. For all samples, a moderate deactivation followed by a stabilization is observed. This deactivation is probably due to the deposition of coke owing to other secondary reactions or to the presence of traces of impurities in the feed. More specifically we identified, in the reactant (97%, Sigma Aldrich), isoprene, which is a common impurity of 33DMB1.[15] We observed that the presence of this impurity

was associated with severe deactivation, probably because this diene was a precursor to coke that poisoned the acid sites.[16] As isoprene has a lower boiling point (34ºC) than 33DMB1 (41ºC), it could be removed by flowing N_2 at low temperature through the saturator. Alternatively, we found another source of 33DMB1 (97.5%, Alfa Aesar) that was free of this impurity. The results reported here were obtained using reactant feeds free of isoprene.

The conversion of GD25-H is higher than that of GD13-H and the conversions after mild dealumination (GD25-0.3CA and GD13-0.2CA) are higher than that of their respective starting ASA. These results are consistent with the increase in the Brønsted acidity after mild dealumination evidenced by adsorption of pyridine. Based on literature, only the Brønsted acid sites that desorb pyridine above 220°C are strong enough to isomerize 33DMB1.[17] Hence, 33DMB1 should mostly correlate with the amount of acid sites that retain pyridine at 250°C (medium BAS, see Table 4-3), but could also correlate with the total amount of BAS, because the BAS desorbing pyridine between 220 and 250°C are included in the weak BAS. GD13-0.4CA displays a lower activity than GD13-0.2CA, close to the one of the starting GD13, which is also consistent with the evolution of the amount of BAS based upon pyridine adsorption.

As 33DMB1 isomerization is sensible to medium strength acid sites, testing the activities of these ASA for other model reactions, sensitive either to mild (e.g. isomerization of methylene cyclohexane) or to strong Brønsted acid sites (such as isomerization of methylcyclopentane) could help identify the nature of the Brønsted sites in these ASA and their evolution with dealumination.[17,18]

4.3.4 Aluminium coordination

^{27}Al MAS NMR has been applied to follow the evolution of the local Al environment as a function of the dealumination treatment. The left part of Figure 4-10 displays the ^{27}Al MAS NMR of the ammonium forms of the two ASA before and after treatment with CA. For the different coordination, the amount of aluminium species have been quantitatively calculated by fitting the peaks and the results are summarized in Table 4-4.

As already commented in **Chapter 3**, the spectrum of GD13-NH_4^+ shows two main peaks

at 56 and 4 ppm, attributed, respectively, to 4-coordinated Al (Al^{IV}) and 6-coordinated Al (Al^{VI}); a third, weaker, peak is also observed at ca. 30 ppm, that can be assigned to 5-coordinated aluminium (Al^{V}).

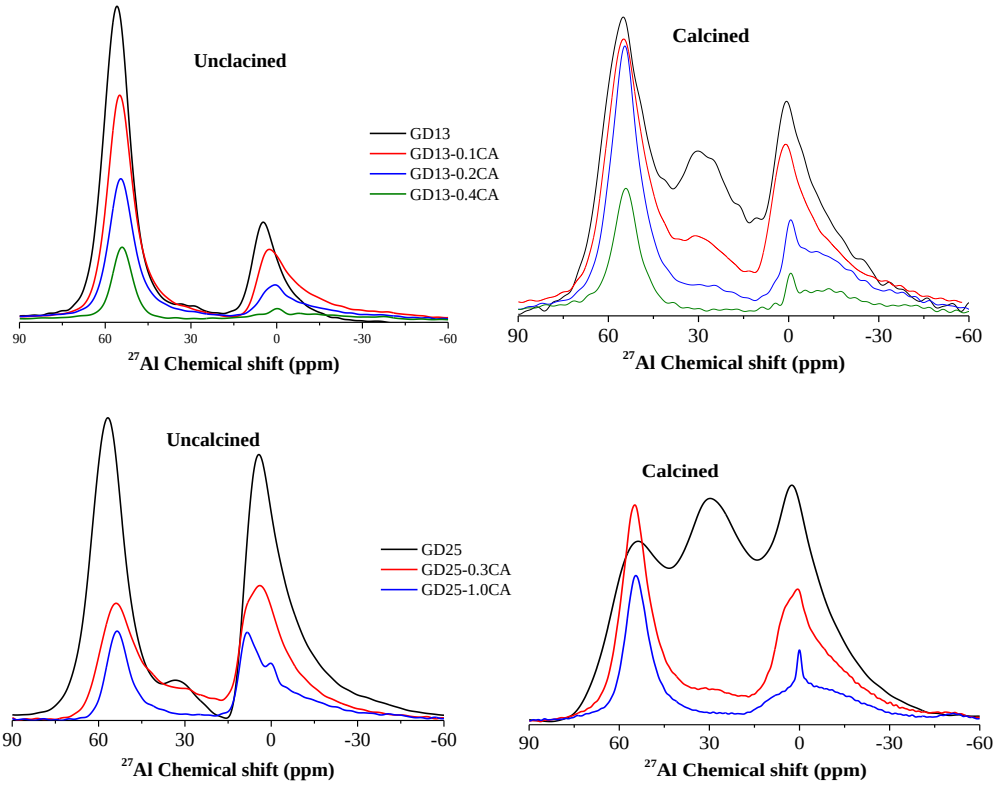

Figure 4-10 ^{27}Al MAS NMR of starting ammonium form and dealuminated samples before (left) and after calcination (right), all curves have been normalized by sample weight and calcined samples were rehydrated before measurement. Left parts correspond to GDxx-nCA-NH_4^+/H_2O and right parts to GDxx-nCA-H/H_2O in **Chapter 5**

After treatment of GD13-NH_4^+ with CA, the overall amount of Al in the samples, based on a quantitative analysis of the ^{27}Al MAS NMR signal area decreases, confirming that dealumination took place. The more severe the dealumination conditions, the stronger the loss of intensity. This result is consistent with the decrease in the aluminium concentration observed by elemental analysis (Table 4-1). Moreover, the peak assigned to tetrahedral aluminium shifts to a lower field, indicating that Al^{IV} are in a more siliceous environment[19] caused by dealumination. After severe dealumination (GD13-0.4CA), the peak corresponding to Al^{IV} becomes slightly narrower and represents more than 80% of all remaining Al atoms, while the intensity of the peak associated Al^{VI} further decreases.

As already commented in **Chapter 3**, compared to GD13-NH_4^+, GD25-NH_4^+, despite an

almost twice higher Al content, displays similar intensity for Al^{IV} (peak at 56 ppm) and therefore, most of the increase in the Al content contributes to Al^{VI} (peak at 4 ppm) and, to a lower extent, to Al^{V} (shoulder at ca. 30 ppm). The effect of dealumination for this ASA is almost the same as the one observed for GD13-NH_4^+: a global loss of intensity, a right shift in the position of the peak associated with Al^{IV} and a narrowing of this peak. However, the proportion of Al^{IV} and Al^{VI} do not seem to vary significantly with dealumination.

Table 4-4 Distribution of various aluminium species in samples based on the deconvolution of their normalized ^{27}Al MAS NMR, Al content was calculated based on the amount of Al in the corresponding sample determined by elemental analysis

Sample	Uncalcined						Calcined					
	Al percentage (%)			Al content (mmol/g)			Al percentage (%)			Al content (mmol/g)		
	Al^{IV}	Al^{V}	Al^{VI}	Al^{IV}	Al^{V}	Al^{VI}	Al^{IV}	Al^{V}	Al^{VI}	Al^{IV}	Al^{V}	Al^{VI}
GD13	64.5	3.6	32.0	1.48	0.08	0.74	43.0	17.8	39.2	0.99	0.41	0.90
GD13-0.1CA	68.0	4.2	31.8	1.16	0.07	0.54	50.3	10.4	39.3	0.86	0.18	0.67
GD13-0.2CA	70.6	2.2	27.2	0.71	0.02	0.27	54.5	6.7	38.4	0.55	0.07	0.38
GD13-0.4CA	81.2	0.0	18.8	0.24	0.00	0.06	64.3	0.0	35.7	0.19	0.00	0.11
GD25	45.2	3.6	51.2	1.81	0.14	2.05	26.6	30.5	42.9	1.06	1.22	1.72
GD25-0.3CA	36.3	6.3	57.4	0.70	0.12	1.11	37.9	11.1	51.1	0.73	0.21	0.98
GD25-1.0CA	49.1	0.2	50.7	0.47	0.00	0.49	55.1	0.0	44.9	0.53	0.00	0.43
GD13-H-0.3CA	54.7	9.3	36.0	0.79	0.13	0.52	45.7	15.2	39.0	0.66	0.22	0.56
GD25-H-0.5CA	44.2	8.0	47.8	1.02	0.18	1.10	37.1	16.4	46.5	0.85	0.38	1.07

Dealumination also strongly modifies the Al speciation on the calcined ASA and the extent of this modification follows the severity of the dealumination conditions: under moderate dealumination conditions (CA concentration of 0.2 M for GD13-NH_4^+ and of 0.3 M for GD25-NH_4^+), dealumination mostly concerns five-fold coordinated Al atoms, whereas, at higher CA concentration, Al^{IV} and Al^{VI} also diminish, but the diminution of Al^{VI} is stronger than that of Al^{IV}.

Figure 4-11 displays the ^{27}Al MAS NMR spectra of the calcined ASAs before and after treatment with CA. CA treatment on calcined ASA also tends to remove preferentially Al^{V}. It is noteworthy that most of these five-coordinated Al species were not 5-coordinated in the

ammonium form. Hence the Al species that are the most prone to dealumination (independently of the choice of the form of the starting ASA-NH_4^+ or -H) correspond to Al atoms with flexible coordination. One possible explanation would be that a flexible coordination favors the interaction with the CA molecules.

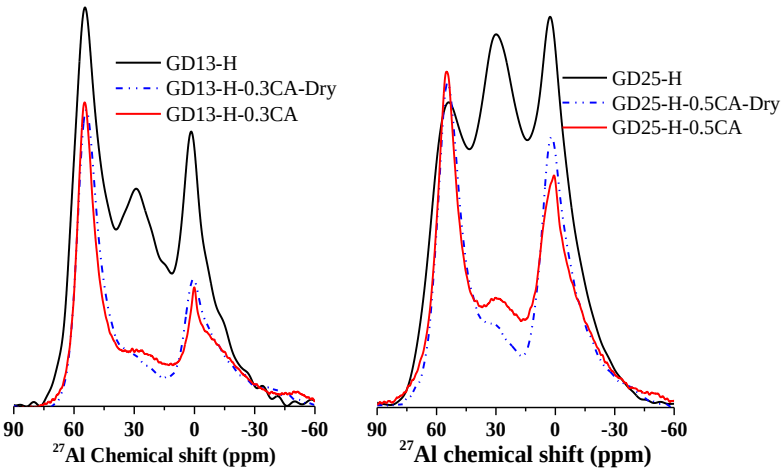

Figure 4-11 ^{27}Al MAS NMR of starting calcined and dealuminated samples, the dash lines stand for samples without calcination. All curves have been normalized by sample weight and calcined samples were rehydrated before measurement

4.3.5 Hydroxyl groups

Figure 4-12 shows ^{1}H MAS NMR spectra of dehydrated calcined H form of GD13 and dealuminated samples derived from this ASA. Decomposition of these ^{1}H MAS NMR spectra has been performed in order to attempt to quantify each type of proton. The peak assignments and their corresponding calculated concentration were summarizing in Table 4-5. As reported in **Chapter 2**, TGA and quantitative ^{1}H NMR experiments using HR-MAS rotors give consistent results. Hence, the total amount of protons was determined by TGA, and, for each sample, the concentration of a specific type of proton was calculated based on the total concentration of protons and the fraction of protons of this type deduced from the decomposition of the ^{1}H NMR spectrum.

For all samples, the dominant signal at 1.8 ppm can unambiguously be assigned to silanol. Based on the literature on aluminas and zeolites, the positions of the three other signals, 2.5, 3.7 and 6.5 ppm could correspond respectively to nonframework Al-OH-Al species[20], framework Si-OH-Al bridging hydroxyl groups located in a large structure units on ASA based on this position in zeolites,[21] and H-bonded Al-OH.[22,23]

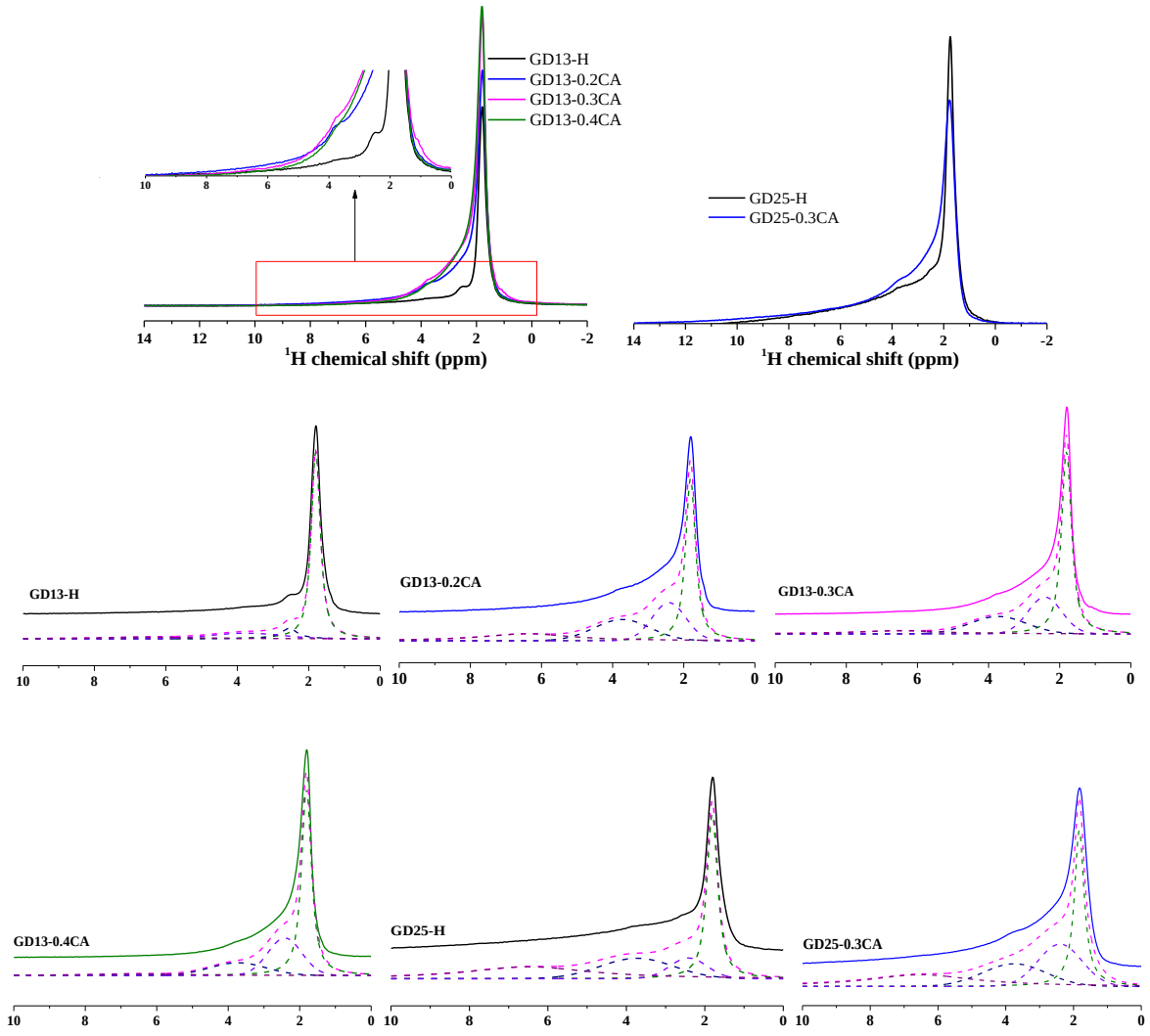

Figure 4-12 ^{1}H MAS NMR of various samples dehydrated at 200°C. Deconvolution with Lorentzian-Gaussian-shape peaks showing the contributions of various sorts of hydrogen groups. Experimental spectra (top) are compared with simulated spectra (middle) and each component spectra (bottom)

After CA treatment upon GD13, the density of hydroxyls (TGA) increases, which is due to the increase in the surface area: the surface density of hydroxyls, that can be calculated based on the density and the surface area, actually decreases gradually from 4.7 OH per nm^2 for GD13-H to 3.4 OH per nm^2 for GD13-0.4CA. This decrease is consistent with the dealumination of the ASA. Indeed the density of surface hydroxyls of alumina (ca. 8 OH/nm^2)[24] is higher than the one of silica (ca. 5 OH/nm^2)[24]. Hence, this decrease could be due to the removal of an alumina like phase. This hypothesis is confirmed by the fact that the density of surface hydroxyls of GD25 is even higher (5.5 OH/nm^2) and decreases even more strongly upon dealumination (3.9 OH/nm^2 for GD25-0.3 CA).

The increase in the amount of hydroxyls upon dealumination is confirmed by the comparison of the ^{1}H MAS NMR spectra of the starting ASA and the derived dealuminated samples. Moreover, this comparison evidences, for the two ASAs, a change in the distribution of protons with a clear increase in the intensity of the left shoulder (corresponding to the peak at 2.6 and 3.8 ppm) after dealumination.

Table 4-5 Assignment of the different bands in ^{1}H MAS NMR and the concentration of the various proton species in the starting and dealuminated samples

Sample	n_H (mmol/g)				
	Total (TGA)	1.8 ppm (Isolated and terminal Si-OH)	2.5 ppm (Al-OH and/or H donor Si-OH)	3.8 ppm (Si-OH-Al bridges and/ or H donor Si-OH)	6.5 ppm (H donor Al-OH)
GD13-H	3.5	2.6	0.3	0.4	0.2
GD13-0.2CA	4.0	2.0	0.8	0.7	0.5
GD13-0.3CA	4.2	2.1	1.0	0.8	0.3
GD13-0.4CA	4.0	2.2	1.0	0.6	0.2
GD25-H	3.6	1.3	0.4	0.8	1.1
GD25-0.3CA	3.5	1.1	0.9	0.8	0.8

The densities of OH groups corresponding to the peaks at 2.5 and 3.8 ppm are quite high for all samples and increase upon dealumination. The intensity of the peak at 2.5 ppm, increases with dealumination for all samples. Although dealumination may generate more Al-OH, the amount of hydroxyls per Al do not make sense for most samples (for example, for the samples prepared by dealumination of GD13 with 0.3 M and 0.4 M CA, the densities of Al are respectively 0.4 and 0.3 mmol/g. Hence densities of Al-OH of 1.0 mmol/g do not make sense and H donor SiOH also contribute to this peak. For the peak at 3.8 ppm, there is a clear inconsistency between the amount of Brønsted acid sites estimated using pyridine adsorption (about 30-40 µmol/g) and the density of hydroxyls associated with this peak, which varies between 0.4 and 0.8 mmol/g. Hence, this peak cannot be assigned to Si-OH-Al bridges exclusively (see Table 4-3) and a large part of the ^{1}H signal detected at this position is probably due to H-bonded silanols or aluminols. This confirms that the direct observation, in ASA, of BAS by ^{1}H MAS NMR spectroscopy is rather difficult.[25] Another point that must be mentioned,

is the difficulty to evaluate correctly the fraction of hydroxyls corresponding to the signals at 2.5, 3.8 and 6.5 ppm, because these hydroxyls are associated with broad and unsolved peaks (the contributions are overlapping), making the decomposition of the NMR signal very challenging. In addition, for technical reasons, the use of HRMAS rotor was not possible. These proton measurements were made with standard rotors, so there may also have a problem of homogeneity of the field.

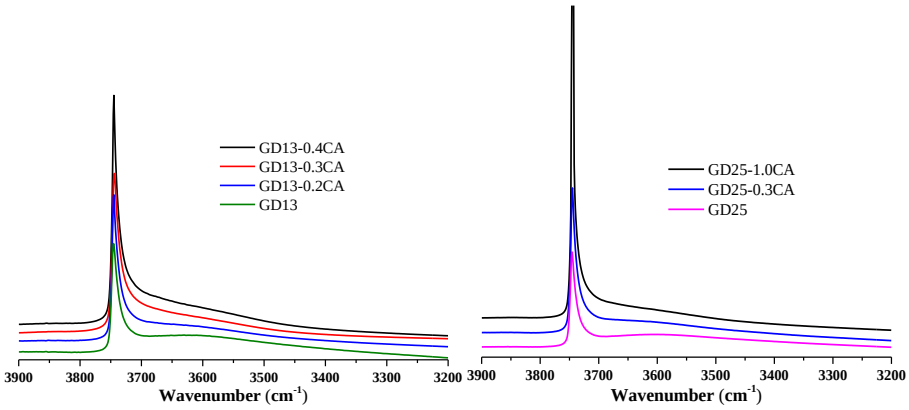

Figure 4-13 υ(OH) ranges of FTIR spectra of different samples activated at 450°C

Further information on the nature of hydroxyl groups in the samples was acquired by FTIR spectra, as shown in Figure 4-13. All the samples displayed one sharp and asymmetric band at 3745 cm^{-1}, attributed to accessible, isolated silanol groups.[26-30] In addition, a broad envelop extending from 3700 to 3300 cm^{-1} can be also detected, generally assigned to hydrogen-bonding Si-OH groups (H-donor).[31] It could also include a contribution of Si-OH-Al groups, but these bridging hydroxyl groups are not detectable in agreement with previously published work on ASA.[9,32] This broad envelop is more intense on starting ASAs than on dealuminated samples. The decrease of the intensity of this signal upon decreasing the Al content could indicate that this envelop also contains, in agreement with NMR data, a contribution of Al-OH-Al bridges (possibly H-bonded).

4.4 Discussion

4.4.1 Mechanism of dealumination with CA

In order to understand better the respective effect of the acidity and the chelating

properties of CA on the dealumination of ASA by CA, two others samples have been prepared using modified conditions. The first one was prepared by replacing the solution of CA by a solution of HCl of the same pH (sample GD13-HCl, initial pH = 1.7, i.e. the almost same initial pH as GD13-0.3CA) with the purpose to explore the effect of acidity. The second one was prepared by increasing the pH of the dealumination solution to 4.9, while keeping the same CA concentration as GD13-0.3CA (sample GD13-0.3CA(OH)), with the purpose to enhance the chelating properties of CA (by increasing the dissociation of this polyacid) and to decrease the effect of the acidity. Both samples were compared to GD13-0.3CA (i.e, the sample and their characteristics are summarized in Table 4-1.) For the sample prepared using the standard conditions, the treatment results in a severe dealumination (removal of 83% of Al species). This dealumination goes with an important increase of the surface area (from 445 to 598 m^2/g), a decrease of the acidity of the solution (from 1.7 to 2.8), together with a small decrease of the pore size.

Table 4-6 The various parameters during dealumination upon CA and texture properties

Sample	c_{CA}	Filtrate			Al[e]	S_{BET}	Pore	Pore
	pH[a]	pH[b]	Al[c]	Si[d]			Size	Volume
			mg/ml	mg/ml	mmol/g	m^2/g	nm	cm^3/g
GD13-H					2.3	445	4.2	0.68
GD13-0.3CA	1.7	2.8	11.9	1.72	0.4	598	3.7	0.69
GD13-0.3CA(OH)	4.9	5.9	3.0	0.78	1.9	434	4.2	0.63
GD13-HCl	1.6	1.7	0.0	0.07	2.3	445	4.2	0.66
GD13-H-0.3CA	1.7	2.2	4.9	0.45	1.5	445	4.2	0.66

[a] the starting CA concentration [b] the first filtrate [c]Al concentration in the filtrate(mg/ml) [d]Si concentration in the filtrate(mg/ml) [e]Al concentration in the calcined sample

When NaOH is added to the aqueous solution to adjust initial pH to 4.9, i.e. a pH that increases the proportion of deprotonated CA in the solution, and should therefore strengthen the chelating properties of CA, see Figure 4-14, the dealumination is strongly reduced and so are the modification of the acidity of the solution (from 4.9 to 5.9, i.e. a relatively weak modification considering the logarithmic scale) and of the textural properties. For the sample prepared without CA and at the same pH (HCl addition), the pH is hardly modified and surface

area and Al content are unchanged. These results indicate that both low pH and the presence of a chelating agent are required for an efficient dealumination. Furthermore, these above results also confirm that all the other modifications in the solution (increase of the pH) and on the texture (increase of the surface area and decrease of the pore size) are related to dealumination.

Citric acid = AH_3 = $HOC(COOH)(CH_2COOH)_2$

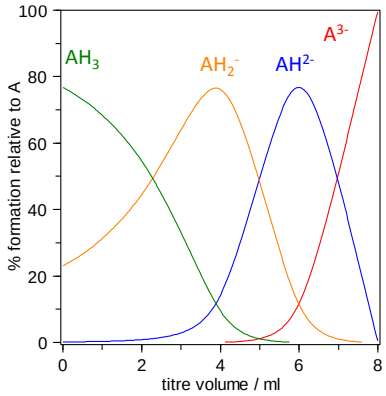

Figure 4-14 Speciation of citric acid and its partially and fully deprotonated associated bases as a function of the pH (calculation performed using HySS 2009[33])

To understand better the relation between dealumination and pH of the solution, we have plotted the speciation of the species present in the dealumination solution using HySS2009 software[33] (Figure 4-15), using beside the constants already included in the software, the stability constants for Al complexation with citric acid reported in the literature.[34] This calculation evidences the complex speciation of aluminium in the dealumination solution. At the starting pH of the dealumination solution, the Al is mostly present as Al^{3+}, but its formation requires the consumption of H^+ (≡Al-O-M + H_3O^+ → ≡Al-OH_2^+ + HO-M, where M = Al or Si). Hence, the pH will gradually increase with the release of aluminium and the speciation of Al will gradually shift toward the formation of other Al species such as AlCA and $AlOHCA^-$ that require less H^+ for their formation.

Hanudin et al.[35] studied the interaction of organic acids (acetic, oxalic and citric acid) with allophane, an aluminosilicate amorphous clay present in volcanic ash soils, at pH ranging from 4 to 10. Although, this study was performed at higher pH than the one used in the present work, the results they obtained and the mechanisms they proposed are still pertinent. They

observed an adsorption of the organic acid on the clay. The amount of adsorbed citric acid increases with the concentration of citric acid in the solution and decreases when the pH of the solution increases. The higher amount of adsorbed citric acid at low pH was assigned to the protonation of aluminol, because the formation of positively charged Al-OH_2^+ species facilitates the interaction of negatively charged citrates (H_2CA^- or HCA^{2-}) with the solid. These authors also studied the Al and Si release in the solution as a function of the pH and the concentration of organic acid. They observed that the amounts of released Si and Al increase with the concentration of organic acid in the solution and decreases upon increasing the pH of the solution. They concluded that, at low pH, protons contribute more than the chelation by the organic acid to the dissolution of the allophane. They also observed that increasing the pH of the solution favors the selective removal of Si. They concluded that increasing the pH results in an increase in the concentration of COO^- in solution (the acid functions being more deprotonated) which have a greater capability of breaking bonds. However, increasing pH also has the revert effect of decreasing the amount of positive charges (and even building negative charges) on the surface of the allophane which results in less favorable electrostatic interaction between the allophane and the carboxylates.

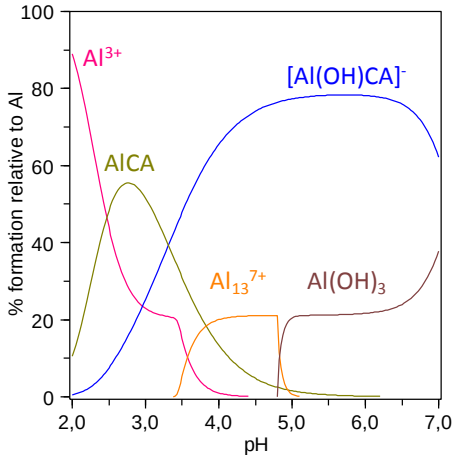

Figure 4-15 Speciation of Al in the citric acid aqueous solution as a function of the pH

Chin et al.[36] studied the dissolution kinetic of kaolinite, an aluminosilicate clay, as a function of pH and concentration of organic acid (such as oxalic acid). They observed that, for a given pH, the dissolution rate of Al increases considerably (by a factor 14) when the solution contains a concentration of oxalic acid of 5 mM, compared to the solution free of organic acid.

Based on experimental data, they determined that the rate of dissolution of Al of kaolinite in presence of oxalic acid is proportional not only to the surface concentration of Al coordinated by oxalic acid but also to the concentration of H^+. They propose that the proportionality of the Al dissolution rate to $[H^+]$ is due to the fact that the protons intervene in the release of Al-ligand complex by protonating O atoms from Al-O bonds and hence favoring their breaking.

Based on these results from the literatures, one can conclude that the dealumination of ASA in presence of oxalic acid occurs in two steps: in the first step, partially deprotonated citric acid (CAH_2^-) interacts with surface Al-OH_2^+ species leading to the formation of a surface chelate; the formation of this chelate polarize the adjacent Al-O-M bonds (where M = Si or Al). Hence, in the second step, the protonation of the M-O-Al leads to the breaking of M-O-Al bond and the release of the Al citrate complex from the solid.

$$\equiv Al\text{-}OH_2^+ + CAH_2^- \rightarrow \equiv Al\text{-}CAH^- + H_3O^+$$

$$(MO)_n Al\text{-}CAH^- + H^+ \rightarrow \equiv MOH + (MO)_{n-1} Al\text{-}CAH$$

This mechanism is slightly different from what has been proposed previously for the dealumination of zeolite with citric acid, where the first step is H^+-assisted hydrolysis of the M-O-Al bonds followed by the formation of the citrate/Al chelate. However, this mechanism is not only supported by the kinetic analysis of Al dissolution data for kaolinite, but seems also consistent with the preferential dissolution of non-acidic Al that we observed.

Indeed, based on the characterization of the ASA by ^{27}Al MAS NMR, the Al atoms that are the most prone to dealumination are also those with flexible coordination. This result is consistent with the fact that the first step of the dealumination is the formation of an Al-CA chelate that requires the capability, for the Al atom to increase its coordination of 1. Moreover, the high stability toward dealumination with CA of framework Al in zeolites and of the strong Brønsted acid sites could be related to their geometrical inability to form chelate complexes with CA due to their position in tetrahedral framework position.

The large increase in the surface area upon dealumination CA, is rather puzzling especially if one considers that only Al is released from the solid (determination of the Si

content in the dealumination solutions indicates negligible Si dissolution) and that the percentage of matter released by the solid is at maximum 10%. Moreover, this important increase in surface area is associated to a slight contraction of the pores (with a decrease of ca. 1 nm in the pore diameter). The contraction of the pores tends to indicate that a reconstruction of the solid takes place after dealumination. This reconstruction is to be expected as the simple removal of Al from the solid surface could increase substantially the density of surface hydroxyls. These surface hydroxyls will likely undergo condensation reaction, either in solution or during the final calcination step that could be responsible for the shrinkage in the pore diameter. A modification in the pore structure of USY zeolite upon dealumination with CA has been reported by Xin-Mei et al.[37] who observed the formation of mesopores after dealumination with CA and assigned it to a reconstruction of the solid. This reconstruction could also be responsible for the increase in the surface area. Alternatively, as proposed by Fan et al.[38] for ZSM-5 zeolites, the increase in the surface area may also result from the removal of alumina-like debris from the solid that were blocking the access to a part of the porosity.

The large difference in the effectiveness of dealumination when performed on the ammonium form and the H form of the ASA, is also puzzling. The lower reactivity of the H form is probably due to the calcination step that is used to transform the ammonium form to the H-form. Indeed, this calcination would decrease the surface hydroxylation of the ASA and could therefore reduce its reactivity toward dealumination.

4.4.2 Effect of dealumination on the acidic properties of the ASA

The characterization of these ASA by ^{27}Al NMR do not show any direct correlation between the concentration of tetrahedrally, pentahedrally, or octahedrally coordinated aluminium atoms and the concentration of acid sites in the ASAs, in accordance with previous reports.[39,40] Penta-coordinated Al is the most prone to dealumination and its elimination from the solid under mild dealumination conditions does not decrease the acidic properties. On the contrary, mild dealumination increases the amount of Lewis and Brønsted sites and also increases the conversion of 33DMB1. Hence, these pentacoordinated Al do not seem to be associated with Brønsted or Lewis sites strong enough to be detected by pyridine adsorption

and to intervene in the conversion of 33DMB1.

The characterization of the acidic properties of the starting ASA and of the derived ASA obtained by dealumination with CA confirmed the fact that a very large fraction of the Al atoms in ASA is silent in terms of acidity, at least based on pyridine adsorption. We detected about 100 µmol/g of acid sites (Lewis and Brønsted) for the two starting ASA that contain, respectively 2.3 and 4 mmol/g of Al. Hence, the percentage of acidic Al in the starting ASAs is below 5.

Based on pyridine adsorption, dealumination significantly enhance the fraction of acidic Al that reaches for a highly dealuminated sample derived from GD13, GD13-0.4 CA, 28.5 %. Whereas pyridine gives very useful information on the amount of Lewis and Brønsted sites and their evolution upon dealumination, CO provide complementary information on the strength of the acid sites and their evolution. It especially shows that mild dealumination results in the detection of strong Brønsted acid sites that could likely be Si-OH-Al bridges. The question whether these strong Brønsted acid sites where already present in the starting ASA but inaccessible or whether these sites were formed during the dealumination process by the reinsertion of extracted Al in adequate position (as reported by Zaiku et al.[2] and Fan et al.[38] for zeolites). More severe dealumination results in a decrease in the densities of Brønsted and Lewis sites (pyridine adsorption), in a decrease in the isomerization of 33DMB1 and in the loss of the weak and mild Brønsted sites while the new (or newly accessible) strong Brønsted sites are preserved (CO adsorption).

4.5 Conclusion

Various techniques have been employed to clarify the influence of treatment of ASA with aqueous solution of citric acid (CA) on their properties. CA can effectively remove up to 80% of Al and results in changes in the texture, acidity and the aluminium distribution. Several conclusions can be drawn:

1) CA dealumination is more effective and selective on the ammonium form ASA compared to the H form.

2) Treatment with CA can effectively remove nonacidic Al sites while preserving or exposing the acidic ones. The release of Al is accompanied by a significant increase of the surface area and a decrease in the pore size. Mild dealumination leads to ASA with improved textural and acidic properties and to an increase catalytic activity of 33DMB1 isomerization.
3) ^{27}Al MAS NMR shows that CA preferentially removes Al with flexible coordination (the Al atoms that are five coordinated in the calcined from of ASA).
4) Characterization of the ASA by CO adsorption reveals the presence of strong and mild Lewis sites in the starting ASA and together with mild and weak Brønsted acid sites. It also shows the presence of strong Brønsted acid sites in the samples obtained after mild dealumination, whereas the amounts of other acid sites are unchanged or slightly increased. After severe dealumination, the strong Brønsted acid sites are preserved while the amounts of other Brønsted and Lewis acid sites decreases.
5) In addition to resulting in enhanced acidic and catalytic performances, CA treatment, by removing a large fraction of nonacidic aluminium species, make the obtained ASA model samples for further research on the nature of acid sites of ASA by advanced NMR.

Reference

(1) Zanjanchi, M.; Mohabbati, E. *Journal of Molecular Structure* **2003**, *645*, 171.

(2) Zaiku, X.; Qingling, C.; Chengfang, Z.; Jiaqing, B.; Yuhua, C. *The Journal of Physical Chemistry B* **2000**, *104*, 2853.

(3) Lin, X.; Fan, Y.; Liu, Z.; Shi, G.; Liu, H.; Bao, X. *Catalysis today* **2007**, *125*, 185.

(4) Fan, Y.; Bao, X.; Lin, X.; Shi, G.; Liu, H. *The Journal of Physical Chemistry B* **2006**, *110*, 15411.

(5) Alexander, G. B.; Heston, W.; Iler, R. K. *The Journal of Physical Chemistry* **1954**, *58*, 453.

(6) Choy, J.-H.; Yoo, J.-S.; Han, Y.-S.; Kim, Y.-H. *Materials Letters* **1993**, *16*, 226.

(7) Apelian, M. R.; Fung, A. S.; Kennedy, G. J.; Degnan, T. F. *The Journal of Physical Chemistry* **1996**, *100*, 16577.

(8) Rodríguez-González, L.; Hermes, F.; Bertmer, M.; Rodríguez-Castellón, E.; Jiménez-López, A.; Simon, U. *Applied Catalysis A: General* **2007**, *328*, 174.

(9) Crépeau, G.; Montouillout, V.; Vimont, A.; Mariey, L.; Cseri, T.; Maugé, F. *The Journal of Physical*

Chemistry B **2006**, *110*, 15172.

(10) Blanchard, J.; Krafft, J.-M.; Dupont, C.; Sayag, C.; Takahashi, T.; Yasuda, H. *Catalysis Today* **2014**, *226*, 89.

(11) Holm, M. S.; Svelle, S.; Joensen, F.; Beato, P.; Christensen, C. H.; Bordiga, S.; Bjørgen, M. *Applied Catalysis A: General* **2009**, *356*, 23.

(12) Cairon, O.; Lavalley, J.-C. *Journal of the Chemical Society, Faraday Transactions* **1998**, *94*, 3039.

(13) Cairon, O. *Physical Chemistry Chemical Physics* **2010**, *12*, 6333.

(14) Hensen, E. J.; Poduval, D. G.; Degirmenci, V.; Ligthart, D. J. M.; Chen, W.; Maugé, F. o.; Rigutto, M. S.; Veen, J. R. v. *The Journal of Physical Chemistry C* **2012**, *116*, 21416.

(15) Stephen, M. K. Sinclair Research Inc. New York, 1968, p US3365511 A.

(16) Haber, J.; Lalik, E. *Catalysis today* **1997**, *33*, 119.

(17) Martin, D.; Duprez, D. *Journal of Molecular Catalysis A: Chemical* **1997**, *118*, 113.

(18) Guisnet, M. R. *Accounts of chemical research* **1990**, *23*, 392.

(19) Caillot, M.; Chaumonnot, A.; Digne, M.; Poleunis, C.; Debecker, D. P.; van Bokhoven, J. A. *Microporous and Mesoporous Materials* **2014**, *185*, 179.

(20) Huang, J.; Jiang, Y.; Marthala, V. R.; Thomas, B.; Romanova, E.; Hunger, M. *The Journal of Physical Chemistry C* **2008**, *112*, 3811.

(21) Hunger, M. *Solid state nuclear magnetic resonance* **1996**, *6*, 1.

(22) Delgado, M.; Delbecq, F. o.; Santini, C. C.; Lefebvre, F.; Norsic, S.; Putaj, P.; Sautet, P.; Basset, J.-M. *The Journal of Physical Chemistry C* **2011**, *116*, 834.

(23) Barrow, B. N. S.; Scullard, A.; Collis, N. *Johnson Matthey Technology Review* **2016**, *60*, 90.

(24) Richards, R. *Surface and nanomolecular catalysis*; CRC Press, **2006**.

(25) Luo, Q.; Deng, F.; Yuan, Z.; Yang, J.; Zhang, M.; Yue, Y.; Ye, C. *The Journal of Physical Chemistry B* **2003**, *107*, 2435.

(26) Janin, A.; Maache, M.; Lavalley, J.; Joly, J.; Raatz, F.; Szydlowski, N. *Zeolites* **1991**, *11*, 391.

(27) Ichihashi, H.; Kitamura, M. *Catalysis today* **2002**, *73*, 23.

(28) Heitmann, G.; Dahlhoff, G.; Hölderich, W. *Journal of Catalysis* **1999**, *186*, 12.

(29) Chu, C. T.; Chang, C. D. *The Journal of Physical Chemistry* **1985**, *89*, 1569.

(30) Kiricsi, I.; Flego, C.; Pazzuconi, G.; Parker, W. J.; Millini, R.; Perego, C.; Bellussi, G. *The Journal of Physical Chemistry* **1994**, *98*, 4627.

(31) Halasz, I.; Senderov, E.; Olson, D. H.; Liang, J.-J. *The Journal of Physical Chemistry C* **2015**, *119*, 8619.

(32) Williams, M.; Fonfé, B.; Sievers, C.; Abraham, A.; Van Bokhoven, J.; Jentys, A.; Van Veen, J.; Lercher, J. *Journal of Catalysis* **2007**, *251*, 485.

(33) Alderighi, L.; Gans, P.; Ienco, A.; Peters, D.; Sabatini, A.; Vacca, A. *Coordination Chemistry Reviews* **1999**, *184*, 311.

(34) Motekaitis, R. J.; Martell, A. E. *Inorganic Chemistry* **1984**, *23*, 18.

(35) Hanudin, E.; Matsue, N.; Henmi, T. *Developments in Soil Science* **2002**, *28*, 319.

(36) Chin, P.-K. F.; Mills, G. L. *Chemical Geology* **1991**, *90*, 307.

(37) Xin-Mei, L.; Zi-Feng, Y. *Catalysis today* **2001**, *68*, 145.

(38) Fan, Y.; Lin, X.; Shi, G.; Liu, H.; Bao, X. *Microporous and Mesoporous materials* **2007**, *98*, 174.

(39) Hahn, M. W.; Copeland, J. R.; Van Pelt, A. H.; Sievers, C. *ChemSusChem* **2013**, *6*, 2304.

(40) Hensen, E.; Poduval, D.; Magusin, P.; Coumans, A.; Van Veen, J. *Journal of Catalysis* **2010**, *269*, 201.

Chapter 5. Identification of the acid sites on dealuminated amorphous silica-aluminas by solid state NMR

Abstract

Representative samples obtained by dealumination of GD13 with CA were chosen as model ASA to investigate the structure of acid sites. The spatial proximity between proton and aluminium was explored in these ASAs by a combination of one and two-dimensional homo- and heteronuclear ^{1}H and ^{27}Al NMR. Based on ^{27}Al DQ-SQ NMR, two separate phases, an alumina phase and silica-alumina phase are present on the starting ASA. Flexible aluminium coordination was found upon ^{27}Al NMR (DP and 3Q MAS) both between ammonium form and H form ASA and between hydrated and dehydrated form. In ammonium form ASA, ammonium and hydroxyls are evenly distributed over the surface (^{1}H DQ-SQ NMR); Brønsted acidity may be associated with both Al^{IV} and Al^{V} (^{27}Al-^{1}H D-HMQC 2D NMR). However, Brønsted acid sites of ASA have a structure that differs from those of zeolites (^{1}H-^{27}Al REAPDOR). For the H form of ASAs, especially in dehydrated state, ^{27}Al spectra experience severe broadening and half Al are invisible. Although current NMR experiments are not (yet) able to provide a complete picture of the structure of acidity on ASA, we were able to propose a structure for non-acidic tetrahedral Al sites and to bring new knowledge on the characteritics of the acid sites of ASAs.

5.1 Introduction

Amorphous silica-aluminas (ASA) are widely used as solid acid catalysts in various chemical reactions including hydrocracking, isomerization, and alkylation, which are important in the oil refining and petrochemical industry.[1,2] The study of ASA acidity is hampered by the difficulty to unambiguously identify the structure of the acid sites. Determining the local structure of the acid sites on the surface of ASA would be of critical interest to understand how to tune/improve their acidic properties and provide guidance in the design of solid acids with improved acidity and enhanced activity.

A reasonable surface model of ASAs contains at least four different types of aluminiums: Al substitutions in the silica network and, at the surface, isolated tetrahedral and octahedral Al as well as more aggregated forms of Al.[3] The aggregation of aluminium may

lead to the presence of a separate alumina phase. Five-coordinated Al has been suggested to make up the interface between these domains and the mixed silica-alumina phase.[3,4] However, it has been recently reported that most of the Al^{V} species are formed independently from the alumina phase and are accessible on the surface.[5] The original structural models of ASA proposed that BAS arise from proton compensating the electronic charge of the surface.[6] Currently, the two more widely shared opinions are, either that strong BAS in ASA is zeolite-like Si-(OH)-Al groups,[3,7,8] which are close or ideally similar in strength to that of zeolites based on probe molecule adsorption,[3,7,9-11] or that ASA possess specific acid sites such as pseudo bridging[12]… The first hypothesis, which seems the most straightforward, remains questionable for two reasons. First it is well-known that the strength of the acid site depends on both the local BAS atomic structure and the confinement effect[13] which depends on the size of the pore where the BAS is located. Hence, obtaining acid sites of similar strength in ASA than in zeolite seems difficult. Second, there is, no conclusive evidence for the presence, in ASA, of strongly acidic bridging hydroxyl groups, because these sites have eluded direct spectroscopic observed.

The standard method to probe acidity in aluminosilicates is IR spectroscopy of adsorbed pyridine. Pioneering works[14,15] have shown the feasibility of this method to simultaneously probe Lewis and Brønsted acid sites. The use of CO as a weak base to probe acidity by IR spectroscopy is also well established.[9,16] Crépeau et al.[14] proposed that ASAs contain sites similar in acidity strength to zeolites through comparison of the red shift of the OH stretching band upon adsorption of CO in ASA to the shift of this band in zeolites.

The reason why the detailed structures of BAS and LAS remains ambiguous and debatable issues is the lack of direct experimental evidence. Thanks to the rapid development of SSNMR, it has become possible to directly observe the spatial connection of atoms. Copéret team,[17] combining advanced NMR techniques and DFT calculation, confirmed that Al^{IV}-(O)-Si^{IV} connectivity was a requirement for BAS. Meanwhile, Huang group[18] directly observed, using $^{27}Al/^{1}H$ DHMQC sequence, a new type of BAS related to 5-coordinated Al (Al^{V}) and concluded that BAS-Al^{V} co-exist with BAS-Al^{IV} and exhibit a similar acidity (based on the protonation of ammonia).

Although SSNMR spectroscopy is indeed a valuable tool to obtain insights into the nature of Al and Si species on ASA, unambiguous identification of the most relevant surface sites has not been achieved yet. One of the problem is that only a small fraction of aluminium species located in ASA contribute to acidity, and these acidity-silent Al species heavily perturb the interpretation of NMR results. Therefore, extracting selectively non acidic Al from the ASA would be greatly beneficial for the comprehension of NMR results. In **Chapter 4**, citric acid (CA) was shown to be a very effective molecule for the removal of a large fraction of nonacidic Al and to improve effective acidity. Samples prepared by this method could therefore be considered as rational ASA model for NMR comprehension. Therefore, in this chapter, representative dealuminated samples were chosen as model ASAs for advanced NMR characterization to investigate the spatial proximity and connectivity between proton, aluminium and silicon and attempt to provide a direct experimental evidence for the structure of BAS and LAS. After presenting in details the results obtained from each NMR sequence (applied either on the ammonium or on the H form of the ASAs), we will summarize briefly the conclusions or hypotheses that can be drawn from the NMR study and attempt to propose a model for the Al atoms in ASAs.

5.1 Experimental

5.1.1 Synthesis

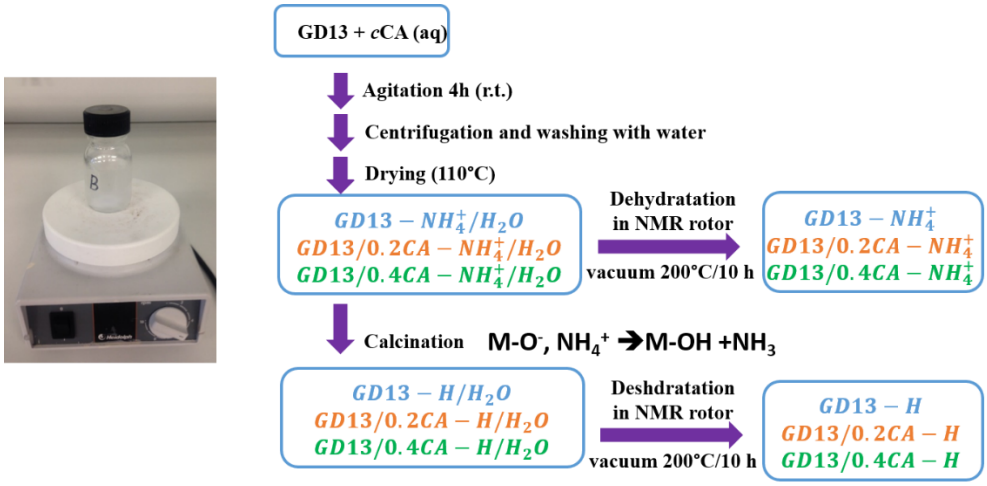

Figure 5-1 Scheme for the synthesis and designation of the samples with different post-treatment

Synthesis protocols and characteristics of all the samples used in this chapter have been detailed in **Chapter 4**. The selected samples were denoted as GD13/cCA-x, where "c" is the concentration of citric acid, CA represents citric acid and x is an extension describing the final treatment of the sample prior to the NMR measurement. The scheme for the synthesis and designation of the x extension of the samples at different stage is displayed in Figure 5-1.

5.1.2 Characterization

Characterization methods (including NMR sequences) were detailed in the **Chapter 2**.

5.2 Results

5.2.1 Brief overview of the characteristics of the selected ASAs

Table 5-1 Al content and texture properties of different samples prepared by CA dealumination (see Figure 5-1 for sample designation)

Sample	Al	S_{BET}	Pore Size	Pore Volume
	mmol/g	m^2/g	nm	cm^3/g
GD13-NH_4^+	2.3	475	4.8	0.68
GD13/0.2CA-NH_4^+	1.0	560	3.7	0.70
GD13/0.4CA-NH_4^+	0.3	668	3.7	0.60
GD13-H	2.3	445	4.8	0.70
GD13/0.2CA-H	1.0	517	3.7	0.78
GD13/0.4CA-H	0.3	699	3.3	0.63

The evolution of the textural properties of the ASA upon dealumination with CA has been studied in details in the previous chapter (**Chapter 4)**. Herein, Table 5-1 simply shows the textural properties of the model ASA used in this present chapter.

In the previous chapter (**Chapter 4**), FTIR of adsorbed pyridine was used to quantify Brønsted acid sites (BAS) and Lewis acid sites (LAS) present on the surface of the ASAs. Table 5-2 displays acid type and strength distribution of the samples of interest. After mild CA dealumination (sample GD13-0.2CA-H), the density of BAS and LAS increases, while under more severe dealumination conditions (sample GD13-0.4CA-H) densities of BAS and LAS decrease slightly compared to the starting GD13-H. Effective acidity (percentage of acid site

per Al atom) increases from 4.4% to 28.5%. Moreover, based on FTIR of adsorbed CO experiments, highly dealuminated sample (sample GD13-0.4CA-H) contains mostly strong Brønsted acid sites. A detailed discussion about this was made in **Chapter 4**.

Table 5-2 Acid type and strength distribution of the samples of interest (based on pyridine-IR)

Sample	Acidity (μmol/g)									Acidic Al
	Total	BAS				LAS				%
	B+L	weak	medium	strong	total	weak	medium	strong	Total	
GD13-H	101	23	11	0	34	21	11	36	67	4.4
GD13/0.2CA-H	130	29	15	0	43	24	13	50	87	12.5
GD13/0.4CA-H	96	22	9	0	31	7	8	49	65	28.5

5.2.2 Characterization of the ammonium form ASA

5.2.2.1 ^{27}Al MAS NMR

A- ^{27}Al DP MAS and MQ MAS NMR

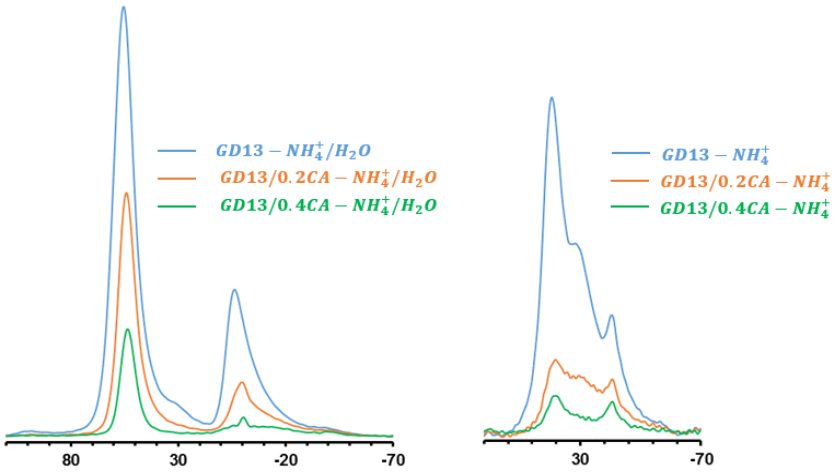

Figure 5-2 ^{27}Al MAS NMR spectra of ammonium form ASA: hydrated (left) and dehydrated (200°C vacuum) (right)

Figure 5-2 displays the ^{27}Al MAS NMR spectra of ammonium form of the GD13-NH_4^+ derived ASA in hydrated (left) and dehydrated (right) state. Hydration makes the aluminium sites more symmetric by decreasing the quadrupolar interaction, thereby enhancing visibility of the aluminium. Conversely, the peak of ^{27}Al NMR of the dehydrated samples are broader due to strong quadrupolar interactions. By integrating the spectra, the total area of Al signals in hydrated samples are similar to that in dehydrated ones, indicating that all the Al species can be visible in dehydrated state. Spectra of hydrated form are acquired under quantitative

conditions with direct-polarization and can be fitted directly using the CzSimple model (Table 5-3).

For the dehydrated forms of the ASAs, the overlay of the peaks, which is due to their broadening makes it difficult to decompose directly the 1D spectra. In this case, ^{27}Al MQ MAS NMR can provide a more detailed and resolved pattern compared with ^{27}Al MAS NMR by averaging out the second-order quadrupole interaction. Figure 5-3 shows the ^{27}Al 3Q MAS NMR spectra of ammonium form of GD13-NH_4^+ and GD13/0.2 CA-NH_4^+ in dehydrated state. Table 5-3 presents the parameters obtained from 3Q MAS NMR spectra for each Al coordination and the fraction of Al atoms in the corresponding coordination. Al fractions were calculated by the decomposition of quantitative 1D ^{27}Al MAS NMR spectra using the quadrupolar product and isotropic chemical shift derived from the 3Q MAS NMR spectra.

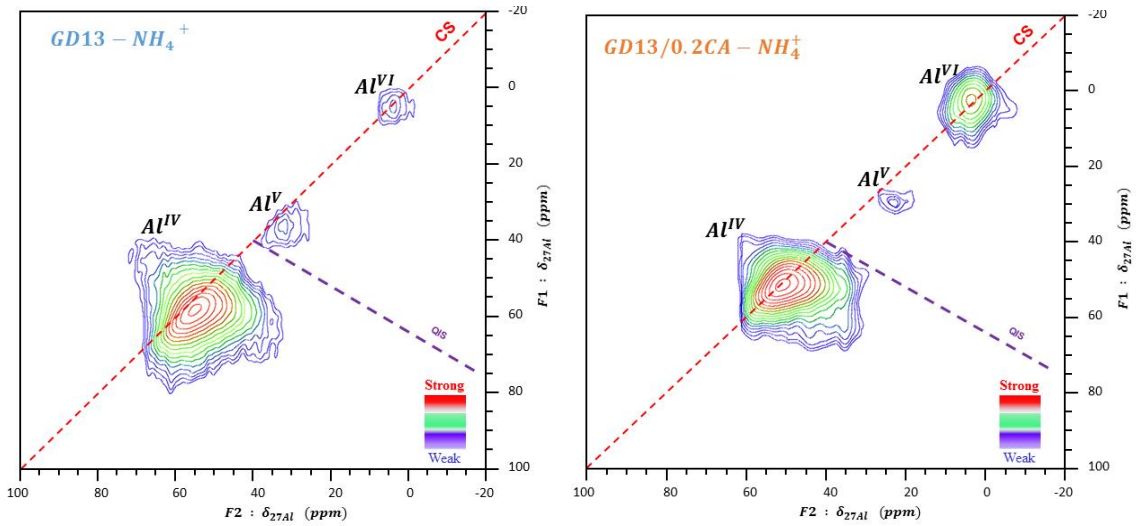

Figure 5-3 ^{27}Al 3Q MAS NMR spectra of GD13-NH_4^+ (left) and GD13/0.2 CA-NH_4^+ (right)

On the 3Q MAS of GD13-NH_4^+ and GD13/0.2CA-NH_4^+ (Figure 5-3), three signals are distinguished: an intense resonance centered at around 55 ppm, attributed to Al^{IV} and two weaker signals at 30 and 0 ppm assigned to Al^{V} and Al^{VI}, respectively. The three signals are circular in shape and close to the diagonal, indicating that all species of aluminium experience a weak quadrupolar interaction. Values of $C_{Q\eta}$ reported in Table 5-3 confirm this observation.

Based on the spectra of the hydrated forms, mild CA treatment does not appear to alter the relative proportion of Al^{IV}, Al^{V} and Al^{VI}. However, dealumination under more severe

conditions seems to remove Al^{VI} species, as already commented in **Chapter 4**.

Table 5-3 The assignment, NMR parameters and relative Al content of ammonium form ASA

Sample	Al coordination	δ_{F1} ppm	δ_{F2} ppm	δ_{ISO} ppm	$C_{Q\eta}$ MHz	Al content %
GD13-NH_4^+/H_2O	Al^{IV}			60.5		64.5
	Al^{V}			34.6		3.6
	Al^{VI}			7.5		32.0
GD13-NH_4^+	Al^{IV}	61.2	54.2	58.9	3.5	53.3
	Al^{V}	36.6	31.6	34.3	3.0	38.9
	Al^{VI}	4.5	3.2	3.8	1.6	7.8
GD13/0.2CA-NH_4^+/H_2O	Al^{IV}			55.1		70.6
	Al^{V}			31.2		2.2
	Al^{VI}			1.1		27.2
GD13/0.2CA-NH_4^+	Al^{IV}	60.9	50.9	57.6	4.2	46.8
	Al^{V}	39.5	25.3	35.3	4.9	38.9
	Al^{VI}	11.4	3.3	8.4	3.8	14.3

Dehydration increases the fraction of Al^{V} at the expense of Al^{VI}, indicating that some of the Al^{V} may be formed by desorption of one water molecular from Al^{VI}. But, especially for GD13/0.2CA-NH_4^+, the quantity of Al^{IV} also decreases upon dehydration indicating that Al^{IV} contribute also to the formation of Al^{V}. An increase of the Al coordination upon dehydration is counter-intuitive as one would rather expect a decrease in the coordination of Al upon dehydration due to the removal of coordination water molecules. A possible explanation would be that the change in the local environment of the Al^{IV} atoms upon dehydration allows some of them to increase their coordination to V by interaction with framework oxygen atoms. This hypothesis is consistent by the work of Busco et al.[19] who showed that, in zeolites, masked Lewis Al are formed by interaction of Al(III) Lewis sites with framework oxygen atoms.

B- ^{27}Al DQ-SQ MAS NMR

^{27}Al-^{27}Al DQ-SQ MAS NMR gives complementary information about the spatial proximity of the various Al species. It was therefore applied to the characterization of the GD13-NH_4^+. A γ-alumina sample was used as reference because it also contains tetrahedral

and octahedral aluminium atoms. The structure of gamma alumina is usually described as a cubic defective spinel, where the O atoms are in a cubic close packed arrangement and the Al atoms occupy partially the octahedral and tetrahedral sites.[20] The ratio between tetrahedral and octahedral Al in gamma alumina is about 1/3 to ¼.[21]

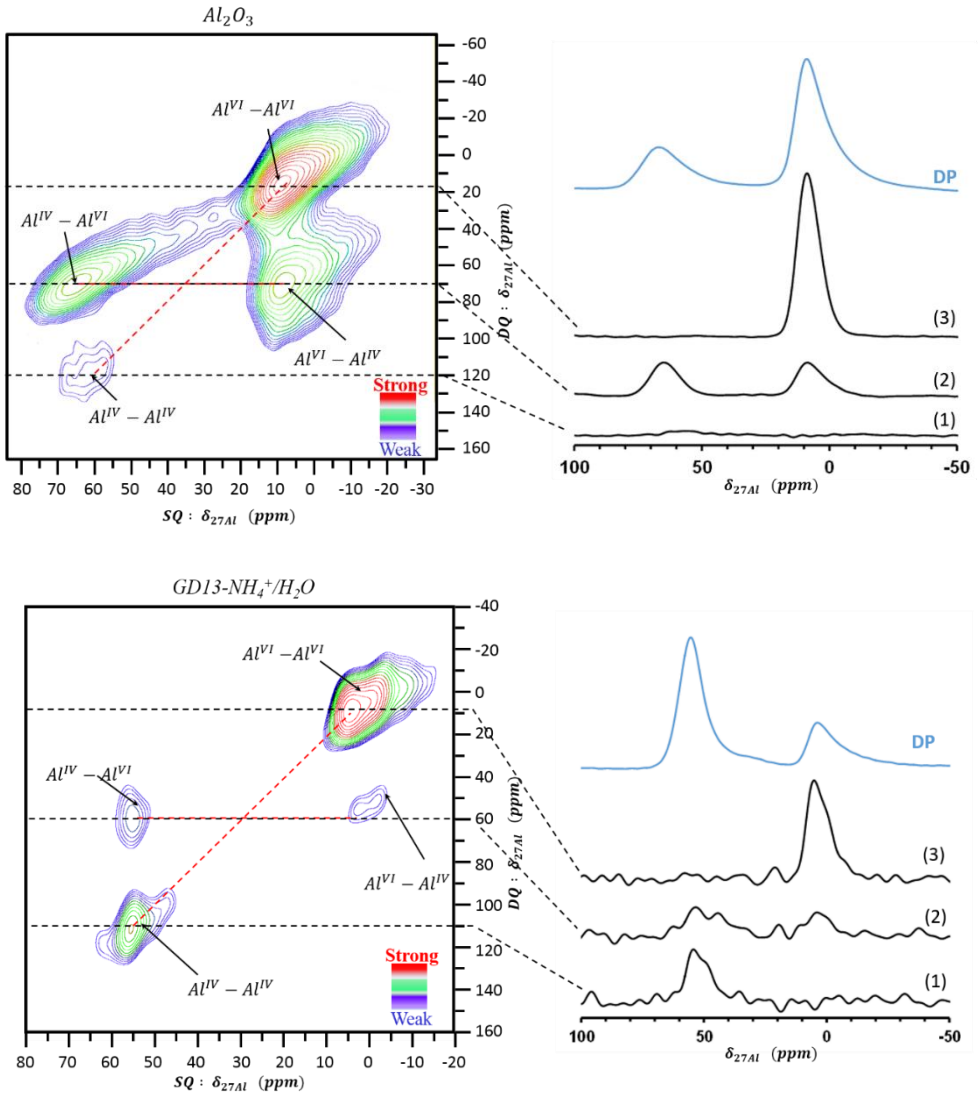

Figure 5-4 ^{27}Al-^{27}Al DQ-SQ MAS NMR spectra of GD13-NH_4^+/H_2O and Al_2O_3. 1D (DP) ^{27}Al NMR (up) and selected slices cut along the SQ-axis are shown on the right part.

The ^{27}Al-^{27}Al DQ-SQ MAS NMR of γ-alumina is shown on Figure 5-4. Beside the 2D spectra, slices cut along the y axis together with the ^{27}Al DP spectra (direct polarization, i.e. standard ^{27}Al MAS NMR spectra) have also been reported on the right part of this figure. It consists in one intense diagonal peak for two coupled octahedral ^{27}Al (Al^{VI}-Al^{VI}) and two off-diagonal peaks for an octahedral ^{27}Al coupled with a tetrahedral ^{27}Al (Al^{VI}-Al^{IV} and Al^{IV}-Al^{VI}).

Besides these three peaks, a much weaker diagonal peak is observed at 60 ppm and corresponds to two coupled tetrahedral ^{27}Al (Al^{IV}-Al^{IV}). The weak intensity of this last peak can be explained by the lower amount of Al^{IV} (the ratio Al^{IV}/Al^{VI} in this γ-Al_2O_3 is 0.4, Table 5-4). Hence Al^{IV} are mostly coupled to octahedral ^{27}Al, but few coupled to other Al^{IV}. The DQ-SQ spectrum of Iuga et al.[22] shows a diagonal peak (Al^{VI}-Al^{VI}) and two off-diagonal peaks (Al^{VI}-Al^{IV} and Al^{IV}-Al^{VI}) but no diagonal peak for two coupled tetrahedral Al.

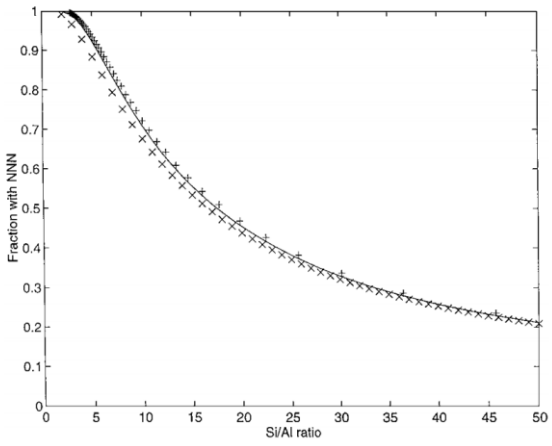

Figure 5-5 Fraction of Al atoms in ZSM-5 with at least one Al atom as second tetrahedral neighbor in versus Si/Al ratio[23]

The spectrum of GD13-NH_4^+/H_2O (Figure 5.4) is, at first sight, quite similar to the one of γ-Al_2O_3 with 4 peaks: two diagonal peaks corresponding to Al^{VI}-Al^{VI} and Al^{IV}-Al^{IV} correlation and two cross-peaks corresponding to Al^{VI}-Al^{IV} correlation. However, the relative intensities of the diagonal peaks (ratio slices Al^{IV}(1)/ Al^{VI}(3) is 0.5) do not reflect the relative intensities of Al^{IV} and Al^{VI} in the DP spectrum (ratio is 2.5). The high relative intensity of the Al^{VI}-Al^{VI} peak suggests a segregation of an Al^{VI}-rich phase. Hence, the question that could be raised is whether the DQ spectra could not be simply the signature of a γ-alumina like phase, separated from a silica-alumina phase. Under this hypothesis, most of six-coordinated aluminium atoms would belong to a pure alumina phase, while four-coordinated ones could be located, either in the pure alumina domains or in a mixed silica–alumina phase.[3]

For the discussion, we could make use of the correlation between Si/Al ratio and the fraction of Al atoms having another Al atoms as second tetrahedral neighbor (Al-O-Si-O-Al) proposed by Rice et al.[23] The GD13-NH_4^+ sample is composed of 64.5% Al^{IV} (Table 5-3) with

a Si/Al ratio of 5.7. Thus the Si/Al^{IV} ratio is around 8.8 and the fraction of Al^{IV} atoms having Al^{IV} atoms as second tetrahedral neighbor is evaluated to 0.78 (Figure 5-5). Hence, if one assumes that almost all Al^{IV} are in a mixed silica-alumina phase, they are largely coupled to one another, which can explain the high intensity of the diagonal peak (Al^{IV}-Al^{IV}).

Table 5-4 Ratios of intensities for different Al types from 1D (DP) ^{27}Al NMR and from ^{27}Al DQ-SQ NMR slices

Sample	Ratio				
	$\frac{Al^{IV}(DP)}{Al^{VI}(DP)}$	$\frac{Al^{IV}(2)}{Al^{IV}(1)}$	$\frac{Al^{VI}(2)}{Al^{VI}(3)}$	$\frac{Al^{IV}(1)}{Al^{VI}(3)}$	$\frac{Al^{IV}(2)}{Al^{VI}(2)}$
γ-Al_2O_3	0.4	5.3	0.3	0.1	1.0
GD13-NH_4^+	2.5	0.7	0.2	0.5	2.0

(DP and the numbers between parentheses correspond to the right part of Figure 5-4)

To facilitate the comparison between G13-NH_4^+/H_2O and γ-Al_2O_3, the ratios of different Al peaks coming from different slices of the 2D and DP spectra are calculated in Table 5-4. The intensity ratio $Al^{VI}(2)/Al^{VI}(3)$ for both samples is similar, indicating that GD13 could contain a γ-alumina like phase, while the obviously much higher ratio $Al^{IV}(1)/Al^{VI}(3)$ in GD13-NH_4^+/H_2O than that in Al_2O_3, implies the presence of an excess of Al^{IV} atoms in GD13-NH_4^+/H_2O (compared to γ-Al_2O_3). These extra Al^{IV} atoms are probably inserted into the silica matrix, in a similar way as in zeolites, in a mixed silica-alumina. Therefore, GD13-NH_4^+/H_2O at least contains two phases: bulk alumina and alumina-silica phase, and based on the similarity of the $Al^{VI}(2)/Al^{VI}(3)$ in GD13-NH_4^+/H_2O and in γ-Al_2O_3, these two phases could be isolated from one another (the cross peaks indicating a proximity of Al^{IV} and Al^{VI} in GD13-NH_4^+/H_2O would almost exclusively come from the Al^{IV} atoms of the γ-Al_2O_3 domains). One must however keep in mind that fully isolated Al atoms are, by essence, not visible on the 2D DQ-SQ spectrum. Hence, one cannot exclude that other (isolated) species are also present, such as, for example, isolated Al^{IV} species.

The intensity variation of the DQ curve allows to discuss about the range of Al-Al distances. 1D DQ-SQ spectra of γ–Al_2O_3 for various excitation times (Figure 5-6 A) show a maximum of intensity for Al^{VI} in pairs at 593 μs (position is marked with a ●) corresponding to Al-Al distances around 4.5 Å.[24] The DQ curve obtained from slices of the 2D spectra of the

γ–Al_2O_3 cut along diagonal peak of Al^{VI}-Al^{VI} is very similar (Figure 5-6 C). The maximum for GD13-NH_4^+/H_2O is identical, indicating that Al^{VI}-Al^{VI} pairs are in the same range of distance that in a pure alumina phase (Figure 5-6 B). For the coupled Al^{IV}, the maximum intensity occurs at a higher recoupling time, at around 900 μs (Figure 5-6 B, position is marked with a *), which suggests longer Al-Al distances (~ 6 Å[24]).

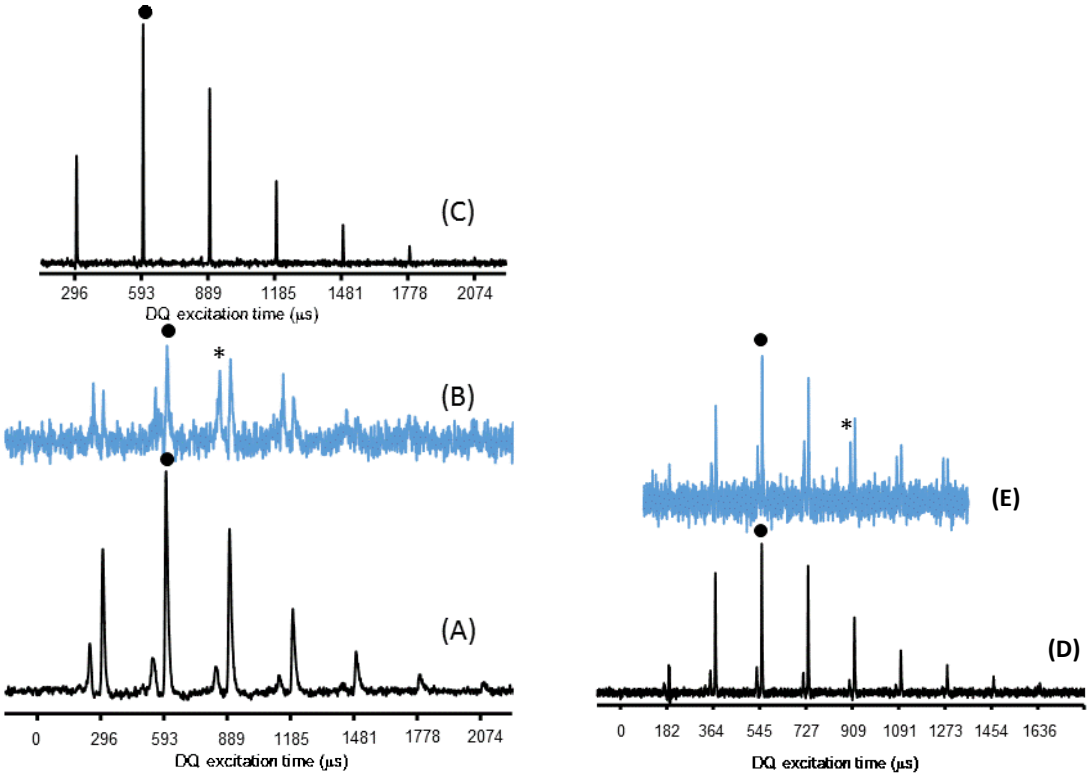

Figure 5-6 **Left part**: ^{27}Al 1D DQ-SQ NMR spectra of γ-Al_2O_3 (A) and GD13-NH_4^+/H_2O (B) samples recorded for various excitation times at Larmor frequency 130.3 MHz (500 MHz spectrometer) and spinning speed 13.5 kHz. (C) Slices along the diagonal peak of Al^{VI}-Al^{VI} of 2D DQ-SQ NMR spectrum of γ-Al_2O_3, for various excitation times. **Right part:** ^{27}Al 1D DQ-SQ NMR spectra of γ-Al_2O_3 (D) and GD13-NH_4^+/H_2O (E) samples recorded for various excitation times and at higher field (700 MHz spectrometer, Larmor frequency 182.5 MHz) and higher spinning speed (22 kHz).

With a higher spinning speed and therefore a shorter increment of DQ duration, the maxima are consistent but a little shorter (Figure 5-6, D & E). The Al^{IV}-Al^{IV} distance obtained by this technique is consistent with Al-O-Si-O-Al distance for large rings in zeolites (6-membered rings or higher). For example, in a faujasite, the distance with a second tetrahedral neighbor is about 4.4 Å for a connection within a 4-membered ring and increases to 5.4 Å in a 6-membered ring and reaches about 6 Å in larger rings (12-membered rings of the supercage). This large Al distance tends to indicate that the tetrahedral Al atoms in GD13-NH_4^+/H_2O follow

the Loewenstein's avoidance rule (absence of Al^{IV}-O-Al^{IV} bonds) and are exclusively surrounded by Si atoms ($Al(OSi)_4$ tetrahedra).

5.2.2.2 ^1H MAS NMR spectra of ammonium ASA

A- ^1H DP MAS NMR

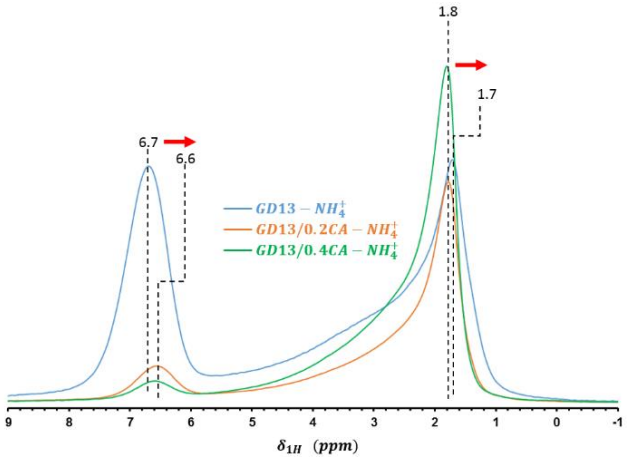

Figure 5-7 ^{1}H MAS NMR spectra of ammonium form ASA dehydrated at 200^{O}C

^{1}H MAS NMR spectroscopy provides direct information about the hydroxyl groups. In the ^{1}H MAS NMR spectrum of GD13-NH_4^+ (Figure 5-7), two major signals at around 1.7 and 6.7 ppm are observed, which can be unambiguously assigned respectively to isolated (or terminal) silanol and ammonium ions NH_4^+ formed by protonation of NH_3 on a Brønsted acid site. The broad feature between 3 and 7 ppm is due either to Si–OH groups interacting through the hydrogen bond[25,26] or bridging hydroxyls of an alumina like phase, also possibly experiencing H-bonding.[27]

After CA treatment, the signal due to the silanol groups increases and the peak assigned to NH_4^+ decreases remarkably in intensity. Considering the low pH at which the dealumination takes place and the increase in the intensity of the silanol peak, a possible reason for the decrease in intensity of this peak is that a large fraction of NH_4^+ acting as counterions to compensate the negative charge has been ion exchanged by H^+ during CA treatment. In addition, the peak assigned to ammonium slightly shifts down from 6.7 ppm in the starting ASA to 6.6 ppm in the dealuminated samples. Yin et al.[28] observed a correlation, on NH_4Y zeolite, between the position of the ^{1}H peak of the ammonium species and the size of the

cavities: this peak shifts from 6.9 ppm (ammonium in the supercage) to 6.5 ppm (ammonium in the sodalite cage). Hence, the remaining NH_4^+ after CA treatment may be located in confined space (and hence more difficult to exchange).

B- 2D ^{1}H DQ-SQ MAS NMR

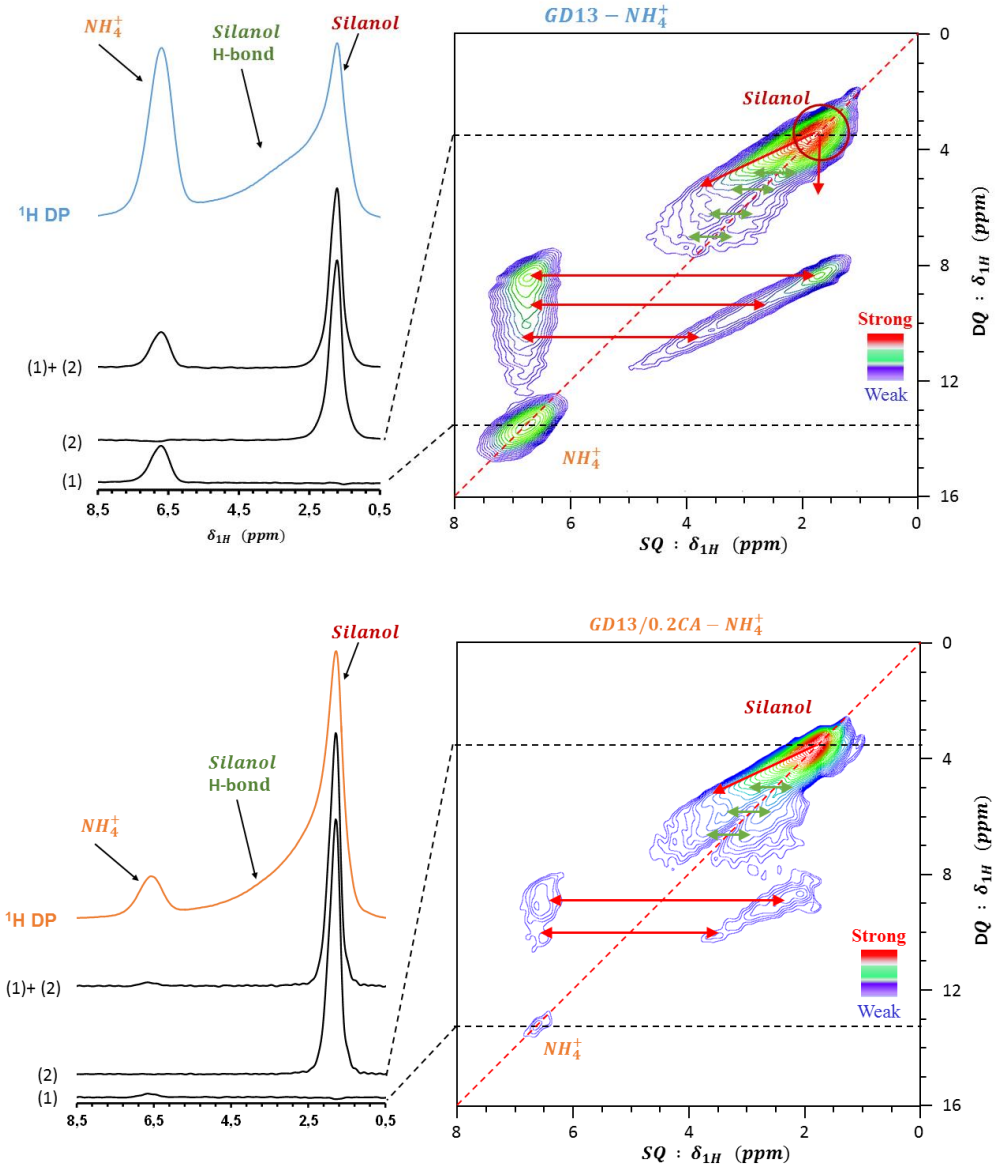

Figure 5-8 ^{1}H DQ-SQ MAS NMR spectra (right part) and corresponding ^{1}H MAS (DP) NMR spectra and slices from selected positions along the vertical axis (left part) of GD13-NH_4^+ (top) and GD13/0.2CA-NH_4^+ (bottom). Sample were beforehand dehydrated under vacuum at 200°C 10 h

To gain more insight into the spatial proximities between protons species based on their dipolar interaction, 2D ^{1}H DQ-SQ MAS NMR was applied to provide an effective and selective view of the dipolar interactions among the various proton groups. Figure 5-8 compares the

spectrum of the parent ASA (GD13-NH_4^+) with the one of the ASA dealuminated with 0.2 M CA (GD13/0.2CA-NH_4^+).

The overall lineshape of both spectra, especially the alignment of the whole spectra along the diagonal clearly indicates that the main contribution to the width of each line is resulting from a distribution of the isotropic chemical shift. Both spectra exhibit a strong autocorrelation peak at (1.7, 3.4) ppm. This indicates that an important fraction of isolated silanols are at a distance below 5 Å from the next isolated silanol. One can compare this result with the average distance between two isolated silanols estimated from surface density of isolated silanols in GD13-NH_4^+: based on ^{1}H NMR and TGA, we have estimated the amount of isolated silanols in GD13-NH_4^+ at 2.7 mmol/g (see Table 3-5 of **Chapter 3**). Considering the surface area of GD13-NH_4^+ (475 m^2/g, see Table 5-1), the surface density of isolated silanols is about 3.4 per nm^2. Hence the average distance between the two silanol, taken, as first approximation as the square root of the surface density, is about 5.4 Å and most isolated silanols have another silanol in close vicinity (at a distance lower than 5 Å) which is consistent with the observation of an intense autocorrelation peak at 1.7 ppm on the ^{1}H DQ-SQ spectrum of GD13-NH_4^+. Beside the silanol peak, a distinct, extended, off-diagonal correlation peak spreading from 1.8 ppm to about 3.5 – 4.0 ppm is observed. It can be attributed to the proximity of the isolated silanol groups with the other type of hydroxyls.[29]

Another autocorrelation peak is observed at (6.7, 13.4) ppm, that can be assigned to ammonium ion. This peak has a higher intensity for GD13-NH_4^+ than for the dealuminated sample. It is to be expected as the density of ammonium is severely decreased by the treatment with CA. The intensity of this autocorrelation peak is nonetheless significantly weaker than the one of the (1.7, 3.4) autocorrelation peak. This seems, at the first sight, surprising as the peaks at 6.7 ppm and 1.7 ppm have similar intensities in the DP spectrum. Moreover, in case of autocorrelation between the four protons of the same ammonium group, one would expect and intense autocorrelation peak at this position. One can therefore postulate that, due to the fact that the four protons of an ammonium group are in rapid exchange with one another, non intense autocorrelation is possible. Hence the autocorrelation observed at 6.7 ppm would

exclusively reflect autocorrelation between neighboring ammonium groups. As the peak at 6.7 ppm stands for the 4 protons of an ammonium ion, the surface density of ammonium is significantly lower than the surface density of isolated silanols (0.7 mmol/g compared to 2.7 mmol/g, see Table 3-5 of **Chapter 3**). Hence the average distance between two NH_4^+ (about 1 nm) is considerably larger than the distance between two isolated silanols, and the probability of two ammonium ions to be in close proximity is reduced (actually one should determine, rather than the average distance between two ammonium ions, the shortest distance between two protons of two adjacent NH_4^+. Although this distance is difficult to evaluate precisely, it could be ca. 2 Å lower than the distance between ammonium. This does however not modify the above conclusion).

Besides, these two intense diagonal peaks, one distinct cross peak pair, corresponding to the interaction between isolated silanol, H-bond silanols (and/or aluminol and/or Si-OH-Al bridges) and ammonium is present on both samples, indicating that ammonium ions NH_4^+ are in close proximity with all types of surface hydroxyls. By comparison with GD13-NH_4^+, all the signals of cross peaks of GD13/0.2CA-NH_4^+ are less intense, in agreement with the much lower density of ammonium in this sample.

Based on the relative intensities of the diagonal cross-peaks of isolated silanols and ammonium, and based on the presence of an off-diagonal peak that links these two types of protons, one can conclude that ammonium and silanols are on the same phase and probably evenly distributed over the silica-alumina phase.

5.2.2.3 Heteronuclear ^{27}Al-^{1}H MAS NMR

A- ^{27}Al-^{1}H D-HMQC 2D NMR

In order to have a better insight in the proton–aluminium spatial connectivity, ^{27}Al-^{1}H D-HMQC 2D NMR was applied for the starting and mildly dealuminated ASA in their ammonium form. Spectra are displayed on Figure 5-9. In addition to the contour plot of the ^{27}Al-^{1}H D-HMQC 2D spectra, slices cut either along the x axis (^{27}Al spectra) or along the y axis (^{1}H spectra) together with the corresponding ^{27}Al and ^{1}H DP spectra are also shown for

analysis assistance. For this experiment, the dehydrated form of the sample was used in order to suppress the overwhelming correlation signal between Al and adsorbed water molecules.

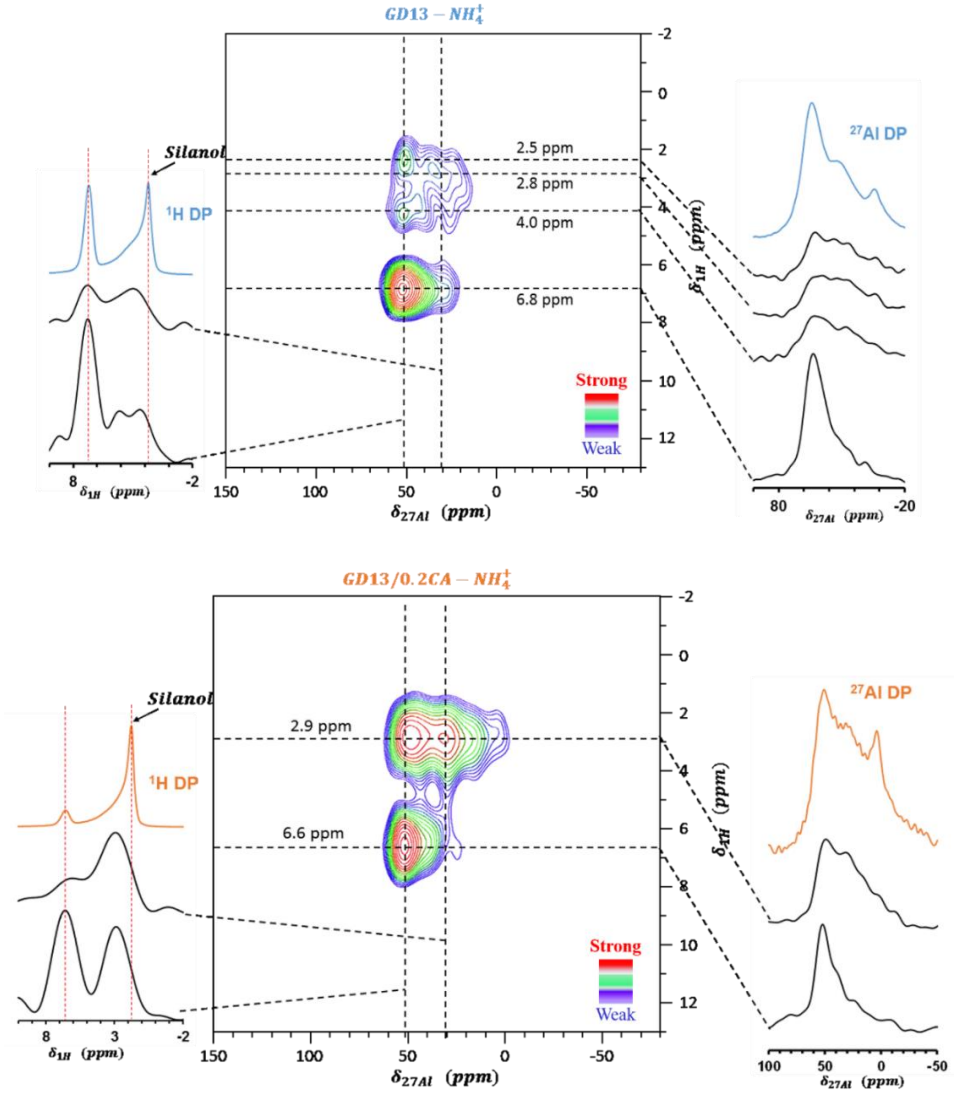

Figure 5-9 ^{27}Al-^{1}H D-HMQC 2D spectra of GD13-NH_4^+ and GD13/0.2CA-NH_4^+. Selected slices are shown aside the spectra: Left part for ^{1}H and right part for ^{27}Al

As these 2D spectra are obtained on dehydrated samples, the peaks are very broad and strongly overlaid on the slices cut along the ^{27}Al axis (see Figure 5-9). Hence, in order to discriminate the Al^{IV}, Al^{V} and Al^{VI} contributions on the ^{27}Al slices extracted from 2D spectra, these spectra have been decomposed (see Figure 5-10) in the same way we did for the DP spectra, i.e. using parameters obtained from corresponding ^{27}Al 3Q MAS NMR spectra (see Table 5-3). The obtained fractions of Al in each coordination for ^{27}Al slices taken at selected ^{1}H values have been reported in Table 5-5.

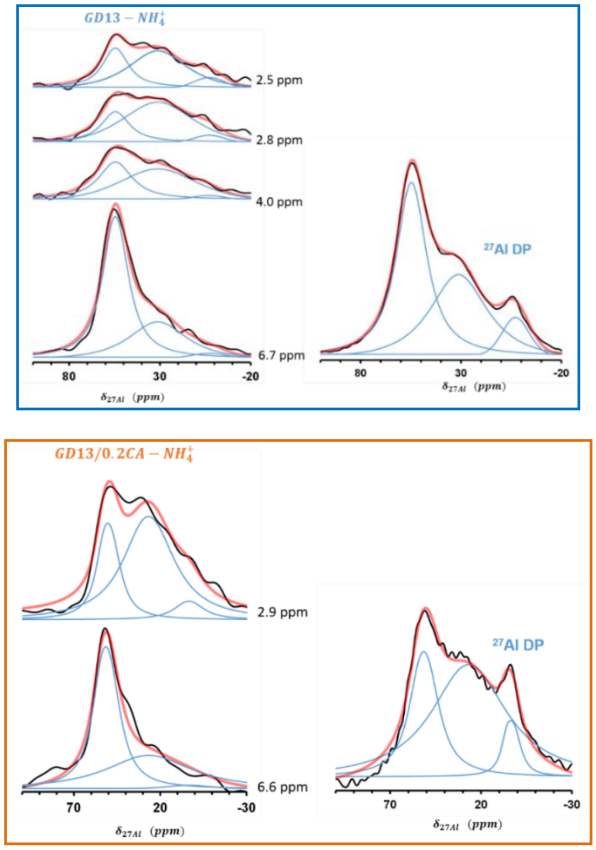

Figure 5-10 Decomposition of Al slices from selected ^{1}H values on ^{27}Al-^{1}H D-HMQC (Figure 5-9) and DP spectra. These decompositions were performed using the parameter from corresponding ^{27}Al 3Q MAS NMR of GD13-NH_4^+ (**top**) and GD13/0.2CA-NH_4^+ (**bottom**)

For the parent ASA (GD13-NH_4^+), the 2D NMR spectrum reveals that the ^{1}H signal of NH_4^+ (6.7 ppm) is strongly correlated with Al^{IV} (52 ppm) indicating that the BAS-Al^{IV} sites are present on the surface of ASAs. The decomposition of the ^{27}Al slice cut at δ_{1H} = 6.7 ppm (Table 5-5 and Figure 5-10) indicates the likely presence of an Al^{V} contribution to this slice. This correlation between Al^{V} and the protons from the ammonium would be consistent with the results reported by Wang et al.[18] who observed a correlation between NH_4^+ protons and Al^{V} on the 2D D-HMQC spectra of their samples and concluded from this result that 5-coordinated aluminium atoms contribute to the Brønsted acidity of the ASA.

Based on the comparison of the hydrated and dehydrated spectra of GD13-NH_4^+, Al^{V} present in dehydrated GD13-NH_4^+ are partly formed by desorption of one water molecule from an Al^{VI} (^{27}Al DP NMR spectra reported on Figure 5-2 and Table 5-3). Part of these Al^{VI} could

be surface species of the alumina-like phase, whose presence was evidenced by the ^{27}Al DQ-SQ experiments (see Figure 5-4). However, the surface Al^{V} species of an alumina-like phase are not expected to have acidic properties. 5-coordinated Al with Brønsted acidic properties are necessarily in the silica-alumina phase. Based on the decomposition of the DP spectra, Al^{V} formed upon dehydration seems to also part originate from a decrease of Al^{IV} (Figure 5-2 and Table 5-3). Hence, acidic Al^{V} may correspond to Al^{V} formed by distortion, upon dehydration, of Al^{IV} of the silica alumina phase. Alternatively, part of the Al^{V} formed upon dehydration could also originate from isolated Al^{VI} at the surface of the silica-alumina phase. Hence, ASA presents two types of BAS, one based on tetra-coordinated aluminium species (Al^{IV}), the other one based on penta-coordinated aluminium species (Al^{V}).

Table 5-5 Al content of the D-HMQC slice and DP spectrum of GD13-NH_4^+ and GD13/0.2CA-NH_4^+

Sample	Al coordination	Al content (%)				
		DP	Slice$^{6.7}$	Slice$^{4.0}$	Slice$^{2.8}$	Slice$^{2.5}$
GD13-NH_4^+	Al^{IV}	53.3	67.9	40.0	26.6	34.4
	Al^{V}	38.9	30.5	57.9	69.1	58.6
	Al^{VI}	7.8	1.6	2.1	4.3	7.0
GD13/0.2CA-NH_4^+	Al^{IV}	28.4	57.1		26.9	
	Al^{V}	64.1	41.4		66.2	
	Al^{VI}	7.5	1.5		6.9	

Beside the correlation with the protons from ammonium, the 2D D-HMQC spectra of the two samples also evidence a correlation between aluminium and hydroxyls. The maxima is located at ca. 3.0 ppm for both samples and there is no evidence of a correlation between the signal of the proton of isolated-terminal silanols (1.8 ppm) and any aluminium. The ^{27}Al NMR spectrum corresponding to a slice cut along the x-axis at $\delta_{1H} \approx 3.0$ ppm shows correlation with Al^{IV}, Al^{V} and Al^{VI}. The position of the maximum (ca. 3.0 ppm) is consistent with Al-OH species (such as μ_2 Al-OH).

B- ^{1}H-^{27}Al REAPDOR

NH_4^+–Al distances (Table 5-6) in GD13-NH_4^+ was obtained by numerical simulation of ^{1}H-^{27}Al rotational echo adiabatic passage double resonance (REAPDOR) experiments using

the protocol proposed by P. P. Man (*http://www.pascal-man.com/pulsesequence/double-resonance/REAPDOR.shtml*). For comparison, this experiment was also performed on a mordenite zeolite in an intermediate H^+, NH_4^+ form.

Table 5-6 ^1H-^{27}Al dipolar interaction constants and Al-H distance in the investigated samples

Sample	Dipolar interaction/Hz	Distance Al-H /pm
$NH_4^+/H^+ mordenite$	507	396
$GD13 - NH_4^+$	848	334

For the mordenite sample, the fit of the experimental curve with theoretical REAPDOR curve gives a dipolar interaction between Al^{IV} and NH_4^+ of 507 Hz. This value is closed to the value obtained by Ganapath et al.[30] for the same zeolite (510 Hz). It corresponds to a distance of 3.96 Å between the Al atom and the protons of the ammonium. This distance is consistent with an ammonium ion charge compensating a Si-O^--Al bridge.

For the GD13-NH_4^+ sample, the calculated value for the dipolar interaction between Al^{IV} and ammonium is stronger (848 Hz) and hence corresponds to a proton of NH_4^+ located at shorter average distance (3.34 Å) from the Al^{IV}. This results tends to indicate that the BAS of ASA have a different structure from the BAS of zeolite.

5.2.3 Characterization of H form ASA

5.2.3.1 ^{27}Al MAS NMR

A- ^{27}Al DP MAS and MQ MAS NMR

Figure 5-11 illustrates the influence of calcination and dehydration on the Al coordination as detected by ^{27}Al MAS NMR. Calcination increases significantly the proportion of Al^V. As discussed in **Chapter 3**, this modification in the speciation of Al between the H form and the NH_4^+ form of the ASAs is probably related to the flexible coordination of some of the Al atoms in ASA, that has been evidenced by Omegna et al.[4] and Parker et al.[31] In the Al^{VI} range, two resonances, a sharp and a broad one can be observed. The sharp resonance corresponds to a small fraction of mobile Al species. The exact nature of these species is not known but they are probably hydrated Al cations $(Al(OH)_{3-x}(H_2O)_{3+x}^{x+})$[32,33]. The broad resonance can be assigned,

at least partly, to alumina domains. For the calcined/dehydrated samples, all the peaks are very broad probably due to both a broad distribution of sites and a strong quadrupolar interaction. This dramatic signal broadening leads to a significant fraction of "NMR-silent" species (about 50% of the signal is lost) in agreement with previous reports.[31] Due to the width of the NMR peaks, decomposition of the spectra is not possible without the input of MQ MAS NMR.

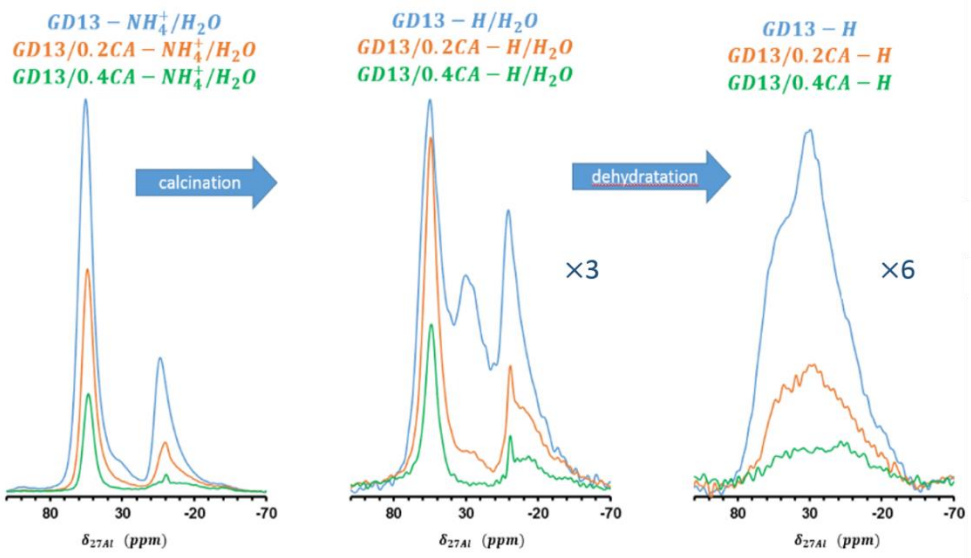

Figure 5-11 ^{27}Al MAS NMR spectra of ASA: hydrated ammonium form (left), calcined (H form) and rehydrated (middle) and calcined (H form) and dehydrated (right)

Figure 5-12 shows the ^{27}Al 3Q MAS NMR spectra of the calcined ASA in hydrated and dehydrated state, respectively. Table 5-7 presents the parameters obtained from the simulation of the 3Q MAS NMR spectra and the fraction of Al in each coordination. As already explained for the spectra of the ammonium forms, these fractions were calculated by decomposition of the 1D ^{27}Al MAS NMR spectra using the quadrupolar product and the isotropic chemical shift derived from the 3Q MAS NMR spectra.

For sample GD13-H/H_2O, in the 40-70 ppm region, i.e. the region of the tetrahedrally coordinated aluminium species, one can, in agreement with previous report by Omegna et al.,[4] distinguishes two different contributions, named Al^{IVa} and Al^{IVb}. The position of the peak Al^{IVa} is close to the diagonal, indicating that the corresponding aluminium atom experiences a relatively small quadrupolar interaction and a weak electric field gradient, hence pointing to a rather symmetric environment. The low C_Q value calculated for this peak confirms that these

Al are in a symmetrical environment and similar to that of Al atoms in tetrahedral substitution in zeolite framework (for hydrated zeolite[34]). This results implies that Al^{IVa} may be located in the silica ($Al(OSi)_4$ units). Peak Al^{IVb}, which appears like a tail to signal Al^{IVa}, deviates from the diagonal in the direction of quadrupolar induced shift, indicating a large anisotropic quadrupolar-induced shift and a substantial electrical field gradient, thus a less symmetric surrounding. The C_Q value calculated for this peak is consistent, either with extraframework Al^{IV} species in hydrated zeolites[34] or with Al^{IV} in an amorphous alumina phase[35] or in γ-alumina[36]. Two other broad signals with a large quadrupolar interaction are observed at around 35 ppm and 0 ppm. They are attributed respectively, to Al^{V} and Al^{VI} (denoted Al^{VIa}). The broad signal Al^{VIa} points toward the presence of a small amount of oligomeric Al, typical of an amorphous alumina zone.[4,35]

After mild dealumination (sample GD13/0.2CA-H), the signal associated with five-coordinated Al is relatively hard to observe by 3Q MAS NMR, and the decomposition of the DP spectra indicates that the fraction of Al^{V} is indeed reduced (from 17.8% to 6.7%). The signal of Al^{IVb} disappears while the fraction of Al^{IVa} is increased and represents a twice higher fraction in the dealuminated sample than in the starting ASA. As the total Al content is divided by ca. 2 between GD13-H and GD13/0.2CA-H (from 2.3 mmol/g to 1.0 mmol/g, see Table 5-1), one can roughly estimate that the Al atoms associated with Al^{IVa} are preserved after mild dealumination. In the region of octahedral Al, the Al^{VIa} is still present. Its fraction decreases slightly from 39.2% to 32.4%, which indicates (considering the twice lower Al content of GD13/0.2CA-H) that this sites also undergo dealumination. Beside this peak, a new, barely detectable peak, Al^{VIb}, is observed. It corresponds, on the DP spectra, to the narrow peak (in agreement with the low C_Q value associated to it) at ca. 0 ppm (that has been assigned to mobile cationic Al species[32,33]).

After severe dealumination (sample GD13/0.4CA-H), the peak associated with Al^{V} has completely disappeared. Al^{IVa}, Al^{VIa} and Al^{VIb} are always present on the MQ-MAS spectra (Al^{VIa} and Al^{VIb} are barely visible on the spectra but can clearly observed on the zoomed insert). The decomposition of the DP spectrum of this sample confirms the complete disappearance of

Al^{IVb} and Al^{V} for this sample.

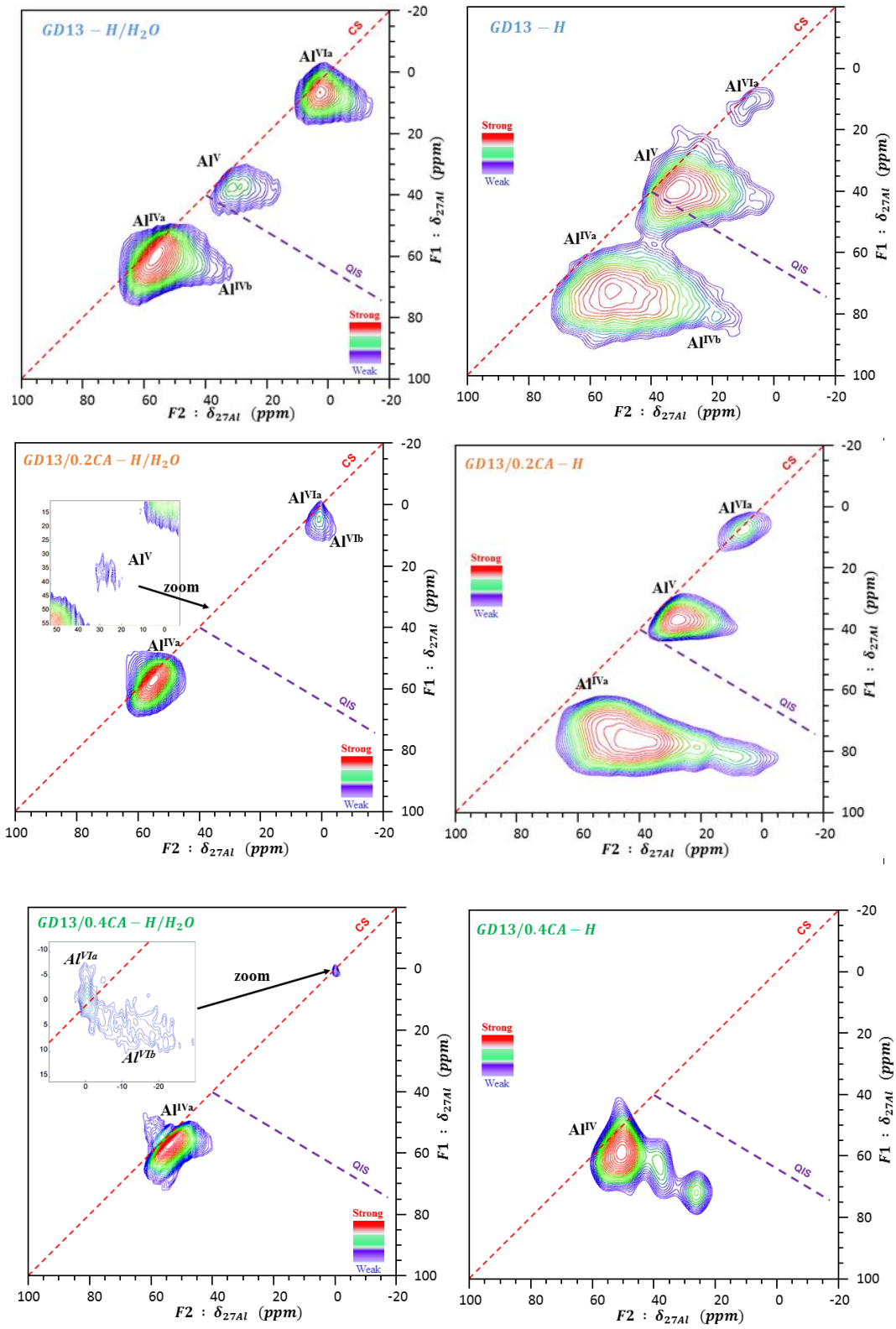

Figure 5-12 ^{27}Al 3Q MAS NMR spectra of H form ASA: hydrated (left) and dehydrated (right)

No extra peaks appear in the spectra of dealuminated samples, indicating that CA

treatment did not lead to the formation of (detectable) new Al species. Dealumination treatment with CA acts differently for the various Al signals. Under mild dealumination conditions, (e.g. concentration of CA = 0.2 M), Al^{IVa} is preserved, whereas all other Al peaks undergo dealumination. Among these others peaks, distorted Al^{IV} (Al^{IVb}) is the most sensitive to dealumination, followed by Al^{V} and finally Al^{VIa}. Under severe dealumination conditions, all peaks, including Al^{IVa} undergo dealumination, but Al^{IVa}, and, to a lower extent Al^{VIa} are less sensitive to dealumination than Al^{IVb} and Al^{V}, which are absent from the spectra of the severely dealuminated sample. Al^{IVa} are, on the severely dealuminated sample, the main Al species.

Table 5-7 The assignment, NMR parameters and relative Al content of hydrated and dehydrated H form ASA

Sample	Al coordination	δ_{F1} ppm	δ_{F2} ppm	δ_{ISO} Ppm	$C_{Q\eta}$ MHz	Al content %
GD13-H/H_2O	Al^{IVa}	59.8	56.8	58.7	2.3	28.3
	Al^{IVb}	63.4	44.6	56.4	5.8	14.7
	Al^{V}	38.0	27.0	33.9	4.4	17.8
	Al^{VIa}	7.2	2.3	5.4	3.8	39.2
GD13/0.2CA-H/H_2O	Al^{IVa}	58.0	54.6	56.7	2.5	54.9
	Al^{V}	35.2	27.6	32.4	3.7	6.7
	Al^{VIa}	6.9	-5.5	2.3	4.7	32.4
	Al^{VIb}	5.5	0.5	3.6	2.9	6.0
GD13/0.4CA-H/H_2O	Al^{IVa}	56.2	54.4	55.5	1.8	64.3
	Al^{VIa}	3.4	-11.4	-2.1	5.1	31.2
	Al^{VIb}	0.1	-0.3	0.0	0.8	4.5
GD13-H	Al^{IVa}	74.5	42.1	62.5	7.6	46.0
	Al^{IVb}	71.8	53.3	64.9	5.7	9.5
	Al^{V}	40.1	25.5	34.7	5.1	23.0
	Al^{VIa}	11.3	7.8	10.0	2.5	21.5
GD13/0.2CA-H	Al^{IVa}	74.9	33.6	59.6	8.6	59.5
	Al^{V}	36.0	22.1	30.9	5.0	27.6
	Al^{VIa}	9.1	5.3	7.7	2.6	13.2
GD13/0.4CA-H	Al^{IV}	63.4	43.6	56.1	5.9	100

The 3Q MAS spectra corresponding to calcined dehydrated samples have been displayed on the right part of Figure 5-12. Quadrupolar parameter and fraction of Al associated with each

coordiantion are reported in Table 5-7. These values are reported for information as they cannot be easily interpreted because only about half of the Al atoms are detected. Hence other Al atoms in unknown coordination are also present and these Al probably have high quadrupolar parameters.

For GD13-H, one still observes two signal in the area corresponding to Al^{IV}. One of the signal has a C_Q value similar to that of Al^{IVb} whereas the other one corresponds to an Al^{IV} in an even more distorted environment. Upon mild dealumination (sample GD13/0.2CA-H) only the Al^{IV} in the most distorted environment remains. Hence one can conclude that the Al^{IV} in the very distorted environment corresponds to Al^{IVa} (which is present on the spectrum of GD13/0.2CA-H/H_2O) and that Al^{IVb} corresponds to the Al^{IV} in less distorted environment, that are absent on the spectra of the hydrated sample. Based on this assignment Al^{IVa} which was in a rather symmetrical environment in the hydrated ASAs is in a much distorted one in the dehydrated environment, while Al^{IVb} has kept its environment and hence is almost insensitive to dehydration. Regarding the strong modification of the symmetry around Al^{IVa} upon dehydration, an even stronger modification in the C_Q parameters (from ca. 3 to ca. 18 MHz[33]) is observed for framework Al atoms of zeolite upon dehydration and is assigned to the formation of the Si-OH-Al bridge. Indeed the formation of this bridge results in one long and three short Al-O bonds[37] and hence in a distortion in the Al^{IV} environment, whereas, in hydrated state, the acid sites form H_3O^+ cations by reaction with water, leading to ($Si\text{-}O^-\text{-}Al$, H_3O^+) pairs. Brønsted acid site of ASA are probably different from those of zeolites, and, anyway, as demonstrated in **Chapter 4**, only a small fraction Al^{IV} of GD13-H and GD13/0.2CA-H have acidic properties. Nevertheless, the behavior of a large fraction of their Al^{IV} is similar to that of Al^{IV} in zeolites. Moreover, the sensitivity of the environment of these Al^{IV} to dehydration indicates that they are located close or at the surface. For the other signal associated to Al^{IV}, Al^{IVb}, the C_Q parameter (and hence the symmetry of the Al) is less influenced by dehydration, clearly indicating that water molecules have no access to Al^{IVb}, which may further confirm that Al^{IVb} correspond to Al atoms from the bulk of the alumina phase. On the dehydrated samples, Al^{VIb} is not observed, in agreement with the assignment of Al^{VIb} to an hydrated Al cation

$(Al(OH)_{3-x}(H_2O)_{3+x}^{x+})$.

Regarding the evolution of the Al environment between GD13-H and GD13/0.2CA-H, one can see that the fraction of Al^{IVa} and Al^{V} both increase upon dealumination. This seems to be at variance with the fact that the Al^{V} decreases upon dealumination for the hydrated samples. However, Al^{V} from hydrated and dehydrated samples are probably different.

We will not discuss sample GD13/0.4CA-H, because, due to its low Al content and strong quadrupolar interaction, the resolutions the DP and MQ spectra are very low and make the interpretation of the spectra too uncertain. Recording the spectra of this sample at higher field and faster speed would probably allow a better interpretation of its DP and 3Q MAS spectra.

B- ^{27}Al DQ-SQ NMR

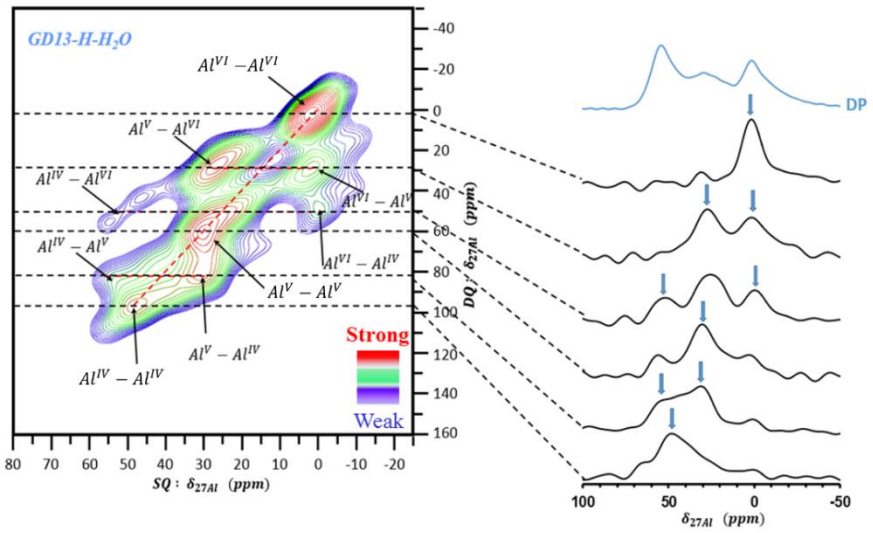

Figure 5-13 ^{27}Al DQ-SQ MAS NMR spectrum of GD13-H/H_2O. For illustrative purposes, selected slices are shown aside the spectrum.

The spatial proximity of various Al environments was studied by ^{27}Al-^{27}Al DQ-SQ MAS NMR on GD13-H/H_2O (Figure 5-13). Three auto-correlation peaks are clearly observable, indicating that Al^{IV}, Al^{V}, Al^{VI} are in close proximity to Al atoms in the same coordination. Apart from the auto-correlation peaks, three pairs of cross peaks between Al^{IV} and Al^{V}, Al^{V} and Al^{VI}, Al^{VI} and Al^{IV} are present, implying that the three kinds of Al coordination are also in close proximity to one another. Looking more closely at the pairs of cross peaks, one can observe the intensities of the signals associated with Al^{IV}-Al^{VI} pairs are weaker than those of

the two other pairs. This observation is consistent with the formation of two phases, an alumina like phase that contains most of the Al^{VI} and a silica-alumina phase that contains most of the Al^{IV}, whereas, Al^{V} are present in the two phases (pure alumina and silica-alumina).

5.2.3.2 ^{1}H MAS NMR

A- ^{1}H DP NMR

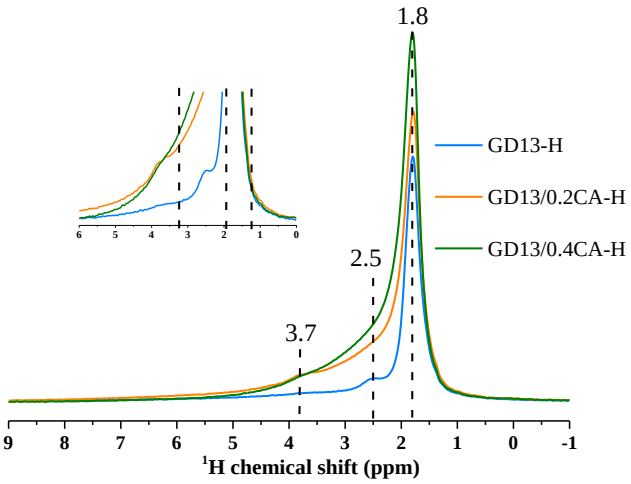

Figure 5-14 ^{1}H MAS NMR spectra of ASAs in their H-form (spectra were recorded on samples freshly dehydrated under vacuum at 200°C)

^{1}H MAS NMR spectra of calcined H-forms of starting and dealuminated ASAs are reported in Figure 5-14. These spectra have already been commented in details in **Chapter 4** and we will simply comment them briefly here. The peak assigned to NH_4^+ is no longer observed, in agreement with complete desorption of NH_3 during calcination. The dominant signal at 1.8 ppm can unambiguously be assigned to isolated or terminal silanol. The signals at 2.5 ppm and 3.7 ppm become better-resolved. After CA treatment, the intensity of the ^{1}H NMR spectrum increases, due to an increase in the intensities of the peaks at 2.6 and 3.7 ppm. However, based on the decomposition of the ^{1}H NMR spectra and their integration, the intensities of these two signals was shown to be too high to be exclusively assigned respectively to bridging $(Al)_xOH$ group and Si-OH-Al, although these hydroxyls may contribute to these peaks. Besides, H bonded hydroxyls also contribute to this broad signal. Other NMR experiments involving ^{1}H are therefore required for an identification of the acidic protons of ASAs.

B- ^{1}H DQ-SQ MAS NMR

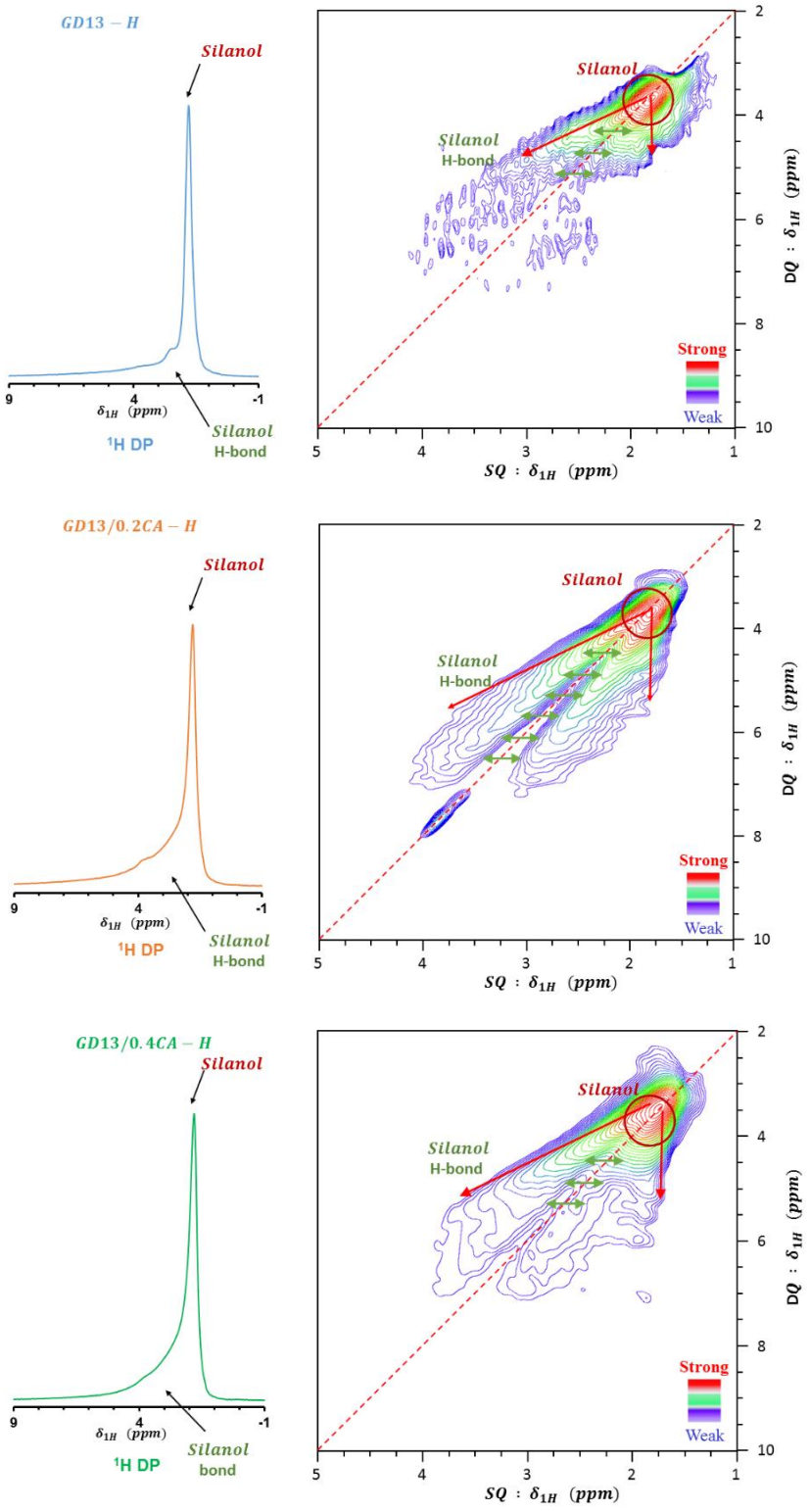

Figure 5-15 ^{1}H DQ-SQ MAS NMR spectra (right) and corresponding ^{1}H MAS NMR spectra (left) of GD13-H (top), GD13/0.2CA-H (middle) and GD13/0.4CA-H (bottom). All spectra were obtained on samples freshly dehydrated at 200°C under vacuum

Figure 5-15 investigates the spatial proximities between proton species with two–

dimensional ^{1}H DQ-SQ MAS NMR. Similar to that of the ammonium form ASA, the spectra of the H-forms exhibit a strong autocorrelation peak assigned to isolated/terminal silanol groups, indicating a spatial proximities (< 5 Å) of the isolated/terminal silanols which is consistent with the surface density of silanols for these ASAs (based on the densities of hydroxyls and surface areas of these two ASA, see Table 4-5), the distance between silanols are: 5.3 Å (GD13-H), 6.6 Å (GD13/0.2CA-H) and 7.3 Å (GD13/0.4CA-H). Along the silanol peak, a distinct long off-diagonal correlation peak spreading from 1.8 ppm to about 3.5 – 4.0 ppm is observed, which indicate the proximity of isolated silanol groups with the hydroxyls responsible for the peak at 2.5 ppm. Hence these hydroxyls are not (or at least not exclusively) surface hydroxyls on a separate alumina phase and a contribution from the silica-alumina phase is also present in this peak (either as H bonded silanols or as surface Al-OH). One can also note the absence of autocorrelation peaks for the signals at 2.6 and 3.8 ppm. This is likely due to the at least twice lower density of these sites, which corresponds to a too high distance (about 10 Å) to allow their observation with the DQ excitation period we used for these experiments.

An extra signal is observed at (3.8, 7.6) ppm for GD13-0.2CA-H only and we observed that this signal disappears when the sample is dehydrated at 350°C for 10 h (the spectrum is not shown here). Whatever the nature of the hydroxyl associated to it, one can be certain that the density of this site is low (as it produces only a very weak signal on the DP spectrum). Hence, the fact that we observe an autocorrelation peak for a species with a low surface density indicates either that, all the hydroxyls of this type are in a separate phase or close to one another or that the species itself contains several hydroxyls. Moreover, this autocorrelation peak is observed only for one sample. Hence, we can discard the hypothesis that this peak is related to acidic proton. That said, this signal cannot be unambiguously assigned, but we can make several suggestions regarding its attribution: it could be due to water molecules adsorbed on Lewis sites, but its position would not be consistent with previous conclusions who usually associate this species with a peak at 6.5 ppm.[34] Alternatively, it could be related to the separate alumina phase (as surface hydroxyls of this phase) whose presence is supported by other NMR experiments. However, according to this attribution, one would expect this peak to be also

present, and more intense on the GD13-H sample. Finally, another possible attribution would be that it is related to the cationic Al species whose presence has been evidenced based on ^{27}Al NMR spectra of some of the samples (in their hydrated form). This last hypothesis would explain why this species is detected only on the spectrum of GD13/0.2CA-H, as the ^{27}Al peak associated with cationic Al species is more intense on the spectrum of than on the spectrum of the other samples (see Figure 5-11).

5.2.3.3 Heteronuclear ^{27}Al-^{1}H NMR

^{27}Al-^{1}H D-HMQC 2D NMR was also utilized to study the spatial proximities between different Al species and various protons in the H-form of the ASAs (Figure 5-16). Only one broad correlation centered at (30, 3.6) ppm appears in the GD13-H spectrum. Considering the width of this signal in the ^{1}H projection, sites associated to this signal could as well be Si-OH-Al bridges (expected at 4.8 ppm) or Al-OH species (from the alumina or from the silica-alumina phases, expected at 2.7 ppm).

Figure 5-17 shows the decomposition of the slice of the ^{27}Al-^{1}H D-HMQC (Figure 5-16) of GD13-H corresponding to δ_{1H} = 3.6 ppm together with the ^{27}Al DP spectrum. These two spectra were fitted using the parameters obtained from ^{27}Al 3Q MAS spectra. Calculated Al fraction for GD13-H are shown on Table 5-8 (we did not attempt to perform the same decomposition on the spectra of and GD13/0.2CA-H and of GD13/0.4CA-H due to a too low signal to noise ratio for these two samples). Although the large widths of the ^{27}Al peaks make it difficult to estimate precisely the type and the fraction of the aluminium species, slice and DP spectrum seem very similar and this is confirmed by their decomposition. Hence the hydroxyls giving rise to the cross peak at 3.6 ppm appear to “see” indifferently Al atoms of all coordinations (including Al^{VI} coordination).

One must also mention that, at variance with the results reported by Wang et al., there is no evidence of a correlation between the signal of the proton of isolated (terminal) silanols (1.8 ppm) and any aluminium.[18] Hence, although we cannot completely discard this hypothesis, an involvement of isolated/terminal silanols in the Brønsted (as proposed by Wang et al.[18]) seems

unlikely because they are too far away from the aluminium.

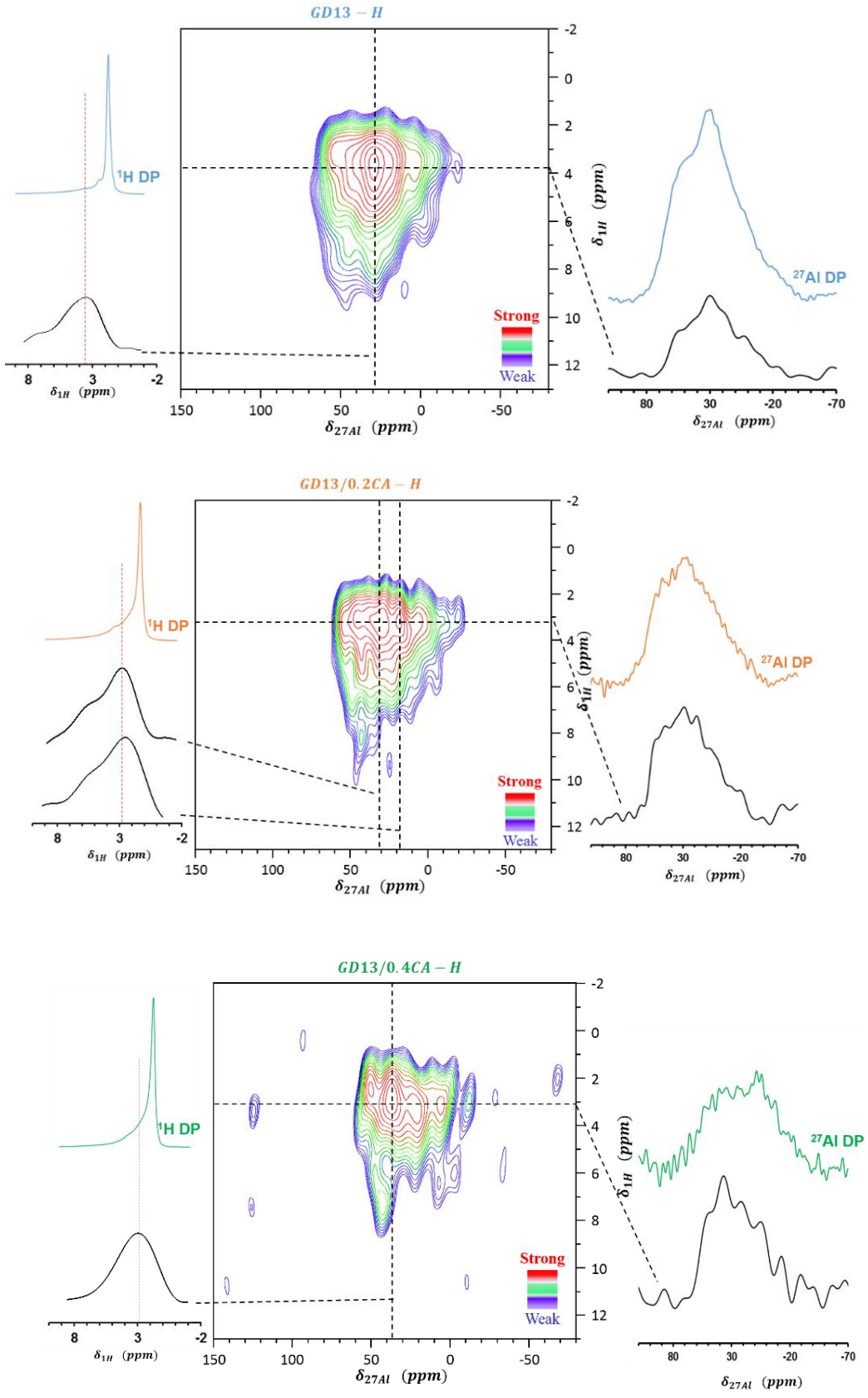

Figure 5-16 ^{27}Al-^{1}H D-HMQC 2D spectra of dehydrated H form ASA

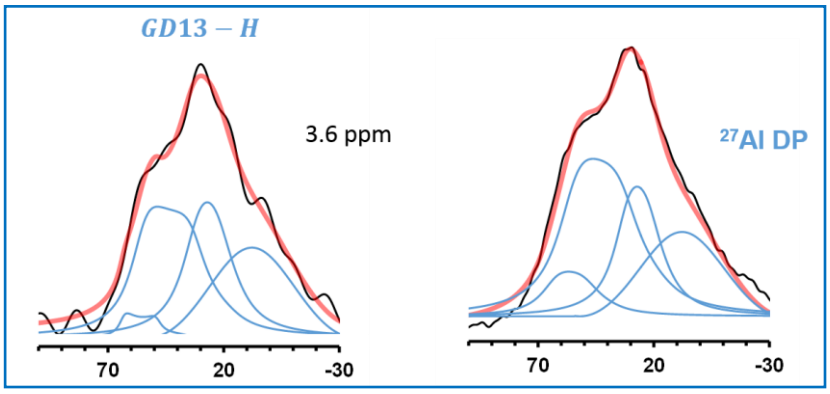

Figure 5-17 **Left**: decomposition of the ^{27}Al slice at δ_{1H} = 3.6 ppm for the ^{27}Al-^{1}H D-HMQC spectra of GD13-H (Figure 5-16); **Right**: decomposition of the ^{27}Al DP spectrum of GD13-H. These decompositions were performed using the parameters extracted from the ^{27}Al 3Q MAS NMR of GD13-H (Figure 5-12)

Results reported here mostly focus on GD13-H sample because the signal to noise ratio of the spectra of GD13/0.2CA-H and GD13/0.4CA-H are too weak to perform a decomposition of a slice of the 2D spectrum. Nevertheless, these two ASA also present, on their ^{27}Al-^{1}H D-HMQC spectra a single correlation signal between protons at 3.2 ppm and aluminium atoms, but coordination of the involved Al atoms cannot be estimated with a reasonable enough accuracy. Recording spectra at higher field and higher speed would be useful for the interpretation of these correlation peaks but could not be performed due to lack of time.

Table 5-8 Al content of the D-HMQC slice at δ_{1H} = 3.6 ppm and DP spectrum of GD13-H

Sample	Al coordination	Al content (%)	
		DP	Slice$^{3.6}$
GD13-H	Al^{IVa}	9.5	3.7
	Al^{IVb}	46.0	40.2
	Al^{V}	23.0	29.9
	Al^{VI}	21.5	26.2

5.3 Summary of NMR results

Before the discussion, we will summarize the facts/hypotheses that have be drawn from the various NMR experiments reported above:

5.3.1 NMR results on ammonium forms of the ASAs:

1) The parent ammonium form ASA GD13-NH_4^+/H_2O at least contains two separated phases: alumina-like and alumina-silica phase (^{27}Al DQ-SQ MAS NMR).
2) Ammonium ions NH_4^+ are in spatial proximity with isolated silanol as well as other types of hydroxyls; hence ammonium and hydroxyls are evenly distributed over the surface of the silica alumina phase (^{1}H DQ-SQ NMR).
3) On hydrated NH_4^+-ASA, Al atoms are mostly 4-coordinated (about 2/3) and 6-coordinated (about 1/3) with a very low fraction of 5-coordinated Al. However, the dehydration of the samples reveals that a large fraction of these atoms have a flexible coordination as a fraction of both Al^{IV} and Al^{VI} converts to Al^{V}. The conversion of Al^{VI} to Al^{V} was interpreted as desorption of a water coordination molecule, whereas the conversion of Al^{IV} to Al^{V} upon dehydration was assigned to the ability of some of the Al^{IV} of the silica-alumina phase to increase their coordination to five by an interaction with a framework oxygen (^{27}Al DP and 3Q MAS NMR).
4) The NH_4^+ cations are located in close proximity of both Al^{VI} and Al^{V}, indicating that beside Al^{IV}, Al^{V} (of dehydrated samples) may also participate to the Brønsted acidity of the ASAs. Beside the interaction of Al atoms with ammonium, another correlation peak is observed between Al atoms of all coordinations (including 6-coordinated Al) and protons responsible for a signal at $\delta_{1H} \approx 3.0$ ppm. These hydroxyls correspond to proton with no or weak acidity (for ammonium forms, acidic protons are expected to participate to the ammonium signal) (^{27}Al-^{1}H D-HMQC 2D NMR). No correlation between Al atoms and isolated/terminal silanols is observed.
5) Al^{VI}-Al^{VI} distances are consistent with Al atoms in an alumina-like phase, whereas Al^{IV}-Al^{IV} distances are consistent with Al^{IV} having another Al^{IV} as second tetrahedral neighbor (Al^{IV}-O-Si-O-Al^{IV}) and hence following the Loewenstein's avoidance rule of zeolites (no Al^{IV}-O-Al^{IV} bond) (^{27}Al 1D DQ-SQ experiments).
6) Distance between ammonium and Al^{IV} in the starting ASA (^{1}H-^{27}Al REAPDOR) is significantly shorter (3.34 Å compared to 3.96 Å) than the distance between

ammonium and Al^{IV} of a reference zeolite (NH_4^+/H-Mordenite).

5.3.2 NMR results on H forms of the ASAs:

1) Calcination increases the fraction of Al^{V} and Al^{VI} in the hydrated samples at the expense of Al^{IV}. This ability of the Al atoms of silica-alumina materials (either amorphous ASAs or crystalline zeolites) to change their coordination between ammonium and H forms has been shown by others[4] to be reversible and indicates that these atoms are accessible to H_2O and NH_3 molecules and hence located at the surface (^{27}Al DP and 3Q MAS NMR on hydrated samples).
2) Always based on ^{27}Al DP and 3Q MAS NMR of the hydrated samples, on can identify 5 types of Al environments:
    - two types of Al^{IV}, one of them (Al^{IVa}) corresponding to a symmetrical environment and assigned to Al^{IV} in substitution in the silica network, whereas the other, Al^{IVb}, which is in a less symmetric environment, corresponds either to extraframework Al^{IV} (by analogy to zeolites) or to Al^{IV} from the alumina phase.
    - one type of Al^{V}, which seems to mostly originate from the surface sites of the silica-alumina phase (based on the evolution of the Al coordination upon calcination)
    - two types of Al^{VI}, the first one, which corresponds to the majority of the Al atoms, Al^{VIa}, is associated to Al atoms in an environment of intermediate symmetry and can be assigned to Al^{VI} of the alumina phase; the second one, Al^{VIb}, is not present on all samples and when present, account only for a small fraction of the Al^{VI}. It corresponds to Al atoms in a very symmetrical environment, and was associated to mobile hydrated Al cations.
3) Mild dealumination with CA, preferentially removes Al^{IVb} and Al^{V} atoms, Al^{VIa} are also removed, but to a lower extent, while Al^{IVa} are preserved; under severe dealumination conditions, all types of Al atoms undergo dealumination but Al^{IVa} and Al^{VIa} are less sensitive to dealumination and Al^{IVa} becomes the predominant species

(^{27}Al DP and 3Q MAS NMR on hydrated samples).

4) For the dehydrated samples, quantitative analysis of ^{27}Al NMR DP signal reveals that about half of the Al atoms are invisible (and hence in an environment of low symmetry, giving rise to very high C_Q values). Therefore, results involving ^{27}Al on calcined dehydrated sample are difficult to interpret as they only concern about half of the effective Al atoms.
5) Dehydration of the calcined ASAs results in an important broadening of the NMR signals. The symmetry of the Al atoms in Al^{IVa} environment is especially strongly decreased. A similar modification of the environment of Al^{IV} atoms upon dehydration is observed for zeolites and assigned to the formation of Si-OH-Al bridges. Although this similarity does not necessary mean that this is what occurs in ASA, this indicates at least that Al^{IVa} atoms are located close to the surface. Mildly dealuminated ASA has a higher fraction of Al^{IVa} than the parent ASA. It also still contains a large fraction of Al^{V}, probably formed by dehydration of Al^{VI}.
6) The starting ASA after calcination is still made of two phases, an alumina phase which contains, when dehydrated both Al^{VI} and Al^{V} (surface atoms) and a silica-alumina phase which contains, when dehydrated Al^{IV} and Al^{V} atoms. As this result is based on ^{27}Al DQ-SQ NMR, isolated Al species may also be present that will not be visible by this technique.
7) Beside isolated silanols, other hydroxyls located at ca. 3.8 and 2.7 ppm are observed by ^{1}H MAS NMR. The close proximity of these sites with isolated silanols (^{1}H DQ-SQ NMR) indicates that they are located in the silica-alumina phase.
8) A spatial proximity between protons and Al atoms is identified by a ^{27}Al-^{1}H D-HMQC 2D NMR. This signal is broad and centered between 3 and 4 ppm in the ^{1}H dimension (and could therefore concerns all hydroxyls except isolated silanols); in the ^{27}Al dimension, it involves indifferently all types of Al.

5.4 Discussion and conclusion

The presence of two phases, an alumina phase (containing mostly Al^{VI}, but also surface

Al^{V}, and a small fraction of Al^{IV}) and a silica-alumina one (containing Al^{IV} and also Al^{V} for the dehydrated and/or calcined samples and a small fraction of cationic Al^{VI} species for the calcined hydrated form), is proposed based on ^{27}Al DQ-SQ NMR (on ammonium and on calcined form of the starting ASAs). Complementary ^{27}Al 1D DQ-SQ experiments (on the ammonium form of the starting ASA) confirmed the distance between Al^{VI}-Al^{VI} was similar to that in γ-alumina.

The close proximity between ammonium and all types of hydroxyls (based on ^{1}H DQ-SQ experiments on the ammonium forms of the ASAs) indicates that all types of hydroxyls (isolated silanols at 1.7 ppm and other hydroxyls at 2.6 and 3.7 ppm) are present in the silica-alumina phase. The exact nature of the hydroxyls (except for isolated hydroxyls) is not known but their quantification (based on ^{1}H NMR experiments, see **Chapter 4**) indicates that they cannot all be related to acidic protons and a fraction of them is probably H-bonded silanols. The fact that the left shoulder of the pic of isolated hydroxyls is also present on the ammonium form of the ASAs confirms that these hydroxyls are not all acidic (otherwise they would be absent in the form of ammonium ion). Part of these hydroxyls are also in close proximity with Al atoms (heteronuclear ^{1}H-^{27}Al NMR experiments on calcined ASAs).

Regarding the results of ^{27}Al NMR (DP and 3Q MAS experiments), they confirm the versatility of coordination of some of the Al (between NH_4^+ and H forms, between hydrated and dehydrated forms) that has been previously evidenced by Omegna et al.[4] This versatility is of course useful, as it indicates that these Al atoms are probably located at (or close to) the surface. However, it also complicates the understanding of the fate of each type of Al atoms during the steps of the preparation of the ASA (dealumination and calcination). Another difficulty we encountered is that, although dealumination allows removing non acidic Al, acidic Al species remains minority (and that is even more true for Brønsted acidic Al species), even in the severely dealuminated ASAs. Moreover, after dealumination (and especially after severe dealumination), the low amount of remaining Al, makes it difficult to obtain good quality 2D NMR spectra in a reasonable time.

Among the Al species that have been identified by ^{27}Al 3Q MAS experiments on calcined

hydrated and dehydrated ASAs, the Al^{IVa} species is of particular interest because its characteristics are very close to those of Al^{IV} in tetrahedral substitution in zeolite framework: on the calcined hydrated samples, this species is in a rather symmetrical environment but the symmetry of its environment strongly decreases upon dehydration (^{27}Al 3Q MAS). Moreover, this species withstands mild dealumination conditions and is the most resistant to dealumination under severe conditions. Furthermore, Al^{IV}-Al^{IV} distance is consistent with Al^{IV} following the Loewenstein exclusion rule: Al^{IV}-Al^{IV} distance of ca. 6 Å (established by ^{27}Al 1D DQ-SQ on the ammonium form of the starting ASA) corresponds to Al distances in Al-O-Si-O-Al ensembles. One can therefore exclude the formation of Al^{IV}-Al^{IV} dimers such as those depicted on the left of Figure 5-18. All these results rather suggest that, in calcined-hydrated form, Al^{IVa} are inserted in the silica matrix forming symmetrical $[Al(OSi)_4]$ units. However, such units are expected to bear a negative charge that must be compensated by a cation, and if this cation is a proton, each Al^{IVa} species should be associated with a Brønsted acid site. This is clearly not the case: based on FTIR of adsorbed pyridine, the density of Brønsted sites in the ASAs is 30-40 µmol/g, a value well below the density of Al^{IVa} in GD13-H and GD13/0.2CA-H (about 600 µmol/g). One could argue that most of the Brønsted sites of ASA are inaccessible or too weak to protonate pyridine. However, their accessibility is established by the fact that their local environment is very sensitive to the hydration/dehydration of the sample (3Q MAS on hydrated and dehydrated calcined samples). Moreover, even if these sites where inaccessible or too weak to protonate pyridine, the presence of Si-OH-Al bridges on dehydrated samples would be observed on the FTIR spectra.

One possibility could be that other species are acting as charge compensating cations. One good candidate would be the cationic Al species whose presence have been evidenced on some of the samples (Al^{VIb} species observed by ^{27}Al DP and 3Q MAS NMR on calcined hydrated samples). However, Al^{VIb} species represent only a small fraction of total aluminium atoms and, although their presence may contribute to decreasing the density of Brønsted acid sites, they cannot account for the strong discrepancy between the amount of Brønsted acid sites and the amount of Al^{IVa}. Ion exchange experiments could be attempted to remove this species

in order to check its effect on the Brønsted acidity (based on FTIR of adsorbed pyridine).

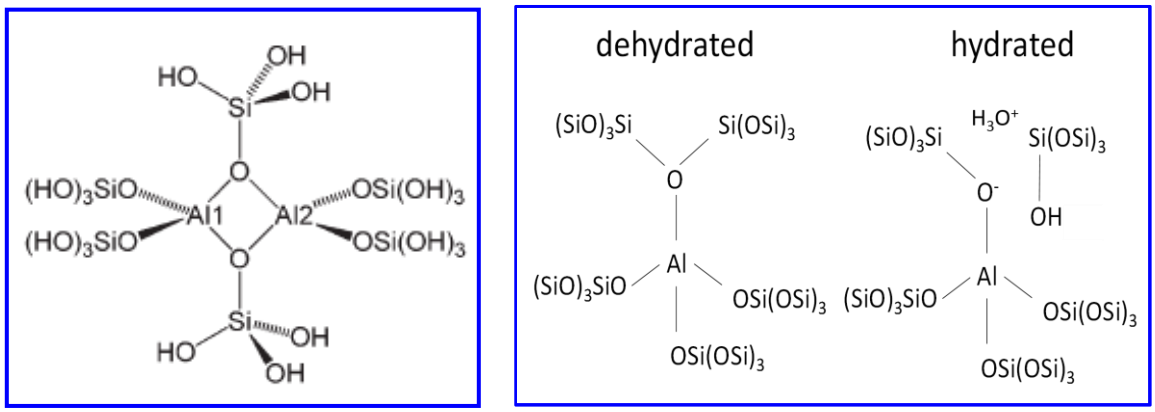

Figure 5-18 Possible structures of a surface tetrahedral Al atoms without significant Brønsted or Lewis acidity: Left: from kermagoret et al [38]; Right: proposed model based on NMR experiments

One must also mention that, although the symmetry around Al^{IVa} decreases substantially after dehydration, this decrease (based on the value of C_Q) is lower than what is usually observed for zeolites. Based on these results, we can propose the following model (Figure 5-18, right) for tetrahedral Al exempt of Brønsted acidity in dehydrated ASA, where the Si-OH-Al of zeolites is replaced by a Si-O-Si-Al bridge. Upon hydration, the bridge is broken, which increases the symmetry around Al atoms.

The short Al-ammonium distance evaluated by the REAPDOR experiments on the ammonium form of the starting ASA implies that, in ASA, NH_4^+ cations are located closer to the Al than in zeolite. This result indicates that Brønsted acid sites are not silanols in proximity with Lewis Al (as this structure would be associated with a longer distance between ammonium and Al^{IV}). The two other possible structures for Brønsted acid sites that are currently envisaged, i.e. pseudo bridging silanols (silanol/Lewis-aluminium pairs that, in presence of a base, react together to form an Si-O^--Al and the protonated base) or a preexisting Si-OH-Al bridge, cannot be discarded but the shorter distance between Al^{IV} and the ammonium remains to explain. Another possible Brønsted acid site consistents with a short ammonium aluminium distance would be Al-OH (Al^{IV} or Al^{V}). Such species would be consistent with the correlation peak at ca. 3 ppm observed on ^{27}Al-^{1}H D-HMQC experiments. However, its detailed structure remains to determine.

Reference

(1) Primo, A.; Garcia, H. *Chemical Society Reviews* **2014**, *43*, 7548.

(2) Weitkamp, J.; Puppe, L. *Catalysis and zeolites: fundamentals and applications*; Springer Science & Business Media, 2013.

(3) Hensen, E.; Poduval, D.; Magusin, P.; Coumans, A.; Van Veen, J. *Journal of Catalysis* **2010**, *269*, 201.

(4) Omegna, A.; van Bokhoven, J. A.; Prins, R. *The Journal of Physical Chemistry B* **2003**, *107*, 8854.

(5) Wang, Z.; Jiang, Y.; Yi, X.; Zhou, C.; Rawal, A.; Hook, J.; Liu, Z.; Deng, F.; Zheng, A.; Baiker, A. *arXiv preprint arXiv:1604.04839* **2016**.

(6) Thomas, C. L. *Industrial & Engineering Chemistry* **1949**, *41*, 2564.

(7) Xu, B.; Sievers, C.; Lercher, J. A.; van Veen, J. R.; Giltay, P.; Prins, R.; van Bokhoven, J. A. *The Journal of Physical Chemistry C* **2007**, *111*, 12075.

(8) Góra-Marek, K.; Derewiński, M.; Sarv, P.; Datka, J. *Catalysis today* **2005**, *101*, 131.

(9) Caillot, M.; Chaumonnot, A.; Digne, M.; Van Bokhoven, J. A. *Journal of Catalysis* **2014**, *316*, 47.

(10) Hensen, E. J.; Poduval, D. G.; Degirmenci, V.; Ligthart, D. J. M.; Chen, W.; Maugé, F. o.; Rigutto, M. S.; Veen, J. R. v. *The Journal of Physical Chemistry C* **2012**, *116*, 21416.

(11) Poduval, D. G.; Van Veen, J. R.; Rigutto, M. S.; Hensen, E. J. *Chemical Communications* **2010**, *46*, 3466.

(12) Chizallet, C.; Raybaud, P. *Angewandte Chemie International Edition* **2009**, *48*, 2891.

(13) Phung, T. K.; Hernández, L. P.; Lagazzo, A.; Busca, G. *Applied Catalysis A: General* **2015**, *493*, 77.

(14) Crépeau, G.; Montouillout, V.; Vimont, A.; Mariey, L.; Cseri, T.; Maugé, F. *The Journal of Physical Chemistry B* **2006**, *110*, 15172.

(15) Matsunaga, Y.; Yamazaki, H.; Yokoi, T.; Tatsumi, T.; Kondo, J. N. *The Journal of Physical Chemistry C* **2013**, *117*, 14043.

(16) Blanchard, J.; Krafft, J.-M.; Dupont, C.; Sayag, C.; Takahashi, T.; Yasuda, H. *Catalysis Today* **2014**, *226*, 89.

(17) Valla, M.; Rossini, A. J.; Caillot, M.; Chizallet, C.; Raybaud, P.; Digne, M.; Chaumonnot, A.; Lesage, A.; Emsley, L.; Van Bokhoven, J. A.; Christophe, C. *Journal of the American Chemical Society* **2015**, *137*, 10710.

(18) Wang, Z.; Jiang, Y.; Lafon, O.; Trébosc, J.; Kim, K. D.; Stampfl, C.; Baiker, A.; Amoureux, J.-P.; Huang, J. *Nature Communications* **2016**, *7*.

(19) Busco, C.; Bolis, V.; Ugliengo, P. *The Journal of Physical Chemistry C* **2007**, *111*, 5561.

(20) Samain, L.; Jaworski, A.; Edén, M.; Ladd, D. M.; Seo, D.-K.; Garcia-Garcia, F. J.; Häussermann, U. *Journal of solid state chemistry* **2014**, *217*, 1.

(21) Williams, M.; Fonfé, B.; Sievers, C.; Abraham, A.; Van Bokhoven, J.; Jentys, A.; Van Veen, J.; Lercher, J. *Journal of Catalysis* **2007**, *251*, 485.

(22) Iuga, D. *Journal of Magnetic Resonance* **2011**, *208*, 225.

(23) Rice, M. J.; Chakraborty, A. K.; Bell, A. T. *Journal of Catalysis* **1999**, *186*, 222.

(24) Martineau-Corcos, C.; Dědeček, J.; Taulelle, F. *Solid State Nuclear Magnetic Resonance* **2017**. *84, 65*

(25) Koller, H.; Lobo, R. F.; Burkett, S. L.; Davis, M. E. *The Journal of Physical Chemistry* **1995**, *99*, 12588.

(26) Huo, H.; Peng, L.; Grey, C. P. *The Journal of Physical Chemistry C* **2009**, *113*, 8211.

(27) Delgado, M.; Delbecq, F. o.; Santini, C. C.; Lefebvre, F.; Norsic, S.; Putaj, P.; Sautet, P.; Basset, J.-M. *The Journal of Physical Chemistry C* **2011**, *116*, 834.

(28) Yin, F.; Blumenfeld, A.; Gruver, V.; Fripiat, J. *The Journal of Physical Chemistry B* **1997**, *101*, 1824.

(29) Brunet, F.; Charpentier, T.; Le Caer, S.; Renault, J.-P. *Solid state nuclear magnetic resonance* **2008**, *33*, 1.

(30) Ganapathy, S.; Kumar, R.; Delevoye, L.; Amoureux, J.-P. *Chemical Communications* **2003**, 2076.

(31) Parker, W. O. N.; Wegner, S. *Microporous and Mesoporous Materials* **2012**, *158*, 235.

(32) Malicki, N.; Mali, G.; Quoineaud, A.-A.; Bourges, P.; Simon, L. J.; Thibault-Starzyk, F.; Fernandez, C. *Microporous and Mesoporous Materials* **2010**, *129*, 100.

(33) Zhao, Z.; Xu, S.; Hu, M. Y.; Bao, X.; Peden, C. H.; Hu, J. *The Journal of Physical Chemistry C* **2014**, *119*, 1410.

(34) Li, S.; Zheng, A.; Su, Y.; Fang, H.; Shen, W.; Yu, Z.; Chen, L.; Deng, F. *Physical Chemistry Chemical Physics* **2010**, *12*, 3895.

(35) Klinowski, J.; Thomas, J.; Fyfe, C.; Gobbi, G. *Nature* **1982**, *296*, 533.

(36) Kim, H. N.; Lee, S. K. *American Mineralogist* **2013**, *98*, 1198.

(37) Bugaev, L. A.; van Bokhoven, J. A.; Sokolenko, A. P.; Latokha, Y. V.; Avakyan, L. A. *The Journal of Physical Chemistry B* **2005**, *109*, 10771.

(38) Kermagoret, A.; Kerber, R. N.; Conley, M. P.; Callens, E.; Florian, P.; Massiot, D.; Delbecq, F.; Rozanska, X.; Copéret, C.; Sautet, P. *Journal of Catalysis* **2014**, *313*, 46.

Chapter 6. Synthesis of ASA with improved acidity by grafting of Al precursors

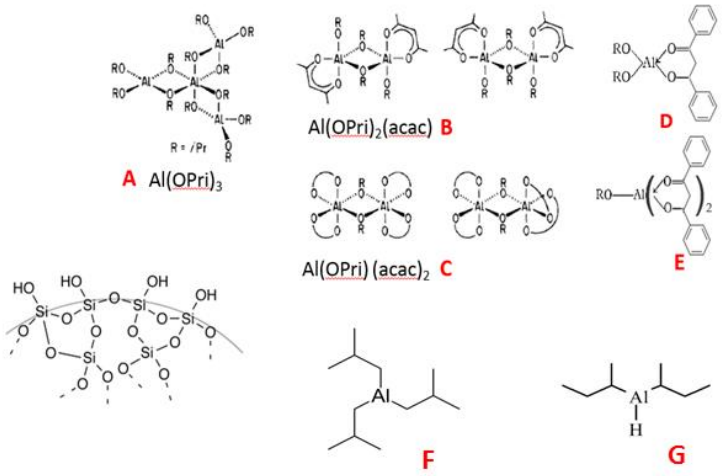

Abstract

Several ASAs were prepared by grafting different types of Al precursors (aluminium alkoxides, triisobutylaluminium, diisobutylaluminium hydride) on silica supports, with the objective to favor the grafting of isolated Al that is expected to be beneficial for obtaining ASA with enhanced acidity. Parameters relevant for a controlled grafting of isolated Al are explored and the prepared ASA are characterized by N_2 adsorption–desorption, FT-IR of adsorbed pyridine and NMR. Only the ASA prepared by grafting diisobutylaluminium hydride displays strong Brønsted acid sites based on pyridine and CO adsorption FTIR experiments. All the grafted ASAs display better performances for 3,3-dimethylbut-1-ene isomerization than a reference zeolite and a commercial ASA, indicating that grafting could be a rational approach for the preparation of ASAs with enhanced acidity.

6.1 Introduction

The Brønsted acidity of amorphous silica-aluminas (ASA) is much weaker in number and in strength than that of zeolites (crystalline microporous aluminosilicates), but their textural porosity and more specifically, their high surface area combined with a large pore size, are very interesting for applications in the field of catalysis. Hence, the development of materials combining the high acid strength and high density of acid sites of zeolites with the open porosity of ASA is greatly desirable. However, the amorphous nature of ASA makes the understanding and optimization of the acidic properties of their surface highly challenging. Commercial ASAs, such as those used in the preceding chapters, are usually prepared by coprecipitation of Al and Si precursors.[1] The characterization of these commercial ASA (^{27}Al NMR and evaluation of the acidity based on pyridine adsorption) has clearly established that, although these ASAs contain a large fraction of tetrahedral Al (from about 50% for the ASA with 25 wt% of alumina to 65% for the ASA with 13 wt% of alumina), less than 5% of the Al atoms of these ASA are associated with Brønsted or Lewis acid sites strong enough to interact with pyridine. Hence, these ASAs contain a large fraction of Al atoms that are silent in terms of acidity. Dealumination, especially dealumination with CA (**Chapter 4**), has proven to be an

efficient method to increase the fraction of acidic Al by selectively removing non acidic ones.

Another approach to the preparation of ASA with a high fraction of acidic Al is the grafting of aluminium precursors on the surface of a high surface area silica. In order to favor the formation of isolated Al sites (i.e. Al sites that are surrounded by Si atoms and hence, Al atoms with potential acidic properties), we have used, for the preparation of these ASA by grafting, monomeric Al precursors.

6.1.1 Parameters relevant for a controlled grafting of isolated Al

Several parameters can be identified as essential for the successful preparation of ASA with enhanced acidic properties: the choice of the silica support, the starting aluminium precursor and the grafting conditions.

6.1.1.1 Characteristics of the silica support

Table 6-1 Concentrations of isolated hydroxyls (OH_i), H-bonded hydroxyls(OH_H) and strained siloxanes(SiOSi) on silica measured by TGA (values are reported in molecules per nm^2)[6]

Functional group	Pretreatment temperature/°C				
	152	320	500	900	1300
OH_H	3.2	2.1	0.2	0.0	0.0
OH_i	1.4	1.4	1.3	0.8	0.0
SiOSi	0.0	1.0	1.5	2.4	0.2

Grafting of Al precursor onto the surface of silica occurs through the reaction between the Al precursors and surface silanols of silica. Therefore, increasing silanol density, could be an effective and straightforward way to increase the amount of grafted Al. When performed at moderate temperature (between 150 and 200°C) thermal pretreatment of the silica supports before grafting only eliminates physisorbed water; when performed at higher temperature, it also reduces their hydroxyl population, and hence the density of anchoring sites. The hydroxyl groups of silica have low or no mobility at moderate temperatures (<= 450°C).[2] Dihydroxylation at intermediate temperature (between 200 and 500°C) proceeds between two adjacent hydroxyl groups with elimination of a water molecule. It decreases therefore significantly the density of hydrogen-bonded silanols. When the surface density of hydroxyls

becomes very low, most of the silanols can be presumed to be isolated.[3] Thermal treatment at 700°C or above results in a reconstruction of the silica surface. It leads to a highly strained reactive surface that may participate in anchoring reactions.[3-5] Hence, different pretreatment temperatures lead to various concentrations of isolated and H-bonded silanol on the silica surface, as summarized in Table 6-1 as reported by Bartram team.[6]

The natural surface density of hydroxyls on silica is always about 4-5 OH per nm^2, independently of the surface area of the silica. Hence silica support with high surface area will be preferred, as they will offer more grafting sites per unit of weight. Moreover, a porosity with large pores is required so as to permit molecular diffusion of the Al precursors as some of them are bulky (see below). This could also be an advantage for the application of the ASA as catalysts for reactions involving bulky molecules. Therefore, silica with large pores and high surface area was synthesized and used (see 2.1.3 on p48).

6.1.1.2 Choice of the Al precursor

Monomeric aluminium precursors are preferable to dimeric or multimeric ones for obtaining isolated surface Al sites. Several Al precursors have been utilized in this study.

1. Aluminium alkoxides

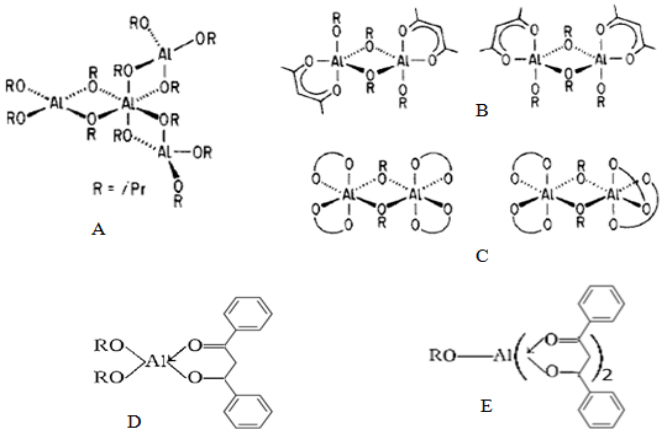

Figure 6-1 The possible structures of aluminium alkoxides. A: $Al(OPr^i)_3$ B: $Al(OPr^i)_2(Acac)$ C: $Al(OPr^i)(Acac)_2$ D: $Al(OPr^i)_2(DBM)$ E: $Al(OPr^i)(DBM)_2$

$Al(OPr^i)_3$ is commonly used as an Al precursor to create acid sites on silica support by grafting.[7-11] This precursor however is not a monomer but a tetramer. The driving force for the

formation of oligomers is the coordinative unsaturation of Al in aluminium alkoxide.[12,13] Grafting this precursor may therefore favor the formation of grafted Al oligomers on the silica surface at the expense of isolated Al. Substitution of one or two OPr^i ligands in $Al(OPr^i)_3$ with a chelating ligand such as acetylacetone (Acac) or its bulkier analog, dibenzoylmethane (DBM), should reduce the coordinative unsaturation of Al complex, resulting in tetrahedral dimers, or even monomeric species when bulky ligand such as DBM is used. Their structure described in Figure 6-1.

2. Triisobutylaluminium (T^iBA)

Benn et al. established, based on ^{27}Al NMR experiments, that T^iBA in solution in toluene is monomeric.[14] The low coordination of Al in this complex (coordination 3), is due to the very bulky character of the triisobutyl groups. Due to its high coordinative unsaturation, this Al complex has a high Lewis acidity and a high reactivity. Therefore, it reacts not only with Si−OH but also with more inert strained siloxane bridges Si−O−Si.[4,15] Copéret team[16] reported on grafting excess T^iBA on SBA15 dehydroxylated at moderate temperature (500ºC). They observed a remarkable incorporation of Al into the framework of SBA15 yielding three different Al sites according to ^{27}Al NMR spectroscopy. They used first principle calculations to propose structures for these three sites and they identified tetrahedral $Al(OSi)_4$ as a possible structure for one of these sites.

3. Diisobutylaluminium hydride (D^iBAH)

D^iBAH exists in solution in nonpolar solvants in a trimeric form[17], however, in low concertation, it may also form monomers or dimers[18]. Werghi et al.[5] investigated the grafting of trimeric D^iBAH on silica surface and proposed the following mechanism, where the trimer reacts successively with three surface silanols in 3 steps, without affecting the siloxane bridges:

Step (1) Trimer + ≡SiOH → Dimer + ^{i}BuH + [(≡SiO)$_2$Al-^{i}Bu] + ≡SiH (Eq. 2)

Step (2) Dimer + ≡SiOH → Monomer + ^{i}BuH + [(≡SiO)$_2$Al-^{i}Bu] + ≡SiH (Eq. 3)

Step (3) Monomer + ≡SiOH → H_2 + [(≡SiO)$_2$Al-^{i}Bu]+ ≡Si-^{i}Bu (Eq. 4)

Therefore, though D^iBAH is not a monomer, it may graft on silica surface as isolated Al.

6.1.1.3 Conditions for grafting

The grafting will be performed under inert atmosphere to prevent the prehydrolysis of the precursor and inhomogeneous deposition.

6.1.2 Objectives

The goal of this study on the grafting of monomeric Al precursors on silica surface, is to prepare well-defined ASA with a controlled Al environment and a high density of acid sites. These ASAs can be regarded as ideal models for further understanding the structure of the acid sites of ASA and also for the enhancement of the acidity of ASAs. Indeed, the amorphous nature of silica makes it impossible to prepare perfectly homogeneous models ASA, but, by using a grafting technique, the mixed oxide phase is restricted to the surface, and this could simplify the comprehension of the structure of the acid sites. Hence, the acidic properties and the Al environment of these ASA will be investigated in order to gain more information on the structure of the acid sites of ASA.

6.2 Experimental

6.2.1 Synthesis

Commercial silica support S4, S6 (Table 2-1 on p47) and two lab-prepared silica with high surface $S4_h$ (HYD9) and S9 (HYD5) (Table 2-2 on p48) have been introduced in **Chapter 2**.

Silica where dehydroxylated at the required temperature under secondary vacuum, either in a pyrex (for $T_{dehydroxy} \leq 500^oC$) or in a quartz reactor (for $T_{dehydroxy} = 700°C$). All the operations were carried out in a moisture free atmosphere of dry argon using standard Schlenk or glove box techniques.

6.2.1.1 Grafting $Al(OPr^i)_3$ and substituted aluminium alkoxides

Silica S4 (2 g) pretreated at 200°C in the oven overnight was added in solution containing 2 mmol $Al(OPr^i)_3$, and respectively 0, 2 and 4 mmol of a chelating ligand (L, where L is Acetylacetone (Acac) or Dibenzoylmethane (DBM)) and 50 ml of anhydrous toluene. Grafting

was performed under an argon atmosphere, because $Al(O^iPr)_3$ is very sensitive to water: in presence of water, it hydrolyzes and forms readily undesired small Al polymers in solution. After 24 h stirring at room temperature, the supernatant was removed by centrifugation and the solid phase was washed with about 20 mL absolute ethanol three times to remove the weakly adsorbed species, and dried overnight at 110°C in an oven. The samples were characterized either in this uncalcined form or after calcination at 550°C for 5 h at a heating rate of 2°C/min. The obtained products were denoted as S4A, S4A-Acac, S4A-2Acac, S4A-DBM, and S4A-2DBM. Grafting of Al was also performed on higher surface area silica $S4_h$ or bigger pore size silica S7 using the same procedure. These samples were denominated with $S4_h$/S7 instead of S4.

6.2.1.2 Grafting of Triisobutylaluminium (T^iBA)

T^iBA is pyrophoric and must be handled with great care. Grafting was performed under argon atmosphere in glove bag and activated 4 Å molecular sieves was put in the glove bog at least 2 h in advance to remove moisture. 2 g silica, pretreated at different temperatures (200°C in the oven overnight or 500°C under secondary vacuum for 10 h), was slurried in a triple Schlenk tube with n mL of a 1.0 M T^iBA in hexanes corresponding to n mmol of T^iBA (n = 2 or 10) and 50 ml of anhydrous toluene. After 3 h stirring at room temperature, the solid phase was left to settle and the supernatant was removed with a pipette. 20 ml toluene were added and the slurry was stirred during several minutes, and then left to settle during several minutes. The supernatant was again removed with a pipette. Another 20 ml toluene containing absolute ethanol was added in order to decompose unreacted M-^{i}Bu (M=Si or Al) groups. Subsequently, the supernatant was separated by centrifugation and the solid phase was extensively wash with absolute ethanol three times to remove weakly adsorbed species, and then dried overnight at 110°C. Finally, the product was calcined at 550°C for 5 h at a heating rate of 2°C/min. The obtained product was denoted as Sx-t-nT, where Sx is one of the silica support, "t" is the pretreatment temperature, "n" is amount of T^iBA (in mmol per 2 g of SiO_2), and "T" stands for T^iBA. A second grafting, on an already T^iBA grafted sample, was also performed in an attempt to increase the Al content (and the density of acid sites). S4-200-(10+2)T was synthesized by

performing the grafting procedure described above on calcined sample S4-200-10T activated at 200°C in the oven overnight.

6.2.1.3 Grafting of Diisobutylaluminium hydride (D^iBAH)

D^iBAH is also pyrophoric and must be handled with care. Silica S9 was calcined at 550°C 5 h before used. The silica support (0.8 g) was pretreated at 150°C in a vacuum oven overnight and 500°C or 700°C for 10 h under secondary vacuum. After pretreatment at high temperature, a highly dehydroxylated silica is obtained that exposes, beside a few isolated silanols, highly strained, reactive siloxane (Si-O-Si) bonds. To avoid traces of moisture, the transfer of the material to the Schlenk tube was performed under dry Ar atmosphere in glove bag. The Schlenk with pretreated silica was purged under vacuum and filled with nitrogen to completely eliminate all the residual in the Schlenk tube. 0.5 ml 1.0 M D^iBAH solution in toluene (corresponding to 0.5 mmol of D^iBAH) was diluted in 10 ml toluene in a glove bag filled with Ar. To slow down the reaction of grafting, the solution of D^iBAH was transferred with syringe to the Schlenk containing the activated silica, that have been, beforehand, placed in a liquid N_2 dewar. A rubber balloon was connected to collect the gases and enable their expansion. After that, the reaction was maintained at RT under stirring for 1 h. Then the solid was washed with about 20 mL anhydrous toluene 3 times to eliminate unreacted D^iBAH. Finally, the solid was dried under vacuum oven at 110°C overnight and then calcined at 550°C for 5 h at a heating rate of 0.2°C/min. The obtained product were denoted as Sx-t-D, where Sx is the name of the silica used as support, "t" is the pretreatment temperature and "D" stands for D^iBAH.

6.2.2 Characterization and catalytic test conditions

Characterization methods and Catalytic test conditions used in this chapter have been already described in § 2.2.

6.3 Results

6.3.1 ASA grafted with $Al(OPr^i)_xL_{3-x}$

6.3.1.1 Composition and textural properties

Aluminium contents of the ASA prepared by grafting $Al(OPr^i)_xL_{3-x}$ (where L stands for

acetylacetone –denoted Acac or Dibenzoylmethane –denoted DBM) are reported in Table 6-2. Grafting of $Al(OPr^i)_3$ on silica S4 yields Al loading of 0.82 mmol/g. The OH density of S4 is 4.36 mmol/g (Table 2-1), which is more than enough for fully grafting the Al introduced in the solution (equivalent to 0.95 mmol of Al per g of SiO_2). This results tends to indicate that other parameters than the density of surface hydroxyls, such as the size of the precursor, determines the maximal amount of Al that can be grafted under these conditions. The complexation of $[Al(OPr^i)_3]_4$ with one or two equivalents of Acac per Al results in derivatives $[Al(OPr^i)_2(Acac)]_2$ and $[Al(OPr^i)(Acac)_2]_2$, respectively. Acac-substituted aluminium alkoxides have, due to their lower coordinative unsaturation, a decreased reactivity toward grafting. Hence, the Al loading, when using these substituted Al alkoxide is about twice lower than when grafting $Al(OPr^i)_3$. On the contrary, DBM-substituted aluminium alkoxides has a similar (2 DMB per Al) or higher grafting efficiency than $Al(OPr^i)_3$. This may be due to a smaller degree of association (and hence a higher reactivity) of this Al complex. Indeed, in $Al(OPr^i)(DBM)_2$, the bulkiness of the two DBM ligands may impedes the formation of dimers (complementary ^{27}Al NMR of the $Al(OPr^i)_xL_{3-x}$ solutions would be helpful to clarify this point but could not be done due to lack of time).

$S4_h$, a silica support with higher surface area, allows to graft a higher amount of aluminium. One must mention here that the values of grafted Al for $S4_h$ may be overestimated as $S4_h$ is a lab-made silica used without prior calcination, which probably contains a larger fraction of adsorbed water than the other samples. As the weight of introduced silica is measured before pretreatment at 200°C, the actual value of dry silica for this sample may be significantly lower than 2 g. This would explain why, for this sample, the Al loading for $S4_h$A-DBM, significantly exceed the maximum expected loading. Lower surface area associated with larger pore size decreases the loading. Hence, the surface loading seems to be mostly controlled by the surface area of the support. This can be verified by calculating the surface density of Al based on the mass density and the surface areas (also reported in Table 6-2). This calculation allows verifying that, for the same Al precursor, the surface density varies only slightly with the silica support (from 0.88 to 1.11 Al per nm^2 for the grafting of $Al(OPr^i)_2$DBM and from

0.39 to 0.54 Al per nm^2 for the grafting of $AlOPr^i(Acac)_2$.

Table 6-2 Designation, Al content and textural properties of ASA prepared by grafting $Al(OPr^i)_xL_{3-x}$ precursors

Sample	Al	S_{BET}	Al	Pore Size	Pore Volume
	mmol/g	m^2/g	At/nm^2	nm	cm^3/g
S4		523		3.7	0.61
S4A	0.82	461	1.07	3.7	0.54
S4A-Acac	0.41	496	0.50	3.3	0.63
S4A-2Acac	0.44	493	0.54	3.3	0.62
S4A-DBM	0.83	449	1.11	3.7	0.53
S4A-2DBM	1.04	462	1.36	3.7	0.56
$S4_h$		1022		3.3	0.89
$S4_hA$-2Acac	0.56	865	0.39	3.3	0.74
$S4_hA$-DBM	1.19	817	0.88	3.3	0.71
S7		381		7.1	0.65
S7A-2Acac	0.26	346	0.45	6.2	0.62
S7A-DBM	0.52	354	0.88	6.2	0.57

Deposition of Al species on the two silica supports with the highest surface area reduces the surface area of about 20% and the pore volume, while the pore size is unchanged, whereas, for the silica with larger pore, the decrease in the surface area is significantly smaller (about 7%). The smaller decrease in the surface area for this support may be related with the lower amount of Al that is incorporated to its surface. For all supports, the decrease in the surface area is moderate but, it still exceeds the value that could be expected based on the weight gain (between 2 and 6 %) due to the incorporation of Al. It could therefore indicate a moderate pore blocking by some alumina like debris.

6.3.1.2 Acidic Properties

FTIR of adsorbed pyridine was used to quantify the various acid sites present on the surface. Values are reported in Table 6-3. The total acidity is 107 µmol/g for sample S4A and decreases to 65 and 89 µmol/g for samples S4A-Acac and S4A-2Acac, respectively. Replacement of one or two OPr^i ligands by acetylacetone, by decreasing the amount of grafted Al, decreases the total acidity. However, it results in higher ratio of BAS to LAS (although

most of the BAS are weak) and higher effective acidity (higher percentage of acidic Al). DBM-substituted aluminium alkoxides result in samples with acidic properties similar to those of S4A. ASA with higher surface area allows to generate higher total acidity while keeping the same percentage of acidic Al. This can be assigned to the fact that higher surface area allows increasing the density of Al per gram of support while keeping the same surface density.

Table 6-3 Type of acid sites (Lewis Acid Sites = LAS), Brønsted Acid Sites = BAS) and acid strength distribution of ASA prepared by grafting $Al(OPr^i)_xL_{3-x}$ precursors on silica, determined by pyridine-IR

Sample	Acidity (µmol/g)									Aciditic Al
	Total	BAS				LAS				
	B+L	weak	medium	strong	total	weak	medium	strong	total	%
S4A	107	8	15	0	24	11	33	39	83	13.1
S4A-Acac	65	18	4	0	21	8	8	27	43	15.8
S4A-2Acac	89	19	5	0	24	19	11	35	65	20.1
S4A-DBM	109	18	9	0	27	28	14	39	82	13.1
S4A-2DBM	102	17	7	0	24	27	14	38	78	9.8
$S4_hA$-2Acac	116	27	18	0	44	9	1	61	71	20.8
$S4_hA$-DBM	136	28	20	0	48	19	15	53	88	11.5

6.3.1.3 Aluminium coordination

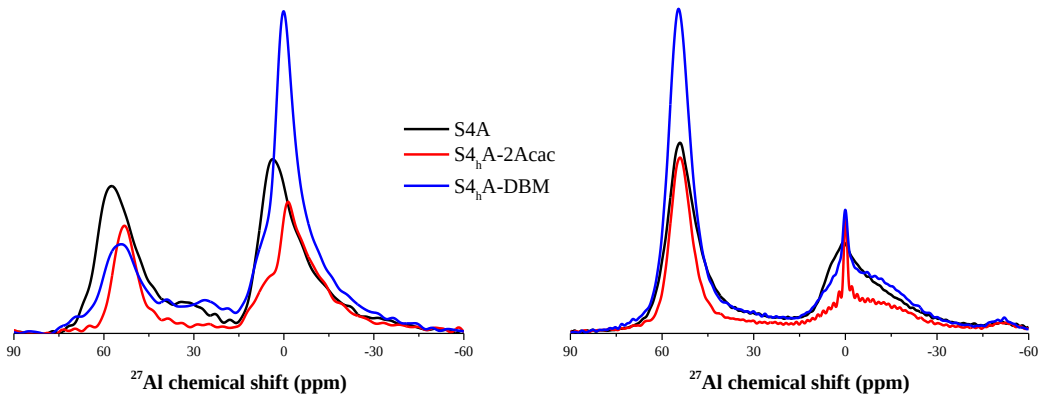

Figure 6-2 ^{27}Al MAS NMR of ASA grafted aluminium alkoxides before (left) and after calcination (right). All curves have been normalized by sample weight and calcined samples were rehydrated before measurement

Selected samples were characterized by ^{27}Al MAS NMR before and after calcination in order to study the Al coordination and its modification after calcination. Spectra are shown in Figure 6-2 and various aluminium species in the samples based on the deconvolution of their

^{27}Al MAS NMR are summarized in Table 6-4. All the spectra exhibit two main peaks at around 56 and 0 ppm, attributed to aluminium in tetrahedral (Al^{IV}) and octahedral (Al^{VI}) environment, respectively. The nonzero intensity between these two main lines, which is more easily observed on sample $S4_hA$-DBM (i.e. the sample with the highest Al loading), indicates the presence of a weak component, corresponding to pentacoordinated aluminium Al^{V}.[19]

Table 6-4 Distribution of various aluminium species in samples grafted $Al(OPr^i)_xL_{3-x}$ based on the deconvolution of their normalized ^{27}Al MAS NMR, Al content was calculated based on the amount of Al in the corresponding sample determined by elemental analysis

Sample	Uncalcined						Calcined					
	Al percentage (%)			Al content (mmol/g)			Al percentage (%)			Al content (mmol/g)		
	Al^{IV}	Al^{V}	Al^{VI}	Al^{IV}	Al^{V}	Al^{VI}	Al^{IV}	Al^{V}	Al^{VI}	Al^{IV}	Al^{V}	Al^{VI}
S4A	37.2	12.3	50.5	0.31	0.10	0.41	49.4	5.6	45.1	0.40	0.05	0.37
$S4_hA$-2Acac	38.1	1.8	60.1	0.21	0.01	0.34	54.9	3.7	41.4	0.31	0.02	0.23
$S4_hA$-DBM	20.7	13.6	65.7	0.25	0.16	0.78	60.6	3.7	35.7	0.72	0.04	0.43

On the spectra of the uncalcined $S4_hA$-DBM and $S4_hA$-2Acac, the peak at ca. 0 ppm seems to be made of two contributions at ca. 0 and ca. 4 ppm. Moreover, a large fraction of the Al atoms are in octahedral coordination in all uncalcined samples but the fraction of Al^{VI} is higher for $S4_hA$-DBM and $S4_hA$-2Acac than for S4A. Calcination converts a large fraction of Al^{VI} species into Al^{IV}, especially for $S4_hA$-2Acac and $S4_hA$-DBM. The conversion of such a large fraction of Al^{VI} species into Al^{IV} upon calcination is not common for aluminosilicate materials. However, this can be partly explained by the fact that, for $S4_hA$-DBM and $S4_hA$-2Acac, a large fraction of the grafted species are AlL chelates where L is either Acac or DBM. Indeed, the chelating ligands are difficult to hydrolyze and will not be easily removed from the Al, even after grafting. These chelating ligands increase the average coordination of the grafted Al. After the final calcination step (550°C), chelating agent are eliminated by decomposition, and the Al atoms change their coordination from octahedral to tetrahedral. Furthermore, according to Hensen et al.,[20] calcination may also result in a redistribution of the surface aluminium species in two competing processes, namely the diffusion of aluminium into the silica network and sintering of aluminium into separate domains of a phase in which octahedral Al is dominant. As for which process plays a dominant role, it depends on the surface density

of grafted Al species. When the surface density of grafted Al species is low, agglomeration to alumina like domains is very limited and calcination favors the insertion of Al into the silica matrix. Conversely, when the surface Al coverage is high, not all Al atoms can be inserted into the mixed phase and agglomeration occurs via formation of Al-O-Al network, leading to an alumina phase similar to transition alumina phase (and hence to a high fraction of Al^{VI} after calcination).

The fraction of Al^{IV} in the calcined samples increases in the order S4A < $S4_hA$-2Acac < $S4_hA$-DBM which could be related to a decrease in the nuclearity of the Al precursor.

6.3.1.4 Hydroxyl groups

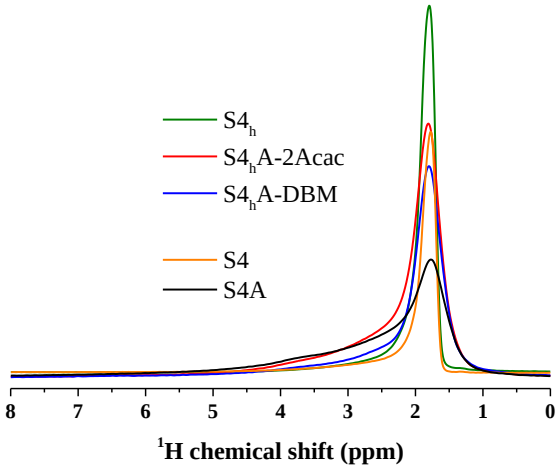

Figure 6-3 ^{1}H MAS NMR of ASA prepared by grafting of aluminium alkoxides on S4 and S4h silicas. Spectra of the starting silica are also shown for comparison; spectra are measured on samples dehydrated at 200°C; all curves were normalized by sample weight

^{1}H NMR spectroscopy was used to distinguish the different types of hydroxyl groups, as illustrated in Figure 6-3. The ^{1}H NMR signal can be decomposed in three contributions at 1.8, 2.6 and 3.8 ppm. For the silica supports, the dominant contribution at 1.8 ppm, can be attributed to isolated silanol Si-OH groups[21] and to terminal (H acceptor) silanols[22] and the weak left shoulder to H bonded (H-donor) silanols. As expected, based on the TGA measurements for these two samples (Chapter 2, §2.1.2 & §2.1.3), $S4_h$ contains a significantly higher density of hydroxyls than S4, thanks to its higher surface area.

For the two silicas, after grafting, the intensity of the band associated to isolated (terminal)

Si-OH decreases significantly, and the higher the Al loading, the stronger the decrease. Moreover, the shoulder on the left of the peak at 1.8 increases in intensity and becomes broader. This could be, at least partially, due to the presence of Al-OH-Al groups (expected at 2.6 ppm, similar to bridging surface μ_2-OH groups in gamma alumina[23]) and also possibly to Si-OH-Al bridging hydroxyl groups (expected at 3.8 ppm based on their position in zeolites[24]). However, as mentioned in **Chapter 4**, the amounts of hydroxyls corresponding to these peaks largely exceed the fraction of Al-OH and Si-OH-Al bridges that can be expected based on the Al content and the density of Brønsted acid sites. Hence these two peaks also contain an important contribution of H bonded silanols. Moreover, since these peaks are very broad, spectral deconvolution is amenable to large errors and will not bring reliable information in terms of relative populations.

6.3.1.5 Conclusion

Al precursors with different reactivities and different nuclearities have been tested by modifying $Al(OPr^i)_3$ with different quantitities of two chelating ligands, Acac and DBM. However, all samples have close density of total Brønsted acid sites and higher Brønsted acidity is obtained only by using a silica support with higher surface area. Using DBM instead of Acac, allows grafting a higher amount of Al on the silica surface, confirming the higher reactivity and hence the lower nuclearity of the Al-DBM chelates, but this does not increase the density of acid sites. The coordination of Al in some of these ASA was investigated by means of ^{27}Al NMR and we observed that the fraction of Al^{IV} increases in the order S4A < $S4_hA$-2Acac < $S4_hA$-DBM. Hence the fraction of Al^{IV} increases upon increasing the L dimension. However, this ranking also reflects the surface density of Al atoms. Hence, one cannot correlate the L/Al ratio and the Al coordination in the ASA. Moreover, there is no direct correlation with the fraction of tetrahedral Al and the acidities (either total acidity or Brønsted acidity) and the acidic Al corresponds only to a fraction of the tetrahedral ones.

6.3.2 ASA Grafted T^iBA

6.3.2.1 Composition and porous properties

Aluminium contents of the ASA prepared by grafting T^iBA are reported in Table 6-5.

For the slurry corresponding to 2 mmol T^iBA for 2 g silica S4 (activated at 200°C, 4.36 mmol/g OH), the grafting of Al is complete (1.0 mmol/g of ASA), whereas, for the slurry corresponding to 10 mmol of T^iBA for 2 g of silica, the amount of grafted T^iBA is only slightly higher (1.5 mmol/g) and much lower than the amount of available silanols (4.4 mmol/g). There are two possible explanations for this result: either the stoichiometry of silanols per grafted T^iBA is very high (close to 4) or the amount of T^iBA that can be grafted on the surface is not controlled by the density of silanols but by size of the precursor (as already observed for the grafting of $Al(OPr^i)_{3-x}L_x$).

Table 6-5 Designation, Al loading and textural properties of silicas and ASA grafted T^iBA

Sample	Al	S_{BET}	Al	Pore Size	Pore Volume
	mmol/g	m^2/g	At/nm^2	nm	cm^3/g
S4		526		3.7	0.61
S4-200-2T	1.0	454	1.33	3.3	0.54
S4-200-10T	1.5	403	2.24	4.8	0.51
S4-200-(10+2)T	2.4	370	3.90	4.2	0.41
S9		902		9.2	1.42
S9-200-2T	1.1	838	0.79	8.1	1.41
S9-500-2T	1.0	868	0.69	9.2	1.42

Repetition of the grafting on calcined S4-200-10T sample allows increasing the amount of grafted Al from 1.5 to 2.4 mmol/g, the increment in the amount of grafted Al is close to 1 mmol/g, i.e. the amount of Al grafted on pure silica under similar conditions. This can be explained by the fact that calcination regenerates surface hydroxyls and removes bulky substitutes from the first grafting. Grafting was also attempted on a silica support with higher surface area. As could be expected, a complete grafting of Al (ca. 1 mmol/g) occurs under the standard conditions. Interestingly, a complete grafting of Al was also observed when the silica support was pretreated at a higher temperature (500°C), despite the much lower surface density of silanols (ca. 1.5 OH per nm^2 based on values reported in Table 6-1, corresponding to a density of 2.1 mmol/g). This could be explained by the fact that silica activated at 500°C contains highly strained siloxane and, according to Werghi et al, T^iBA reacts not only with

silanols but also with strained siloxane.[4]

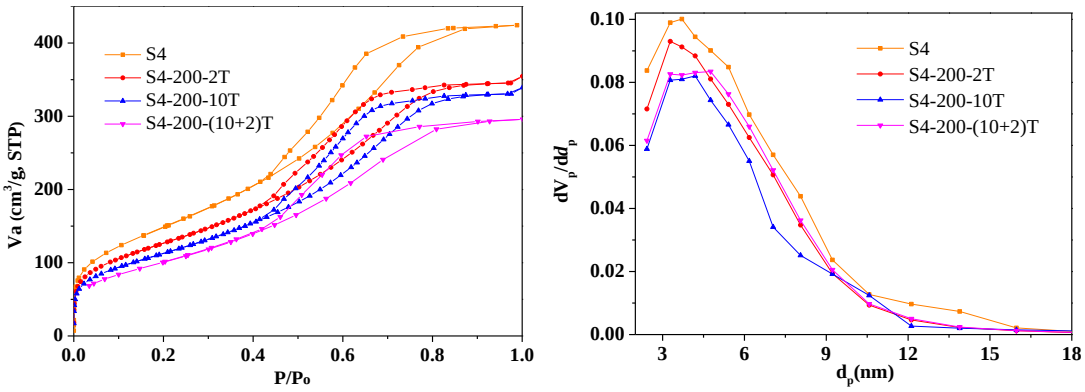

Figure 6-4 N_2 physisorption isotherms (left) and related pore size distribution (right) of ASA prepared by grafting of T^{i}BA on S4 silica (results for S4 silica are also reported for comparison)

The textural characteristics of the grafted samples are also reported in Table 6-5 and Figure 6-4 shows the nitrogen adsorption desorption isotherms and pore size distribution curves of these samples. All samples exhibit a type IV isotherm with a type-H1 hysteresis loop, which is characteristic of mesoporous materials with a relatively narrow pore size distribution, meaning that after grafting Al the mesoporosity of the initial silica is retained.

For the ASA prepared by T^{i}BA grafting on silica S4, the surface area and the pore volume decrease after grafting. The higher the Al loading, the stronger the decrease (up to -38% of surface area for the twice grafted sample), while the pore size (at the maximum of the pore size distribution) is unchanged. As observed for the grafting of Al(OPr^i)$_3$ derivatives, this decrease exceeds the loss of surface area due to the incorporation of 12 wt% of Al_2O_3. Hence, it could indicate that Al atoms form alumina clusters are blocking the pore channel. For the silica with larger pores and pore size (S9), the decrease in the surface area is very low and consistent with the gain weight associated with the incorporation of ca. 6% Al_2O_3. Hence, for this support one can exclude the blocking of the pores by Al debris, probably thanks to its large pore size.

6.3.2.2 Acidic Properties

FTIR of adsorbed pyridine

FTIR of adsorbed pyridine was performed to quantify Brønsted and Lewis acidities.

Values are summarized in Table 6-6. Grafting more Al results in higher total acidity, but tends to form more LAS while the number of BAS is almost unchanged. Though a higher Al loading results in a higher total acidity, it also decreases the percentage of acidic Al. At the highest Al loading (2.4 mmol/g), the percentage of acidic Al is quite similar to that in commercial GD13-H (2.3 mmol of Al per g).

Table 6-6 Type of acid sites (Lewis Acid Sites = LAS), Brønsted Acid Sites = BAS) and acid strength distribution of ASA prepared by grafting T^{i}BA on silica, determined by pyridine-IR

Sample	Acidity (μmol/g)									Acidic Al
	total	BAS				LAS				
	B+L	weak	medium	strong	total	weak	medium	strong	total	%
GD13-H	101	23	11	0	34	21	11	36	67	4.5
S4-200-2T	93	17	15	0	32	15	19	33	67	9.3
S4-200-10T	101	26	0	0	26	31	13	32	76	6.7
S4-200-(10+2)T	116	24	7	0	31	32	18	35	86	4.8
S9-200-2T	109	19	25	0	43	8	1	57	66	9.9
S9-500-2T	106	24	18	0	42	13	2	49	64	10.6

Preparing ASA by grafting the same amount of T^{i}BA on a silica with higher surface area (S9-200-2T prepared using S9 silica) generates an only slightly higher total acidity (and only slightly higher percentage of acidic Al) despite a lower surface density of Al. However, the lower surface density of Al seems to be favorable to the formation of mild Brønsted sites.

Another ASA was prepared by grafting T^{i}BA on S9, but after activation of the silica support at high temperature (sample S9-500-2T). Based on the literature[4], this process should change the mode of grafting of T^{i}BA by allowing, in addition to the reaction with silanol, the grafting by reaction with strained siloxane. However, the ASA produced by grafting on silica activated at 200 and 500°C have almost identical acidic properties.

6.3.2.3 Aluminium coordination

^{27}Al MAS NMR was used to characterize the local Al environment after grafting and calcination for the series of ASA derived from S4 silica. Spectra are shown in Figure 6-5. Fractions and concentrations of aluminium atoms in each coordination, based on the

deconvolution of ^{27}Al MAS NMR spectra, are summarized in Table 6-7.

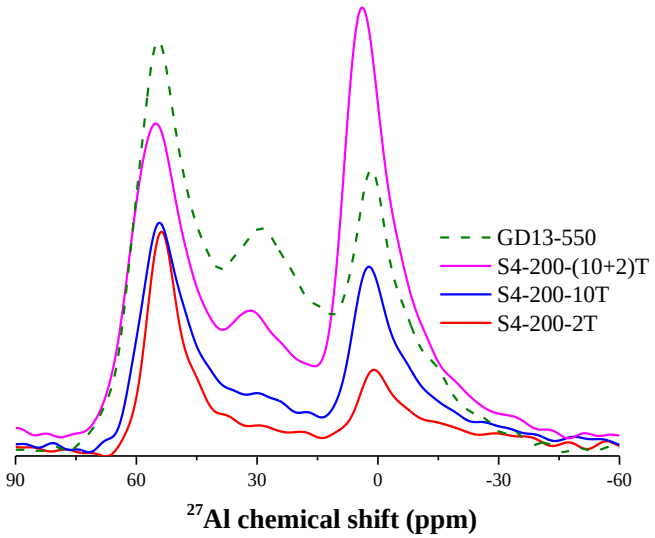

Figure 6-5 ^{27}Al MAS NMR of ASA prepared by grafting of T^{i}BA; all curves have been normalized by sample weight and samples have been rehydrated before measurement

Spectrum of S4-200-2T, the ASA with the smallest amount of Al is dominated by the peaks of four-coordinated at ca. 55 ppm and six-coordinated aluminium at around 0 ppm. For the ASA prepared with an excess of T^{i}BA in the solution (sample S4-200-10T), the intensity of the ^{27}Al NMR spectrum globally increases, in agreement with the 1.5 higher density of grafted Al, but Al^{IV} intensity increases only slightly, while that of the peak associated with Al^{VI} increases distinctly. Besides, a small contribution of five-coordinated becomes visible.

Table 6-7 Fractions and concentrations of Al atoms for each coordination for ASA samples prepared by grafting T^{i}BA. Fraction were determined via the decomposition of normalized ^{27}Al MAS NMR spectra; concentrations were calculated based on the fractions and on the amount of Al in the corresponding sample determined by elemental analysis

Sample	Al percentage (%)			Al content (mmol/g)		
	Al^{IV}	Al^{V}	Al^{VI}	Al^{IV}	Al^{V}	Al^{VI}
S4-200-2T	55.6	2.2	42.3	0.56	0.02	0.42
S4-200-10T	45.3	8.2	46.6	0.68	0.12	0.70
S4-200-(10+2)T	35.1	12.7	52.2	0.84	0.30	1.25

Repeated grafting (sample S4-200-(10+2)T) leads to an increase in the intensities of all peaks, and the peak associated with Al^{V}, at ca. 30 ppm, becomes clearly visible. These Al^{V} species could be related to the deposition of aluminium atoms over the first layer of isolated aluminium species.[25]

Another interesting point is that the position of the Al^{IV} peak shifts to higher ppm as the Al loading increase (from 53.3 ppm in S4-200-2T to 55.3 ppm in S4-200-(10+2)T), indicating that part of the Al^{IV} atoms are in an Al-rich environment.[25]

6.3.2.4 Hydroxyl groups

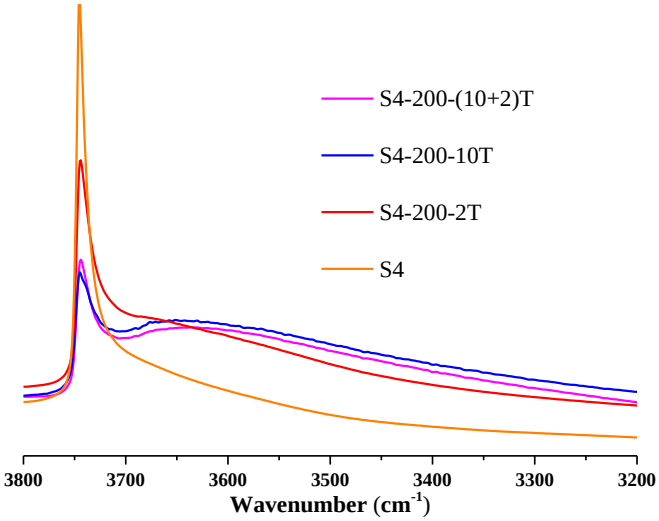

Figure 6-6 υ(OH) ranges of FTIR spectra of silica and ASA grafted T^iBA after activation at 450°C, all curves have been normalized by sample weight

Figure 6-6 displays the IR spectra of the samples derived from S4 in the OH stretching region. All samples exhibit one sharp band at 3745 cm^{-1}, attributed to accessible, isolated silanol groups, together with a broad left shoulder. On the starting silica, the intensity of the left shoulder, that can be assigned to H-bonded silanols,[26-30] is relatively weak, which is consistent with the activation of the silica at 450°C, i.e. at a temperature at which a large part of the H-bonded silanols have undergone dehydroxylation (see Table 6-1). After grafting, the intensity of the band associated to isolated OH decreases significantly while that of other hydroxyls increases, and, the higher the Al, the stronger the variations. The decrease of the band associated with isolated silanols is consistent with the grafting of T^iBA on these sites. After grafting new hydroxyls will likely be formed during drying and calcination and these new hydroxyls will be either aluminols (Al-OH, $(Al)_2$-OH or $(Al)_3$-OH surface hydroxyls), whose FTIR signature is mostly expected at lower wavenumber, and gives rise in transition alumina to multiple bands between 3790 and 3590 cm^{-1}[31] or Si-OH-Al bridges, whose FTIR signature is expected at 3600-3550 cm^{-1}. Hence the modification in the ν(OH) range between

the starting silica and the ASAs reflects the grafting of TIAB on the silica surface (decrease in the density of isolated silanols) and the formation of new type of surface hydroxyls, which could include Si-OH-Al bridges.

6.3.2.5 Conclusion

In this part, several ASAs were prepared by grafting of a highly reactive monomeric Al precursor triisobutylaluminium, using different protocols and two silicas with different surface areas. Grafting of $T^{i}BA$ allows producing ASAs with Brønsted and Lewis acidities. However, the increase in the density of acid sites upon increasing Al surface loading is limited.

6.3.3 ASA Grafted $D^{i}BAH$

6.3.3.1 Composition and porous properties

Table 6-8 Designation, Al loading and textural properties of silica supports and ASA made by grafting $D^{i}BAH$ on these silica

Sample	Al	S_{BET}	Al	Pore Size	Pore Volume
	mmol/g	m^2/g	At/nm^2	nm	cm^3/g
S4		526		3.7	0.61
S6		477		4.8	0.90
S9-150		902		9.2	1.42
S4-700-D	1.0	464	1.30	3.7	0.48
S6-700-D	1.0	409	1.47	6.2	0.70
S9-700-D	1.8	742	1.46	7.1	1.17
S9-150-D	0.7	862	0.49	8.1	1.41

Aluminium contents of the ASA prepared by grafting of $D^{i}BAH$ are reported in Table 6-8. Grafting of $D^{i}BAH$ on silica was performed in the presence of an excess of $D^{i}BAH$ (corresponding to 3.5 mmol of $D^{i}BAH$ per g of silica) on three different silica supports S4, S6, S9 that had been pretreated beforehand at 700°C under vacuum. After pretreatment at such a high temperature, the surface density of silanols is low (about 1.3 OH/nm^2 according to Werghi et al.[5] and silanols are mostly isolated). The Al loading of the prepared ASA are 1.0 mmol/g for silica S4 and S6 (two silica support with similar surface area but different pore size) and 1.8 mmol/g for silica S9. Hence, higher surface area allows the grafting of a higher amount of Al, whereas pore size does not influence the amount of grafted Al despite the large size of the

trimeric Al precursor. If one considers the Al surface loading of these three ASA, it varies between 1.3 and 1.5 and is therefore close to the surface density of silanols. Hence, the grafting of D^{i}BAH seems to be controlled solely by the surface density of silanols.

For the silica S9, grafting of D^{i}BAH was also attempted after activation of the silica at a lower temperature. Although pretreatment at a lower temperature ensure a much higher density of silanols, the amount of grafted Al in these conditions is 2.5 times lower. This may be caused by the low reactivity of siloxanes bridges after pretreatment at 150°C (absence of strained siloxanes) compared to the highly trained siloxanes present on the silica surface after pretreatment at 700°C. According to Werghi et al.,[5] T^{i}BA grafting occurs first by the reaction:

$$\equiv Si\text{-}OH + {}^{i}Bu\text{-}Al({}^{i}Bu)(H) \rightarrow \equiv Si\text{-}O\text{-}Al({}^{i}Bu)(H) + {}^{i}Bu \qquad \text{(Eq. 5)}$$

and is followed by a second reaction between a strained siloxane bridge and the Al-H bond.

$$\equiv Si\text{-}O\text{-}Si\equiv + \equiv Si\text{-}O\text{-}Al({}^{i}Bu)\text{-}H \rightarrow \equiv Si\text{-}O\text{-}Al({}^{i}Bu)\text{-}O\text{-}Si\equiv + \equiv Si\text{-}H \qquad \text{(Eq. 6)}$$

Based on the lower density of grafted Al in absence of strained siloxane, one can postulate that when the grafting is limited to the first reaction, the anchoring of Al is too weak and the ≡Si-O-Al= bond is broken during the subsequent step (e.g. washing). Another possible explanation would be that the two above reactions occur simultaneously.

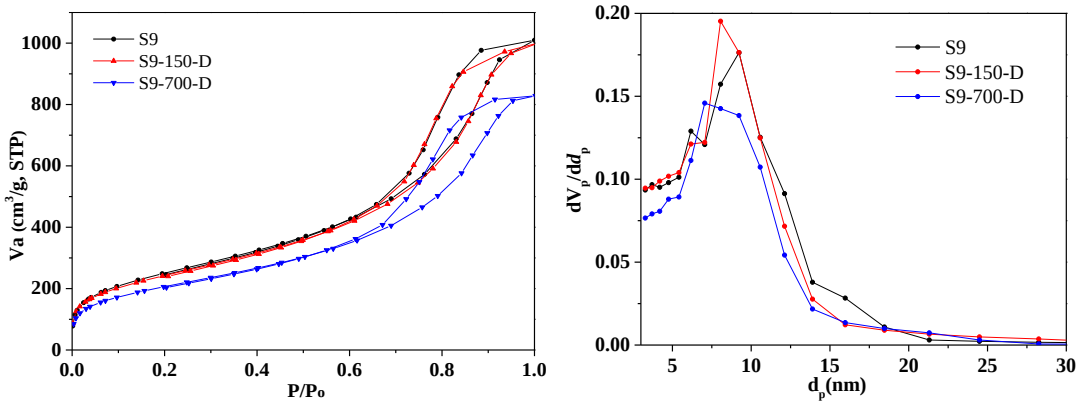

Figure 6-7 N_2 physisorption isotherms (left) and related pore size distribution (right) of S9 and ASAs made by grafting D^{i}BAH on S9

Textural characteristics of the ASAs are summarized in Table 6-8 and Figure 6-7 shows the nitrogen adsorption-desorption isotherms and pore size distribution curves of ASAs

obtained by grafting D^{i}BAH on S9. All samples exhibit a type IV isotherm with a type-H1 hysteresis loop, which is characteristic of mesoporous materials with a relatively narrow pore size distribution. After the grafting process, the pore size slightly shifts to smaller values, which may be due to the incorporation of Al on the pore walls. The modification of the textural properties after grafting are more pronounced for the ASA obtained by grafting on the silica pretreated at 700°C with a decrease of the surface area of about 18%. However, this decrease could partly be due to the pretreatment of the silica support at 700°C.

6.3.3.2 Acidic Properties

1. FTIR of adsorbed Pyridine

Table 6-9 Type of acid sites (Lewis Acid Sites = LAS), Brønsted Acid Sites = BAS) and acid strength distribution of ASA prepared by grafting D^{i}BAH on silica, determined by pyridine-IR

Sample	Acidity (µmol/g)									Acidic Al
	Total	BAS				LAS				
	B+L	weak	medium	strong	total	weak	medium	strong	total	%
GD13-H	101	23	11	0	34	21	11	36	67	4.5
S4-700-D	92	17	3	0	20	32	15	24	71	8.9
S6-700-D	97	20	5	0	25	31	15	26	72	9.2
S9-700-D	155	34	7	6	47	29	5	74	108	10.5
S9-150-D	93	20	7	11	37	10	1	44	56	13.2

FTIR of adsorbed pyridine was used to quantify the Brønsted and Lewis acid sites. Values are summarized on Table 6-9. The ASA prepared with S4 and S6, the two silica supports with similar surface area, have close acidic properties, in agreement with their similar Al loadings. The ASA obtained using the high surface silica support (S9-700-D) has a 1.5 higher amount of acid sites, thanks to its higher Al loading. The total acidity of this ASA is quite high (with regards to the other ASA described in this chapter) but about 2/3 of the total acid sites are LAS. It also contains a small fraction (6 µmol/g) of strong BAS, which had not yet been observed in the previous ASA. S9-150-D, prepared by grafting D^{i}BAH on S9 activated at low temperature (150°C) also has interesting properties with a higher fraction of Brønsted acid sites (including 11 µmol/g of strong Brønsted acid sites). These two last samples will be further

investigated in the next parts of this chapter.

2. *FTIR of adsorbed CO*

FTIR of adsorbed CO at low temperature was used to further investigate the nature of the acid sites of S9-150-D. Figure 6-8 presents the difference spectra (left ν(OH) range, right ν(CO) range), after adsorption of increasing amount of CO.

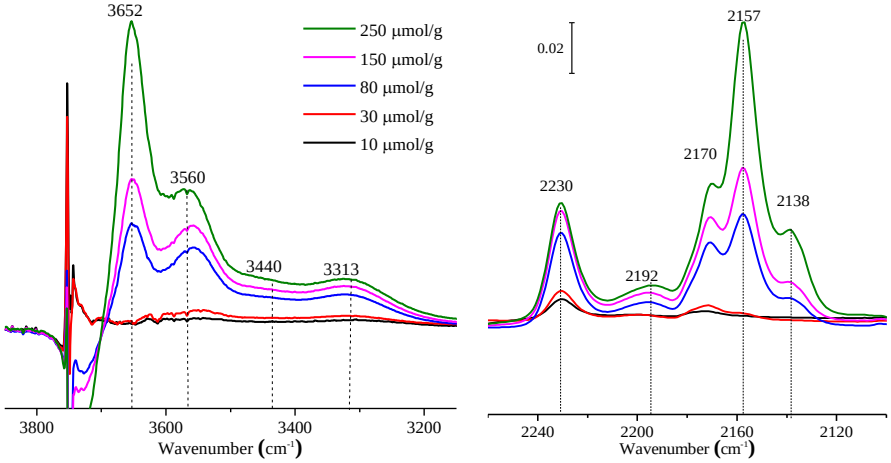

Figure 6-8 Difference FTIR spectra in the ν(OH) (left) zone and ν(CO) (right) zone after CO adsorption on S9-150-D for various CO coverage.

In the ν(OH) zone, four contributions are observed at 3313, 3440, 3560 and 3652 cm^{-1}. The first band is assigned to strong Brønsted sites (with a strength similar to that of the Si-OH-Al bridges of zeolites), while the band at 3440 cm^{-1} indicates the presence medium Brønsted sites. The existence of strong BAS is in agreement with the results found by pyridine adsorption FTIR. The band at 3560 cm^{-1} is indicative of the presence of weakly acidic OH groups with an acidity only slightly stronger than that of silanols (band at 3654 cm^{-1}). In the CO region, at low CO coverage, the peaks at 2230 and 2192 cm^{-1} correspond to CO adsorbed on strong Lewis acid sites, medium and weak Lewis acid sites, respectively. Another peak is observed at 2172 cm^{-1} with a left shoulder at 2178 cm^{-1}. These two contributions correspond respectively to CO adsorbed on mild and strong Brønsted acid sites. Upon increasing the CO loading all these bands increase in intensity and new bands at 2157 (CO adsorbed on silanols) and 2139 cm^{-1} (physisorbed CO) are observed.[32] Upon increasing the CO loading the band at 2172 shifts to 2170 cm^{-1} but the contribution at ca. 2178 cm^{-1} remains present.

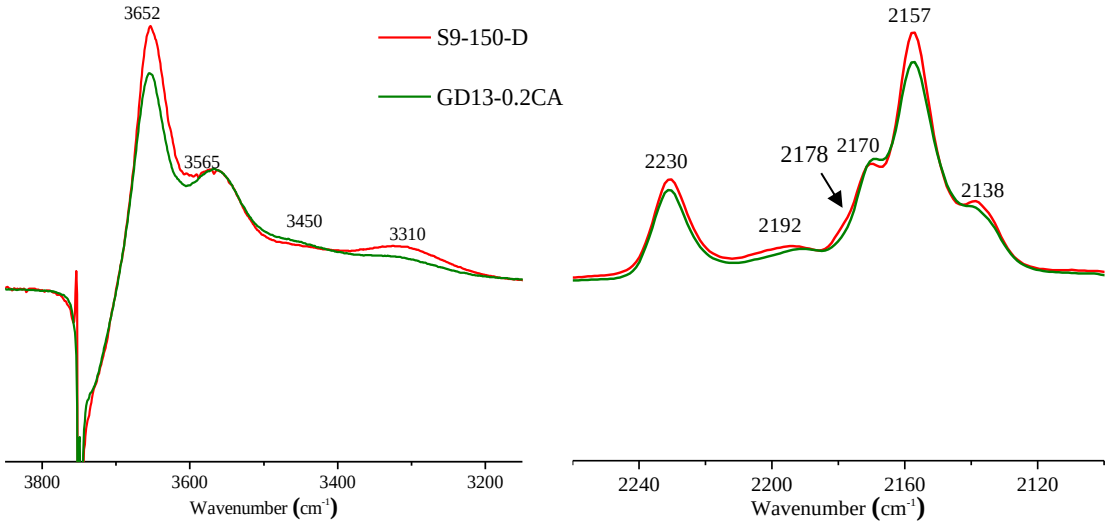

Figure 6-9 Comparison of the difference FTIR spectra in ν(OH) (left) zone and ν(CO)(right) zone of CO adsorption on S9-150-D (black) and GD13-0.2CA (green) at a CO coverage of ca. 250 µmol/g. Spectra of both samples were normalized on structure bands located between 1500 and 2100 cm^{-1}

Figure 6-10 compares the difference spectra after adsorption of ca. 250 µmol/g CO on S9-150-D and GD13-0.2CA (obtained by mild dealumination of a commercial ASA with citric acid, see **Chapter 4**). The spectra of the two samples are quite similar and they both present, in the ν(OH) range, the band at ca. 3310 cm^{-1} that indicates the presence of strong Brønsted sites, likely Si-OH-Al bridges. However, this band is more pronounced on S9-150-D. In the ν(CO) range the shoulder at ca. 2178 cm^{-1} is also more visible on this sample than on GD13-0.2CA.

6.3.3.3 Aluminium coordination

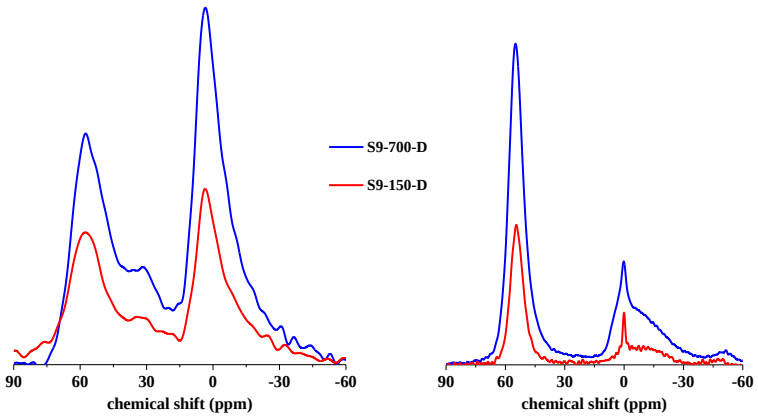

Figure 6-10 ^{27}Al MAS NMR of S9-150-D and S9-700-D before (left) and after calcined (right), all curves have been normalized by sample weight and calcined samples were rehydrated before measurement.

^{27}Al MAS NMR was used to determine the coordination of the Al in S9-150-D and S9-700-D and monitor any changes in the Al environment after calcination. Spectra are shown in Figure 6-10. Fractions and concentrations of aluminium atoms in each coordination, based on the deconvolution of ^{27}Al MAS NMR spectra, are summarized in Table 6-10. Before calcination, both spectra are similar and exhibit three peaks at ca. 56, 30, 0 ppm, attributed to aluminium in Al^{IV}, Al^{V} and Al^{VI} environments, respectively.

Table 6-10 Fractions and concentrations of Al atoms for each coordination for ASA samples prepared by grafting $D^{i}BAH$. Fraction were determined via the decomposition of normalized ^{27}Al MAS NMR spectra; concentrations were calculated based on the fractions and on the amount of Al in the corresponding sample determined by elemental analysis

Sample	Uncalcined						Calcined					
	Al percentage (%)			Al content (mmol/g)			Al percentage (%)			Al content (mmol/g)		
	Al^{IV}	Al^{V}	Al^{VI}	Al^{IV}	Al^{V}	Al^{VI}	Al^{IV}	Al^{V}	Al^{VI}	Al^{IV}	Al^{V}	Al^{VI}
S9-150-D	31.6	22.8	45.6	0.22	0.16	0.32	65.8	0.0	34.2	0.46	0.00	0.24
S9-700-D	31.3	19.2	49.5	0.56	0.35	0.89	64.7	1.4	34.0	1.16	0.02	0.61

After calcination, two main peaks are observed at ca. 56 (Al^{IV}) and 0 ppm (Al^{VI}) whereas the peak ascribed to Al^{V} becomes negligible or even disappears. The fraction of Al^{IV} and Al^{VI} are still similar in the two samples and the relative intensities of their spectra still reflects the amounts of Al in these two samples. For these two samples, calcination results in an increase in the fraction of Al^{IV} at the expense of Al^{VI}. Hence, calcination may result in the incorporation of some of the Al atoms in the silica framework, as previously proposed by Hensen et al.[33] As already mentioned for the other ASAs, the fraction of Al^{IV} in the spectra after calcination exceed by far the amounts of acid sites determined by pyridine adsorption.

^{27}Al MQ MAS NMR was used to provide a more detailed information on the environment of Al atoms in calcined S9-150-D. Figure 6-11 shows the ^{27}Al 3Q MAS NMR spectra of S9-150-D in hydrated and dehydrated state, respectively. Table 6-11 presents the parameters obtained from 3Q MAS NMR spectra and Al content, which was calculated by the decomposition of the 1D ^{27}Al MAS NMR spectra using the quadrupolar and isotropic parameters derived from the 3Q MAS NMR spectra.

The spectrum of calcined-hydrated S9-150-D is characterized by an intense resonance

centered at 55 ppm, attributed to Al^{IV}. The signal of Al^{IV} is close to the diagonal, which indicates that the corresponding aluminium species experience a relatively small quadrupolar interaction and weak electric field gradient. This points toward a rather symmetric environment, corresponding probably to Al^{IV} inserted in the silica network. In the region corresponding to octahedral Al, two resonances, a sharp one, Al^{VIb}, assigned to mobile cationic Al species^{+})[34,35] and a broad one, Al^{VIa}, are clearly visible in the 1D spectrum of the hydrated sample. These two resonances produce a weak signal on the MQ MAS spectrum and could only discerned from one another on the zoomed insert. According to Malicki et al., the peak associated to Al^{VIb} is hardly observed on the MQ MAS spectrum because the efficiency of multiple-quantum (MQ) coherence generation tends to zero for species with very small quadrupolar couplings.[34]

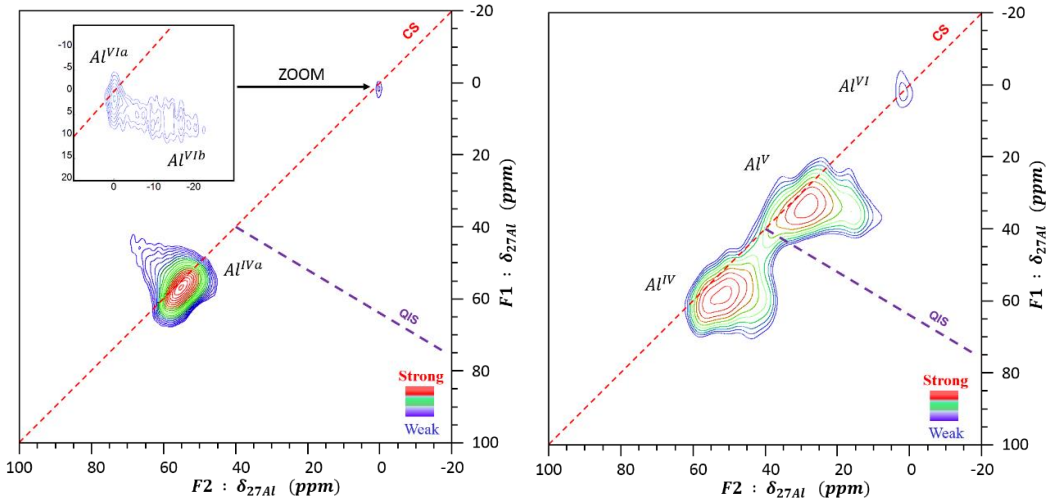

Figure 6-11 ^{27}Al 3Q MAS NMR spectra of S9-150-D: hydrated (left) and dehydrated at 200°C (right); F1 dimension = isotropic dimension; F2 dimension = 2^{d} order quadrupolar line shape

After dehydration, a new signal is observed at δ_{ISO} = 32.5 ppm, which can be attributed to Al^{V}. This Al^{V} species was absent from the spectrum of the hydrated sample but account for a large fraction (65%) of the signal in the dehydrated sample, and probably originates from both Al^{IV} and Al^{VI} from the hydrated sample. Conversion of Al^{IV} to Al^{V} upon dehydration was also observed in **Chapter 5**, and we proposed that the change in the local environment of the Al^{IV} atoms upon dehydration allows some of them to increase their coordination to V by interaction with framework oxygen atoms. Moreover, Al^{VI} contribution almost vanishes from the spectrum of S9-150-D after dehydration. This indicates the absence, in this sample, of an

alumina like phase. Another point that is worth mentioning is that Al^{IV} in this ASA is in a more symmetrical environment after dehydration than what was reported for the ASAs investigated in **Chapter 5**.

Table 6-11 The assignment, NMR parameters and relative Al content of hydrated and dehydrated S9-150-D by ^{27}Al 3Q NMR

Sample	Al coordination	δ_{F1} ppm	δ_{F2} ppm	δ_{ISO} ppm	$C_{Q\eta}$ MHz	Al content %
S9-150-D-hy	Al^{IV}	56.8	54.9	56.1	1.8	65.8
	Al^{VIa}	1.5	-0.1	0.9	1.7	6.9
	Al^{VIb}	5.7	-13.5	-1.4	5.8	27.3
S9-150-D-dehy	Al^{IV}	59.5	52.4	56.9	3.6	33.5
	Al^{V}	34.8	28.5	32.5	3.4	65.0
	Al^{VI}	2.8	1.8	2.4	1.3	1.5

6.3.3.4 Hydroxyl groups

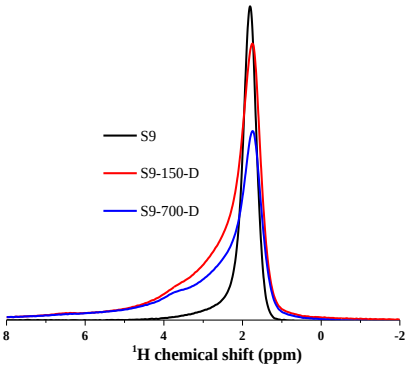

Figure 6-12 ^{1}H MAS NMR of spectra on S9, S9-150-D and S9-700-D dehydrated at 200°C, all curves have been normalized by sample weight

^{1}H NMR spectroscopy on the dehydrated ASAs was used to distinguish the different types of hydroxyl groups. Spectra of S9-150-D, S9-700-D together with the spectrum of S9 are shown in Figure 6-12. For all samples, the dominant signal is located at 1.8 ppm and can be attributed to isolated silanols.[21] For the starting silica, a weak shoulder is visible on the left side of this peak that can be assigned to H-bonded silanols. After Al grafting, the intensity of the peak associated with isolated silanols decreases. This is to be expected as silanols which are the anchoring points for the grafting of D^{i}BAH *(see* (Eq. 5)*, p188*). The loss of isolated silanols is more pronounced for S9-700-D than for S9-150-D. This could have two origins: first,

treatment of the silica at 700°C may cause irreversible dihydroxylation, hence decreasing irreversibly the density of surface silanols; second, the grafting of 2.5 higher amount of $D^{i}BAH$ will result in the consumption of more of the surface silanols.

Compared to pure silica S9, the peak associated with isolated silanols is slightly broader in the ASAs, probably because of the incorporation of Al into the silica network.[36] A small peak at about 3.8 ppm, can be distinguished on the spectra of the two ASA, i.e. at the position where one would expect Si-OH-Al hydroxyl groups based on the position of bridging hydroxyls in zeolites.[24] Beside this peak, a broad shoulder is clearly visible on the left side of the peak associated to isolated silanols indicating the presence of other types of hydroxyls such as Al-OH-Al (expected at 2.6 ppm)[23] and also H-bonded hydroxyls. The strong overlap of the signals impedes a better interpretation of the ^{1}H NMR spectra of these two samples.

6.3.3.5 ^{27}Al-^{1}H D-HMQC 2D NMR

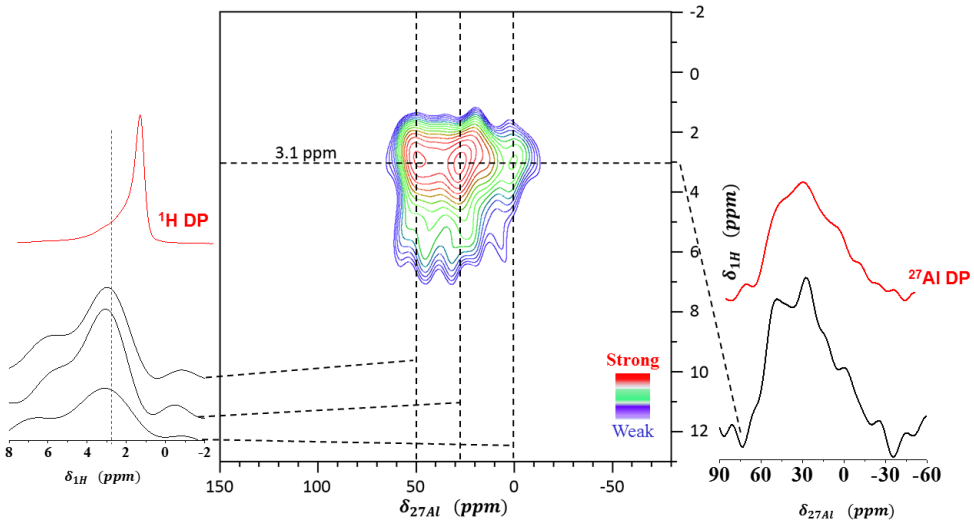

Figure 6-13 ^{27}Al-^{1}H D-HMQC 2D spectra of S9-150-D dehydrated at 200°C

^{27}Al-^{1}H D-HMQC 2D NMR spectra of S9-150-D is shown on Figure 6-13. In addition to the contour plot of the ^{27}Al-^{1}H D-HMQC 2D spectra, slices cut either along the x axis (^{27}Al spectra) or along the y axis (^{1}H spectra) together with the corresponding ^{27}Al and ^{1}H DP spectra are also shown for analysis assistance. For this experiment, the dehydrated form of the sample was used in order to suppress the overwhelming correlation signal between Al and adsorbed water molecules. The 2D spectrum and its projections along the ^{1}H axis clearly shows the

absence of correlation between isolated silanols and Al atoms, whatever the coordination of the Al atom. The maximum of the correlation peak on the ^{1}H projection is located between 2 and 4 ppm, i.e. in the broad left shoulder of the DP ^{1}H NMR signal. This signal could be due to Si-OH-Al (expected at ca. 3.8 ppm) and/or Al-OH-Al (expected at 2.6 ppm). On the ^{27}Al dimension, the projected 2D and the DP spectra are quite similar, seeming to indicate that ^{1}H-^{27}Al correlation is not limited to Al^{IV} but may also occurs with Al^{V} (based on MQ MAS experiments, Al^{VI} are, after dehydration, almost absent from this sample). This conclusion should however be taken with caution: indeed, due of the large widths of the NMR peaks in the dehydrated sample, a strong overlap of the peaks assigned to Al^{IV} and Al^{V} occurs (as emphasized on the insert showing the ^{27}Al projections) and because of the low signal to noise ratio of the 2D spectrum (which is due to the low Al content of S9-150-D) we could not attempt a decomposition based on the 3Q parameters (as we did for the ^{27}Al-^{1}H DHMQC spectra of **Chapter 5**).

6.3.3.6 Conclusion

Grafting of $D^{i}BAH$ on high surface silica results in strong Brønsted acid sites which were not observed for the grafted samples prepared with the others precursors. These strong Brønsted acid sites are, based on CO adsorption, similar to those observed in the ASAs obtained by dealumination with CA of commercial ASA (**Chapter 4**). The fraction of strong Brønsted acid sites is nevertheless more important in the ASAs obtained by grafting of $D^{i}BAH$ than in those obtained by dealumination. The most acidic ASA of the $D^{i}BAH$ series was further characterized by advanced NMR. We observed, for this ASA, the absence of an alumina-like phase and a high fraction of tetrahedral Al. Nevertheless, the fraction of acidic Al remains well below the fraction of Al^{IV}. ^{27}Al-^{1}H D-HMQC experiments show a correlation peak at about 3 ppm in the ^{1}H dimension that correlate with both Al^{IV} and Al^{V} in the ^{27}Al dimensions. Similar experiments on the ammonium form of this ASA, would certainly help to the identification of acidic Al.

6.3.4 Catalytic Performance for the isomerization of 3,3-dimethylbut-1-ene

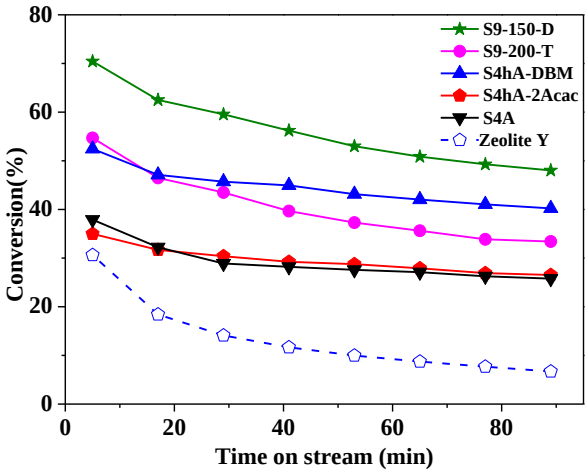

Figure 6-14 Conversion of 33DMB1 as a function of time on stream for the representative grafted samples

Figure 6-14 compares the conversion of the representative grafted ASAs as a function of time on stream. The conversion vs. time on stream of a commercial zeolite Y (ammonium form, surface area 730 m^2/g, mole ratio SiO_2:Al_2O_3 = 12:1, converted to H-form for catalytic test with the calcination procedure used for the ASAs and described in **Chapter 2**) is also shown for comparison. For all samples, the conversion decreases quickly during the first half hour, then deactivation slows down and a steady state is reached for most samples within one hour. The conversion at steady state increases in the order: S4A ≈ $S4_hA$-2Acac < S9-200-T < $S4_hA$-DBM < S9-150-D, which is generally consistent with the Brønsted acidity (medium or total) measured by FTIR of adsorbed pyridine, except S9-150-D. S9-150-D, the sample for which we have evidenced the presence of strong Brønsted acid sites (with strength and structure similar to those of zeolites based of FTIR of adsorbed CO and pyridine), displays the highest conversion indicating that strong BAS are remarkably beneficial for the reaction. However, this is, with the zeolite, the sample that also shows the highest deactivation. Nevertheless, at variance with the zeolite, which loses 80% of its initial activity after 90 min time-on-stream, S9-150-D only loses 30% of its initial activity. Hence, this sample is less sensitive to deactivation than the zeolite despite its strong Brønsted acid sites, either because it also possesses mild Brønsted sites or thanks to its more open porosity.

Compared to the commercial ASAs (Figure 3-4, GD13-H and GD25-H), the grafted

samples all display better catalytic performance, suggesting that preparation of ASA by grafting of aluminium precursors on high surface silicas is a promising approach for the synthesis of ASA with enhanced acidic properties and improved performance.

6.4 Discussion

In this chapter, different types of Al precursors were used for the preparation of ASA by grafting them on silica supports. As mentioned in the introduction, the purpose was to favor the formation of isolated grafted Al species. We therefore privileged low nuclearity Al precursors.

For the first series of Al precursors, we used $Al(OPr^i)_{3-x}L_x$, where L is either acetylacetone or dibenzoylmethane (DBM), i.e. bidentate chelating ligands. The addition of a chelating ligands, especially a bulky one such as DBM is expected to decrease the nuclearity of the Al precursor by decreasing its coordinative unsaturation. However, it is also expected to decrease its reactivity. For the second and third series, we used highly reactive alkylaluminium (hydride) precursors, which are either monomeric is solution (T^iBA) or expected to graft as isolated Al on silica (D^iBAH).

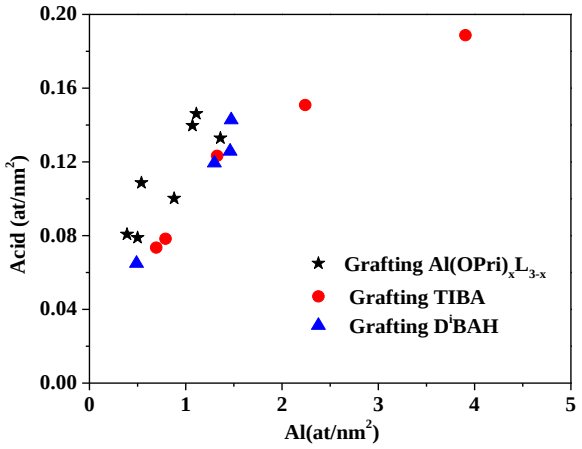

Figure 6-15 Evolution of the surface density of acid sites (FTIR of adsorbed pyridine) as a function of the surface density of Al atoms

As we used silica of various surface areas as support, we compared the acidity data (based on FTIR of adsorbed pyridine experiments) as a function of surface densities (rather than density by unit of weight). The acidity characteristics of the three series of ASAs are

summarized in the three following figures: in Figure 6-15, the surface density of acid sites is plotted vs the surface density of Al; in Figure 6-16, the fraction of acidic Al is plotted vs the surface density of Al and finally, in Figure 6-17 the ratio of BAS/LAS (Brønsted acid sites/Lewis acid sites) is plotted vs the surface density of Al and of acid sites.

One can clearly see, on these three figures, that, although the three series of ASA were prepared using different Al precursors, they all follow the same trends. Hence, the type of Al precursor and the choice of other experimental conditions (such as temperature of pretreatment or surface area of the silica support) mostly control the amount of grafted Al (and the surface density of Al), that, in turns, control the acidic properties of the ASA. Therefore, increasing significantly the density of acid sites per g of ASA seems to be only achievable by increasing the surface area of the silica support. One must however mention that, although the total amount of BAS and LAS are controlled by the surface density of Al, the choice of the Al precursor may play a role in the strength of the acid sites, as strong Brønsted acid sites (desorbing pyridine above 350°C) are only detected for one precursor, D^{i}BAH. The formation of strong acid sites for this precursor may be associated to high reactivity of D^{i}BAH that favor the multiple grafting of this Al precursor on the silica surface.

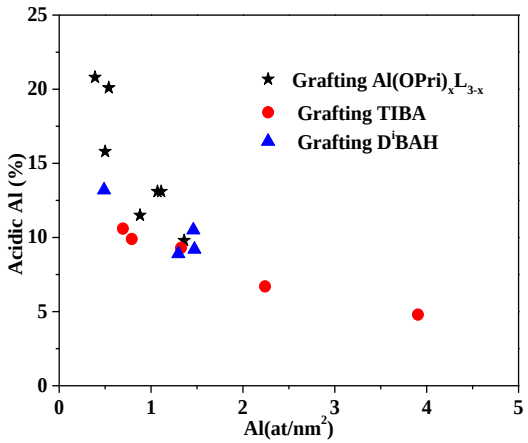

Figure 6-16 Evolution of the percentage of acidic Al (FTIR of adsorbed pyridine) as a function of the surface density of Al atoms

On Figure 6-15, one can see that the surface density of acid sites increases with the surface density of Al, but that this increases is moderate (when the surface density is multiplied

by 8, the surface density of acid sites is multiplied by 3). Moreover, the increase of the surface density of acid sites with the surface density of Al seems to level off at high Al loading. This could be due to the fact that a high Al loading is detrimental to the formation of isolated Al. The decrease in the fraction of acidic Al with the surface density of Al is better seen on Figure 6-16. Low Al loading (which were mostly obtained by using the low reactivity $Al(OPr^i)(Acac)_2$ precursor) corresponds to a quite high fraction of acidic Al (from 20 to 15%) and the fraction of acidic Al decreases sharply with the Al loading.

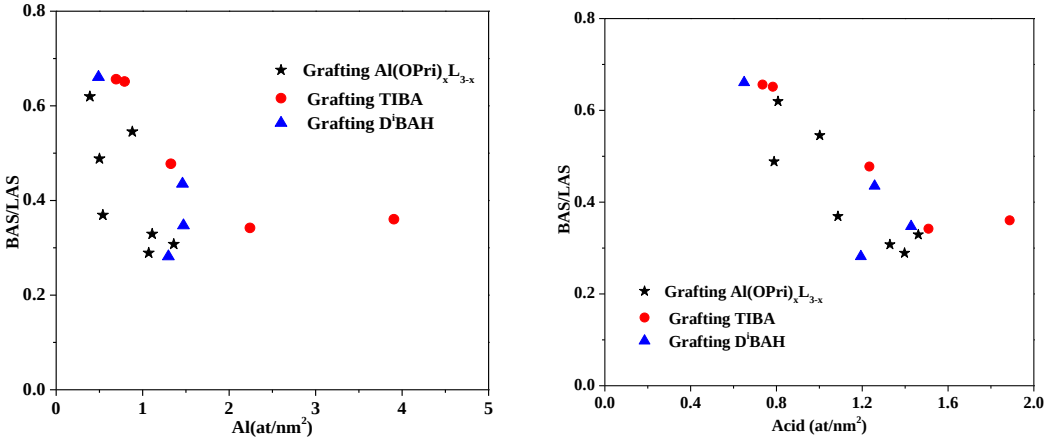

Figure 6-17 Evolution of the percentage of BAS/LAS ratio (FTIR of adsorbed pyridine) as a function of the surface density of Al (left) and the surface density of acid sites (FTIR of adsorbed pyridine) (right)

On the last figure, Figure 6-17 which reports the evolution of the BAS/LAS as a function of the surface density of Al (left) and of acidic Al (right), one can see that the BAS/LAS ratio also decreases, for all ASAs prepared by grafting, upon increasing the density of surface Al. This also could be due to the fact that a high surface concentration of Al is detrimental to the formation $Al(OSi)_4$ species leading. More surprisingly, when the BAS/LAS ratio is plotted vs the surface density of acid sites, the correlation of all datas seems even better, indicating that, the higher the surface density of acid sites, the lower the fraction of BAS (and the higher the fraction of LAS). This result is however difficult to explain, especially when one takes into account the very low surface density of acid sites (maximum 0.2 acid sites per nm^2), that excludes an interaction between them.

6.5 Conclusion and perspectives

In this chapter, we explored the preparation of ASA by grafting Al precursors ($Al(OPr^i)_{3-}$

$_xL_x$, Al(^{i}Bu)$_3$, Al(^{i}Bu)$_2$H on high surface area silica. ASA with wide range of Al loading have been prepared but the acidic properties of these ASA seems to be mostly controlled by the surface density of Al atoms, independently of the choice de the Al precursor, the silica support and the experimental conditions for grafting.

Nevertheless, the choice of the Al precursor may play a role on the strength of the acid sites as a small amount of strong Brønsted acid sites (based on pyridine adsorption experiments and confirmed by CO adsorption experiments) were observed solely when using D^{i}BAH as Al precursor. Strong Brønsted acid sites are very rarely observed on ASA and they may indicate the presence of Si-OH-Al bridges on D^{i}BAH derived ASA. Although the amount of these strong Brønsted acid sites is low (maximum 11 µmol/g), it is similar to the amounts reported previously by Hensen et al.[33]

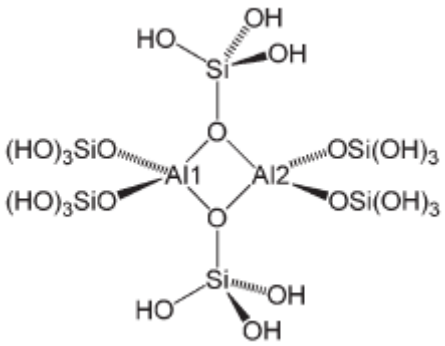

Figure 6-18 Possible structure of a surface tetrahedral Al atoms without significant Brønsted or Lewis acidity (from kermagoret et al.[37])

For all the ASA prepared in this chapter, the fraction of Al^{IV} (^{27}Al MAS NMR) after calcination exceed by far the amounts of acid sites determined by pyridine adsorption. This was also true for the ASA prepared by dealumination (see **Chapter 3** and **4**). However, in this chapter, the ASAs were prepared by grafting followed by thermal treatment at moderate temperature (550°C). The formation of buried Al^{IV} is therefore probably very limited and most of the Al atoms are located at the surface. This is particularly true for sample S9-150-D, for which the very low loss of surface upon grafting allows excluding pore blocking. Hence, one can conclude to the presence of accessible Al in tetrahedral coordination but without acidic properties. A possible model (Figure 6-18) for these sites would be Al dimers, as proposed by

Kermagoret et al.[37]

Sample S9-150-D, which contains strong Brønsted sites and 13% of acidic Al, was further characterized using advanced NMR sequences. However, drawing conclusions regarding the structure of the acid sites of this ASA remains challenging because, the fraction of acidic Al remains low and, as the density of Al sites is also relatively low, obtaining NMR data with good signal to noise is difficult and would probably necessitate the access to a high field NMR spectrometer.

Due to limited time, there is still ample space to improve the grafting procedure and possibly produce ASA with enhanced acidic properties and/or reach a better understanding of the factors controlling the acid type and acid site density of ASAs.

For the ASA prepared using $Al(OPr^i)_{3-x}L_x$ precursors, the amount of grafted Al remains low due to the low reactivity of these Al precursors, whereas, for the ASA prepared using D^iBAH, the amount of grafted Al is limited by the low density of silanols (grafting after thermal treatment at 700°C) or by the low reactivity of the siloxane bridges (grafting after pretreatment at 150°C). We could nevertheless attempt to increase the Al loading on the ASAs prepared using these two precursors by applying repeated grafting. For the ASA derived from $Al(OPr^i)_{3-x}L_x$, experiments could also be performed using silica supports with higher surface area and bigger pore size such as S9 in order to increase the density of acid sites per unit of weight.

For the ASAs prepared by grafting T^iBA, attempts could be made using diethylether (Et_2O) as solvent or additive. Indeed, when reacted with diethylether Et_2O, monomeric neutral etherate adduct T^iBA /Et_2O are formed, which prevent T^iBA dimerization and also serves as adsorption competitor to facilitate unreacted and physisorbed T^iBA removing from the surface conveniently.[38]

The conditions of calcination (atmosphere and temperature) could be varied. For these experiments, calcination was performed in an oven under air and in static conditions, but the moisture from air has been previously reported to promote aggregation of surface species. In order to favor the formation of isolated Al species (and hence the formation of acid sites),

calcination under an O_2 stream could be used, as reports on the preparation of alumina-rich ASA by grafting (grafting of tetraethoxysilane on γ-alumina) have concluded to important role of calcination conditions for the preservation of the acid sites of these ASA during the calcination step.[39,40] Regarding the temperature of calcination, as proposed by Hensen et al.,[33] calcination at higher temperature could be attempted (700°C or higher) in order to favor the migration of Al atoms in Si-rich environment.

Reference

(1) Seese, M. A.; Albers, E. W.; Magee Jr, J. S.; Patents US4226743 A, **1980**.

(2) Van Ginhoven, R. M.; Jonsson, H.; Park, B.; Corrales, L. R. *The Journal of Physical Chemistry B* **2005**, *109*, 10936.

(3) Fleischman, S. D.; Scott, S. L. *Journal of the American Chemical Society* **2011**, *133*, 4847.

(4) Werghi, B.; Bendjeriou-Sedjerari, A.; Sofack-Kreutzer, J.; Jedidi, A.; Abou-Hamad, E.; Cavallo, L.; Basset, J.-M. *Chemical Science* **2015**, *6*, 5456.

(5) Werghi, B.; Bendjeriou-Sedjerari, A.; Jedidi, A.; Abou-Hamad, E.; Cavallo, L.; Basset, J.-M. *Organometallics* **2016**, *35*, 3288.

(6) Bartram, M.; Michalske, T.; Rogers Jr, J. *Journal of Physical Chemistry* **1991**, *95*.

(7) Anwander, R.; Gerstberger, G.; Palm, C.; Groeger, O.; Engelhardt, G. *Chem. Commun.* **1998**, 1811.

(8) Mokaya, R. *Chemical Communications* **1997**, 2185.

(9) Mokaya, R. *Angewandte Chemie International Edition* **1999**, *38*, 2930.

(10) Caillot, M.; Chaumonnot, A.; Digne, M.; Van Bokhoven, J. A. *ChemCatChem* **2014**, *6*, 832.

(11) Pan, Y.-S.; Lin, H.-P.; Cheng, H.-H.; Cheng, C.-F.; Tang, C.-Y.; Lin, C.-Y. *Chemistry letters* **2006**, *35*, 608.

(12) Wengrovius, J. H.; Garbauskas, M. F.; Williams, E. A.; Goint, R. C.; Donahue, P. E.; Smith, J. F. *Journal of the American Chemical Society* **1986**, *108*, 982.

(13) Abraham, A.; Prins, R.; van Bokhoven, J. A.; van Eck, E. R.; Kentgens, A. P. *The Journal of Physical Chemistry B* **2006**, *110*, 6553.

(14) Benn, R.; Janssen, E.; Lehmkuhl, H.; Rufínska, A. *Journal of organometallic chemistry* **1987**, *333*, 155.

(15) Charoenchaidet, S.; Chavadej, S.; Gulari, E. *Macromolecular rapid communications* **2002**, *23*, 426.

(16) Kermagoret, A.; Kerber, R. N.; Conley, M. P.; Callens, E.; Florian, P.; Massiot, D.; Copéret, C.; Delbecq, F.; Rozanska, X.; Sautet, P. *Dalton Transactions* **2013**, *42*, 12681.

(17) Parfenova, L. V.; Kovyazin, P. V.; Nifant'ev, I. E.; Khalilov, L. M.; Dzhemilev, U. M.

Organometallics **2015**, *34*, 3559.

(18) VESTIN, R.; VESTIN, U.; KOWALEWSKI, J. *Acta Chem. Scand. A* **1985**, *39*.

(19) Crépeau, G.; Montouillout, V.; Vimont, A.; Mariey, L.; Cseri, T.; Maugé, F. *The Journal of Physical Chemistry B* **2006**, *110*, 15172.

(20) Hensen, E.; Poduval, D.; Magusin, P.; Coumans, A.; Van Veen, J. *Journal of Catalysis* **2010**, *269*, 201.

(21) Trébosc, J.; Wiench, J. W.; Huh, S.; Lin, V. S.-Y.; Pruski, M. *Journal of the American Chemical Society* **2005**, *127*, 3057.

(22) Brunet, F.; Charpentier, T.; Le Caer, S.; Renault, J.-P. *Solid state nuclear magnetic resonance* **2008**, *33*, 1.

(23) Delgado, M.; Delbecq, F. o.; Santini, C. C.; Lefebvre, F.; Norsic, S.; Putaj, P.; Sautet, P.; Basset, J.-M. *The Journal of Physical Chemistry C* **2011**, *116*, 834.

(24) Asakawa, N.; Motokura, K.; Yashima, T.; Koyama, T.-r.; O-nuki, T.; Miyaji, A.; Baba, T. *The Journal of Physical Chemistry C* **2012**, *116*, 17734.

(25) Goldbourt, A.; Landau, M. V.; Vega, S. *The Journal of Physical Chemistry B* **2003**, *107*, 724.

(26) Janin, A.; Maache, M.; Lavalley, J.; Joly, J.; Raatz, F.; Szydlowski, N. *Zeolites* **1991**, *11*, 391.

(27) Ichihashi, H.; Kitamura, M. *Catalysis today* **2002**, *73*, 23.

(28) Heitmann, G.; Dahlhoff, G.; Hölderich, W. *Journal of Catalysis* **1999**, *186*, 12.

(29) Chu, C. T.; Chang, C. D. *The Journal of Physical Chemistry* **1985**, *89*, 1569.

(30) Kiricsi, I.; Flego, C.; Pazzuconi, G.; Parker, W. J.; Millini, R.; Perego, C.; Bellussi, G. *The Journal of Physical Chemistry* **1994**, *98*, 4627.

(31) Busca, G. *Catalysis Today* **2014**, *226*, 2.

(32) Phung, T. K.; Hernández, L. P.; Lagazzo, A.; Busca, G. *Applied Catalysis A: General* **2015**, *493*, 77.

(33) Hensen, E. J.; Poduval, D. G.; Degirmenci, V.; Ligthart, D. J. M.; Chen, W.; Maugé, F. o.; Rigutto, M. S.; Veen, J. R. v. *The Journal of Physical Chemistry C* **2012**, *116*, 21416.

(34) Malicki, N.; Mali, G.; Quoineaud, A.-A.; Bourges, P.; Simon, L. J.; Thibault-Starzyk, F.; Fernandez, C. *Microporous and Mesoporous Materials* **2010**, *129*, 100.

(35) Zhao, Z.; Xu, S.; Hu, M. Y.; Bao, X.; Peden, C. H.; Hu, J. *The Journal of Physical Chemistry C* **2014**, *119*, 1410.

(36) Luo, Q.; Deng, F.; Yuan, Z.; Yang, J.; Zhang, M.; Yue, Y.; Ye, C. *The Journal of Physical Chemistry B* **2003**, *107*, 2435.

(37) Kermagoret, A.; Kerber, R. N.; Conley, M. P.; Callens, E.; Florian, P.; Massiot, D.; Delbecq, F.; Rozanska, X.; Copéret, C.; Sautet, P. *Journal of Catalysis* **2014**, *313*, 46.

(38) Pelletier, J.; Espinas, J.; Vu, N.; Norsic, S.; Baudouin, A.; Delevoye, L.; Trébosc, J.; Le Roux, E.;

Santini, C.; Basset, J.-M. *Chemical Communications* **2011**, *47*, 2979.

(39) Mouat, A. R.; Kobayashi, T.; Pruski, M.; Marks, T. J.; Stair, P. C. *The Journal of Physical Chemistry C* **2017**.

(40) Mouat, A. R.; George, C.; Kobayashi, T.; Pruski, M.; Van Duyne, R. P.; Marks, T. J.; Stair, P. C. *Angewandte Chemie* **2015**, *127*, 13544.

Conclusions and perspectives

The purpose of this thesis was twofold: first we aimed at preparing amorphous silica-alumina (ASA) with enhanced acidic properties and second, we aimed at studying the local structure around Al atoms in ASAs using advanced NMR experiments, with the ultimate purpose to discriminate non-acidic Al atoms from acidic ones. These two objectives are inter-related: on the one side, preparation of ASA with a high fraction of acidic Al will be very useful for NMR investigation as the high fraction of acidity-silent Al in ASA renders the NMR characterization of acid sites very challenging; on the other side, a better understanding of the structure of acidic and non-acidic Al could be helpful to the development of ASAs with improved acidic properties.

To reach the above described objectives, the following scientific approach has been adopted in this thesis:

First, two experimental strategies have been developed for the preparation of ASAs with enhanced acidic properties. The first one was based on the dealumination of commercial ASAs with the objective to remove selectively non acidic Al while leaving acidic ones. For this strategy two molecules have been tested: acetylacetone which is a chelating agent and citric acid which combines chelating properties with acidic ones. The second strategy was based on the preparation of ASAs by grafting isolated Al atoms on the surface of a silica material. Again different Al precursors have been tested (either aluminium alkoxides or aluminium alkyl or alkyl hydride). In order to understand and optimize the preparation of ASAs by these two approaches, the textural and acidic properties of these materials have been carefully characterized using N_2-sorption (for the characterization of the texture) and NH_3-TPD, FTIR of adsorbed basic probe molecules (pyridine and CO) and the model reaction of isomerization 3,3-dimethylbut-1-ene (a reaction that characterizes mild and strong Brønsted acid sites). Moreover, routine NMR experiments have been performed on these ASAs, in order to investigate (i) Al coordination and its evolution upon dealumination or as a function of the grafting strategy (^{27}Al MAS NMR) and (ii) the nature of the surface hydroxyls (^{1}H MAS NMR).

Second, model ASAs selected among those prepared using the above described

procedures, have been investigated by a combination of one and two-dimensional homo- and heteronuclear ^{1}H and ^{27}Al NMR, with the purpose to highlight spatial proximities (within ca. 5 Å, based on their dipolar interaction) between Al atoms (^{27}Al DQ-SQ 1D and 2D experiments), between H atoms (^{1}H DQ-SQ 2D experiments) and also between an H and an Al atom via heteronuclear dipolar interaction between ^{1}H and ^{27}Al (D-HMQC 2D and REAPDOR experiments). 3Q MAS NMR was also used to get a more precise image of the local environment of the Al atoms, especially in dehydrated samples).

Regarding the synthesis of model ASAs by dealumination of commercial ASAs either with Acetylacetone (Acac, **Chapter 3**) or with Citric Acid (CA, **Chapter 4**), we have shown that:

-When dealumination is performed on the ammonium (uncalcined) forms of the commercial ASAs, acetylacetone can remove more than half of the Al present in the starting ASA and this removal is accompanied by an increase of the surface area (up to 40% extra surface area). This Al removal does not decrease the acidity (acidity even slightly increases for some of the samples, based on measurements of FTIR of adsorbed pyridine). Dealumination also leads to an increase in the conversion (isomerization) of 33DMB1. Dealumination with Acac has also been attempted on the calcined (H-forms) of the ASAs but the results are shown to be less efficient under these conditions. Characterization of the Al coordination by ^{27}Al NMR and of its evolution with the extent of dealumination shows that 5-coordinated Al in the calcined ASA (which probably correspond to Al^{IV} with flexible coordination in the uncalcined ASA, based on the comparison of the ^{27}Al NMR spectra before and after calcination) are the most easily removed. The high reactivity of these Al atoms toward dealumination with Acac was associated with their flexible coordination (which will favor their interaction with Acac).

-CA treatment also modifies the textural properties, acidity and catalytic activity of ASAs. CA can effectively extract up to 80% of Al atoms present in the starting ASA and results in a significant increase of the surface area (up to 57% extra surface area), of total acidity (up to 41% extra acid sites) and of conversion of 33DMB1 (up to 1.7 times higher conversion). Dealumination with CA, thanks to its efficiency and selectivity also increases dramatically the

fraction of acidic Al (by a factor of 5). Moreover, FTIR of adsorbed CO reveals that dealumination also creates (or reveals) new Brønsted acid sites of zeolitic strength (and also probably of zeolitic structure). Similar to Acac, CA dealumination is more effective and selective on the (uncalcined) ammonium form than on the (calcined) H-form of the ASAs and preferentially extract Al with flexible coordination.

Based on the comparison of the acidic properties of the ASA dealuminated by these two protocols, CA is superior to acetylacetone for selective dealumination and allows obtaining a higher fraction of acid sites per Al atoms. This higher dealumination efficiency is most probably related to the fact that it combines chelating and acidic properties. Therefore, ASA dealuminated by CA would be more suitable than those obtained by dealumination with Acac for the second objective of this thesis (Advanced NMR characterization of the environment of Al and H atoms).

The other strategy that has been investigated in view of obtaining ASAs with improved acidic properties was the preparation of ASA with well controlled Al environment through grafting of monomeric Al precursor on silica supports. Monomeric (or low nuclearity) Al precursors have been specifically targeted because the objective was to favor the grafting of isolated Al, as grafted polymeric Al species are expected to be mostly silent in terms of acidity. This synthesis approach is developed in Chapter 6. Al precursors that have been investigated are:

-Aluminum alkoxides modified by chelating ligands ($Al(OPr^i)_xL_{3-x}$, where L = acetylacetone or dibenzoylmethane), an alkylaluminium (triisobutylaluminum), and an aluminium alkylhydride (diisobutylaluminum hydride). Several ASAs have been prepared using these precursors with wide range of Al loading and parameters relevant for a controlled grafting of isolated Al have been explored. Based on the comparison of the acidic properties of these ASA, the overall acidity seems to be mostly controlled by the surface density of Al atoms, independently of the choice of the Al precursor, silica supports and the experimental conditions for grafting. However, the choice of the Al precursor may influence on the nature of the acid sites that are formed as only ASAs prepared by grafting diisobutylaluminum hydride

displayed strong Brønsted acid sites based on pyridine and CO adsorption FTIR experiments. Nevertheless, all ASAs prepared by grafting displayed enhanced performances for 3,3-dimethylbut-1-ene isomerization compared to a reference zeolite and to commercial ASAs, indicating that grafting could be a promising approach for the synthesis of ASA with enhanced acidic properties and improved catalytic performances.

The two synthesis strategies we have explored (dealumination or grafting) have allowed developing ASAs with enhanced acidity and a higher fraction of acid sites per Al atoms compared to commercial ASAs. Among the ASAs prepared using these two strategies, those presenting the most promising properties were selected for advanced NMR characterization to investigate the spatial proximity and connectivity between proton and aluminum, in order to provide information on the local environment of Al atoms, and attempt to identify the Al atoms associated with the acid sites. These NMR results are mostly reported in **Chapter 5** (ASAs prepared by dealumination with CA) but a preliminary study on one of the ASA prepared by grafting of $D^{i}BAH$ is also included in **Chapter 6**. The main results of this NMR investigation are the following:

-Based on ^{27}Al DQ-SQ NMR experiments, at least two phases (an alumina phase and a silica-alumina phase) are present on the starting ASA. The silica-alumina phase contains mostly 4-coordinated Al, but also 5-coordinated and probably 6-coordinated ones (depending on the hydration of the ASA); the alumina phase contains mostly 6-coordinated Al (similar to A^{VI} of γ-alumina) but also 4-coordinated Al (similar to Al^{IV} of γ-alumina) and also probably Al^{V} at the surface of the alumina phase.

-For all ASAs prepared by dealumination, large fraction of their Al atoms experience a flexibility of their coordination (or at least a modification in the symmetry around the Al atom) between ammonium and H form or between hydrated and dehydrated samples. This modification of the Al environment, which was evidenced by ^{27}Al NMR (DP and 3Q MAS), is a clear indication that most of Al atoms are located at or close to the surface.

-For the starting ASA in its ammonium form, ammonium and all types of hydroxyls

(isolated silanols and other types of hydroxyls responsible for a broad shoulder on the left side of the ^{1}H NMR signal of isolated silanols) are in close proximity. This indicates that all these species are located on the same phase, which is necessarily the silica-alumina phase (^{1}H DQ-SQ NMR).

-^{27}Al-^{1}H D-HMQC 2D NMR of the starting ASA shows a close proximity between ammonium and not only Al^{IV}, but also Al^{V}. Hence, Brønsted acidity may be associated not only to Al^{IV} but also to Al^{V}.

-Among the Al species that are identified thanks to ^{27}Al 3Q NMR experiments on calcined ASAs, Al^{IVa} is particularly interesting because all its characteristics (and especially the modification of its environment upon dehydration) are close to those of the framework Al^{IV} of zeolites. Moreover, the comparison of the NMR spectra of the starting ASA and of dealuminated ASAs reveals that Al^{IVa} is resistant to dealumination. Furthermore, the Al^{IV}-Al^{IV} distance (about 6 Å based on 1D ^{27}Al DQ-SQ experiments) is consistent with isolated Al (no direct Al^{IV}-O-Al^{IV} linkage). Hence, Al^{IV} sites are necessarily $Al(OSi)_4$. However, the quantitative analysis of the ^{27}Al NMR spectra clearly indicates that the amount of Al^{IVa} largely exceeds the amount of acid sites (let alone the amount of Brønsted acid sites). To reconcile these two contradictory conclusions, we proposed that (some) Al^{IVa} sites are engaged in Si-OSi-Al bridges (the charge compensating proton found in zeolites and responsible for their Brønsted acidity is replaced by a Si atom), that can be opened by water in the hydrated samples.

-Regarding the structure of the Brønsted acid sites, we could not draw a final conclusion, but based on the shorter distance between Al and ammonium in the ASA compared to the Al-ammonium distance in a zeolite (^{1}H-^{27}Al REAPDOR experiments), we can exclude the hypothesis that acid sites are silanols, whose acidic properties are modified by a nearby aluminium. Although other possible structure such as bridging or pseudo bridging silanols cannot be discarded, this shorter Al-ammonium distance could point toward an acidity related to aluminol sites.

As mentioned above, grafting has a high potential for the synthesis of ASA with

enhanced acidic properties and allows preparing ASAs with strong Brønsted acid sites. However, due to limited time, we could not completely optimize the acidic properties of the ASAs prepared by this method and their acidic properties could probably be improved by adjusting more carefully the conditions of synthesis (including the conditions of calcination).

Regarding NMR experiments, there are, in theory, still many more experiments that could be done on these samples in order to get a clearer view of the nature of the acid sites of ASAs. Moreover, we were able to prepare ASAs with a percentage of acid site per Al as high as 28%. These ASA, would, in principal, be ideal samples for the characterization of the acid sites by advanced NMR. However, the concentration of acid sites in all these samples is very low and this low concentration is definitely a bottleneck for 2D NMR studies, except, maybe, when using dynamic nuclear polarization (DNP) which allows a strong enhancement in the sensitivity. NMR experiments at higher field are also an interesting option.

Annexes

Annex I Reactor Draft

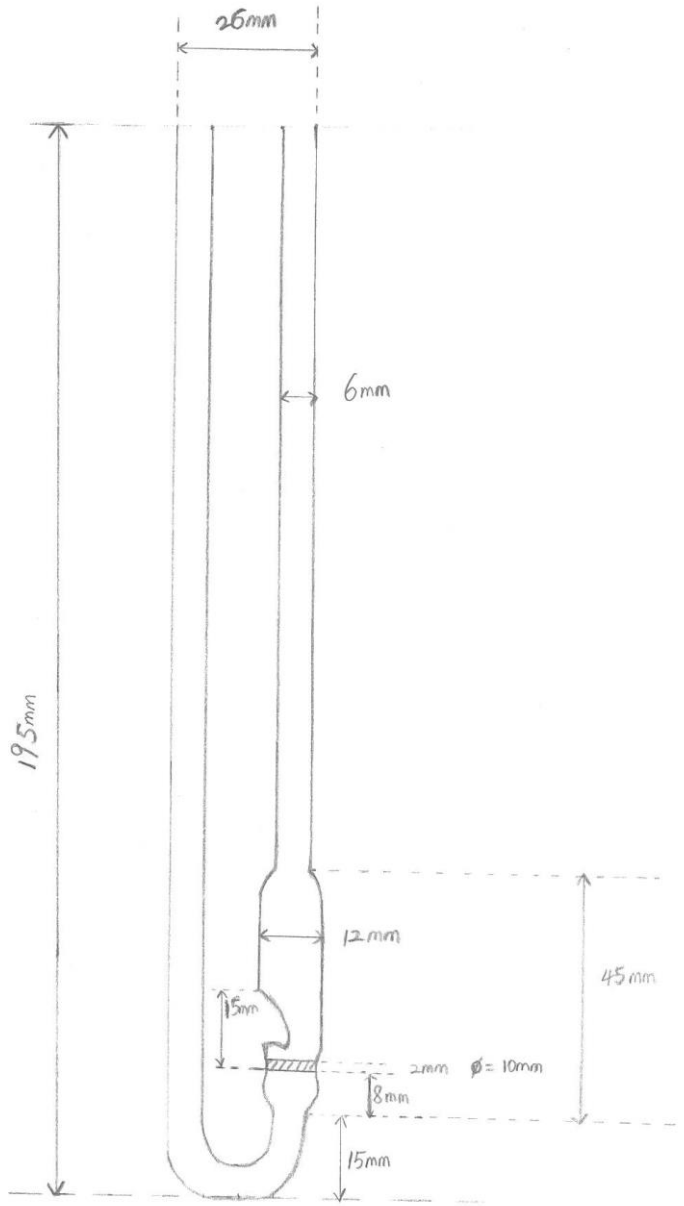

Annex II Gas chromatography results of 33DMB1 isomerization

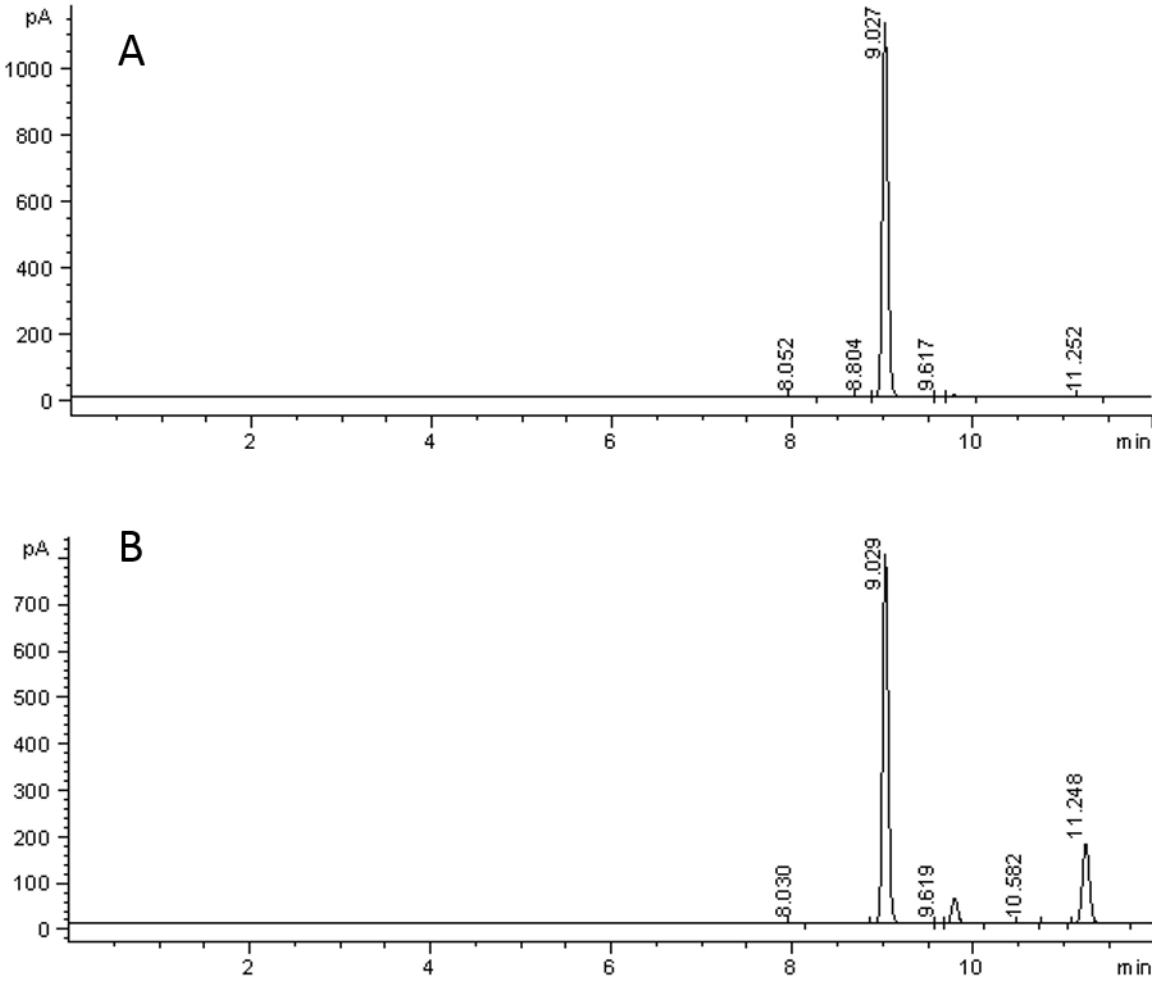

A: Blank test; B: Catalytic test on GD13-H

Retention time (min)	Molecule	Area (a.u)	
		A	B
8.0		1.4	0.6
8.8		0.8	
9.0	33DM1B	4901.2	3465.0
9.6		2.1	1.0
9.7	23DM1B	27.6	255.1
10.5			0.5
10.8			1.6
11.2	23DM2B	2.0	933.2

Annex III In situ infrared cell for FTIR adsorption pyridine/CO

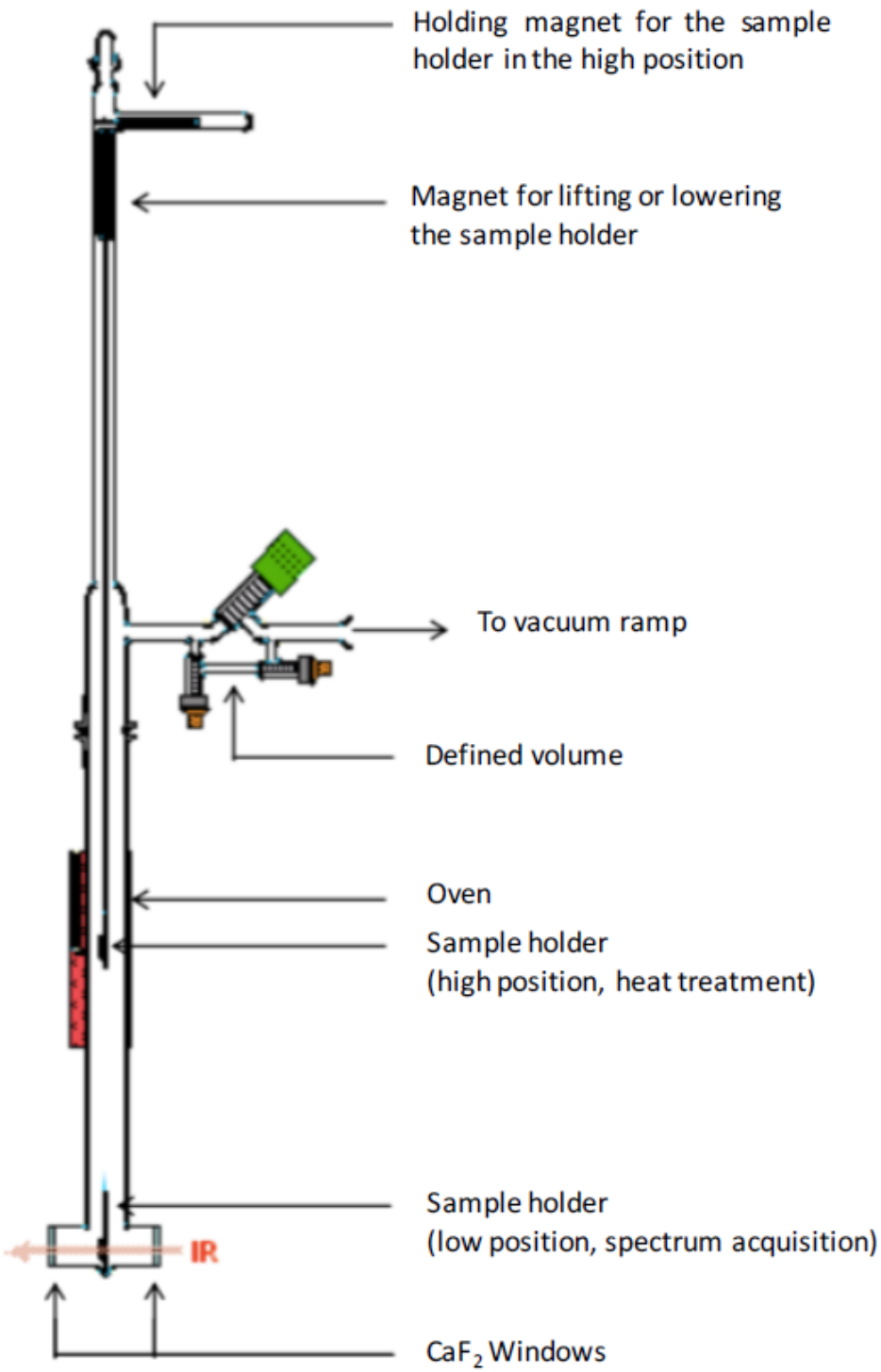

Annex IV Assembly for FTIR adsorption pyridine

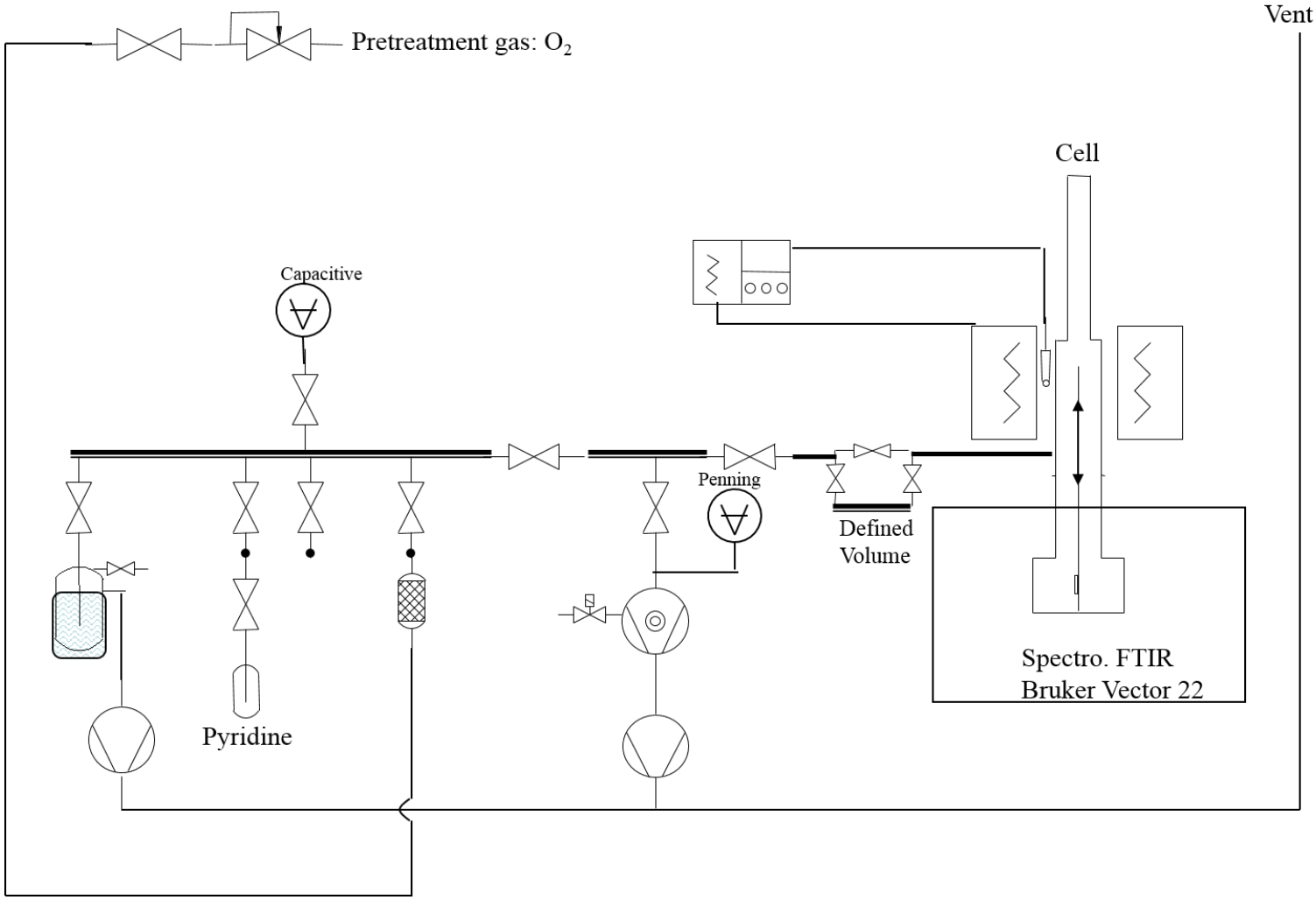

Annex V Assembly for FTIR adsorption CO

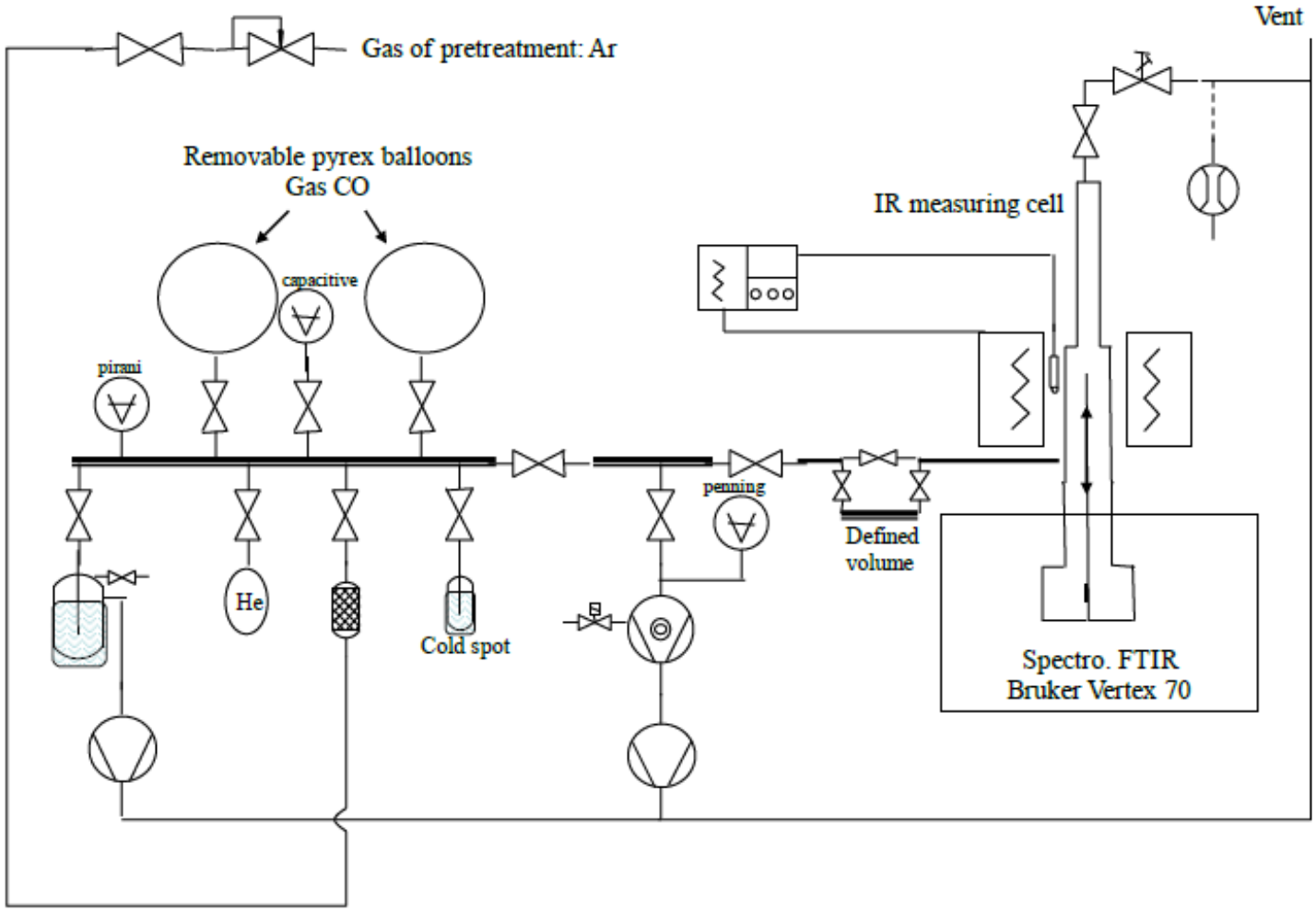

Annex VI Catalytic test scheme

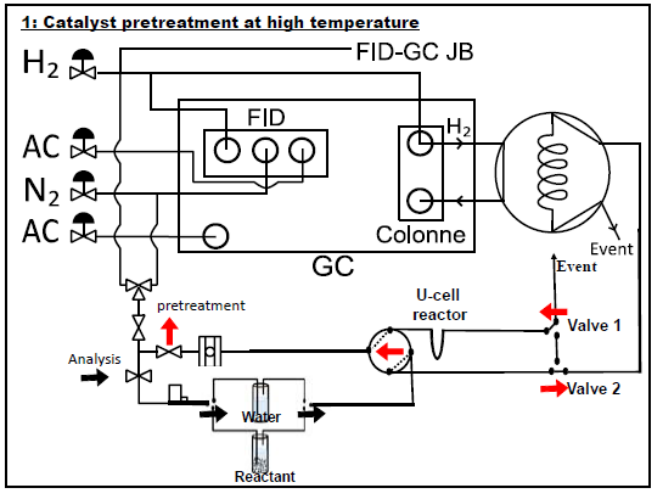

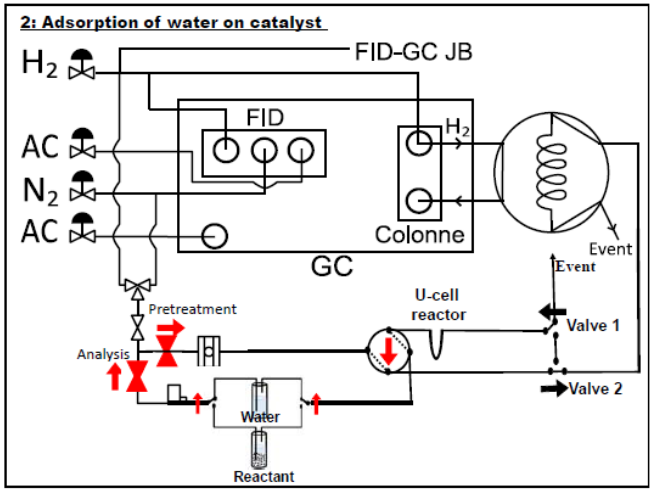

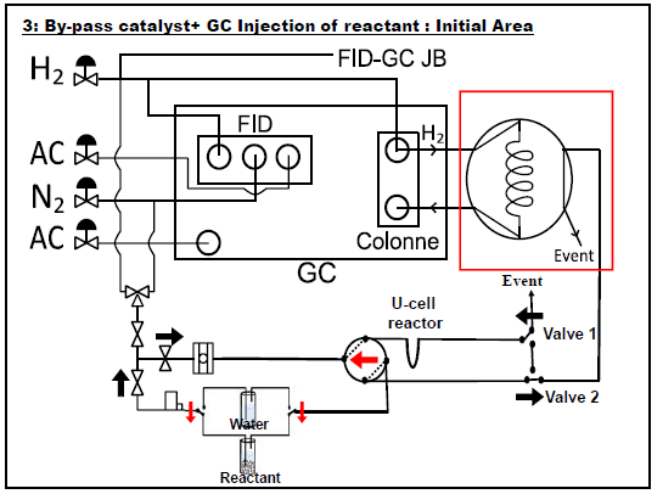

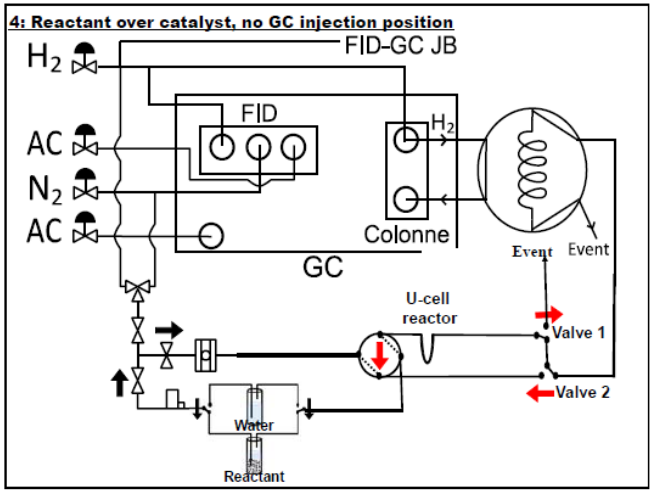

List of Tables

List of Figures

JIN xiaojing – Preparation of amorphous silica-aluminas with enhanced acidic properties and spectroscopic identification of their acid sites - 2017

Résumé

Des silice-alumines (SA) avec des propriétés acides améliorées et une fraction plus élevée d'aluminium acides ont été préparées en utilisant deux stratégies de synthèse. Leurs propriétés texturales ont été étudiées par physisorption de N_2 et leurs propriétés acides par suivi FTIR de l'adsorption de molécules sondes (pyridine ou CO). Par ailleurs, la réaction d'isomérisation du 33DMB1 a été utilisée pour caractériser leurs performances catalytiques et leurs propriétés acides. La première stratégie de synthèse a été de désaluminer des silice-alumines commerciales avec de l'acetylacetone (Acac) ou de l'acide citrique (CA). CA est plus actif et plus sélectif que Acac et permet de retirer jusqu'à 87% des Al initialement présents tout en augmentant la quantité de sites acides (jusqu'à 41%) et en multipliant par 5 la fraction d'Al acides. La seconde stratégie a été de greffé des précurseurs d'aluminium ($Al(OPr^i)_xL_{3-x}$, T^iBA, D^iBAH) sur des silices. Toutes les SA obtenues par greffage présentent une activité catalytique plus élevées que les SA commerciales et la zéolithe, mais seules certaines de SA obtenues par greffage de D^iBAH ont des sites acides de Bronsted forts.

Des SA représentatives de ces deux séries ont été caractérisées par RMN, avec comme objectif d'étudier la structure des sites acides en utilisant des séquences RMN 1D et 2D, homo- et héteronucléaires impliquant ^1H et ^{27}Al. Cette étude a mis en évidence : (i) la présence, pour la plupart des SA, de deux phases, l'une d'alumine, l'autre de silice alumine (^{27}Al DQ-SQ NMR); (ii) une localisation des atomes d'Al près de la surface sur la base de leur flexibilité de coordination ^{27}Al NMR (DP and 3Q MAS); (iii) l'implication possible des Al^V (en plus des Al^{IV}) dans les sites acides de Bronsted (^{27}Al-^1H D-HMQC 2D NMR); (iv) la probable différence de structure des sites acides des SA par rapport à ceux des zéolithes (^1H-^{27}Al REAPDOR).

Mots clés: [Silice-alumine amorphe; Préparation; Acidité; Désalumination; Acétylacétone; Acide Citrique; Greffage; RMN du solide; Activité catalytique en isomérisation du 33DMB1]

Abstract:

ASAs with enhanced acidity and a higher fraction of acidic Al were prepared by two experimental strategies. Their textures have been investigated by N_2 adsorption–desorption and their acidic properties by FTIR of adsorbed probe molecule (pyridine or CO). Besides, isomerization of 33DMB1 was selected as model reaction to check their activity and characterize their acidity. The first strategy is based on dealumination of commercial ASAs with acetylacetone (Acac) or citric acid (CA). CA is superior to Acac for selective dealumination. It allows removing up to 87% of Al, increases total acidity up to 41%, and fraction of acidic Al by a 5 fold factor. The second strategy is based on the grafting Al precursor ($Al(OPr^i)_xL_{3-x}$, T^iBA, D^iBAH) on silica. All the grafted ASAs display better performance for 33DMB1 isomerization than commercial ASA and zeolite, but strong Brønsted acid sites are observed solely for some D^iBAH derived samples.

Representative samples of these two series were selected as model ASAs for advanced NMR characterization, with the purpose to investigate the structure of acid sites by a combination of one and two-dimensional homo- and heteronuclear ^1H and ^{27}Al NMR. On most ASAs, two separate phases are present: alumina and silica-alumina (^{27}Al DQ-SQ NMR). Localization of most of the Al atoms was evidenced based on the flexibility of their coordination (^{27}Al NMR DP and 3Q MAS). Brønsted acidity may be associated with both Al^{IV} and Al^V (^{27}Al-^1H D-HMQC 2D NMR) but the structure of these sites is probably different from those of zeolites (^1H-^{27}Al REAPDOR).

Keywords: [Amorphous silica-alumina; Preparation; Acidity; Dealumination; Acetylacetone; Citric acid; Grafting; SSNMR; Catalytic activity for 33DMB1 isomerization]